Cerebrovascular integrity maintenance and inflammation in atherosclerosis animal models

Vanessa Di Cataldo

N°d'ordre NNT : 2016LYSE1290

THESE de DOCTORAT DE L'UNIVERSITE DE LYON
opérée au sein de
l'Université Claude Bernard Lyon 1

Ecole DoctoraleED205
Ecole Doctorale Interdisciplinaire Science-Santé

Spécialité de doctorat : Physiologie
Discipline: (Biologie)

Soutenue publiquement le 16/12/2016, par :
Vanessa Di Cataldo

Cerebrovascular integrity maintenance and inflammation in animal models of atherosclerosis: a biomarker approach

---

Devant le jury composé de :

Pialoux, Vincent	Université Lyon 1	Président
Arnaud, Claire	Grenoble	Rapporteure
Badaut, Jérôme	Bordeaux	Rapporteur
Boisseau, Nathalie	Clermont-Ferrand	Examinatrice
Lahoutte, Tony	Bruxelles	Examinateur
Millon, Antoine	Université Lyon 1	Co-directeur
Canet-Soulas, Emmanuelle	Université Lyon 1	Directrice de thèse

UNIVERSITE CLAUDE BERNARD - LYON 1

Président de l'Université	**M. le Professeur Frédéric FLEURY**
Président du Conseil Académique	M. le Professeur Hamda BEN HADID
Vice-président du Conseil d'Administration	M. le Professeur Didier REVEL
Vice-président du Conseil Formation et Vie Universitaire	M. le Professeur Philippe CHEVALIER
Vice-président de la Commission Recherche	M. Fabrice VALLÉE
Directeur Général des Services	M. Alain HELLEU

COMPOSANTES SANTE

Faculté de Médecine Lyon Est – Claude Bernard	Directeur : M. le Professeur J. ETIENNE
Faculté de Médecine et de Maïeutique Lyon Sud – Charles Mérieux	Directeur : Mme la Professeure C. BURILLON
Faculté d'Odontologie	Directeur : M. le Professeur D. BOURGEOIS
Institut des Sciences Pharmaceutiques et Biologiques	Directeur : Mme la Professeure C. VINCIGUERRA
Institut des Sciences et Techniques de la Réadaptation	Directeur : M. X. PERROT
Département de formation et Centre de Recherche en Biologie Humaine	Directeur : Mme la Professeure A-M. SCHOTT

COMPOSANTES ET DEPARTEMENTS DE SCIENCES ET TECHNOLOGIE

Faculté des Sciences et Technologies	Directeur : M. F. DE MARCHI
Département Biologie	Directeur : M. le Professeur F. THEVENARD
Département Chimie Biochimie	Directeur : Mme C. FELIX
Département GEP	Directeur : M. Hassan HAMMOURI
Département Informatique	Directeur : M. le Professeur S. AKKOUCHE
Département Mathématiques	Directeur : M. le Professeur G. TOMANOV
Département Mécanique	Directeur : M. le Professeur H. BEN HADID
Département Physique	Directeur : M. le Professeur J-C PLENET
UFR Sciences et Techniques des Activités Physiques et Sportives	Directeur : M. Y.VANPOULLE
Observatoire des Sciences de l'Univers de Lyon	Directeur : M. B. GUIDERDONI
Polytech Lyon	Directeur : M. le Professeur E.PERRIN
Ecole Supérieure de Chimie Physique Electronique	Directeur : M. G. PIGNAULT
Institut Universitaire de Technologie de Lyon 1	Directeur : M. le Professeur C. VITON
Ecole Supérieure du Professorat et de l'Education	Directeur : M. le Professeur A. MOUGNIOTTE
Institut de Science Financière et d'Assurances	Directeur : M. N. LEBOISNE

REMERCIEMENTS

Une fois le gros travail de recherche et de rédaction fait, reste à écrire la seule partie dont on est sûrs que tout le monde la lira : les remerciements !

Je tiens tout d'abord à remercier les membres de mon jury. Merci aux rapporteurs pour avoir pris le temps de critiquer mon travail et d'être là aujourd'hui : Claire Arnaud et Jérôme Badaut. Merci pour votre temps et vos remarques constructives sur ce manuscrit. Merci également à Nathalie Boisseau d'être présente aujourd'hui en tant qu'examinatrice.

Emmanuelle, merci pour m'avoir prise sous ton aile, pour m'avoir formée au métier de la recherche durant mon Master 2 et mes 3 années de thèse. Merci pour ta confiance, les opportunités que tu m'as apportées, et tout ce que tu m'as appris. Tu as toujours été derrière moi et m'a permis de participer à de nombreux congrès, formations et à l'EMIDS. Merci aussi pour toutes ces grandes discussions, scientifiques ou non. Merci Antoine pour avoir co-encadré ma thèse et pour son œil de clinicien qui nous a été très utile.

Enfin, merci Vincent pour m'avoir le premier donné ma chance dans ton laboratoire pour mon stage de Master 1, merci de m'avoir fait confiance et de m'avoir donné l'envie de continuer dans la recherche. C'est grâce à toi que j'ai rencontré Emmanuelle et que j'en suis là aujourd'hui. Merci pour ton soutien et tes conseils tout au long de ces années. Et merci encore à vous deux pour votre persévérance concernant nos articles ☺

Je remercie maintenant tous les collègues du laboratoire, je ne peux pas tous vous nommer mais je ne vous oublie pas. Merci à Hubert pour m'avoir accueillie dans son laboratoire pendant ces quatre années et pour être toujours disponible pour répondre à nos questions et prodiguer des conseils. Merci aux techniciennes toujours prêtes à nous aider et à nous former quand on arrive petits M2 : Marie-Agnès pour tes bons conseils, ta gentillesse et ton franc-parler, Claudie pour ta gentillesse et nos longues conversations concernant nos animaux que nous aimons tant, Nathalie pour la formation hygiène et sécurité et pour être toujours sur notre dos, Vanessa qui est toujours prête à aider sans oublier Stéphanie, Aurélie, Audrey, Christine et Nadia.

Merci aux chercheurs Jennifer, Brigitte, Danielle, Béatrice, Guillaume, Luciano, Etienne, Assia, Anne-Marie, Charles et Sophie pour leurs questions et remarques toujours constructives lors de

nos présentations. Merci à Brigitte Roux pour gérer le laboratoire, les commandes et autres choses indispensables à la vie du laboratoire.

Merci ensuite aux post-docs pour vos conseils toujours utiles et les discussions qui nous remontent le moral : Emily, merci pour avoir été notre marraine et nous avoir fait profité de ton expérience et pour les bonnes tranches de rigolade, Kassem merci pour ta gentillesse, ton humour et tes magnifiques gâteaux !

Je remercie également les autres doctorants : Hala, Marine, Poupinou (et oui comme ça ça restera ^^) et Benoît. Certains ont fini récemment, d'autres sont en plein milieu de leur thèse, bonne chance à tous !

Merci à Jean-Baptiste, Radu, Franck et Danielle pour les imageries au CERMEP, merci à CYNBIOSE de nous avoir fournis les primates et d'en avoir pris soin. Merci également à Alain de l'INSA pour les samedis de dissection et pour les dosages lipidiques.

Maintenant passons aux choses sérieuses : les « gens » du deuxième étage !!! Merci aux filles du plateau pour leur expertise et leur disponibilité pour m'aider dans mes analyses ou mes questions (sauf le mercredi après-midi hein ;-) . Manue M. pour tes conseils et ton aide concernant la mise en place de nos protocoles génomiques, Sandra et Manue L. pour votre aide dans les moments de rush, les matinées passées ensemble à préparer nos runs et les rigolades qui allaient avec ! Manu Combe, tu n'es pas à proprement parler membre du plateau génomique mais tu y résides, merci pour les playlists de Bob Marley qui mettaient de l'ambiance dans la salle culture du 2è.

On arrive au bureau des doctorants ! Que dire sur ce bureau à part que j'y ai trouvé des amis aussi dingues que moi, voire même plus ☺, en tout cas de vrais amis.

Caroline merci pour ses deux semaines à Turin qui ont sifflé le coup d'envoi de ma thèse et nous ont permis de nous découvrir. Je t'adore ma blonde et j'adore m'engueuler avec toi ! ;) Et oui, on n'est pas d'accord sur grand-chose mais c'est cool aussi, ça met de l'ambiance et ça fait des discussions animées ☺ Merci aussi pour être aussi attentionnée avec les gens, tu es toujours prête à te décarcasser pour nous aider (que ce soit pour la thèse, la mécanique, etc). On t'a longtemps appelée Marc mais on aurait aussi bien te surnommer 'Caro les bons tuyaux' ;) Bravo à toi et Aurel pour votre petite Lilou et je vous souhaite plein de bonheur.

Merci ma couillasse droite, Pierre, pour le concert d'Arsenic (et Seth Gueko hein ^^), pour les grandes discussions sur Star Wars sur lesquelles on ne sera jamais d'accord (je ne désespère pas de

te faire un jour changer de côté ^^), les délires et les crasses qu'on se faisait dans le bureau (sans oublier celle qu'on a fait à Caro, la plus belle, elle s'en souvient aussi je suis sûre ^^) le bureau est beaucoup moins pailleté et « polystyrénisé » depuis que tu es parti ☺. Et merci pour être parti vivre en Italie et avoir (enfin !) compris que c'est un beau pays !

Merci Jujube pour tes connaissances en statistiques qui nous ont sauvées plus d'une fois, pour ton incroyable personnalité et les fous rires que tu as provoqués !

Vous êtes tous partis les uns après les autres mais on ne se lâche pas et merci à vous d'être toujours là pour nous conseiller et nous soutenir, particulièrement en cette fin de thèse !

Merci Morgane et Elena pour votre bonne humeur et vos sourires qui ont illuminé l'aquarium du rez-de-chaussée pendant 1 an ! Et tous mes vœux de réussite pour votre thèse et carrière future.

Reste les survivants, les meilleurs !! Merci Marwa (avec l'accent hein !) pour tes répliques de sniper (qui sont maintenant cultes) mais surtout pour ta fraîcheur ! C'est un plaisir de t'avoir dans le bureau !! Et qu'est-ce que tu as pu nous faire rire !!

Sabrina merci pour tous les délires, les discussions de mecs, les gros fous rires ! On se ressemble pas mal finalement et c'est assez drôle (enfin sauf pour Marwa qui a deux fois plus de sources de choc au final ^^). On peut discuter de tout et surtout on est toujours là pour se soutenir. On aura d'ailleurs bien pêter des câbles ces derniers mois mais à plusieurs c'est toujours mieux ☺ Et encore merci pour tous les gâteaux dont tu nous a fait profiter pendant ces années dont certains semblaient clairement faire partir d'un protocole de surnutrition !

Manu, notre scout toujours prêt et toujours de bonne humeur, merci pour les fous rires avec toi aussi, pour ton langage sans nul autre pareil (pour lequel je mériterais d'ailleurs un diplôme s'il existait ^^), pour ta gentillesse et les conneries que tu dis ! Merci aussi pour tes commentaires très pertinents sur nos Messieurs du jour (on sait que tu aimais ça ^^) et ta participation très personnelle à la plupart de nos conversations. Ça va beaucoup me manquer les conversations à retardement et les phrases qu'il faut finir soi-même lol. Merci aussi à Alice qui a partagé notre bureau pendant quelques semaines et l'a égayé de sa bonne humeur. Et bravo pour Charlotte, tout le bonheur possible à vous aussi ! Sans oublier Kiwi dont je suis l'heureuse marraine !

Vous avez tous les deux finis avant moi mais vous êtes resté un soutien moral important que ce soit en live ou à distance (hein Manu le déserteur ! ^^). En tout cas on aura vécu de belles années dans ce bureau, à tout partager (parfois même trop au goût de certains, n'est-ce pas les mecs Pierre et Manu !), à se goinfrer, à rigoler, à se perdre dans des grandes discussions philosophiques et souvent quand même à parler de sciences. RIP à toutes nos super idées de recherche exotique qui n'ont jamais

pu voir le jour et à notre historique Google. En tout cas même si Sabrina part se réchauffer au pays des Vikings (tmtc ^^), que Pierre est sous le soleil de l'Italie et qu'on ne sait pas encore où on va finir, je sais qu'on ne se perdra jamais de vue. On a survécu à une thèse ensemble, plus rien ne peut nous arriver !

Je n'oublie pas bien sur mes amis non-thésards (et heureusement qu'on en a pour parler d'autre chose des fois ☺): merci à mes deux supers kupines, Lola et Sandra, qui sont toujours là depuis tant d'années même si on ne se voit que trop peu. Je vous adore les filles et bien sûr je n'oublie pas non plus vos petites familles, Yannick, Axel, Cloé et Geoffrey !

Merci à Vivian et Audrey pour les gros fous rires à la fac, le voyage à Dublin (on y retourne quand ???) et pour vous aussi être toujours là malgré nos vies bien prises et le temps qui passe. Une pensée également pour vos moitiés Martial et Ben qui maintenant font partie du groupe.

Lise, en arrivant au magasin ce fameux matin d'été, je ne m'attendais pas à ce que la « blondasse » arrivée le même jour devienne une amie et pourtant ! Qu'est-ce qu'on a pu rigoler au boulot toutes les deux et faire tourner en bourrique les autres !

Merci aux copains d'Olivier (qui sont un peu les miens aussi depuis le temps ;p). Merci les Chagneux pour votre gentillesse et votre bonne humeur, pour le grain de folie de Marie et son champignon des années 80. Merci aux Da Silva, Vilain et Christine pour votre gentillesse aussi et vos soirées où on ne mange jamais ^^ Merci aussi à Richard et Viviane pour votre prévenance et votre grand cœur. Merci à tous pour votre soutien durant cette thèse et vos efforts pour me faire sortir la tête de mon travail de temps en temps.

Merci Maman pour ton soutien et ton amour inconditionnels, qui m'ont aidée à arriver jusqu'ici, et pour tout ce que tu m'as transmis. Merci de t'être battue pour pouvoir être présente aujourd'hui à ma soutenance. Papa, merci pour m'avoir appris qu'on peut triompher de tous les obstacles (« on est beaucoup plus forts que ça ! »), pour ta curiosité dont j'ai hérité (en plus du sale caractère hein ;)) et qui m'a permis d'arriver jusqu'ici. Je vous aime tous les deux très fort. Claudette merci de m'avoir acceptée comme un membre de votre famille et merci Jacky pour votre gentillesse, votre prévenance et vos supers confitures maison !

Merci au reste de la famille : Arnaud, Ludivine, Kévin et leur famille ; Mamie, Jean-Michel, Mimi, Morgane, Charles, Claire et Maëva !

Arnaud, Virginie (cloklicloooo ! ^^), Laure et Enzo, merci pour les délires geek, les mangas et pour si bien soutenir la Squadra Azzura ☺ Ludivine, merci pour toutes nos sorties mémorables et les actions qui en ont découlé ^^ et Nina, le pti monstre, je ne désespère pas qu'un jour tu finisses par

écouter de la bonne musique ;p. Charles, tu as une vraie curiosité de scientifique et tu feras peut-être le même parcours plus tard. Je vous aime tous.

Kévin, mon petit frère adoré, on a tout partagé depuis toujours, je peux toujours compter sur toi et tu me soutiens même si « c'est pourri ce que tu fais à ces pauvres petits animaux ! ». Tu le sais déjà mais je t'aime très fort. Laurie, ma belle-sœur blonde, partenaire de sorties et de délires (dont je ne peux pas parler ici ^^), on recommence les sorties bientôt !! Merci de ton soutien depuis toutes ces années et d'être une oreille réconfortante quand le besoin s'en fait sentir. Et surtout, merci à vous deux pour Jules, le petit dernier de la famille.

On arrive à la fin, merci à mon Ours, Olivier, de partager ma vie et d'avoir un univers tellement différent du mien que cela nous permet de nous enrichir mutuellement chaque jour. Je nous souhaite d'arriver à réaliser nos projets et je t'aime de tout mon cœur.

Enfin, et non des moindres, une pensée pour Lys qui m'a accompagnée la plus grande partie de ma vie et de ma thèse et qui me manque chaque jour.

TABLE OF CONTENTS

RESUME

Intégrité cérébrovasculaire et inflammation dans des modèles animaux d'athérosclérose : une approche biomarqueurs

Les accidents vasculaires cérébraux sont la première cause mondiale d'handicap et l'athérosclérose en est le principal facteur. Cette pathologie, liée à une mauvaise prise en charge du cholestérol pourra avoir des conséquences plus pernicieuses comme la fragilisation des unités cérébrovasculaires qui, combinée à une inflammation systémique et locale, peut entraîner d'importantes répercussions cérébrales.

Pour être au plus proche de l'humain nous avons utilisé des modèles animaux murins et primate non-humain (PNH) âgés sous régime gras. Une approche translationnelle avec suivi longitudinal de biomarqueurs sanguins et d'imagerie combinée à la caractérisation tissulaire de l'inflammation a été effectuée pour tenter d'élucider les spécificités de la réponse inflammatoire dans la paroi vasculaire des grosses artères et le tissu cérébral.

Nous avons montré que chez des souris $ApoE^{-/-}$ âgées l'exercice physique peut contrecarrer les effets délétères d'un régime gras lorsque l'apport calorique est contrôlé mais plus lorsqu'il ne l'est pas. La dégradation de la barrière hémato-encéphalique pourrait expliquer l'inflammation observée *in vivo* et confirmée par l'analyse tissulaire. L'étude des PNH a montré l'intérêt d'associer imagerie multimodale et dosages sanguins dans la stratification du risque cardiovasculaire ainsi que l'importance d'associer des marqueurs métaboliques, inflammatoires et anti-inflammatoires.

Nous avons montré l'intérêt de contrôler les apports caloriques pour bénéficier des effets protecteurs de l'exercice sur l'athérosclérose et l'importance d'avoir une vue globale du patient pour une stratification individuelle précise du risque cardio et cérébrovasculaire.

MOTS-CLES

Athérosclérose, imagerie, neuroinflammation, modèles animaux, stratification, exercice physique

SUMMARY

Cerebrovascular integrity maintenance and inflammation in atherosclerosis animal models: a biomarker approach

Stroke is the leading cause of disabilities worldwide and is mainly caused by atherosclerosis. But this is not the only risk for patients. Indeed, as this pathology is due to a lack of circulating cholesterol management and could lead to more pernicious outcomes such as the disorganization of cerebrovascular units that, when combined with systemic and local inflammation, can result in serious repercussions in the brain.

Aged murine and non-human primate (NHP) animal models fed high cholesterol diets were used as they are closest to the human pathology. A translational approach with longitudinal follow-up of circulating and imaging biomarkers combined with a tissular characterization of inflammation was performed in order to elucidate the specificities of the inflammatory response in the vascular wall of large vessels and brain tissue.

We showed that in old ApoE-/- mice exercise can counterbalance the deleterious effects of a high fat diet when caloric intake is controlled, but not when food is given *ad libitum*. The leakage of the blood-brain barrier might explain the neuroinflammation observed *in vivo,* and confirmed by tissular analysis. The study on NHP showed the interest of combining multimodal imaging with blood dosage for cardiovascular risk stratification and the importance of associating metabolic, inflammatory and also anti-inflammatory markers.

We highlighted the importance of controlling calorie intake in order to benefit from the protective effects of exercise on atherosclerosis and the relevance of having an overview of the patient's status for an accurate individual stratification of cardio and cerebrovascular risk.

KEY WORDS

Atherosclerosis, imaging, neuroinflammation, animal models, stratification, exercise

ABBREVIATIONS

24-OHC: 24-hydroxycholesterol

A

ACAT: acyl-CoA cholesterol acyltransferase

ACEi: angiotensin converting enzyme inhibitor

AD: Alzheimer's disease

AHA: American Heart Association

ANT: adenine nucleotide transporter

AOPP: advanced oxidization protein products

AP-1: activator protein 1

ApoB: apolipoprotein B

ApoE: apolipoprotein E

ARB: angiotensin II type I receptor blocker

Arg1: arginase 1

B

B cell: B lymphocyte

BBB: blood-brain barrier

BP: blood pressure

C

CA: contrast agent

CACS: coronary artery calcium score

CAD: coronary artery disease

CCL: chemokine (C-C motif) ligand

CCR2: C-C chemokine receptor

CD: cluster of differentiation

CE: cholesteryl ester

CETP: cholesterol ester transfer protein

CHF: congestive heart failure

CMB: cerebral microbleed

CNS: central nervous system

CSF: cerebrospinal fluid

CT: computer tomodensitometry

CVD: cardiovascular disease

CX3CR: CX3C chemokine receptor

CXCL: chemokine (C-X-C motif) ligand

E

EAT: epicardial adipose tissue

ECM: extracellular matrix

eNOS: endothelial nitric oxide synthase

ER: endoplasmic reticulum

ESAM: Endothelial cell-selective *adhesion* molecule

ESC: European Society of Cardiology

F

FDG: fluorodesoxyglucose

FFA: free fatty acid

FGF: fibroblast growth factor

FH: familial hypercholesterolemia

FLAIR: fluid attenuated inversion recovery

G

Gd: gadolinium

GPx: glutathione peroxidase

H

Hb: hemoglobin

HDL: high-density lipoprotein

HDL-C: high-density lipoprotein cholesterol

HF: High fat

HMG-CoA: 3-hydroxy-3-methylglutaryl coenzyme A

hsCRP: high-sensitivity C-reactive protein

I

ICAM-1: intercellular adhesion molecule-1

IFNγ: interferon gamma

IL: interleukin

IMT: intima-media thickness

K

KLF: Krüppel-like factor

L

LDL: low-density lipoprotein

LDL-C: low-density lipoprotein cholesterol

LDLR: low-density lipoprotein receptor

LPS: lipopolysaccharide

LysoPC: lysophosphatidylcholine

M

MCP-1: monocyte chemoattractant protein-1 (also known as CCL2)

MDA: malondialdehyde

MI: myocardial infarction

MIS: mycobacterial infection induces suppressor macrophage

MMP: matrix metalloproteinase

MMR: mannose receptor

MPIO: micron particles of iron oxide

MPO: myeloperoxidase

mPTP: mitochondrial permeability transition pore

MRI: magnetic resonance imaging

mRNA: messenger ribonucleic acid

MTX: methotrexate

MUFA: monounsaturated fatty acid

N

NADPH: **reduced** Nicotinamide adenine dinucleotide phosphate

NAFLD: non-alcoholic fatty liver disease

NF-κB: nuclear factor kappa B

NHP: non-human primate

NIRF: near-infrared fluorescence

NIRS: near-infrared spectroscopy

NLRP3: NOD-like receptor family, pyrin domain containing 3

NMR: nuclear magnetic resonance

NO: nitric oxide

NPC1L1: Niemann-Pick C1-like-1 protein

NSTEMI: non-ST elevation myocardial infarction

O

oxLDL: oxidized low-density lipoprotein

P

PAT: pericardial adipose tissue

PBR: peripheral benzodiazepine receptor

PCSK9: pro-protein convertase subtilisin/kexin type 9

PDGF: platelet derived growth factor

PECAM-1: Platelet endothelial cell adhesion molecule

PET: positron emission tomodensitometry

PI3K: phosphoinositide 3-kinase

PUFA: polyunsaturated fatty acid

R

ROS: reactive oxygen species

S

SAA: serum amyloid A

SAT: subcutaneous adipose tissue

SOD: superoxide dismutase

SPECT: Single photon emission computed tomography

SR-A: scavenger receptor A

STEMI: ST elevation myocardial infarction

STH: St Thomas' Hospital

STIR: short time of inversion recovery

T

T cell: T lymphocyte

TC: total cholesterol

TE: echo time

TG: triglycerides

TR: repetition time

TGFβ: transforming growth factor beta

Th: T helper

TIA: Transient ischemic attack

TLR: toll-like receptor

TNFα: tumor necrosis factor alpha

TRL: triglyceride-rich lipoprotein

TSPO: translocator protein

U

USPIO: ultrasmall superparamagnetic particle iron oxide

V

VAT: visceral adipose tissue

VCAM-1: vascular cell adhesion molecule

VDAC: voltage-dependent anion channel

VLDL: very low-density lipoprotein

VSMC: vascular smooth muscle cell

W

WHHL: Watanabe hereditary hypercholesterolemic

WHO: World Health Organization

ILLUSTRATIONS

CONGRESS COMMUNICATIONS

Printemps de la Cardiologie

Strasbourg, France
April, 24-25th 2014

Poster presentation

European Atherosclerosis Society Congress

Madrid, Spain
May, 31st – June, 3rd

Award for the Best Poster: *Body weight gain impairs physical training benefits in old ApoE$^{-/-}$ mice*

European Molecular Imaging Meeting

Antwerpen, Belgium
June, 4-6th 2014

Poster presentation

EDISS Doctoral School Meeting

Villeurbanne, France
October, 16th 2014

Oral presentation: *Sport and ad libitum high fat diet: body weight gain impairs benefits of exercise in old ApoE$^{-/-}$ mice*

Hot Topics in Molecular Imaging (TOPIM) – Inflammation

Les Houches, France
February, 1-6th 2015

Oral presentation: *MR and PET/CT Imaging use to stratify cardiovascular risks in Non-Human Primates under atherogenic diet*

European Atherosclerosis Society Congress

Glasgow, Scotland
March, 22-25th 2015

Poster presentation

European Molecular Imaging Meeting

Tübingen, Germany
March, 18-20th 2015

Title of the oral: *MR and PET/CT Imaging use to stratify cardiovascular risks in Non-Human Primates under atherogenic diet*

European Molecular Imaging Doctoral School Meeting

Tübingen, Germany
March, 17th 2015

Title of the oral: *Molecular imaging of macrophage dysfunction*

OPeRa (Organ Protection and Replacement) Institute Meeting

Bron, France
May, 29th 2015

Title of the oral: *Molecular imaging of macrophages*

Hot Topics in Molecular Imaging (TOPIM) – Cardiovascular

Les Houches, France
January, 31st - February, 5th 2016

Title of the oral: *What would be the optimal combination of inflammation imaging and tissue analysis for cardiovascular risk assessment? – A study in Non-Human Primates under atherogenic diet*

European Molecular Imaging Meeting

Utrecht, Netherlands
March, 8-10th 2016

Poster presentation

European Atherosclerosis Society Congress

Innsbruck, Austria
May, 29th – June, 1st 2016

Title of the oral: *Markers of vulnerable plaques in Non-Human Primates under atherogenic diet*

Congrès de la Nouvelle Société Française d'Athérosclérose

Biarritz, France
June, 16 – 18th2016

Poster presentation

World Molecular Imaging Congress

New York, USA
September, 7 – 10th 2016

Poster presentation

PUBLICATIONS

MRI Biomarkers of Exercise-Induced Improvement of Oxidative Stress and Inflammation in the Brain of Old High Fat Fed ApoE$^{-/-}$Mice

Erica N Chirico, **Vanessa Di Cataldo**, Fabien Chauveau, Alain Geloen, David Patsouris, Benoît Thézé, Cyril Martin, Hubert Vidal, Jennifer Rieusset, Vincent Pialoux, Emmanuelle Canet-Soulas

Journal of Physiology 2016. doi: 10.1113/JP271903

Exercise Does Not Protect Against Peripheral and Central Effects of a High Cholesterol Diet Given *Ad Libitum* in Old ApoE$^{-/-}$ Mice

Vanessa Di Cataldo, Alain Geloën, Jean-Baptiste Langlois, Fabien Chauveau, Benoît Thézé, Violiane Hubert, Marlène Wiart, Erica N Chirico, Jennifer Rieusset, Hubert Vidal, Vincent Pialoux, Emmanuelle Canet-Soulas

Frontiers in Physiology, 06 October 2016 | http://dx.doi.org/10.3389/fphys.2016.00453

Safety and Imaging Contrast Properties of Gadolinium-Based Nanoparticles in Healthy and Atherosclerosis Non-Human Primates

Shady Kotb, Joao Piraquive, Franck Lamberton, François Lux, Michaël Verset, **Vanessa Di Cataldo**, Hugues Contamin, Olivier Tillement, Emmanuelle Canet-Soulas, Lucie Sancey

Scientific Reports, October 2016, DOI: 10.1038/srep35053

At-risk profiles from imaging and tissue biomarkers combine inflammatory and anti-inflammatory features in carotid atherosclerosis

Vanessa Di Cataldo, Joao Piraquive, Alain Geloën, Michaël Verset, Adeline Paturet, Emmanuel Labaronne, Emmanuelle Loizon, André Sérusclat, Franck Lamberton, Danielle Ibarrola, Franck Lavenne, Didier Le Bars, Hugues Contamin, Emmanuelle Canet-Soulas

In preparation

RESUME SUBSTANTIEL

L'athérosclérose est la plus importante cause de mortalité dans le monde avec plus de 30% des morts associées à cette pathologie en 2012 selon l'Organisation Mondiale pour la Santé (soit environ 17.5 millions de morts). En France, l'athérosclérose est responsable de 150 000 morts par an et est reconnue comme la principale cause de maladies cardiovasculaires telles que l'infarctus du myocarde (7.4 millions) et l'accident vasculaire cérébral (AVC, 6.7 millions), ce qui en fait un réel problème de santé publique.

L'athérosclérose est une pathologie complexe induite et aggravée par des facteurs environnementaux tels que l'obésité, le diabète de type 2, l'hypertension, l'âge et le mode de vie (tabagisme, consommation d'alcool, sédentarité). C'est une pathologie silencieuse qui ne montre pas de réels symptômes et n'est souvent découverte qu'au moment où l'occlusion de l'artère conduit à des conséquences cliniques telles que l'infarctus du myocarde (120 000 cas par an en France), l'artériopathie oblitérante des membres inférieurs, l'insuffisance rénale ou encore l'infarctus mésentérique. Au niveau central, l'athérosclérose peut conduire à un accident ischémique transitoire, un déficit neurologique bref et sans répercussion qui est considéré comme le signal d'alerte d'un prochain accident vasculaire cérébral. Cependant, la cascade de réaction menant de l'inflammation cérébrale chronique à l'accident aigu reste inconnue.

Lorsqu'une plaque d'athérosclérose rompt, elle pourra former un thrombus au niveau de la zone de rupture ou envoyer un embole qui ira boucher une artère de faible diamètre. Mais cela ne représente pas le seul risque pour le patient. En effet, cette pathologie est avant tout liée à une mauvaise prise en charge du cholestérol circulant, souvent due à une consommation excessive de graisses. Dans ce contexte, et notamment avec une inflammation chronique qui se développe, l'athérosclérose pourra entraîner des effets plus pernicieux que les conséquences cardiovasculaires les plus connues (infarctus et AVC). L'excès de graisses dans le régime alimentaire peut en effet induire une fragilisation des unités cérébrovasculaires qui, combinées avec une inflammation systémique et locale, entraîneront des répercussions cérébrales importantes qui sont aujourd'hui encore peu explorées et mal expliquées.

A l'heure actuelle, un patient présentant une hypercholestérolémie est mis sous traitement générique (aspirine, statines et inhibiteurs de l'enzyme de conversion de l'angiotensine) et se voit prescrire une modification de son mode de vie si celui-ci est à risque cardiovasculaire (faire de l'exercice, arrêter le tabac, diminuer sa consommation d'alcool, faire un régime). Une intervention chirurgicale telle que la pose de stent ou l'endartériectomie sera préconisée sur le seul critère du degré

de sténose. Ce paramètre reste le paramètre de choix pour justifier ou non une chirurgie alors même qu'il est maintenant fortement débattu. D'où la nécessité d'identifier une combinaison de biomarqueurs, accessibles de façon non invasive, afin d'évaluer plus précisément et de façon individuelle la prise en charge optimale pour chaque patient.

La complexité de l'athérosclérose en fait une maladie difficile à étudier dans sa globalité. Cela nécessite l'utilisation de modèles animaux le plus proche possible de la pathologie humaine afin d'en étudier les paramètres et les cascades de réactions menant à l'évènement clinique. L'âge est notamment un facteur essentiel à prendre en compte lors du choix de son modèle animal, un âge avancé permettant d'avoir un contexte cardio-métabolique à risque avec un statut inflammatoire et oxydatif important. De plus, afin de pouvoir translater les découvertes de l'animal à la clinique humaine, l'utilisation de méthodes d'explorations non invasives et translationnelles est nécessaire.

Au cours de ma thèse, j'ai donc travaillé sur deux modèles d'athérosclérose impliquant des animaux âgés sous régime gras afin d'être au plus proche des conditions multifactorielles de la pathologie humaine. Le modèle souris nous a permis de caractériser les lésions cérébrovasculaires grâce à l'imagerie et aux analyses tissulaires. Concernant notre étude sur les biomarqueurs d'intérêt dans la stratification individuelle du risque cardiovasculaire, nous avons choisi un modèle primate non-humain, physiologiquement et génétiquement beaucoup plus proche de l'Homme, nous permettant une étude translationnelle.

Le modèle souris ApoE$^{-/-}$ est le modèle murin le plus utilisé pour les études sur l'athérosclérose du fait de la délétion du gène ApoE qui permet une accumulation de cholestérol circulant et en fait donc un modèle prédisposé à l'athérosclérose. Lorsqu'elles sont nourries avec un régime riche en graisses et en cholestérol, les souris ApoE$^{-/-}$ développeront des plaques avancées. Cela, combiné avec notre choix de prendre des animaux âgés, en fait un bon modèle de risque cardio-métabolique avancé. Notre étude sur les souris ApoE$^{-/-}$ avait pour but d'utiliser l'imagerie par résonance magnétique (IRM) et les analyses tissulaires pour caractériser les lésions cérébrovasculaires induites par l'athérosclérose et l'effet d'une activité physique régulière sur ces lésions. Pour cela nous avons donc réalisé des tests métaboliques (dosage du cholestérol plasmatique, test de tolérance à l'insuline, dosage de marqueurs d'inflammation et de stress oxydant dans différents tissus d'intérêt) et de l'imagerie IRM couplée à l'utilisation de deux agents de contraste. Le Gadolinium (Gd-DOTA) nous a permis de visualiser les lacunes de la barrière hématoencéphalique (BHE) et le P904, qui est constitué de particules d'oxyde de fer, permet de mettre en avant l'activité phagocytaire des macrophages et donc leur

accumulation. Nos souris étaient divisées en deux groupes, l'un ayant libre-accès à des roues d'exercice et le second non et recevaient un régime gras constitué de 21% de graisses et 0.15% de cholestérol.

Notre étude a montré que dans un contexte de consommation régulée de régime gras (les souris étaient rationnées selon leurs besoins métaboliques), l'exercice physique régulier a un effet modulateur bénéfique sur l'inflammation et le stress oxydant périphérique, sur la progression de l'athérosclérose mais aussi sur l'inflammation et le stress oxydant central et les lésions cérébrovasculaires observées (lacunes de la BHE et accumulation de macrophages) et localisées au niveau de l'hippocampe et des zones périventriculaires.

Nous avons ensuite voulu voir si l'exercice conservait sa modulation positive sur les lésions centrales lorsque la consommation de graisses n'était plus régulée. Pour cela, nous avons reproduit la même étude que précédemment, à la différence près que les souris avaient accès à la nourriture grasse à volonté. Ce régime est apporté aux souris déjà âgées (uniquement un mois avant le début des tests), ce qui constitue un stress calorique important. Nous avons également choisi de réaliser deux sessions d'imagerie et deux tests de tolérance à l'insuline, le premier avant de commencer l'entraînement et le second à la fin de l'étude afin d'avoir une vision longitudinale des lésions cérébrovasculaires. Cette étude a montré que les souris entraînées ont pris du poids de façon importante et que cette prise de poids correspond à de la prise de masse grasse. Les effets bénéfiques sur le cholestérol plasmatique, l'inflammation et le stress oxydant périphérique n'ont pas été retrouvées et nous avons même observé une aggravation de la résistance à l'insuline chez les souris entraînées. Au niveau central, aucune amélioration n'a été observée en termes d'inflammation et de stress oxydant, et surtout, les souris entraînées ont présenté une aggravation des lésions cérébrovasculaires plus importante que les sédentaires.

Mes travaux de thèse sur des souris ApoE$^{-/-}$ âgées ont donc montré que l'exercice physique régulier permettait de contrecarrer les effets délétères d'un régime gras aussi bien au niveau périphérique que central dans le cadre d'un apport alimentaire contrôlé mais que son action protectrice ne suffisait plus quand le régime gras est donné à volonté. Dans ce modèle, la dégradation de la perméabilité de la barrière hémato-encéphalique (BHE) au niveau de l'hippocampe et des zones péri-ventriculaires est évaluée en IRM via l'injection de gadolinium avant et après l'intervention. Nos travaux ont permis de conclure que cette progression de la rupture de la BHE permet d'expliquer l'activité inflammatoire importante observée in vivo grâce aux USPIO et confirmée par l'analyse tissulaire.

Dans un second temps, nous nous sommes intéressés aux marqueurs permettant de stratifier efficacement le risque cardiovasculaire à l'échelle de l'individu. Dans une optique de translation vers la clinique, nous avons cette fois opté pour un modèle de primate non-humain, présentant de très grandes similarités avec l'Homme, aussi bien au niveau physiologique, anatomique et génétique. Seize macaques Cynomolgus (*Macaca fascicularis*) âgés ont été nourris durant 24 mois avec un régime

gras riche en cholestérol et acides gras saturés (HC, n=13) ou avec un régime standard (SD, n=3). Le suivi longitudinal via des biomarqueurs sanguins et d'imagerie, la caractérisation tissulaire de l'inflammation d'abord par l'imagerie *in vivo* puis par l'analyse de l'expression génique et protéique ont été effectués pour tenter d'élucider les particularités de la réponse inflammatoire dans différents microenvironnements, à savoir la paroi vasculaire des grosses artères comme la carotide ou la crosse aortique, et le cerveau. Durant ces 24 mois, plusieurs prélèvements sanguins ont été effectués afin de nous fournir un suivi des profils lipidiques et des cytokines inflammatoires. De multiples modalités d'imagerie ont été utilisées : l'échographie réalisée à 12 et 18 mois afin de localiser les plaques et d'observer leur progression, une session TEP/CT avec injection de deux traceurs, le [18F]-FDG afin d'étudier le métabolisme cellulaire et le [11C]-PK11195 qui est un analogue du TSPO et est utilisé comme marqueur d'inflammation au niveau cérébral et dans la plaque d'athérosclérose. Enfin, une session d'imagerie IRM a été réalisée à 24 mois et a permis de mesurer la surface de la plaque et la prise de contraste après injection de Gd-DOTA afin d'évaluer la perméabilité vasculaire. Une analyse génomique translationnelle a également été réalisée sur les carotides des primates non-humains ainsi que sur des prélèvements de carotides humaines provenant d'endartériectomies de patients, centrée sur le phénotypage des macrophages contenus dans la plaque. Ainsi, 20 gènes ont été dosés, associés au métabolisme cellulaire et mitochondrial, aux différents types de macrophages (totaux, M1 et M2) et aux lymphocytes.

Une inversion brutale des profils lipidiques a été observée chez les animaux sous régime gras avec une importante augmentation du taux de cholestérol plasmatique et un écrasement du ratio HDL/LDL dès le 1er mois de régime. De plus, le suivi du profil lipoprotéique a montré chez ces animaux une augmentation du nombre de LDL mais surtout la présence de sous-fractions de LDL connues pour être à risque métabolique. Les analyses histologiques des territoires vasculaires ont mis en avant trois animaux HC présentant des plaques sténosantes au niveau des artères coronaires et des plaques sévères et diffuses dans les carotides. Parmi ces trois animaux, un a montré des signes de fibrose myocardique et un AVC lacunaire, signe d'évènements cliniques antérieurs probablement dus à ces plaques. Le suivi échographique et systémique entre 12 et 18 mois de régime a montré que ces trois animaux ont présenté une augmentation de leur score échographique et de leur taux d'hsCRP au cours des six mois de suivi, confirmant leur profil à risque. L'analyse génomique a elle aussi mis en lumière ces animaux, qui sont très distinctement groupés à part des autres animaux de l'étude confirmant notre modèle de plaques vulnérables. Etonnamment, alors que les études sur les macrophages réalisées chez la souris montrent une très claire dichotomie M1/M2 avec une importante présence de macrophages M1 'inflammatoires' dans les plaques à risque, nos résultats chez le macaque et chez les patients montrent que les deux types de marqueurs M1 et M2 sont fortement exprimés chez les sujets à risque et/ou inflammatoires, remettant en cause le paradigme observé chez la souris.

Mes travaux ont permis de souligner l'intérêt des biomarqueurs d'imagerie pour observer de façon non invasive et *in vivo* la présence et la progression des lésions cérébrovasculaires induites par l'athérosclérose et son utilité pour évaluer l'effet de l'intervention utilisée (exercice physique, régime, …). L'étude sur les primates non-humains sous régime athérogène a montré l'intérêt d'associer les différentes modalités d'imagerie à disposition en clinique humaine (à savoir échographie, IRM, TEP/CT) et les dosages biologiques dans la stratification du risque cardio et cérébrovasculaire. Cette stratification a permis d'identifier des animaux dont les plaques d'athérosclérose complexes ont été à l'origine d'évènements ischémiques, caractérisés par des cicatrices myocardiques et cérébrales, confirmée par l'histologie au niveau cardiaque et l'IRM au niveau cérébral. En parallèle, l'imagerie *in vivo* de l'inflammation et les études de biologie moléculaire sur les tissus d'intérêt ont permis de souligner l'importance de l'association des marqueurs métaboliques, inflammatoires et, plus surprenant, de marqueurs anti-inflammatoires dans l'équation de stratification des sujets et de remettre en question le paradigme de la dichotomie M1/M2.

INTRODUCTION

Atherosclerosis is the underlying cause of death and morbidity worldwide: 17.5 million of death in 2012 e.g. 31% of all deaths and the second in France with 150 000 deaths per year (World Health Organization). 80% of cardiovascular diseases deaths are due to myocardial infarction (MI; 7.4 million) or stroke (6.7 million) making this a public health issue.

Atherosclerosis is a complex pathology, worsened by environmental factors such as obesity, type 2 diabetes mellitus, dyslipidemia, hypertension, smoking and sedentarity. Atherosclerosis is a silent disease with no real symptoms which is revealed only when the arterial obstruction lead to outcomes such as myocardial infarction (120 000 per year in France), stroke (130 000 per year), peripheral vascular disease, kidney failure or mesenteric infarction. In the brain, it can also lead to transient ischemic attack (TIA) corresponding to a brief and harmless neurological deficit considered as an alert signal for upcoming stroke. But the exact reaction cascade leading to outcomes is still elusive.

Indeed, it combines inflammation with a dyslipidemic context and mainly results in vascular lesions but also in cerebrovascular outcomes still poorly explained. This complexity of atherosclerosis requires animal models closer to human pathology, notably aged animals, an essential factor to encounter both peripheral and central alterations of oxidant/antioxidant balance and inflammation. Translational techniques for atherosclerosis exploration are also needed to assess circulating biomarkers such as lipidic profile, inflammation, and oxidative stress. The combined use of imaging biomarkers provides local information on plaque morphology and function, and even if it is still explorative, in situ inflammation follow-up in arterial vessel wall and in cerebrovascular tissues.

Studies on animal models permit the end-point tissue evaluation of the atherosclerosis completing the in vivo imaging approach, especially for inflammatory and oxidative stress status. It enables the validation of the best combination of biomarkers (circulating and imaging) transposable in human clinic and diagnosis. In this work, we successively tested these biomarkers to evaluate the modulating effects of exercise in old ApoE$^{-/-}$ mice when high fat/high cholesterol diet is given under a controlled regimen or ad libitum. We then transposed these combinations of biomarkers to study the modulation of inflammation in a non-human primate (NHP) model of atherosclerosis under high fat/high cholesterol diet. We finally evaluate the clinical relevance of our findings by analysis of gene expression in endarterectomy samples from symptomatic and asymptomatic patients. The manuscript is organized in four parts: an introduction of atherosclerosis and the different biomarkers strategies followed by the experimental studies in mice and in NHP, and a general discussion and conclusion.

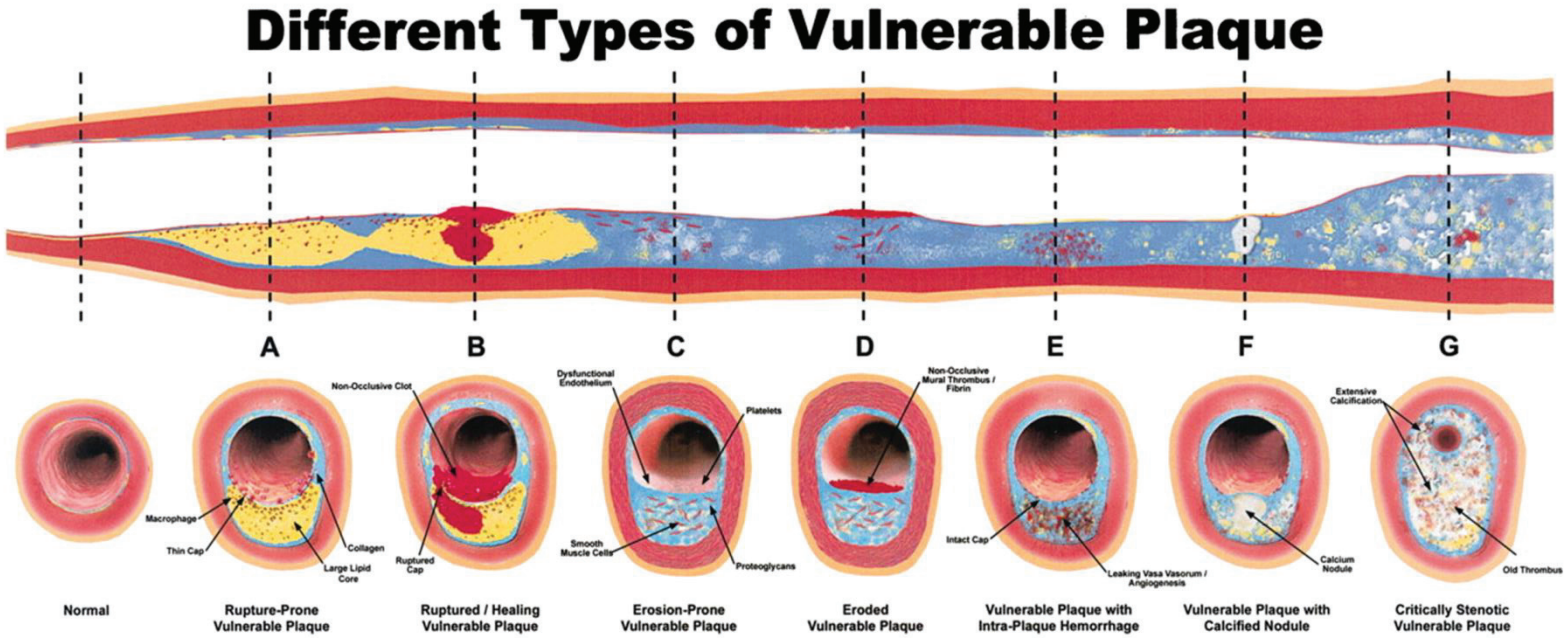

Figure 1: Different types of vulnerable plaque as underlying cause of acute coronary events and sudden cardiac death . (A) Rupture-prone plaque with large lipid core and thin fibrous cap infiltrated by macrophages. (B) Ruptured plaque with subocclusive thrombus and early organization. (C) Erosion-prone plaque with proteoglycan matrix in a smooth muscle cell-rich plaque. (D) Eroded plaque with subocclusive thrombus. (E) Intraplaque hemorrhage secondary to leaking vasa vasorum. (F) Calcific nodule protruding into the vessel lumen. (G) Chronically stenotic plaque with severe calcification, old thrombus, and eccentric lumen.

From Naghavi et al, Circulation, 2003

I. ATHEROSCLEROSIS: A COMPLEX PATHOLOGY WITH MULTIPLE OUTCOMES

My thesis, as emphasized in this chapter, focused on cerebrovascular outcomes of atherosclerosis in humans and animal models.

The first part will illustrate the physiopathology of atherosclerosis, from the plaque development to the progression of advanced pathology and vulnerability and to the cerebrovascular outcomes of plaque rupture. This will lead to the second section on the connections between main metabolic organs (e.g. liver and adipose tissue) andatherosclerosis. And finally, this chapter will focus on different animal models available for research purpose and well-known interventions such as lifestyle behavior and drugs (lowering cholesterol drugs, mitochondrial protection, oxidative stress and inflammation modulation).

A. Atherosclerosis and its cerebrovascular outcomes

Atherosclerosis is a complex and multisite vascular disease leading to a numerous different phenotypes of vulnerable plaque: rupture-prone, erosion-prone, calcified, hemorrhagic or stenotic plaques (Naghavi, 2003) **(Figure 1)**. Several features can be found in the same plaque, increasing its vulnerability. Cerebrovascular outcomes of atherosclerosis, such as transient ischemic attack or stroke lead to many important sequels such as hemiplegia or facial paralysis, and even to death (Toole JF et al., 1975).

1. Atherosclerosis: a lipidic and inflammatory chronic disease

Atherosclerosis is the underlying cause of stroke, heart attack and peripheral vascular disease. Virchow discovered a century ago that atheroma plaque contained fatty element that Windaus lately identified as cholesterol, suggesting an important role for lipids in the pathogenesis of atherosclerosis (Mayerl et al., 2006). More recently, the acceptance of atherosclerosis as an inflammatory disease has led to appealing advances in the understanding of this pathology (Ross, 1999). In this section, we will rapidly discuss the development of atheroma plaque and then focus more on the different characteristics of atherosclerosis such as the lipidic side, the role of immune cells and inflammation and then the participation of oxidative stress.

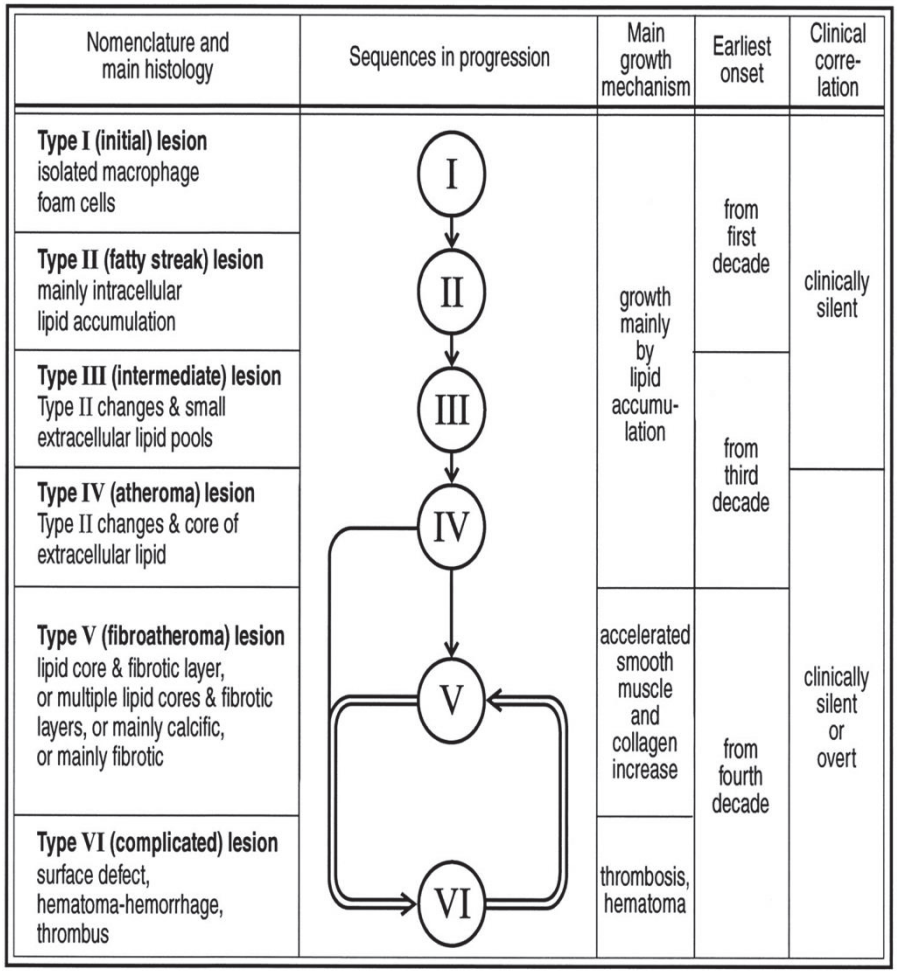

Figure 2: Stary's classification for atheroma lesion. The direction of arrows indicates sequence in which characteristic morphologies may change. From type I to type IV, changes in lesion morphology occur primarily because of increasing accumulation of lipid. The loop between types V and VI illustrates how lesions increase in thickness when thrombotic deposits form on their surfaces. Thrombotic deposits may form repeatedly over varied time spans in the same location and may be the principal mechanism for gradual occlusion of medium-sized arteries. From Stary et al, Circulation, 1995

a) Plaque development

In the 50's, the World Health Organization (WHO) published a classification of the different plaque progression stages, described more precisely by Stary et *al.*in 1995(Stary et al., 1995). The atherosclerotic lesions are divided into six types of plaque; from the initial lesion (type I) characterized by isolated macrophage foam cells in the intima to the complicated lesion (type VI) marked by a defect of the plaque's surface and a thrombus **(Figure 2)**.Atherosclerosis is a progressive disease, evaluating throughout the life, and in the following paragraphs we will describe the initiation and evolution of the plaque.

i. Atherosclerosis lesion initiation and fatty streak phase

Vascular endothelium reacts to different mechanical (shear stress and blood flow) and molecular (cytokines, oxidized molecules) stimuli in order to maintain homeostasis, arterial tone and proper inflammation control(Dahlbäck, 2000; Lüscher et al., 1991; Luscinskas and Gimbrone Jr, 1996).

Physiological endothelium, found in normal shear stress regions, has polygonal and flattened shaped cells with a basal membrane and joined by tight junctions to form an efficient barrierbetween arterial lumen and vessel wall. In these cells, transcription factors Krüppel-like factor (KLF) 2 and 4 are activated, enhancing eNOS expression and contributing to cell migration and survival (Chiplunkar et al., 2013; Topper et al., 1996). There is also increased expression of superoxide dismutase (SOD) which decreased cellular oxidative stress (Topper et al., 1996), allowing maintenance of an effective barrier (Lei et al., 2013). Regions with normal shear stress and efficient endothelial function are resistant to atherosclerosis formation.

In perturbed blood flow and low shear stress regions such as arterial bifurcations or curves (also called atheroma-prone regions), endothelial cells suffered because of hemodynamics perturbations (Gimbrone et al., 2000). It leads to a morphological modification, cells become cuboidal, and alignment is impaired resulting in an increased senescence and apoptosis (Hansson et al., 1985; Nerem et al., 1981). The lowering of endothelial nitric oxide synthase (eNOS) and SOD expression leads to an increased oxidative stress which enhances the low-density lipoproteins (LDL), very low-density lipoproteins (VLDL) and chylomicrons subendothelial retention and oxidation(Ross, 1999). The resulting activation of nuclear factor-kappa B (NF-κB) signaling pathway promotes the expression of monocytes adhesion molecules (intercellular adhesion molecule 1, ICAM-1;vascular cell adhesion molecule 1, VCAM-1, P-selectin), cytokines (macrophage chemoattractant protein 1, MCP-1;interleukine 8, IL-8) and proinflammatory receptor (toll like receptor, TLR) conducting to an subendothelial monocyte infiltration (Hamik et al., 2007; Moore and Tabas, 2011; Yurdagul et al.,

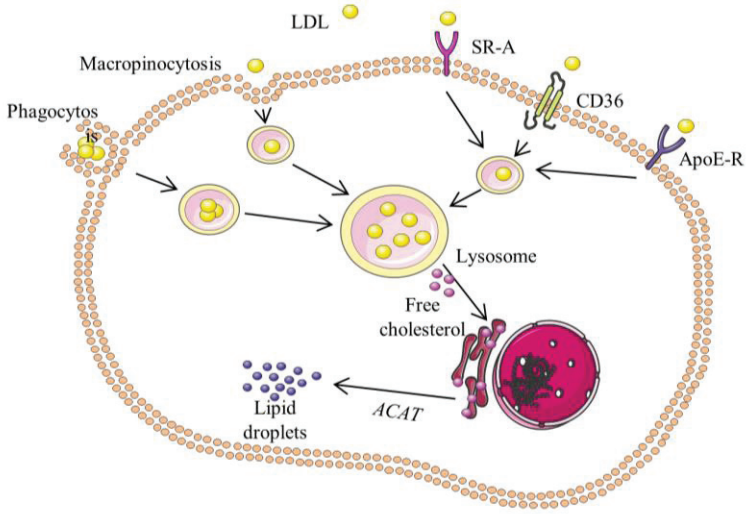

Figure 3: Foam cell formation. Macrophage internalizes LDL and oxLDL via CD36, SR-A, ApoE receptor, macropinocytosis or phagocytosis. Once in the macrophage, LDL are degraded by lysosomes and release free cholesterol (FC) in the cell. FC is then uptaked by endoplasmic reticulum and reconverted in cholesteryl esters (CE) by ACAT. CE obtained accumulates in the cell into lipidic droplets leading to foam cell formation. ACAT, acetyl-CoA acyltransferase; SR-A, scavenger receptor A.

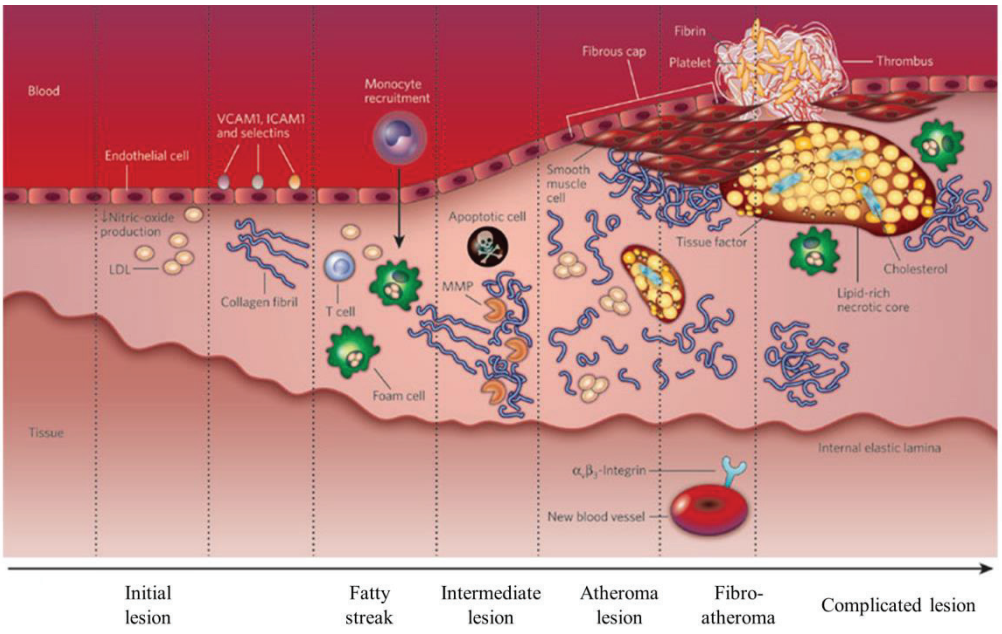

Figure 4: Atherosclerotic plaque progression from initial lesion to advanced, complicated plaque. Adapted from Orbay et al, Theranostics, 2013

2013). Endothelial dysfunction arises from all these and is characterized by a lacunar, prothrombotic and proinflammatory barrier (Gimbrone and García-Cardeña, 2013).

Endothelial activation causes monocyte recruitment via a cascade including monocyte rolling mainly mediated by P-selectin, adhesion via VCAM-1 and ICAM-1 (Galkina and Ley, 2007), activation and transendothelial migration mediated by cytokines, MCP-1 and IL-8 (Gerszten et al., 1999; Gu et al., 1998). Though macrophages are the principal infiltrating cells, several other cells supply to plaque development such as T cells, mast cells and dendritic cells (Paulson et al., 2010; Rocha and Libby, 2009). T cells modulate the macrophage phenotype: Th1 cells produce interferon gamma (IFNγ) which induces proinflammatory macrophage phenotype also called M1; when Treg produce transforming growth factor beta (TGFβ) and IL-10, inducing anti-inflammatory macrophage profile or M2.

In this first phase of atherosclerosis, monocyte-derived macrophages internalize LDL and VLDL which are then degraded by lysosomes resulting in the release of excess free cholesterol. It is then directed to the ER when it will be esterified by acyl-CoA cholesterol acyltransferase (ACAT). The resulting cholesteryl ester (CE) is then batched into lipidic droplets, a characteristic feature of foam cells. OxLDL and to a lesser extent glycated LDL are easily uptake via numerous non cholesterol down-regulated receptor (CD36, SR-A) (Moore and Freeman, 2006), phagocytosis (Torzewski et al., 2004), via apolipoprotein E (ApoE)receptor(Schwartz and Reaven, 2012) or pinocytosis(Kruth, 2013) **(Figure 3)**. Foam cells leads to fatty streak formation, which is the first hallmark of atherosclerosis **(Figure 4)**.

ii. Progression to advanced lesion

Fatty streak lesions do not induce clinical complications and can regress. But, once vascular smooth muscle cells (VSMCs) have proliferated in the endothelium, regression is less prone to occur. There is a small pool of VSMCs in the endothelium and their proliferation is mediated by growth factors secreted by inflammatory macrophages e.g. Platelet-Derived Growth Factor (PDGF) or Fibroblast Growth Factor (FGF) (Raines, 2004; Yang et al., 2015) Macrophages also release chemoattractants such as Matrix Metalloproteinases (MMP) inducing migration of VSMCs from media to intima and proliferation (Johnson, 2007). Accumulation of these VSMCs builds a complex extracellular matrix including collagens, proteoglycans and elastin leading to the formation of a fibrous cap above the lipidic core of foam cells (Libby, 2000). The more the plaque progress, the more lipids accumulates in the core, mainly due to enriched-CE particles from dead foam cells**(Figure 4)**.

VSMCs also have the ability to load CE but as they express less ABCA1 and have a poor lysosomal activity and cholesterol trafficking, they contribute to an inefficient cholesterol efflux

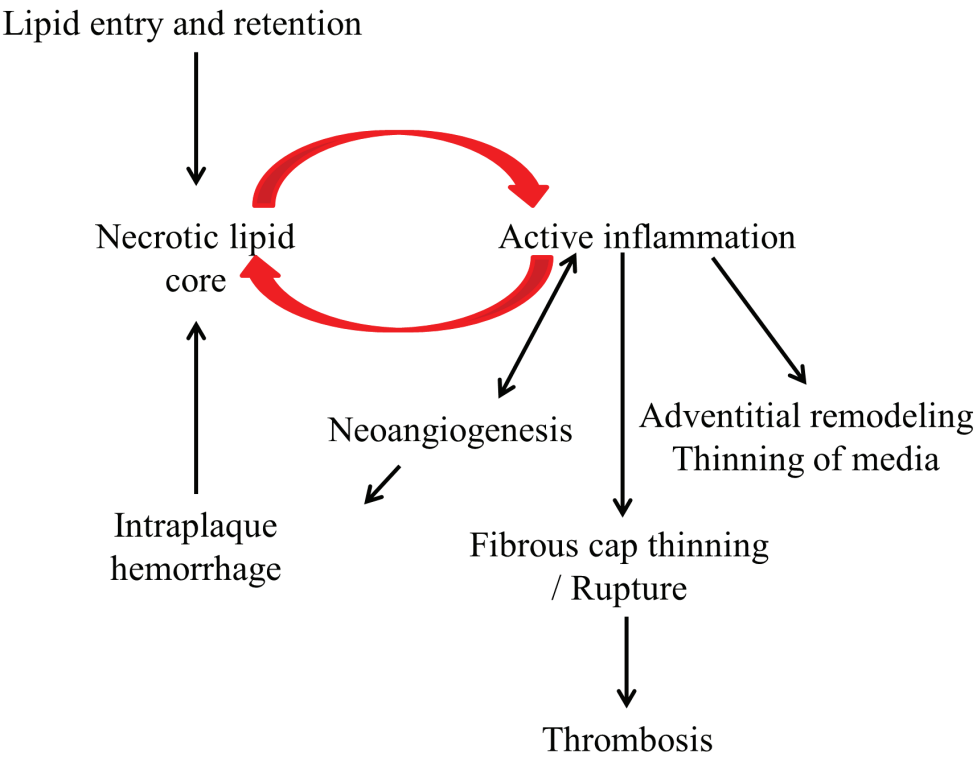

Figure 5: Determinants of plaque vulnerability. Inflammation has a key role in atherogenesis leading to all features of plaque vulnerability. Adventitial remodeling can lead to stenosis, neoangiogenesis and its resulted intraplaque hemorrhage, as well as fibrous cap thinning can result in plaque rupture and thrombus formation leading to clinical outcomes.

Adapted from Shah, Curr Cardiol Rep, 2014

(Jerome et al., 1991; Li et al., 1993). In this environment, macrophages also show an impaired lysosomal function resulting in a decrease of free cholesterol and CE uptake and to the accumulation of lipids in the plaque (Jerome, 2006) suggesting that lysosomal dysfunction is part of the plaque worsening. While accumulation of cells in the subendothelial space leads to a protrusion in the artery, the vessel is remodeling in order to keep the lumen in a physiological range. Thus, the lumen occlusion decrease leads to few clinical symptoms of atherosclerosis during most of the life of the plaque (Alexander et al., 2012; Heusch et al., 2014).

Likewise, during the life of the plaque, the maintained oxidative stress feeds the low-grade inflammation in enhancing M1 polarization of macrophages leading to a vicious circle at the origin of the plaque progression (Dutta et al., 2012).

iii. Vulnerable plaque and rupture

Non resolved inflammation is the cause of advanced plaque, leading to the formation of vulnerable plaque. Vulnerable plaque is morphologically characterized by several parameters such as a necrotic core and a thin fibrous cap (Libby, 2013a; Virmani et al., 2002). These features turn the plaque in a rupture-prone configuration (Virmani et al., 2002) **(Figure 5)**.

The necrotic core contains high quantity of dead macrophages due to an important oxidative stress or a nutrient deprivation (Tabas, 2010a) and the remaining macrophages present a defective efferocytosis (Tabas, 2010b). This defect impairs the phagocytosis of apoptosis-dead macrophages and lead to a necrotic death which release several oxidized intracellular components and inflammatory molecules. Inflammation, oxidative stress and cell death are increased in this microenvironment (Thorp and Tabas, 2009). On the other hand, the thinning of the fibrous cap is the result of the extracellular matrix (ECM) loss, mainly due to the death of the VSMCs of the cap caused by both macrophages (Geng et al., 1997), inflammatory cytokines (Boyle et al., 2003) and oxidation products (Fruhwirth et al., 2006).

Besides the inflammation, the lipidic composition of the plaque is also an important parameter to take into account. Recent studies showed that stable and unstable plaque present differences in their lipid composition. Stable plaques hold more CE-containing polyunsaturated fatty acids (PUFA) when unstable plaques present more CE-containing monounsaturated fatty acids (MUFA) and lysophosphatidylcholine (lysoPC) more prone to oxidation (Stegemann et al., 2011).

When the plaque ruptures, it exposes the necrotic core prothrombotic and procoagulant factors to the pool of platelets procoagulant factors in the vessel lumen resulting in a thrombus formation. The thrombus is the main cause of clinical outcomes. Indeed, the lumen occlusion leads to

myocardial infarction, unstable angina, sudden cardiac death and even stroke when the thrombus migrates or is formed in the cerebrovascular territory (Libby, 2013a; Virmani et al., 2002).

b) Lipidic physiopathology

Anitsckow evidenced the causal role of cholesterol in the atherosclerosis pathogenesis in the early 1900s showing that rabbit fed with cholesterol developed atheroma in a similar way than humans (ANICHKOV, Nikolai Nikolaevich and CHALATOV, Semen Sergeevich, 1913). But several decades passed before it was confirmed by epidemiological studies as the Framingham study (Kannel et al., 1961) and the Multiple Risk Factor Intervention Trial (MRFIT) (Stamler et al., 1986)that elevated blood cholesterol levels were associated with increased risk of cardiovascular outcomes. LDL-C levels are directly correlated with cardiovascular events (Castelli et al., 1986)while high-density lipoproteins cholesterol (HDL-C) levels are inversely associated with the cardiovascular risk (Gordon et al., 1977).

The physiological path that cholesterol follows in the body is very complex. Moreover, cholesterol can be absorbed from diet or synthesized *de novo* and can pass through various modes of transport, storage and metabolism. In this paragraph, we will discuss LDL and HDL,the principal cholesterol-loading particles, and triglycerides.

i. LDL

LDL particles represent a heterogeneous group of lipoproteins from 18 to 25nm of diameter produced by the liver from VLDL. LDL are composed of 78% of lipids and 22% of proteins including apolipoprotein B100 (ApoB100), phospholipids, triglycerides and antioxidant liposoluble vitamins (vit E and carotenoids). Their function is the transport of free or esterified cholesterol to the cells via the blood. Because of is implication in atherogenesis, LDL are commonly called “bad cholesterol” on contrary to HDL, called “good cholesterol” because of its atheroprotective effects.

LDL can be separated by gradient polyacrylamide electrophoresis in non-denaturing condition. Seven LDL subfractions are distinguished, allowing classifying the subjects in two phenotypes: A phenotype is characterized by large LDL (mean diameter > 255 Å) and B phenotype when LDL mean diameter is lower (Austin et al., 1990). Most of the population (70%) have an A or intermediate phenotype. Small and dense LDL are prevalent in individuals with cardiovascular disease (Stampfer et al., 1996). Numerous prospective studies have shown that LDL diameter is a predictive factor of coronary artery disease (CAD) risk even if this link was not independent from HDL-C or triglycerides (TG) levels (Arsenault et al., 2007; Lamarche et al., 1998; Stampfer et al., 1996).Even if

small and dense LDL cannot be considered as an independent risk factor for cardiovascular disease, these LDL subfractions are highly atherogenic particles mainly due to a lower affinity for LDL-C receptor (LDLR) (Galeano et al., 1994) which increases the plasmatic residence time (Campos et al., 1996; Packard et al., 2000)and so favors their oxidization (Chait et al., 1993) and phagocytosis by macrophages. Moreover, small LDL have an increased affinity for proteoglycans (Anber et al., 1996) resulting in an intensification of their transfer into the subendothelial space (Björnheden et al., 1996). Finally, dense LDL are associated with endothelial dysfunction (Vakkilainen et al., 2000) and increase of intima-media thickness (IMT) (Liu et al., 2002). Recent study by Grammer et *al.*, showed that both small and large LDL are associated with a cardiovascular risk in patient referred for coronary angiography (Grammer et al., 2015).

LDLR was discovered in the 1972 by Goldstein and Brown from studies on familial hypercholesterolemia (FH) (Goldstein and Brown, 2009). Indeed *Ldlr* gene mutation is the main cause of this disease associated with high levels of LDL-C and increased risk for premature cardiovascular disease. LDLR is a surface receptor mediating the internalization of LDL particles, which are hydrolyzed by lysosomal enzymes leading to the release of cholesterol in the cell. It follows several regulations such as the decrease of the 3-hydroxy-3-methylglutaryl coenzyme A reductase (HMG-CoA reductase) activity, the decrease of *Ldlr* gene transcription leading to a lowering of LDLR on the cell surface and an increase of ACAT activity. ACAT stimulates the storage of excess cholesterol as cholesteryl ester droplets in the cytoplasm (Brown and Goldstein, 1979) **(Figure 6)**.

LDL infiltration in the intima through dysfunctional endothelium initiates atherosclerotic plaque formation in the arteries (Bonetti et al., 2003). LDL are then retained in the subendothelial space because of their high binding affinity to proteoglycans. The oxidization of LDL lipids in the intima leads to modification on the ApoB residues, which are then recognized by macrophages scavenger receptors and internalized, converting the macrophages to cholesterol-loaded foam cells (Brown and Goldstein, 1983; Greaves and Gordon, 2009). The foam cells release numerous cytokines, initiating an inflammatory response (Hansson and Jonasson, 2009; Libby et al., 2011) inducing the oxidization/inflammation vicious circle at the origin of plaque progression (Higashi et al., 2009).

More details on LDL oxidization will be given in the following chapter on oxidative stress.

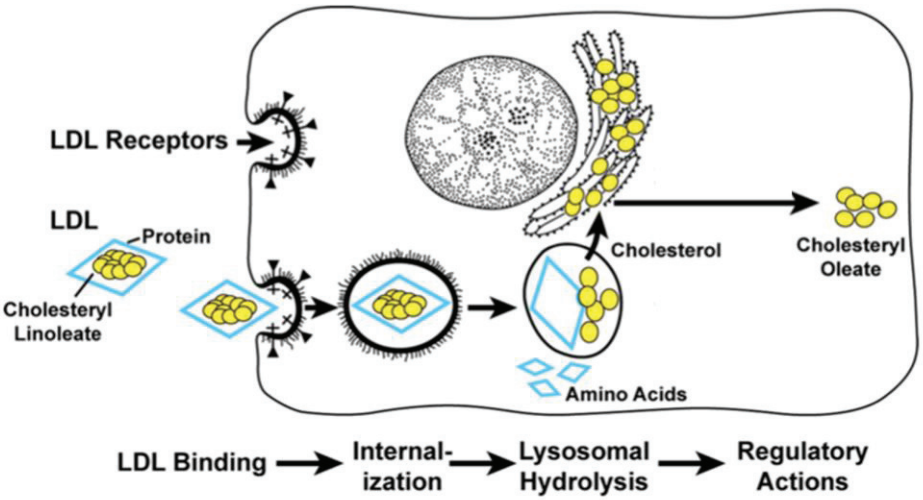

Figure 6: The key role of the LDL receptor in cholesterol metabolism. LDLR is present at the surface of hepatocytes and binds LDL from plasma. Once internalized, LDL undergo hydrolysis in the lysosomes, releasing free cholesterol (FC) in the cell. Then FC is re-converted in cholesteryl esters to constitute HDL particles.

Adapted from Goldstein and Brown, ATVB, 2009

ii. HDL

HDL are lipoproteins of high density responsible of cholesterol trafficking to the liver where it will be eliminated, thereby avoiding cholesterol accumulation in blood vessels and so atherosclerosis risk. HDL are composed of 48% lipids and 52% proteins (mainly apolipoprotein A1,

ApoA1 but also apolipoprotein E, ApoE). They can be divided into 5 subfractions, differing by their proteic content (Davidson et al., 2009). HDL3 subfraction is the only one correlated with a decreased cardiovascular risk (Martin et al., 2015). HDL can inhibit endothelial cells apoptosis excepted in subject with cardiovascular diseases, probably due to a variation of the apolipoprotein content: those containing only ApoA-I seems to be more cardioprotective than those with ApoA-I and ApoA-II (Genest et al., 1991; Riwanto et al., 2013). High plasmatic HDL-C level might be correlated with a lowering of CVD occurrence (Emerging Risk Factors Collaboration et al., 2009)but there is still no evidence of a causal mechanism: genetic or pharmacological-induced HDL increase does not present a protective effect on CVD (Haase et al., 2012; Khera et al., 2011; Voight et al., 2012). Moreover, HDL function might be more important than HDL-C level which is not a reliable biomarker of it (Khera et al., 2011).

iii. Triglycerides-rich lipoproteins (TRLs)

TRLs group very low density lipoproteins (VLDL), chylomicrons and theirs remnants and are the main transporter of triglycerides in plasma. They form a group of heterogeneouslipoproteins of different size, density and composition and are differently associated to the cardiovascular risk (Ginsberg, 2002). TRLs are directly and indirectly contributing to atherosclerosis progression (Hodis, 1999; Rosenson et al., 2014). First, TRLs remnants can penetrate into the intima and be scavenged by macrophages without oxidative modification, contributing to foam cell formation and plaque progression (Nordestgaard et al., 1995; Rosenson et al., 2014).They were found to be as atherogenic as LDL, and even more due to the higher cholesterol volume carried by TRL particle compared to LDL (Rosenson et al., 2014) and promoteendothelialdysfunction(Aung et al., 2013). Secondarily, TRLs hydrolysis by lipoprotein lipase (LPL) releases a large amount of lipolytic products such as oxidized free fatty acids (FFA)in the arterial lumen leading to an increase of inflammatory cytokines resulting in endothelial inflammation (Aung et al., 2013; Wang et al., 2009). Furthermore, TRL remnants have been shown to upregulate the expression of ICAM-1 and VCAM-1 on the endothelium (Wang et al., 2013b), increase the production of reactive oxygen species (ROS)(Wang et al., 2009) and enhance platelet aggregation and intensify the coagulation cascade (Olufadi and Byrne, 2006). They also inhibit the protective effect of HDL (Patel et al., 2009). Moderately elevated triglycerides level (1.7 – 5.6 mmol/L) are independently associated with CVD risk even in patients under statins, suggesting that TRLs are important to take into account for the medical care of patients (Boekholdt et al., 2012).

Although numerous epidemiological studies have shown the association between triglycerides and CVD (Assmann and Schulte, 1992; Emerging Risk Factors Collaboration et al., 2009; Faergeman et al., 2009; Freiberg et al., 2008) the inconsistence of the results of triglycerides-lowering agents on cardiovascular events leaves the question of a direct causal role of TRLs in CVD (Hegele et al., 2014).

c) Low-grade inflammation

Monocytes are peripheral mononuclear blood cells belonging to the innate immunity originate from a common myeloid progenitor cell in the bone marrow. They will differentiate into macrophages since they entered into a tissue; at this stage they are called "steady-state" macrophages or M0 (Gordon and Taylor, 2005). Then, according to the tissular microenvironment, i.e. the cytokines and chemokines expressed in the tissue, they will differentiate and express several cell surface markers and secrete cytokines, which are used to determine the phenotype of the macrophages.

As macrophages are the more represented immune cells in plaque and can also be approached by in-vivo imaging, we will focus on them even if other immune cells such as lymphocytes also play important roles in this pathology. In this section, we will consider the setup of low-grade inflammation in atherosclerosis context from macrophage recruitment to context-adapted phenotypic expression. Then we will focus on knowledge about subsets from *in vitro* to *in vivo* studies in mice, non-human primates and humans and finally we will discuss the relevance of the M1/M2 dichotomy.

i. Low-grade inflammation: from macrophages recruitment to advanced plaque

Monocytes migrate from the blood through tissues to replace long-lived tissue-specific macrophages of the bones (osteoclasts), alveoli, connective tissue (histiocytes), gastrointestinal tract, liver (Küpffer cells), central nervous system (CNS; microglia), spleen and peritoneum (Gordon and Taylor, 2005). In the blood, monocytes are not a homogenous population of cells, and the question whether specific monocytes leads to specific tissue macrophages is still under debate (Nahrendorf et al., 2007). A theory exists that monocytes are still developing and maturing in the blood and can be recruited to the tissues at different time point during the maturation continuum (Sunderkötter et al., 2004), distinguishing 'inflammatory' and 'resident' monocytes. In some cases, local proliferation of tissue-resident macrophages can directly give mature macrophages, such as microglia in the CNS (Ajami et al., 2007).

Macrophages have a crucial role in the totality of atherosclerosis stages: from initiation of the lesion and its expansion to necrosis inducing rupture, and even to resolution and regression of the plaque (Tabas and Bornfeldt, 2016). There are the principal immune cells in atheroma plaque; risk factors of CVD as hypercholesterolemia enhance bone marrow production of monocytes (Swirski et al., 2007) and increase of circulating monocytes is a known independent risk factor for atherogenesis (Dutta and Nahrendorf, 2014; Schlitt et al., 2004). Monocytes enter in the vessel in regions of abnormal hemodynamic stress via adhesion to endothelial cell (Gerhardt and Ley, 2015). Once in the intima, they differentiate to lesional macrophages (Randolph, 2014) depending on lesional microenvironment which is different according to the area and the stage of lesion development. Thus, systemic factors such as dyslipidemia, low-grade inflammation induced by diabetes mellitus and infection can affect the microenvironment. There are three plausible and seriously associated actors of macrophage phenotype: the cholesterol and lipid loading, the metabolic state and the balance between proinflammatory and proresolving molecules (Tabas and Bornfeldt, 2016).

Microenvironment is responsible of pro-atherogenic effect of the lipid loading in foam cells (Spann et al., 2012). The determination of inflammatory status of macrophages depend on the balance between free cholesterol efflux and CE storage (Lim et al., 2008; Tall and Yvan-Charvet, 2015). Free cholesterol efflux and *in vivo* reverse transport are inhibited by inflammation (McGillicuddy et al., 2009), evidencing that inflammation and lower cholesterol efflux supply this detrimental vicious circle. The finely settle of the balance between cholesterol uptake, intracellular handling and efflux can be viewed as a complex apparatus and any perturbation in it can induce macrophage dysfunction, inflammation, altered activation of nuclear receptor and atherosclerosis (Moore et al., 2013; Spann et al., 2012).

An inalienable link exists between the metabolic phenotype of a macrophage and its inflammatory phenotype (Tabas and Bornfeldt, 2016). *In vitro* studies demonstrate that there are important differences in M1 and M2 metabolism: M1 phenotype reposes on an increase glycolysis for energy metabolism while M2 phenotype mainly relies on fatty acid oxidation (Vats et al., 2006). Indeed, glycolysis is essential for activation of inflammation and survival of M1 (Tannahill and O'Neill, 2011; Tawakol et al., 2015) and fatty acid oxidation seems to be necessary for M2 (Vats et al., 2006).

Lesional macrophage proatherogenic effect results in a sensitive equilibrium amongst pro and anti-inflammatory processes (Tabas, 2010b). Main proinflammatory cytokines are interleukin

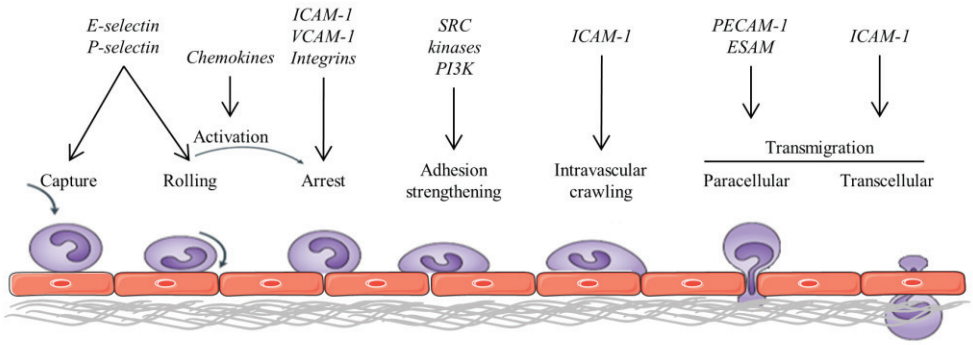

Figure 7: The initial step of inflammation: the leukocyte adhesion cascade. Leukocyte adhesion to endothelial cells and infiltration is a complex process requiring several steps from capture of the leukocyte by the selectins present at the endothelial cells surface to transmigration enabling leukocyte entry in the subendothelial space. Key molecules involved in each step are indicated in italic. ESAM, endothelial cell-selective adhesion molecule; ICAM-1, intercellular adhesion molecule 1; PECAM-1, platelet/endothelial-cell adhesion molecule; PI3K, phosphoinositide 3-kinase; VCAM-1, vascular cell-adhesion molecule 1

Adapted from Ley et al, Nat Rev Immunol, 2007

(IL-1, IL-6, IL-12, IL-15, IL-18), TNFα and chemokine ligand (e.g. MCP-1)when major proresolving and antiatherosclerotic molecules are IL-10, TGFβ (Galkina and Ley, 2009). In mice model, IL-13, IL-27 and CXCL5 can be added (Cardilo-Reis et al., 2012; Koltsova et al., 2012; Rousselle et al., 2013).

Subendothelial macrophage accumulation is one of the first steps of lesion initiation. Monocytes enter in the intima attracted by oxLDL in the subendothelium and expression of adhesion molecules on endothelial cell surface (Williams and Tabas, 1995). The recruitment of monocytes to the intima occurs due to the leukocyte adhesion cascade: capture and rolling (mediated by E and P-selectins), activation (via chemokines), arrest (mediated by ICAM-1, VCAM-1 and integrins), adhesion strengthening and spreading (mediated by SRC kinases and PI3K), intravascular crawling (mediated by ICAM-1) and then paracellular (mediated by PECAM-1, ESAM) or transcellular transmigration (mainly mediated by ICAM-1) (Ley et al., 2007) **(Figure 7)**.Adhesion of monocyte on endothelium activates the transcription factor signal transducers and activators of transcription 1 (STAT1) involved in the monocyte to macrophage maturation process by modulating the expression of functional genes such as ICAM-1 (Coccia, 1999). The fatty streak expands mainly due to more macrophage accumulation and by increase of foam cells. Proliferation of resident macrophages can also participate to the accumulation of cells in this region (Robbins et al., 2013; Rosenfeld, 2014).

In advanced lesions, apoptosis of macrophages is increased, partly due to endoplasmic reticulum (ER) stress induced by free cholesterol or fatty acids (Thorp et al., 2009). Furthermore, advanced lesional macrophages present a defective efferocytosis, contributing to plaque necrosis and increased inflammation due to the release of inflammatory molecules from uncleared post-apoptotic cells (Ridker et al., 2011; Stoneman et al., 2007). Moreover, macrophages have a defect in autophagy resulting in inflammasome activation (NLRP3, NF-κB) in response to cholesterol crystals and leading to larger plaque (Razani et al., 2012). A recent study from Libby suggests that macrophages can contribute to the thinning of the fibrous cap and therefore to plaque rupture by secreting MMPs (Libby, 2013b). Likewise, macrophages can sometimes be associated to intraplaque hemorrhage in advanced human lesions (Kolodgie et al., 2003). All of this shows that macrophages are important actors of development of lesions, especially concerning the necrotic core formation leading to unstable lesion and promoting acute clinical cardiovascular events.

Regression of plaque in mice is characterized by the reduction of the macrophage content and an alteration of gene expression in the remaining macrophages (Feig et al., 2011a; Willecke et al., 2015). In regressing lesion, some studies showed that macrophage phenotype is not completely anti-inflammatory. Indeed, remaining CD-68^{+} cells display high level of *Arg1* and *Cd163* (genes generally considered as M2 markers) and reduced levels of *Tnfa* and *Ccl2* mRNA but also an upregulation of *Cxcl2* and *Il1b* mRNA expression (Feig et al., 2011a). Evenly, CD68+ smooth muscle cells can

contribute to the observed gene expression variation. Recently, Nagareddy et *al.* proposed that the impaired regression of atherosclerotic lesions might be caused by an increase of macrophage recruitment rather than a reduction of macrophages egress (Nagareddy et al., 2013).

ii. Macrophages subsets in plaque

Two different populations of monocytes can be differentiated in mice based on the expression of cell-surface markers: inflammatory monocytes are defined as $CCR2^{+}$ (C-C motif chemokine receptor 2), $CX3CR1^{low}$ (C-X-C motif chemokine receptor 1) and $Ly6^{+}$ (lymphocyte antigen 6 complex) and resident monocytes are defined as $CCR2^{-}$, $CX3CR1^{high}$, $Ly6^{-}$ (Geissmann et al., 2003). Extrapolate mouse data to humans becomes very delicate because human monocytes seem to have distinct physiology from that of mouse (Strauss-Ayali et al., 2007). In humans, monocytes are mainly (90%) $CD14^{high}CD16^{-}$ and referred as "classical" or $CD14^{+}CD16^{+}$ and referred as "non-classical" (Passlick et al., 1989).

Concerning macrophages, two major macrophages subsets were identified *in vitro* that are phenotypically and functionally different: "classically activated" or M1 phenotype considered as pro-inflammatory and "alternative activated" induced *in vitro* by IFNγ or LPS and M2 considered as anti-inflammatory and induced by IL-4 or IL-13 (Mills et al., 2000; Nathan et al., 1983; Pace et al., 1983; Stein et al., 1992).

But the more macrophages are studied, the more the M1/M2 model seems to be inadequate especially as this model is based on *in vitro* studies with unknown relevance to *in vivo* states. (Mantovani et al., 2002; Tabas and Bornfeldt, 2016). In *in vitro* studies the stimulation was reduced to 1 or 2 stimuli (INFγ and LPS for M1, IL-4 and IL-13 for M2) while in atherosclerosis, macrophages are exposed to a profusion of stimuli that will induce different functions and cell-surface markers. For example, in human endarterectomy lesions, the microenvironment of atherosclerotic plaque has been identified as Th1 dominant with more INFγ than IL-4 (Frostegård et al., 1999). But the M1/M2 paradigm is limited because it does not take account of the source and context of the stimuli and strict M1/M2 stimuli do not exist alone in the tissues (in contrary of *in vitro* situation). In contrast with *in vitro* situation, *in vivo* macrophages respond to the tissular microenvironment and interact with T and B cells which will determine whichever phenotype they will have (Cruz-Leal et al., 2014; Mantovani et al., 2004; Mosser and Edwards, 2008).

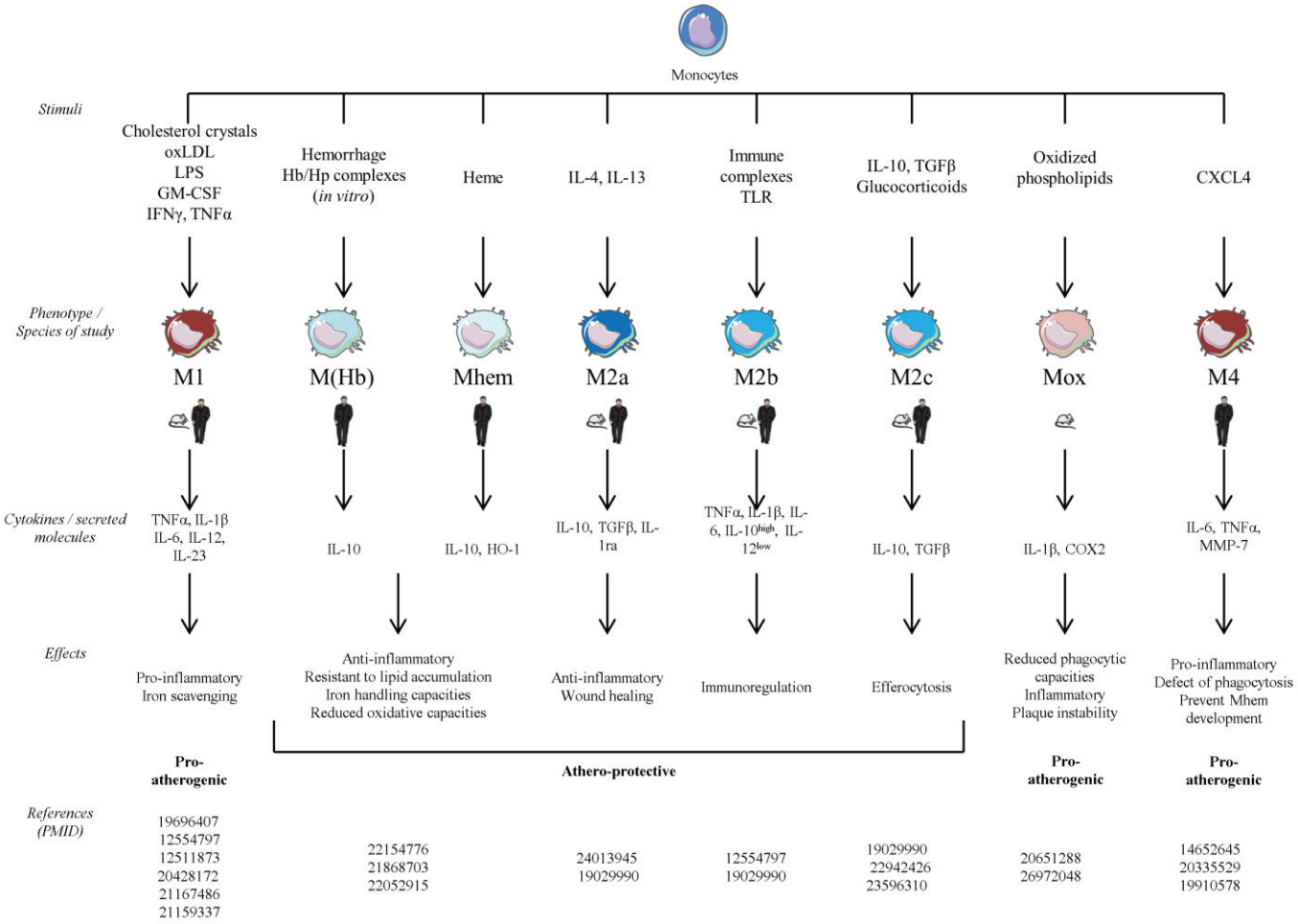

Figure 8: Macrophages subsets and functions. Macrophages phenotypes are modulated by various stimuli such as cytokines, growth factors, chemokines, hemoglobin, bacterial products and lipids. Here are summarize the different macrophage phenotypes according to the stimuli encountered, the molecule they released and their effects on atherosclerosis.

Macrophages phenotype and functions in atherosclerosis were intensively studied in atherosclerosis during the last decades and there is still a lot to discover. Studies showed that M2 phenotype can be divided into three subclasses: M2a, M2b and M2c; all having atheroprotective effect but in different ways (Mantovani et al., 2004). Since the last decade, others populations of macrophages have been suggested in atherosclerosis plaque. M(Hb) and Mhem induced by exposure to hemoglobin/haptoglobin complexes *in vitro* and hemorrhage or neovascularization *in vivo* and are resistant to lipid loading (Boyle et al., 2009), Mox induced by exposure to oxidized phospholipids in vitro in mice (Kadl et al., 2010), M4 induced by CXCL4 and showing protective effects (Chinetti-Gbaguidi et al., 2015), and a population of macrophages stimulated by IL-17A (Erbel et al., 2014).More details are presented in the **Figure 8**.

One cell-surface marker cannot be sufficient to distinguish which phenotype macrophages are expressing. Indeed, only a few markers are specific for a given phenotype and some are shared by multiple subclasses resulting in overlapping macrophage phenotypes **(Figure 8 and Table 1)**. One of the greatest properties of macrophages is that they are remarkably plastic and are able to switch from one phenotype to another regarding on the microenvironment (Lee et al., 2011; Porcheray et al., 2005). Atherosclerotic plaque microenvironment is complex and heterogeneous and influences the phenotyping of macrophages. In the same way, macrophage subtypes influence plaque structure and evolution by their activities (e.g. phagocytosis, cytokine release) (Tabas and Bornfeldt, 2016). Macrophage plasticity has also been observed during plaque regression (Feig et al., 2011b).

iii. Relevance of M1/M2 dichotomy and perspectives

Based on all the discoveries on macrophage phenotype, one only thing remains certain: the M1/M2 dichotomy is no longer applicable. In atherosclerosis as in other diseases involving macrophages, lesional macrophages can be best viewed as representing a wide continuum of phenotypes and functions. There is still a lot to discover and lighten concerning subclasses of macrophages and how they are determined. In mycobacterial infection for example, a new phenotype of macrophage, called mycobacterial infection induces suppressor macrophage (MIS macrophage), has been highlighted by Tatano et *al.*in mycobacterial-infected mice(Tatano et al., 2014). These specific macrophages, down-regulates both Th1 and Th2 cytokine release but increases IL-17A and IL-22 production. This new subset is functionally completely different from M1 and M2 and presents a unique phenotype mixing M1 and M2 markers: IL-12^{+}, IL-1β^{high}, IL-6^{+}, TNF^{+}, NOS2^{+}, CCR7^{high}, IL-10^{high}, Arg1^{-}, MMR^{low}, Ym1^{high}, Fizz^{low} and CD163^{high}.

Phenotype	Markers		Plaque characterisitcs
	Mouse	Human	
M1	Il-1β, TNFα, IL-6, IL-12, IL-23, CXCL9, CXCL10, CXCL11, Arginase II	Il-1β, TNFα, IL-6, IL-12, IL-23, CXCL9, CXCL10, CXCL11	Necrotic core
M2a	Arginase I, Ym1, Ym2, CD163	MMR, IL-1ra, CD200R, CCL18, CD163	Areas of neovascularization or hemorrhage
M2b	IL-10^{high}, IL-12^{low}	IL-10^{high}, IL-12^{low}	
M2c	Arginase I	MMR	
M4		MMP-7, MMR	
Mox	HO-1, NFE2L2		Advanced lesion
M(Hb)		CD163	Areas of neovascularization or hemorrhage
Mhem		CD163^{high}, HLA-DR^{low}	

Table 1: Macrophages markers in mouse and human and the associated plaque characteristics.

CCL18, C-C motif chemokine ligan 18; CXCL, C-X-C motif chemokine ligand; HLA, human leukocyte antigen; HO-1, heme oxygenase; MMP-7, matrix metalloproteinase 7; MMR macrophage mannose receptor; NFE2L2, nuclear factor erthroid-derived 2 like 2; TGFβ, transforming growth factor beta; TNFα, tumor necrosis factor alpha

The phenotype of these macrophages is very interesting and need to be studied also in an atherosclerosis model.

d) Oxidative stress

ROS are highly reactive molecules either endogenous or exogenous which can damage all classes of macromolecules (Holmström and Finkel, 2014). In atherosclerosis pathogenesis, oxidative stress has been established to be an important actor, particularly by promoting oxidation of LDL, one of the earliest hallmark of atherogenesis (Peluso et al., 2012).

Atherosclerosis has three fundamental features: inflammation, disturbed blood flow and abnormal shear stress, arterial wall remodeling and immoderate ROS production is involved in all of these characteristics (Alexander, 2003). Recent studies corroborate the hypothesis of ROS contribution to the structural remodeling of arterial wall by VSMCs proliferation and inflammation (Park and Lakatta, 2012; Patel et al., 2011). Thus, ROS are known to increase adhesion on the endothelium, and to take part tothe signaling pathway forinflammatory cytokines production such as TNFα or IL-1β. ROS accelerate the atherosclerotic process by increasing the differentiation of monocytes to macrophages, which produce ROS in return to feed the vicious cycle (Higashi et al., 2009).

Indeed, disturbed blood flow, low or oscillatory shear stress has pro-oxidative and pro-inflammatory effects on vessels leading to deleterious consequences on endothelial function while laminar blood flow has protective effects (Cunningham and Gotlieb, 2005). Disturbed blood flow commonly appears at bifurcations, curvatures and branch points (Hajra et al., 2000). The chronic exposure to oscillatory shear stress enhances endothelial NADPH oxidase (Nox) generation of $O_2^{\bullet-}$ resulting in monocytes adhesion (Hwang et al., 2003). The stimulation of adhesion molecules (e.g. P-selectin, E-selectins, and VCAM-1) induces more inflammation by increasing leukocytes attraction. This intensifies phagocytosis-induced ROS production leading to the vicious circle mentioned above (Higashi et al., 2009; Hwang et al., 2003).

Nox is expressed in macrophages, neutrophils, endothelial cells, VSMCs and fibroblasts (Li and Shah, 2002) and is the main source of ROS production induced by non-laminar shear stress in vessels (Hwang et al., 2003).

Then, during the inflammatory phase of atherogenesis, others sources of ROS emerged: infiltrated monocytes/macrophages, dysfunctional endothelial cells, migrated VSMCs (Griendling et al., 2000; Li and Shah, 2002). Migration of LDL from the artery lumen to the media initiates the injury of

vessel wall (Navab et al., 1996). Once in the arterial wall, LDL are oxidized by excessive ROS and phagocytized by macrophages, creating lipid droplets characteristics of foam cells (Steinberg et al., 1989). In addition, oxidative stress activates matrix metalloproteinases (MMPs) of endothelial cells, foam cells and VSMCs which degrades the extracellular matrix leading to plaque rupture (Galis and Khatri, 2002).

Some other tissues are affected by abnormalities in cholesterol trafficking, one of the most exposed (even if it is not the most classical organ studied in this context) is the brain, which will be the purpose of the following section.

2. Cerebrovascular outcomes of high fat diet induced atherosclerosis

As seen above, high fat diet and resulting defect in cholesterol handling are the first cause of atherosclerosis and lead to cardio and cerebrovascular diseases. Indeed, the brain is very sensitive to reduced blood flow due to stenotic plaques but even more to emboli coming from carotid plaques and obstructing cerebral arteries leading to stroke. Based on this, this section will focus on cholesterol metabolism in the brain and outcomes resulting from an excess of cholesterol from the diet such as brain inflammation and stroke.

a) Cholesterol metabolism in brain

The brain contains 20% of the whole body cholesterol, it is the most cholesterol-rich organ (15-20 mg/g of tissue) (Björkhem and Meaney, 2004). This is mainly unesterified cholesterol. In the brain, cholesterol is essential for neuronal physiology from development to adulthood due to its involvement in synapse development and formation, dendrite differentiation, axonal elongation and long-term potentiation (de Chaves et al., 1997; Fester et al., 2009; Goritz et al., 2005). Cholesterol depletion in neurons impairs neuronal functions and defects in its metabolism lead to neurodegenerative diseases such as Niemann-Pick disease, Huntington's disease, Parkinson's disease and Alzheimer's disease (AD) (Block et al., 2010; Di Paolo and Kim, 2011; Madra and Sturley, 2010; Wang et al., 2011). Hence, there is a real necessity to closely maintain the cholesterol content in the brain in order to keep brain functions.

Because of the blood-brain barrier (BBB), cholesterol metabolism in the brain is different and separated from that in peripheral tissues. Thereby, brain cholesterol in adult is principally supplied by *de novo* synthesis (Jeske and Dietschy, 1980). Cholesterol synthesis rate is correlated with myelinisation processes, thus higher during perinatal stage and adolescence (Saher et al., 2005) and remains at very low rate during adulthood. Indeed, except during myelinisation processes, the turnover

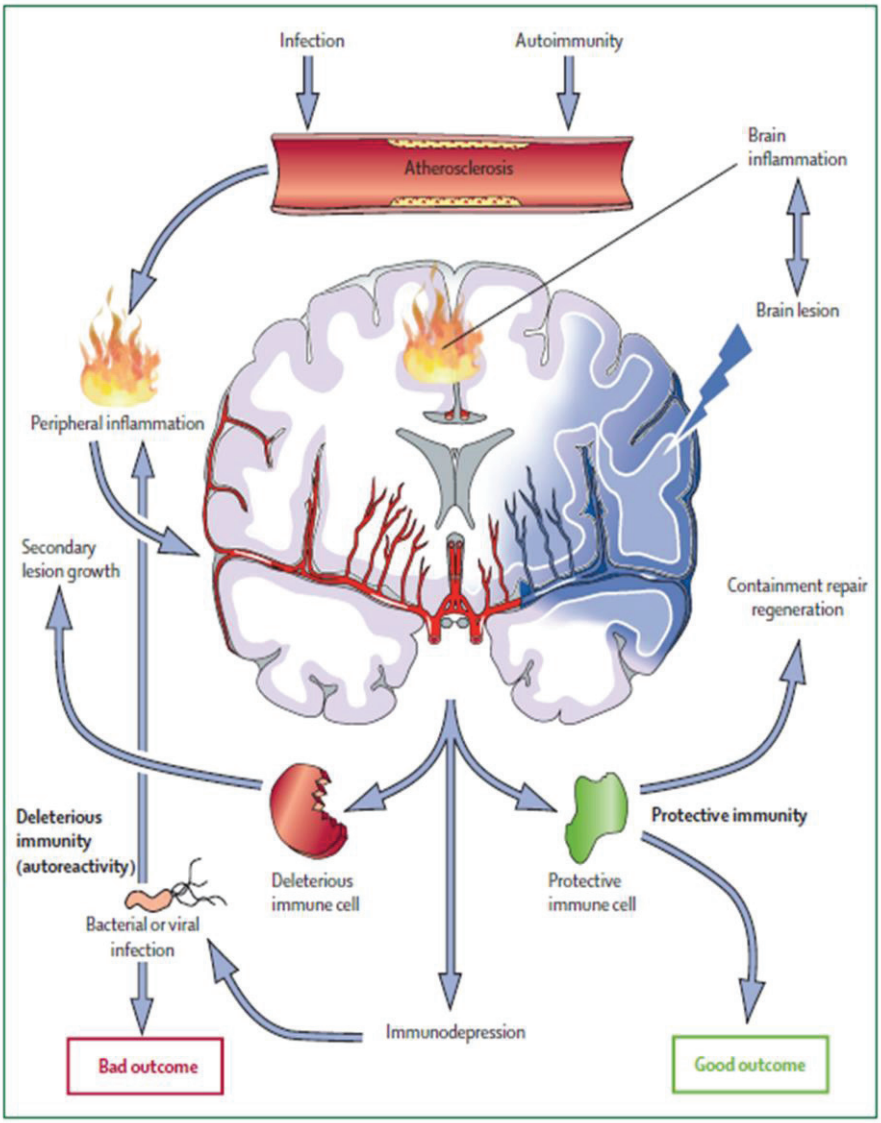

Figure 9: Vicious circle between peripheral inflammation and stroke. Complex interactions exists between peripheral inflammation (which might underlie stroke occurrence or atherosclerosis), stroke – induced brain inflammation, and responses of the peripheral innate and adaptive immune systems to stroke (inflammation, immunodepression, autoreactivity or protective immunity).
From Macrez et al, Lancet, 2011

of cholesterol in the brain is very low because of the minimal losses (Morell and Jurevics, 1996). In the brain, the half-life of cholesterol is comprised between 6 months and 5 years when its only few days in the plasma (Björkhem et al., 2006; Dietschy and Turley, 2004). Although a minimal availability of cholesterol is required for neuronal function, this function can be impaired not only because of a lack of cholesterol but also due to an excess in cholesterol content (Ko et al., 2005; Pooler et al., 2006). Excess of cholesterol leads to 24-hydroxycholesterol (24-OHC) accumulation which have toxic effects on the cells (Matsuda et al., 2013).

ApoE is highly expressed in brain (second most ApoE-rich organ after the liver) and is involved in cholesterol homeostasis (Linton et al., 1991). The major source of ApoE in

brain is astrocytes and in a lower way neuron-supporting cells (Mahley et al., 2006); neurons may express ApoE after excitotoxic injury acting as modulators of the inflammatory response (Iwata et al., 2005; Xu et al., 1999). In humans, ApoE isoform ε4 is correlated with amyloid plaques in Alzheimer's disease (Liu et al., 2013). Likewise, brain cell membranes of AD patients were found to be enriched in cholesterol (Xiong et al., 2008). LDLR is the main receptor for ApoE-containing lipoprotein uptake in the brain and is mostly expressed in glial cells (Rebeck et al., 1993). Furthermore, ApoE-containing lipoproteins have a potent anti-apoptotic effect and protect brain against neurodegeneration(Hayashi et al., 2009).

Dysregulation of cholesterol handling in the brain lead to chronic disorders such as neurodegenerative pathologies (e.g. Alzheimer's, Parkinson's or Niemann-Pick's disease) or chronic inflammation resulting later in transient ischemic attack or stroke.

b) Brain inflammation induced by high fat diet

Brain inflammation and oxidative stress, induced by systemic inflammation, are suspected of increasing the overall cardio and cerebrovascular risk(Drake et al., 2011; Macrez et al., 2011) **(Figure 9)**. In adult brain, oxidative stress is a well-known factor of neurodegenerative disorders, stroke, seizures or trauma (Coyle and Puttfarcken, 1993). Furthermore, Yates et *al.* have shown that carotid atherosclerosis was linked to cognitive impairments and increased brain atrophy suggesting a relationship between metabolic inflammation and neurodegeneration (Yates et al., 2012). Peripheral metabolic chronic inflammation is at the origin of a vicious circle involving vascular changes, oxidative stress and insulin resistance. All together, these pathophysiological phenomena deteriorate the cerebrovascular function. They are also known to activate transcriptional factors such as activator protein 1 (AP-1) and NF-κB causing stimulation of inflammatory factors receptors and adhesion molecules that results in inflammatory markers (TNFα, IL-1β, NO) release in brain parenchyma

(Saavedra, 2012). This inflammatory status in brain may induce abnormalities in BBB, microglia activation and brain insulin resistance, themselves likely causing cognitive decline.

c) Stroke

There is a complex relationship between lipids and acute stroke. Although in most cohort studies there is a direct relationship between cholesterol level and ischemic stroke, this relationship varies by the stroke subtype and the lipid component considered. High total cholesterol (TC) and LDL-C levels are associated with higher risk of ischemic stroke

(Horenstein et al., 2002; Kurth et al., 2007) while lower levels are associated with higher risk of brain hemorrhage (Wang et al., 2013a). Concerning HDL-C levels, it exists an inverse association with cerebrovascular diseases(Sacco et al., 2001; Shahar et al., 2003). But this association is more a function of HDL-C subfractions rather than of total HDL-C (Bots et al., 2007). HDL3 seems to be atheroprotective whereas HDL2 does not. Indeed, there is a direct relationship between HDL2 and carotid plaque thickness and an inverse relationship between HDL3 and plaque area (Tiozzo et al., 2014).

Atherosclerosis stroke subtypes are highly associated with cholesterol levels as showed in some studies (Cui et al., 2012; Imamura et al., 2009; Tirschwell et al., 2004). In contrast, association between dyslipidemia and lacunar stroke is still controversial: case-control studies showed relationship between LDL-C and TC and lacunar stroke (Amarenco et al., 2006; Tirschwell et al., 2004), whereas other studies did not (Cui et al., 2012; Imamura et al., 2009). Finally, despite the fact that dyslipidemia is a known coronary heart disease risk factor, no association between this and embolic stroke were found (Tirschwell et al., 2004).

Others cerebrovascular diseases as lacunar infarcts and cerebral microbleeds can also be found in atherosclerotic patients. Lacunar infarct refers to a small subcortical ischemic lesion probably resulting from an intracerebral arteriole occlusion associated with acute neurological symptoms. It can be due to microatheroma or fibrinoid necrosis (Arauz et al., 2003; Khan et al., 2007). Internal carotid artery stenosis and LDL-C are associated with lacunar stroke (Mok and Kim, 2015). Cerebral microbleeds (CMBs) refers to small perivascular hemosiderin deposits associated with macrophages, resulting from leakage through cerebral small vessels and characterized by hypointense lesions on T2*-weighted gradient-recalled echo MRI. Low triglyceride levels are associated with CMBs while HDL or LDL-C are not (Wieberdink et al., 2011). Moreover, meta-analysis showed that ApoE ε4 allele carriers have higher risks of CMBs (Maxwell et al., 2011).

B. Others metabolic organs

Besides cardiovascular organs and brain, other organs are also affected by high fat and high cholesterol consumption. Here, we will briefly discuss in in which way and the high fat/high cholesterol-induced consequences in two metabolic organs of reference such as liver and adipose tissue.

1. Liver

The liver is an important metabolic organ involved in glucose and lipid homeostasis. The link between liver and atherosclerosis was showed by studies on non-alcoholic fatty liver disease (NAFLD), showing the relationship between dysregulation of lipid metabolism and storage in the liver and subclinical atherosclerosis (Al Rifai et al., 2015; Santos et al., 2007; Sung et al., 2012). Intrahepatic lipid depots are closely linked to cardiovascular outcomes (Fabbrini et al., 2009; Speliotes et al., 2010), NAFLD being an independent predictor of cardiovascular events (Hamaguchi et al., 2007; Targher et al., 2010).

It also has a key role in inflammatory response as it releases acute phase reactant such as CRP or serum amyloid A (SAA). These liver-derived inflammatory markers were found to rapidly increase after consumption of an excessive amount of dietary lipids (Kleemann and Kooistra, 2005; Tannock et al., 2005).In an interesting transcriptomic and metabolomics study, Kleemann et *al*, showed that pro-atherogenic inflammatory factors originate from the liver. Indeed, mice fed with high cholesterol diet (1% w/w) showed faster atherogenesis than mice fed with no or low cholesterol (0.25% w/w). Moreover, genomic analysis showed that a high cholesterol load leads to an extended reprogramming in the liver, involving not only metabolic adaptations to cholesterol but also inflammatory stress (cell proliferation and adhesion apoptosis, immune and inflammatory response) (Kleemann et al., 2007). Furthermore, diet-induced metabolic changes observed in the liver were different according to the amount of cholesterol intake, demonstrating that the switch to a proinflammatory gene expression profile in the liver was accompanied by the development of a new metabolic hepatic state significantly different from the metabolic state at baseline (Kleemann et al., 2007).

2. Adipose tissue / ectopic fat deposits

Adipose tissue represents 15 to 30% of the body weight in humans. It is dispersed throughout the body in discreet depots which constitute separate “mini-organs” (Cinti, 2001). The cardio-metabolic impact of adipose tissue of each individual depends on the size of each depots and

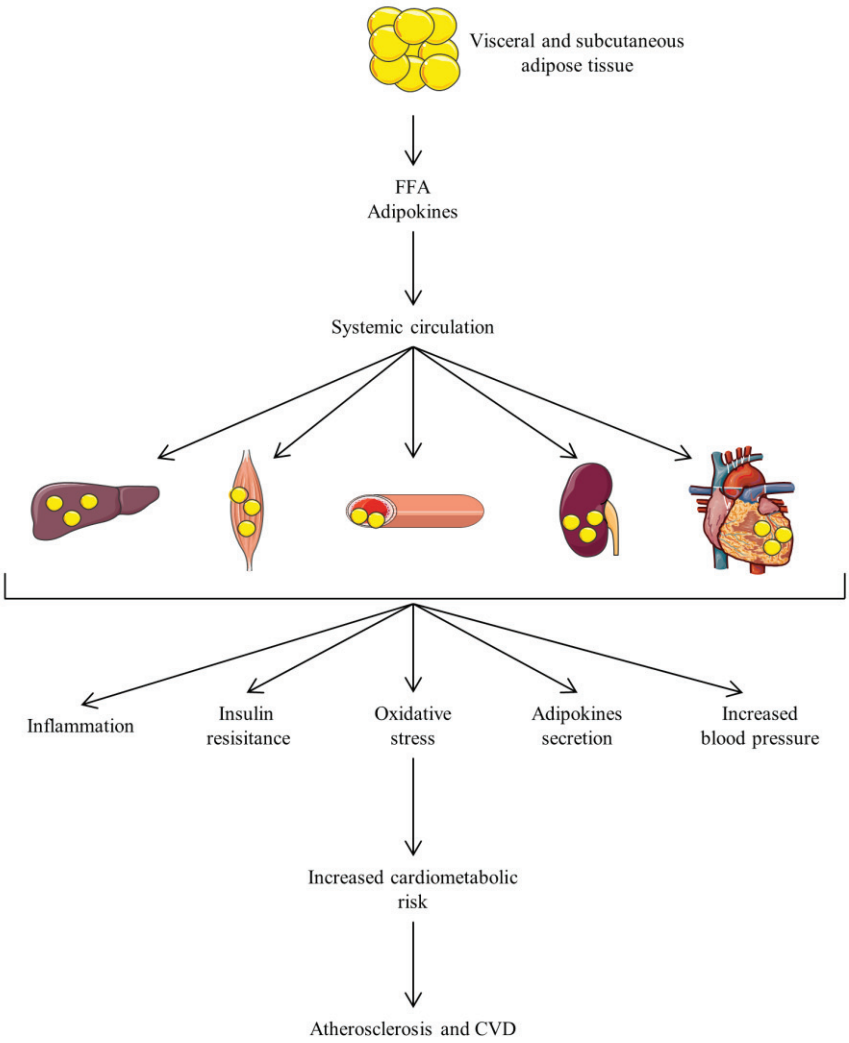

Figure 10: Implication of adipose tissues in atherosclerosis and related cardiovascular diseases. Subcutaneous and (mainly) visceral adipose tissues released FFA and adipokines in the systemic circulation, leading to ectopic depots of fat in the peripheral organs such as liver, skeletal muscles, vasculature, kidneys and heart. The deleterious resulting effects are systemic inflammation, insulin resistance, oxidative stress, adipokines secretion and increased blood pressure leading to the progression of atherosclerosis and increased risk of CVD.

FFA, free fatty acids; CVD, cardiovascular disease

the balance between them. Indeed, peripheral fat distribution, as in the limbs, is favorable while central fat, as in the trunk, is detrimental (Lee et al., 2013) and even leading to poorest survival in patients with CAD (Coutinho et al., 2013). On the contrary, peripheral fat distribution is correlated to a lower BP, insulin sensitivity and healthy lipid profile, resulting in the metabolically healthy obese phenotype (Appleton et al., 2013; Manolopoulos et al., 2010).

Adipose tissue exerts endocrine effects on numerous tissues such as the vasculature, liver and skeletal muscle **(Figure 10)**. In obese condition, various pro-inflammatory cytokines and

molecules are upregulated which will affect all of the stage of atherosclerosis contributing indirectly to CVD (Berg and Scherer, 2005; Mattu and Randeva, 2013).

The ratio between visceral (VAT) and subcutaneous adipose tissue (SAT) showed close correlations to cardio-metabolic risk (Preis et al., 2010; Smith et al., 2012) as accumulation of fat in the visceral compartment and in smaller internal depots (neck, muscle, perivascular) reflects the inability of the SAT for additional TG storage has detrimental effects on the surrounding tissues, especially the liver, skeletal muscle and heart (Carobbio et al., 2011). In this context, VAT increases the delivery of FFA to the liver leading to insulin resistance (Iacobellis et al., 2011; Kabir et al., 2005), and release IL-6 in the portal vein inducing synthesis of CRP by the liver thus contributing to low-grade inflammation (Shoelson et al., 2006)

Fat depots around heart, epicardial (EAT) and pericardial adipose tissue (PAT), were found to be associated with higher occurrence of CVD(Gaborit et al., 2015). Volume and expansion of EAT were related to an increase in coronary calcification (Yerramasu et al., 2012) and PAT to reduced left ventricular function and increased risk of atrial fibrillation (Kim et al., 2011; Thanassoulis et al., 2010) suggesting a locally toxic effect of them.

The effect of dietary cholesterol on liver and adipose tissue is summarized in **Figure 11**.

C. Animal models of atherosclerosis

Pharmacologically or mechanically induced vulnerable plaque animal models are commonly used but do not representthe whole destabilization process leading to a vulnerable plaque. For this reason, we will only address diet-induced or genetically modified models of atherosclerosis plaque, as they are more systemic models for pre-clinical and translational studies.

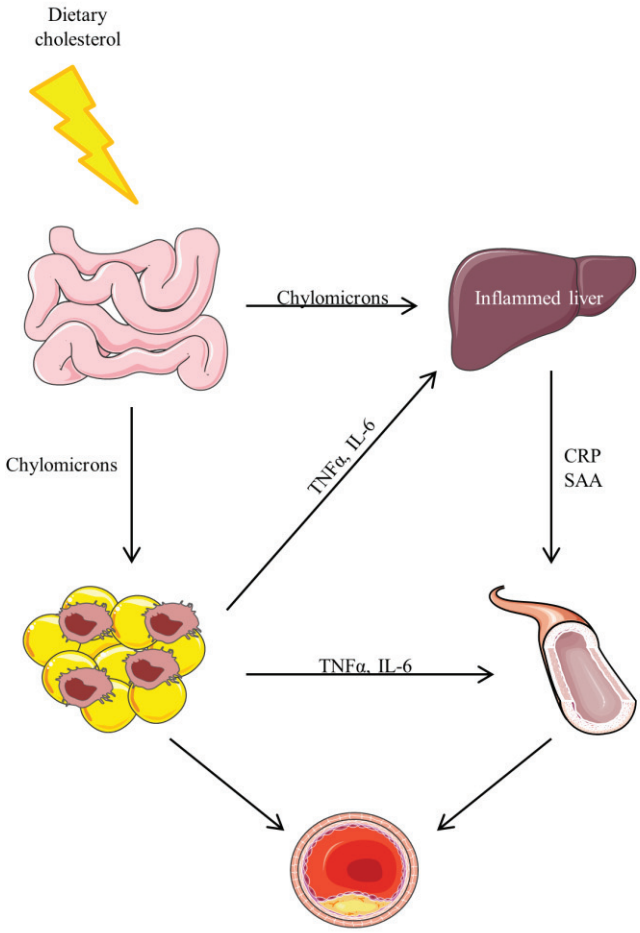

Figure 11: Dietary cholesterol-mediated adipose tissue inflammation can lead to atherosclerosis. Dietary cholesterol absorbed by the intestine is transported by chylomicrons and their remnants to adipose tissue and liver. Cholesterol can directly affect the liver and induce an inflammatory response. In addition, cholesterol could directly cause an inflammatory response in adispoe tissue, with macrophage accrual and production of cytokines, which could indirectly affect the liver. The systemic inflammatory response thus induced could in turn influence atherogenesis at the arterial wall. CM, chylomicrons; CRP, C-reactive protein; SAA, serum amyloid A

Adapted from Subramanian and Chait, Curr Opin Lipid, 2009

1. Mouse models

Mice models are the most commonly used in atherosclerosis research, especially the C57BL/6J strain-derived mice. They present some significant advantages such as their easy breeding, their low cost of maintenance and the fact that their genetic background is well-known. The principal inconvenients are their small size and their plasmatic lipoprotein profiles that are highly different than humans. Actually, wild-type mice do not develop atherosclerosis due to their lack of cholesteryl ester transfer protein (CETP) and to the fact that their plasmatic cholesterol is mainly contained in HDL compared to LDL for humans (Salmon and Hems, 1973). Furthermore, mice dietary cholesterol absorption is weak (Carter et al., 1997) while this is around 50% in humans, resulting in a limiting factor for diet-induced atherogenesis in wild-type C57BL/6J mice. For this reason, numerous genetically modified mouse models were generated, and we will discuss the two most used: ApoE null and LDLR null.

a) ApoE null mice

ApoE null mice are the most widely used mouse model for atherosclerosis study due to their spontaneous development of complex vascular lesions comparable to human ones even under chow diet and since 8-10 weeks of age in the aortic root. Beyond 20 weeks, fibrous plaques are observable.

High fat high cholesterol diet notably accelerate atherogenesis with a significant increase of plasmatic cholesterol level (>1000 mg/dL) and lesions enriched in foam cells(Nakashima et al., 1994). Indeed, advanced lesions contain cholesterol crystals, necrotic core and calcifications. In older ApoE null mice lesions can present hemorrhage suggesting plaque instability (Rosenfeld et al., 2000). On the contrary, no significant coronary artery lesions were showed in this model.

Although his widespread use, ApoE null mice had some inconvenients mostly due to the differences between lipoprotein metabolism in mice compared to human (e.g. plasmatic cholesterol are mostly carried by remnants while LDL in humans). Furthermore, ApoE has numerous other functions affecting macrophage and adipose tissue physiology and immune function (Getz and Reardon, 2009) that impact atherogenesis and plaque progression independently of plasmatic lipid levels (Fazio et al., 1997; Van Eck et al., 2000).

b) LDLR null mice

As seen above LDLR is extremely important for lipoprotein homeostasis but do not have plethora effects as ApoE which is the great advantage of this model. Indeed, the lack of LDLR mainly influences lipoprotein uptake and clearance, increasing the preponderance of LDL in chow diet fed mice but presenting only limited lesions in older animals (Barcat et al., 2006; Teupser et al., 2003). A high fat diet is needed for a significant lesion development. This diet induces an accumulation of VLDL and remnants and a higher plasmatic cholesterol level and more foam cells than ApoE null under chow diet. Thus, an LDLR null mouse is a good model for intermediate atherosclerosis.

2. Rabbits

Rabbits are a widely used animal model for atherosclerosis studies due to their high sensitivity to dietary cholesterol overload (Duff, GL, 1935). Moreover, they share several aspects of lipoprotein metabolism with humans such as the composition of their ApoB-containing lipoprotein (Fan et al., 1995), hepatic production of VLDL (Duverger et al., 1996), the presence of plasmatic CETP and a high absorption rate of cholesterol (Hoeg et al., 1996). The disadvantages of this animal model is that rabbits lack of hepatic lipase, and when fed with atherogenic diet, rabbits develop atherosclerotic lesions in aortic arch and thoracic aorta rather than abdominal aorta while this location is almost always affected in humans (Warren et al., 1991).

Two strains of rabbits are known to be relevant models for human hyperlipidemia: Watanabe Hereditary Hypercholesterolemic (WHHL) which are defective for LDLR and present pathology similar to familial hypercholesterolemia (Aliev and Burnstock, 1998; Kondo and Watanabe, 1975) and the St Thomas' Hospital (STH) which are good models for combined human hypertriglyceridemia and hyperlipidemia (Beaty et al., 1992; Nordestgaard and Lewis, 1991). Transgenic animals are also available such as New-Zealand White-human apoB100 that mimic a hyperlipidemia combined to a reduced HDL-C concentration (Fan et al., 1995) but transgenic rabbits are not so easy to product and allow less genetic manipulation than mice.

3. Pigs and mini-pigs

Pigs develop atherosclerosis spontaneously when fed with standard diet (Skold et al., 1966) and this process can be accelerated by an atherogenic diet (Koskinas et al., 2010).

The large size of pigs is an advantage for atherosclerosis studies; it enables the non-invasive measurement of arteries (Czernuszewicz et al., 2015; Millon et al., 2015) and provides a sufficient

amount of arterial tissues for biological analysis. Moreover, they are physiologically close to humans with a similar lipoprotein profile and develop lesions in coronary arteries. The counterpart of their large size is the quantity of food needed and the technical difficulties of housing and transportation for imaging as well as the lack of tools available for molecular biology or antibodies.

4. Non-human primates

Non-human primates are the closest to humans so are very useful for translational research. Although atherogenesis can differ according to the different species of monkeys, all of them present humanoid lipoprotein metabolism with a predominance of non-HDL, CETP expression and the

same HDL subclasses than humans. Furthermore, non-human primates respond differently to cholesterol thus they can be divided into "hyper" or "hyporesponders" to cholesterol, resulting in a heterogeneous repartition of profiles among individuals in the same way as in humans (Bullock et al., 1975; Clarkson et al., 1971). Another similarity with human is that males develop more atherosclerosis than females under high fat diet.

The two most used species are Rhesus and Cynomolgus monkeys, which even if they are evolutionary close, show different responses to atherosclerosis. Rhesus monkeys fed with high fat diet develop complex coronary lesions with an increase of *vasa vasorum* density in the media and a thickened intima (Heistad and Armstrong, 1986). Cynomolgus are more responsive to high fat diet and atherosclerosis progression is faster than in Rhesus with plasmatic cholesterol levels two-fold higher and a large density of skin xanthomas and more lipid-rich monocytes in the blood (Davis et al., 1984a, 1984b). Macacas are also widely used to study the impact of social status on atherosclerosis progression showing that submissive status in the group favor atherogenesis in females (Kaplan et al., 2009).

Others species of monkeys were used for atherosclerosis research such as baboons, microcebus, squirrel monkeys, spider monkeys but are less close to human than Macaca, which are nowadays the best available animal model for translational research.

D. Intervention modalities

There are several steps in CVD prevention; they range from seek to maintain health to drugs and/or surgery in order to minimize the impact of a chronic clinical disease as presented in **Figure**

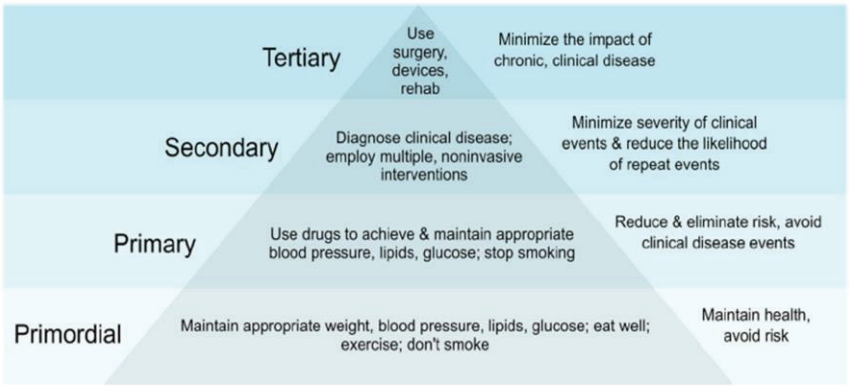

Figure 12: Prevention levels for cardiovascular diseases. Definitions of levels of prevention vary somewhat depending on the disease context. This illustrates typical definitions in the context of cardiovascular disease. Primordial prevention is foundational, seeking to maintain health in individuals and populations free of risk. Typically, interventional strategies used in lower levels of prevention are also important in the higher levels.
From Claas and Arnett, Curr Cardiol Rep, 2016

12. This section will firstly discuss lifestyle factors and then briefly overview the range of drugs available for CVD prevention and/or treatment.

1. Systemic and central modulators

Atherosclerosis is a multifactorial pathology caused by both environmental and genetic factors, environmental being the most important and furthermore the easiest to control. Numerous studies showed that lifestyle factors such as dietary intake, physical activity and behavior (smoking, sleep, stress, etc.) are the first factors of prevention of CVD. Before any treatment, a healthy lifestyle is the better way to avoid the development of atherosclerosis and thus CVD whence its name of primordial prevention.

a) Diet

The first step for a healthy lifestyle is a healthy diet. Indeed, except for genetic lipidic pathologies, the first cause of atherosclerosis and related CVD is an uncontrolled diet. The dietary intake influences all biological parameters such as blood pressure (BP), cholesterol level, and lipidic homeostasis. European Society of Cardiology (ESC) and American Heart Association (AHA) went to a global consensus concerning dietary intake of different nutrients. BP homeostasis is important in the prevention of atherogenesis, as an increased BP lead to hemodynamic changes and to endothelial dysfunction. So a reduced consumption of salt and an increased consumption of potassium is beneficial for maintain BP at normal range (Ekmekcioglu et al., 2016; Stamler, 1993) whence diets rich in fruits and vegetables are cardioprotective (Aaron and Sanders, 2013). A moderate consumption of alcohol is recommended and associated with a reduced risk of coronary arterial disease whereas more than two drinks per day increases the risk of hypertension in men (Klatsky, 2015).

As stated above, diet is a significant factor influencing the risk of dyslipidemias development. Caloric restriction from saturated fats (especially if replaced with PUFAs) is associated with a reduction of LDL-C level. An additional benefit is observed when saturated fats are replaced with PUFAs, resulting in an increase of HDL-C (Berglund et al., 2007; Ginsberg et al., 1998; Obarzanek et al., 2001). Carbohydrates, specifically refined sugars also have a role in the development of CVD and its related adverse outcomes. Indeed, a significant association between added dietary sugar and CVD mortality was showed (Yang et al., 2014). The increase of added sugar consumption was related to increased BP but also to dyslipidemias by increasing the circulating lipid and lipoprotein level (Jayalath et al., 2015; Malik et al., 2014; Stanhope et al., 2015).

In summary, a dietary pattern is highlighted from all this recommendations: high consumption of fruits, vegetables and whole grains, add poultry and fish and low-fats such as nuts and limited consumption of red meat and refined sugar (American Heart Association; US Department of Health and Human Services); offering protective effects on BP and lipid profile.

The diet is obviously an important parameter to take into account for atherosclerosis prevention but it is also beneficial in each step of CVD prevention, indeed, control of food and dietary intake is requested in individuals presenting risk factors or clinical events.

a) Physical exercise

As physical inactivity is a well-known risk factor for cardiovascular diseases, its opposite may have beneficial effects. Moreover, beneficial effect of exercise on health is discussed since Hippocrate "All parts of the body, if used in moderation and exercised in labours to which each is acustomised, become thereby healthy and well developed and age slowly". Numerous epidemiological studies have shown the preventive and protective effect of exercise on atherosclerosis and cardiovascular disease (Kramsch et al., 1981; O'Connor et al., 2009; Pedersen and Saltin, 2015; Swift et al., 2013). Indeed, as primordial prevention requires a healthy lifestyle, physical activity is one of the cardinal points with diet and non-smoking. Moderate exercise enables maintain of glucose and blood pressure homeostasis and balance between calories intake and energy expenditure (Colberg et al., 2010; Cornelissen and Smart, 2013; Millar et al., 2014). Moreover, exercise wad showed to decrease oxidative stress by upregulating anti-oxidant system (Bloomer and Fisher-Wellman, 2008; Cunha et al., 2012), decrease the release of inflammatory cytokines and CRP and increase that of anti-inflammatory (Goldhammer et al., 2005; Lara Fernandes et al., 2011; Schumacher et al., 2006; Sjögren et al., 2010), to reduces the expression of adhesion molecules such as ICAM and the leukocyte recruitment at the plaque location (Schumacher et al., 2006; Sjögren et al., 2010). Furthermore, moderate exercise can also lower the LDL concentration in plasma and protect the remaining LDL against oxidization (Medlow et al., 2015; Nickel et al., 2011) and limit the plaque progression (Cardinot et al., 2016) **(Figure 13)**. In patient with clinical symptoms of cardiovascular disease, practice of a regular exercise was shown to lower the incidence of cardiovascular mortality (O'Connor et al., 2009).

As Paracelsus said "Poison is in everything, and no thing is without poison. The dosage makes it either a poison or a remedy." And it is also valid for physical exercise. Indeed, as stated above, a moderate exercise have notable beneficial effect every step of cardiovascular disease prevention, but several clinical studies have shown that is practiced at high intensity and/or with a high frequency, and even more if rare and acute, exercise may have deleterious effects (Eijsvogels et al., 2016). Indeed, an

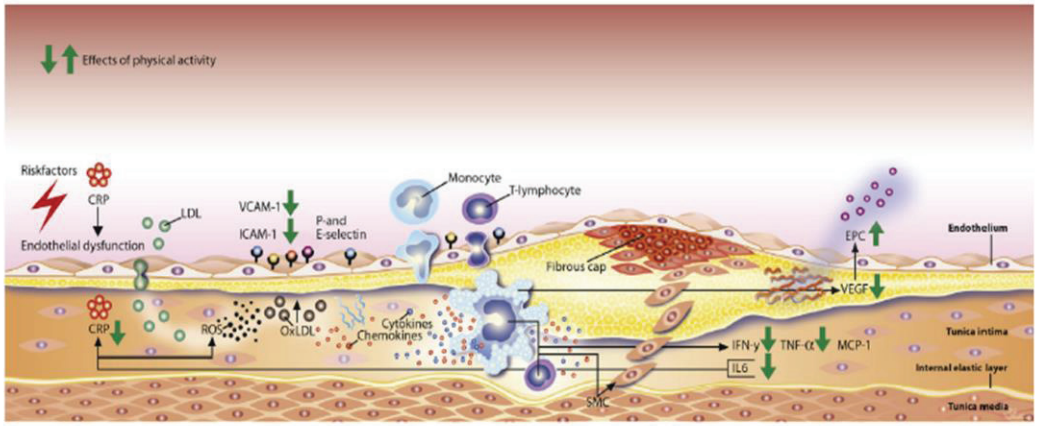

Figure 13: Effect of physical activity / exercise on key factors in the atherosclerotic process. The green arrows show the effect of physical activity and exercise. CRP, C-reactive protein; ROS, reactive oxygen species; VCAM-1, cascular cell-adhesion molecule 1; ICAM-1, intercellular adhesion molecule 1; MCP-1, monocyte chemoattractant protein 1; IFNγ, interferon gamma; TNFα, tumor necrosis factor alpha; IL-6, interleukin 6; EPC, endothelial progenitor cell; VEGF, vascular endothelial growth factor.

Adapted from Palmefors et al, Atherosclerosis, 2014

advanced coronary artery atherosclerotic plaque can result in a cardiac ischemia and lead to sudden cardiac death in asymptomatic patient, as well as the increase of catecholamine spill over can lead to arrhythmia and thus to ventricular fibrillation (Kim et al., 2012). In symptomatic patients, sudden cardiac death are mostly caused by plaque rupture during exercise or by arrhythmia induced by myocardial scar or ischemia (Kim et al., 2012; Thompson et al., 2007).

To summarize, physical activity is one of the cornerstone of cardiovascular health but an excessive practice can lead to opposite deleterious effects. Based on this, the American College of Cardiology and the European Society of Cardiology advocate a minimal daily physical activity or a moderate exercise training several days per week in order to maintain a physical health and avert cardiovascular diseases(Eckel et al., 2014; Piepoli et al., 2016). In the same way, individualization of exercise training would have a greater effect on CVD risks (Josephson RA).

2. Drugs

Atherosclerosis is a complex process involving the interplay of many actors and numerous steps. Nowadays, treatments can concern patients with atherosclerosis and CVD risk factors thus called primary prevention treatment (most of the time hypocholesterolemiant drugs) or patients who already have outcomes resulting of their plaques, then there are secondary prevention drugs. Treatment for these patients are mostly focus on decreasing the inflammatory process and oxidative stress in order to stabilize the progression of the plaque and avoid the occurrence of others deleterious outcomes.

The followingparagraph will sum up in a non-exhaustive way the most used treatment for primary and secondary prevention such as cholesterol lowering drugs, anti-inflammatory and anti-oxidant treatments.

a) Cholesterol lowering drugs

Since Anitschkow highlighted the major role of cholesterol in atherogenesis and plaque progression and afterdecades of research on cholesterol in atherosclerosis, the decrease of LDL-C seemed to be the best target for patients' treatment.

The first success was the development of statins which still are the most used medication for cholesterol lowering and are administered for both first and secondary prevention since late 80s (Alberts, 1988). Statins are hypolipemiant drugs inhibiting the HMC-CoA reductase, a crucial enzyme in the cholesterol synthesis pathway. This allows the decrease of plasmatic cholesterol, particularly LDL-C, which is the main actor of atherogenesis **(Figure 14)**. Besides their hypocholesterolemiant

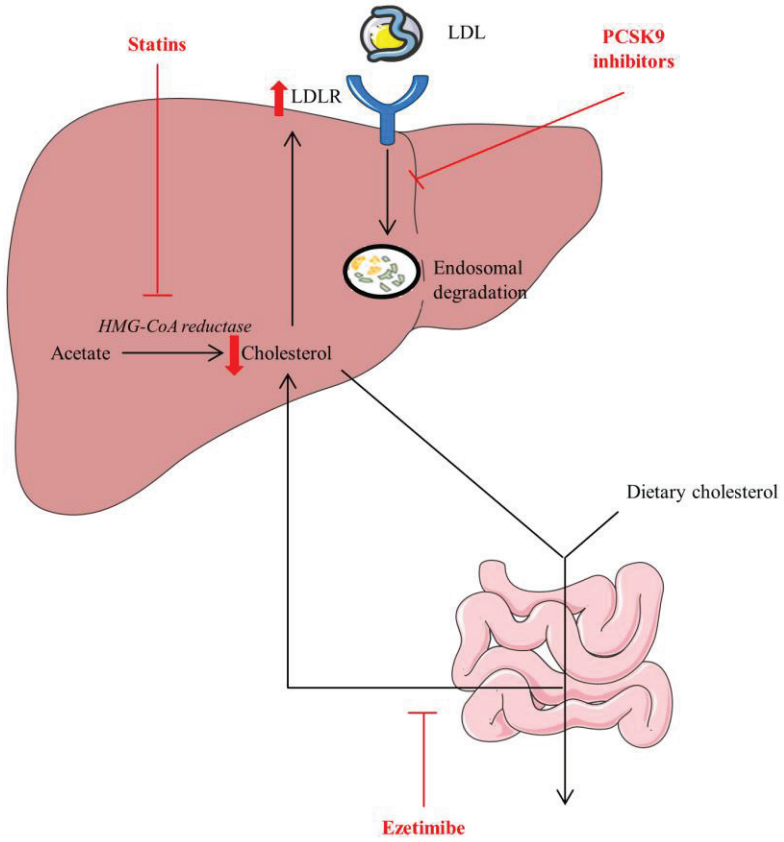

Figure 14: Main cholesterol–lowering drugs and their target. Statins inhibit HMG-CoA reductase, the key enzyme for cholesterol synthesis in the liver; ezetimibe inhibit intestinal absorption of dietary cholesterol and PCSK9 inhibitors stop the internalization and endosomal degradation of LDLR. All of them increase the expression of LDLR and reduce plasmatic LDL-cholesterol levels.

Adapted from Grundy, Nature Rev Cardiol, 2015

effect, statins decrease the vascular inflammation and the endothelial dysfunction, resulting in a potent effect on atherosclerosis(Davignon, 2004; Robinson et al., 2005).Numerous clinical studies showed the beneficial effect of statins on patients with risk factors and/or CVD (Cannon et al., 2004; Downs et al., 1998; LIPID Study Group, 1998; Sacks et al., 1996; Scandinavian Simvastatin Survival Study Group, 1994) and stroke (Amarenco and Labreuche, 2009; Cholesterol Treatment Trialists' (CTT) Collaboration et al., 2010; Heart Protection Study Collaborative Group, 2002). Nevertheless, despite striking achievements of statins, there is always occurrence of two-third of the expected CVD events in statins-treated patients. Furthermore, many patients do not tolerate statins or cannot reach adequate LDL-C levels under treatment whence the need to develop in the future additional therapies.

Ezetimibe is a hypocholesterolemiant molecule decreasing cholesterol absorption in the small intestine. It acts by binding the Niemann-Pick C1-like-1 protein (NPC1L1) resulting in a moderate decrease of LDL-C in range of 20% (Cannon et al., 2015) **(Figure 14)**. It is mostly used

when patients do not tolerate others statins but can also be administered in combination with statins when patients cannot reach the targeted LDL-C level. The efficiency of Ezetimibe was showed by many clinical studies, confirming its utility in combination of statins for LDL-C and CVD reduction (Baigent et al., 2011; Kastelein et al., 2005; Rossebø et al., 2008; Villines et al., 2010) and reduction of stroke occurrence (Cannon et al., 2015; De Caterina et al., 2010).The principal inconvenient of Ezetimibe is that it can cause adverse side effects like liver disease.

Another available drugsto decrease thecholesterol level is proprotein convertase subtilisin/kexin type 9 (PCSK9) inhibitors **(Figure 14)**. PCSK9 is a protein playing a critical role in cholesterol homeostasis by binding the LDLR and inducing its endocytosis and then its lysosomal degradation(Lopez, 2008). The reduced number of LDLR available at the surface of liver cells lead to a lower LDL-C internalization by hepatocytes and thus an increase of plasmatic LDL-C levels. Monoclonal antibodies against PCSK9 were shown to be efficient in decreasing cholesterol, cardiac event and other CVD (Lambert et al., 2012; Navarese et al., 2015). A vaccine is also available and exhibit significant reduction in TC, FC, phospholipids and triglycerides concentrations (Crossey et al., 2015). On the contrary to statins and ezetimibe, PCSK9 inhibitors showed no beneficial effects on stroke occurrence both at primary and secondary prevention (Milionis et al., 2016), and even exhibited neurocognitive deficits (Sabatine et al., 2015).

Other classes of drugs are available such as triglycerides lowering therapies or drugs increasing HDL concentration but these will not be discussed in this chapter.

b) Inflammation modulators

As a substantial proportion of atherosclerosis-related CVD occurs in individuals without apparent hyperlipidemia, targeting the inflammatory side of the pathology seemed attractive for reducing CVD risk mainly for secondary prevention.

As stated above, statins showed, in addition of their lipid-lowering effects, anti-inflammatory properties resulting in a reduction of plasmatic hs-CRP levels (Bohula et al., 2015; Nissen et al., 2005; Ridker et al., 2010). A humanized anti-human IL-6 antibody (tocilizumab) is also available and allows reduction of hs-CRP and troponine T levels resulting in a beneficial attenuation of inflammatory response in patients with non-ST elevation myocardial infarction (NSTEMI) (Kleveland et al., 2016). The principal inconvenient of tocilizumab is that it increases LDL-C levels (Ridker and Lüscher, 2014).

As the "master cytokine" in atherosclerosis, IL-1β seems to be a good target for anti-inflammatory therapies (Dinarello, 2011). Treatment with IL-1ra recombinant, anakinra, blocking IL-1β significantly decreases the inflammatory state in patients (Dinarello, 2010). Anakinra administration in ST elevation myocardial infarction (STEMI) patients showed a reduction of the acute inflammatory response in the three months following the event and a long-term reduction in new-onset heart failure (Abbate et al., 2015).

Methotrexate (MTX) is a commonly used immune modulator which directly targets the inflammatory process in atherosclerosis. It effect was firstly showed in rheumatoid arthritis patients which exhibited a decrease of 21% of cardiovascular and cerebrovascular events when treated with MTX (Choi et al., 2002; Micha et al., 2011) suggesting a concomitant improvement of atherosclerosis in these patients (Westlake et al., 2010).

An alternative classic anti-inflammatory drug, colchicine, commonly used to treat gout appears to be an interesting candidate due to its apparent blocking properties of NLRP3 inflammasome resulting in a decrease of IL-1β and IL-6 (Martinon et al., 2006). Although frequent gastrointestinal side effects, colchicine was found to significantly reduce CVD up to 60% (Nidorf et al., 2013; Verma et al., 2015).

The **Figure 15** shows a summary of the mechanism of action of the anti-inflammatory drugs presented in this paragraph.

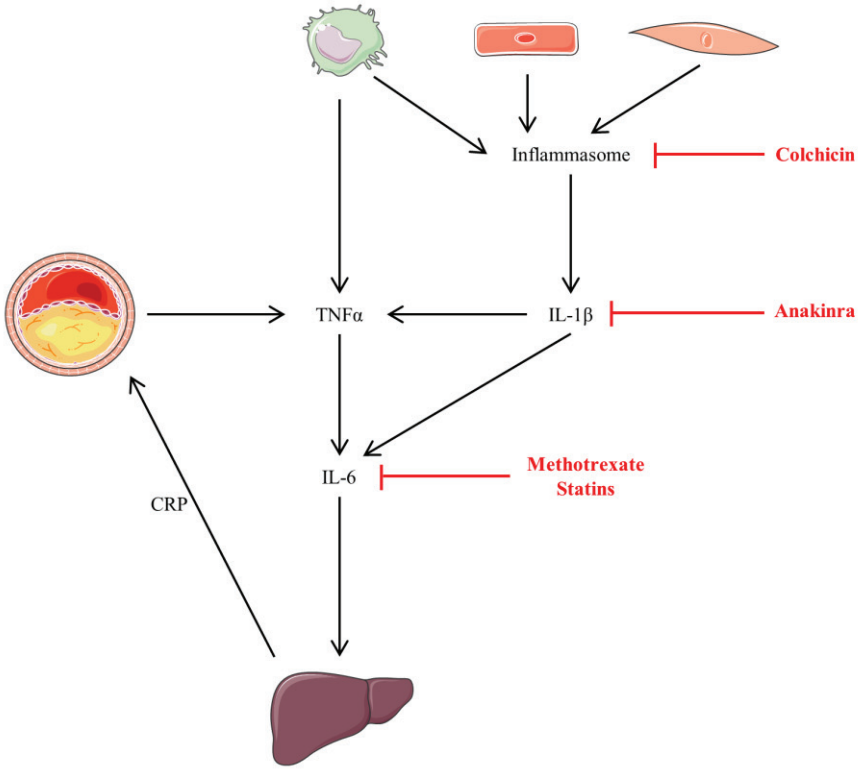

Figure 15: Main anti-inflammatory drugs used in atherosclerosis treatment. Methotrexate and statins target IL-6, Anakinra is an anti-IL-1β antibody and colchicin inhibit the inflammasome activation. CRP, C-reactive protein; TNFα, tumor necrosis factor alpha; IL-1β, interleukin 1 beta; IL-6, interleukin 6

c) Oxidative stress modulators

Oxidative stress is another factor of atherosclerosis progression and CVD and can be the target of some treatment. The first one is, due to their pleiotropic effects, statins. They can act as an indirect antioxidant by inhibiting HMG-CoA reductase, a limiting enzyme for $O_2^{\bullet-}$ production. They also have the ability to enhance eNOS expression thus improving the vascular NO bioavailability (Baigent et al., 2005; Node et al., 2003; Takemoto et al., 2001).

Angiotensin II, when present at high concentration, contribute to the release of $O_2^{\bullet-}$ whence use of angiotensin converting enzyme inhibitors (ACEi) may have a beneficial effect on oxidative stress (Schmidt-Ott et al., 2000). Another way to decrease angiotensin II levels in blood is the administration of angiotensin II type I receptor blocker (ARB), of the sartans family, which enhance NO production and lower oxidative stress leading to a significantly decrease of the carotid intima-media thickness(Ono et al., 2008).

Calcium channel blockers (CCBs) have antihypertensive and antioxidant properties thereby there are widely used in secondary prevention for CVD treatment (Hernández et al., 2003). CCB administration reduces the risk of stroke even if it does not further slowdown the progression of atherosclerosis than usual treatment (i.e. ACEi)(Costanzo et al., 2009; Survase et al., 2005).

A wide variety of food supplements are available to increase the concentration of antioxidants such as vitamin A, C and E, beta carotene, lycopene, CoQ10 or quercetin as well as regular consumption of antioxidant-rich nourishments. Although vitamins were associated with a lower occurrence of peripheral arterial disease (Lane et al., 2008) and vitamin E was specifically found to reduce the rate of non-fatal MI (Stephens et al., 1996), the effectiveness of antioxidant therapies remains debated.

In this first part of the introduction, I have presented the atherogenesis and plaque development cycle, its main cerebrovascular outcome and briefly resume the different animal models used for research and the different interventions available to counteract plaque development and progression. In particular the strong link between inflammation and lipids handling, in vessels as in brain.

II. Translational exploration of atherosclerosis: circulating, tissular and imaging biomarkers

Translation of knowledge from animal models to human is important for improvement of patient care. For this purpose, identification of biomarkers and imaging tools enabling the exploration of atherosclerosis is critical. Therefore, this section will focus on different biomarkers and imaging modalities used in both animals and humans.

A. Circulating and tissular biomarkers

Biomarkers are medical signs that can be objectively measured and evaluated as an indicator of normal biological processes, pathogenic processes, or pharmacologic responses to a therapeutic intervention(Biomarkers Definitions Working Group., 2001). The first characteristic of a biomarker is that it needs to be easily measured. Thus most of them are present in systemic circulation or tissues of interest for animal models. My thesis work is focused on inflammation in atherosclerosis, so we will solely discuss of oxidative stress and inflammatory biomarkers used in human clinic and then rapidly evoke biomarkers used in preclinical studies.

1. Oxidative stress

All organisms using oxygen for their energetic metabolism produce endogenous ROS. The presence of effective antioxidant mechanisms maintains homeostasis. When the ROS production exceeds the capacities of antioxidant system to scavenge and inactivate ROS, oxidative stress appears. In atherosclerosis, as seen in previous chapter, oxidative stress have an important role as it is involved in cell adhesion to arterial wall, lipids oxidization, proliferation and migration of VSMCs, endothelial cell apoptosis, MMP activation and alteration of vasomotricity. Consequently, oxidative stress markers can serve as biomarkers of cardiovascular and cerebrovascular risk in patient (Khoury et al., 2016; Ritzenthaler et al., 2013).

a) Advanced oxidization protein products (AOPP)

Elevated plasmatic AOPP levels were found in patients with coronary artery disease (Kaneda et al., 2002). AOPP was shown to correlate with plasmatic fibrinogen level, which plays an important role in inflammatory processes and atherogenesis (Selmeci et al., 2006). Thus, AOPP could represent a biochemical marker of specific importance (Kalousová et al., 2003). Furthermore, in a

recent review, Klafke et al (Klafke et al., 2016) highlighted the importance of AOPP as biomarker for CVDs as it provides information on level of proteins modifications and metabolic control.

b) Malondialdehyde (MDA)

MDA has been documented in either chronic and acute diseases associated with high levels of oxidative stress such as cardiovascular, metabolic or neurodegenerative diseases. Although MDA levels in plasma of healthy individuals have shown great variability and the detection methods possessed numerous limitations(Del Rio et al., 2005), MDA is still used as biomarker of oxidative stress. Indeed, during oxidative modification occurring in atherosclerosis, LDL lipids undergoes peroxidation leading to generation of different particles including MDA-particles. MDA-modified LDL possesses a potent chemotactic potential and can be engulfed more easily by macrophages. Recently, Tsiantoulas et al, (Tsiantoulas et al., 2015)showedthatplasmatic MDA levelfrom the culpritlesion site of patient withmyocardialinfarction are increasedcompared to levelsfrom the periphery.

c) Superoxide dismutase (SOD)

Anti-oxidant enzymes serve for prevention of vascular tissue damages (and in other tissues). In early atherosclerosis, anti-oxidant activity is upregulated for maintenance of homeostasis but since the oxidative stress gets chronically high, this compensation ceases leading to an oxidative status (Gupta et al., 2009). A significant decrease of SOD activity was also observed in obese postmenopausal women compared to normal weight matched women (Uppoor et al., 2015). Consequently, analysis of SOD activity can be interesting in patientspresenting risk factor for follow-up of atherosclerosis progression.

d) Glutathion peroxidase (GPx)

Previous study showed the inverse correlation between dietary cholesterol level and GPx activity, confirming the impact of cholesterol burden on anti-oxidant activity (Shih et al., 2008). An epidemiologic study on black versus white people showed that GPx activity is lower in black women than in white women and that its increase is correlated with a high BP(van Zyl et al., 2016). The relation between GPx and some risk factor of atherosclerosis make its measurement interesting for atherosclerosis.

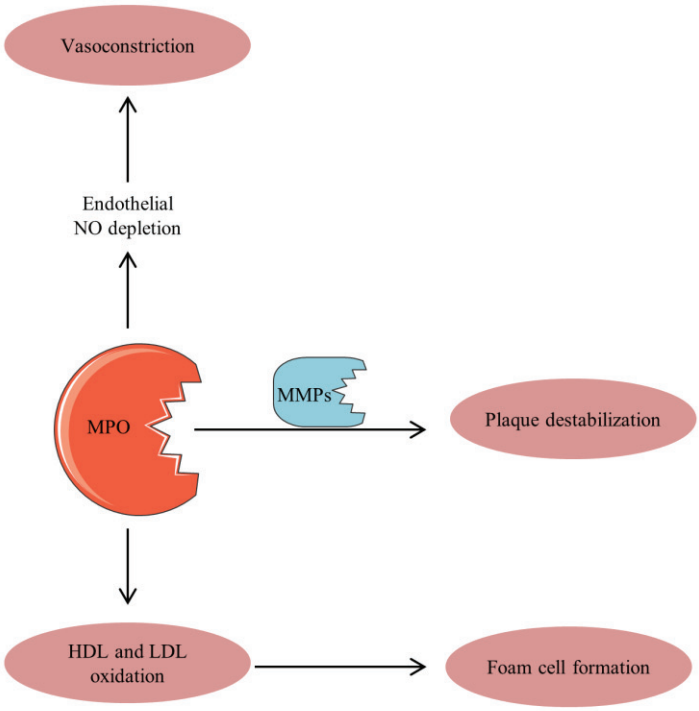

Figure 16: Influence of myeloperoxidase (MPO) in the atherosclerotic process. MPO induces vasoconstriction by consuming a large amount of endothelial-derived NO,foam cell formation due to oxidation of lipoproteins such as LDL and HDL and plaque destabilization.
Adapted from Anatoliotakis et al, Curr Top Med Chem, 2013

e) Myeloperoxidase (MPO)

MPO is an enzyme contained in immune cells, notably monocytes, involving in pathogen destruction via ROS production (hypochlorous acid). This enzyme is known to have an important role in cardiovascular diseases (Schindhelm et al., 2009; Zhang et al., 2001).MPO can be seen both as an oxidative stress or an inflammation biomarker, because of is implication at both level.

In atherosclerosis, MPO is involved in LDL peroxidation and HDL modification leading to foam cell formation (Podrez et al., 1999; Zheng et al., 2004), consumption of endothelium-derived NO leading to depletion of NO(Hazen et al., 1999) and plaque destabilization and rupture through MMP activation(Anatoliotakis et al., 2013) **(Figure 16)**.Numerous epidemiologic studies showed direct correlation between plasmatic or serum MPO levels and CVD events independently of all others CVD risk factors (Anatoliotakis et al., 2013).

2. Key inflammatory circulating biomarkers

There is a complex interplay of cytokines and proteins actors during the time course of chronic inflammatory process. The following section will discuss the use of some of them as biomarkers based on their physiopathological role and to epidemiologic studies.

a) High-sensitivity C-reactive protein (hs-CRP)

C-reactive protein (CRP) is a non-glycosylated circulatory pentraxin composed of 5 identical subunits produced by hepatocytes (Tillett and Francis, 1930) and adipose tissue (Ouchi et al., 2003). CRP is part of the immune system: it binds to immunoglobulin G and activates complement system. CRP is a well-known marker of inflammatory reaction because of its precocity, sensitivity and specificity. In atherosclerosis, pentameric CRP is dissociated by platelets and lysoPC in a monomer that settles on atheroma plaque and enhance inflammation (Eisenhardt et al., 2009).

i. In cardiovascular diseases

Baseline plasma CRP concentrations were found to be higher among men with myocardial infarction or ischemic stroke than among men without vascular event. This shows that the baseline plasma concentration of CRP predicts the risk of future myocardial infarction or stroke but not those of venous thrombosis (Ridker et al., 1997, 2000a). These findings were later confirmed in more than 50 epidemiological studies worldwide (Emerging Risk Factors Collaboration et al., 2010).

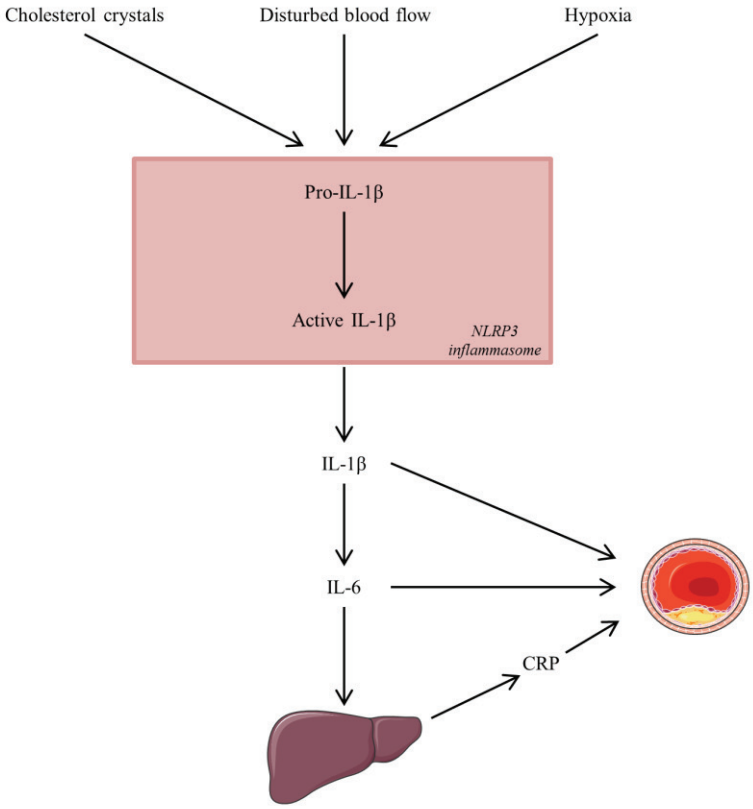

Figure 17: Downstream pathway of CRP. Activation of the NLRP3 inflammasome by cholesterol crystals, hypoxia, and atheroprone flow result in production of pro-IL-1β to IL-1β with consequent downstream effects on IL-6 and CRP, as well as increased vascular atheroma.
Adapted from Ridker, Circ Res, 2016

Global risk algorithms that include hs-CRP, as the Reynolds Risk Scores outperform those solely using Framingham covariates (Cook et al., 2012). Hs-CRP correlates closely to the risk of plaque rupture and vascular thrombosis but not really to the underlying atherosclerotic burden (Ridker, 2016a). Risks of cardiovascular event-free survival with hs-CRP are similar to those with LDL-C and in an independent manner (Ridker et al., 2002).

Hs-CRP levels are associated with numerous features of metabolic syndrome and their severity, and predict vascular risk among patients already defined as insulin-resistant. In patients with unusual or moderate cardiovascular risk profiles, hs-CRP can be measured in order to refined risk assessment (Vlachopoulos et al., 2015). Thereby, hs-CRP level >3mg/l indicate high vascular risk when interpreted in the context of other risk factors. A potential limitation of hs-CRP testing lies in that biological impact of inflammation on vascular risk can be underestimated due to the non-specificity of hs-CRP.

A strong debate existed on whether hs-CRP is a marker or a mediator in atherothrombosis (Anand and Yusuf, 2010; Bisoendial et al., 2010; Yousuf et al., 2013). Mendelian randomization studies suggest that CRP is a predictor of cardiovascular events but improbable to itself be a causal factor in the pathway of disease expression (Dehghan et al., 2011; Zacho et al., 2008) which was confirmed in recent epidemiological studies (Lane et al., 2014; Noveck et al., 2014). CRP is thus viewed like animportant downstream biomarker of cardiovascular disease, suggesting that upstream pathways analysis (IL-1β and IL-6)can provide more information **(Figure 17)** (IL6R Genetics Consortium Emerging Risk Factors Collaboration et al., 2012; Ridker, 2016b).

ii. In cerebrovascular diseases

A recent meta-analysis on stroke and hs-CRP showed that males exhibiting high levels of hs-CRP had 46% greater risk of ischemic stroke, but no of hemorrhagic stroke (Zhou et al., 2016). The Framingham study showed that baseline hs-CRP levels predict the risk of stroke (Rost et al., 2001). Consequently, even if the mechanism underlying high hs-CRP concentration and ischemic stroke risk is still not clearly understood, hs-CRP can be used as complementary tool to predict ischemic stroke.

CRP and inflammatory cytokines secreted after an acute ischemic stroke are associated with the brain infarct volume (Beamer et al., 1995). An increase in CRP levels 12-24 hours after thrombolysis is negatively correlated with neurological outcomes as a reduction of National Institutes Health Stroke Scale (NIHSS) is observed (Gill et al., 2016). As CRP levels are associated with post-infarct lesion size, larger area of necrosis and elevated inflammatory response (Di Napoli et al., 2001),measurement of CRP concentration at 12-24 hours may be considered as an accurate prognostic biomarker (Gill et al., 2016; VanGilder et al., 2014).

Acute stroke patients presenting increased levels of inflammatory markers at admission have poor recurrence, complication and mortality outcomes (Audebert et al., 2004) and elevated baseline CRP is correlated with adverse long-term functional outcome (VanGilder et al., 2014). In a recently published prospective study,Frøyshov et *al* .showed that stroke-survivors suffered more comorbidity and higher level of leukocytes, fibrinogen, IL-6 and hs-CRP during the sixteen years follow-up than stroke-free subjects. However, hs-CRP was not independently associated with mortality in these subjects in contrary to its upstream cytokine IL-6 (Frøyshov et al., 2016).

b) Interleukin-6 (IL-6)

IL-6 is a major cytokine secreted by macrophages and T cells involved in acute and chronic inflammation regulation and playing the role of secondary messenger in these processes. It is capable of crossing the BBB and initiating fever. IL-6 can also be secreted by endothelial cells and smooth muscle cells in blood vessels and can induce the B cells maturation in plasmocytes with efficient antibodies production.

In addition to controlling immune cells, IL-6 is also important in hepatocytes regulation, hematopoiesis, skeleton, cardiovascular system, nervous and endocrine systems and placenta (Kishimoto et al., 1995).

i. In cardiovascular diseases

IL-6 levels measured in healthy populations predict future vascular risk (Ridker et al., 2000a, 2000b). Kaptoge et *al*confirmed in their prospective studies and meta-analysis of others studies that each standard deviation increase in log IL-6 correlates with 25% increase in risk of future vascular events(Kaptoge et al., 2014). Others studies also showed that this cytokine correlates with endothelial dysfunction, arterial stiffness and subclinical atherosclerosis events (Esteve et al., 2007; Lee et al., 2008; Mahmud and Feely, 2005). Despite this, no clinical studyhas yet confirmed these findings and the IL-6 assessment remains difficult because of its short half-life and circadian and post-prandial variations.

Although IL-6 is the main cytokine inducing CRP production by hepatocytes, it also relies on atherosclerotic plaque initiation and vulnerability (Schieffer et al., 2004; Yudkin et al., 2000), microvasculardysfunction(Guo et al., 2014) and on deleteriousevents in acute ischemia(Lindmark et al., 2001). Consequently, IL-6 has a causal role in atherosclerosis. It also can be produced by

cardiomyocytes at the moment of infarcted zones reperfusion, and is involved in reperfusion injuries (Gwechenberger et al., 1999).

ii. In cerebrovascular diseases

IL-6 is also a well-known neuropoeitin by its effects on hematopoietic and nervous system. In the CNS, IL-6 is secreted by astrocytes, oligodendrocytes, microglia and neurons. Endothelial cells in the brain can also produce IL-6 in abundance, acting on neighboring cells and regulating via an autocrine way IL-6 synthesis.

In physiological context, IL-6 plays an important role in adult neurogenesis (Bauer et al., 2007) and long-term memorization processes (Tancredi et al., 2000).

In neuropathological situation like stroke, the detrimental role of inflammation is known (Ekdahl et al., 2003; Whitney et al., 2009) and upregulation of IL-6 may have a role on neurogenesis. In vitro studies of IL-6 upregulation in the hippocampus showed that it significantly decreases the differentiation of neural stem cells into neurons (Monje et al., 2003). A clear increase of serum and cerebrospinal fluid (CSF) concentration of IL-6 have been observed shortly after ischemic stroke and correlates with infarct volume (Smith et al., 2004; Tarkowski et al., 1995). Besides these findings, Acalovschi et *al.* showed that IL-6 expression after stroke depends on IL-6 haplotype (Acalovschi et al., 2003). Indeed, in animal models, an upregulation of IL-6 in neurons and in a lower way in glial and endothelial cells was demonstrated (Suzuki et al., 2009).

IL-6 may be a critical factor coordinating responses in stroke such as control of oxidative stress (Jung et al., 2011)and angiogenesis (Gertz et al., 2012). Furthermore, IL-6 was found to be an independent mortality predictor in stroke-survivors patients (Frøyshov et al., 2016).

c) Interleukin-1 beta (IL-1β)

IL-1β is a resulting of the member of the interleukin 1 family. It is produced by macrophage as a precursor (pre-IL-1β) which is activated when cleaved by cytosolic caspase 1. IL-1β is an important mediator of the inflammatory response and is involved in numerous cellular activities, including cell proliferation, differentiation and apoptosis. An increased secretion of IL-1β leads to different autoinflammatory syndromes.

i. In cardiovascular diseases

IL-1 is known to play a role in numerous diseases and their maintenance in peripheral organs andin the central system. It induces the production of fibronectin, resulting in clinical evolution

of coronary artery diseases and their adverse outcomes such as congestive heart failure (CHF) or angina (Rabinovitch, 1995). The InCHIANTI study showed that patients suffering from CHF or angina have higher levels of IL-1β than controls whereas there was no significant difference between other diseases and controls (Di Iorio et al., 2003).

IL-1β is a good inflammatory biomarker for research purpose due to its great biological basis and its implication in the atherosclerosis process (Packard and Libby, 2008) but its short half-life and large circadian variations makes its use difficult in clinical routine (Biasillo et al., 2010). Since several years, IL-1 receptor antagonist (IL-1Ra) emerges as a more accurate biomarker for diagnosis of acute coronary syndrome and stable angina and prognostic of acute myocardial infarction in the same way than IL-18 (Biasillo et al., 2010).

Consequently, in cardiovascular clinic, IL-1β seems to be rather an indirect marker of a chronic low-grade inflammation and depict a fraction of the activated monocytes/macrophages production (Di Iorio et al., 2003).

ii. In cerebrovascular diseases

In cerebrovascular context, things are different. Inflammation contribution prior to and after a stroke is of major importance for outcomes determination after an acute CNS injury. Indeed, pre-existing inflammation and high levels of IL-1β can affect the susceptibility and the severity of CNS injury (Denes et al., 2010; McColl et al., 2009). Moreover, a raised inflammatory status, notably due to IL-1β increase, is the common element of all co-morbidities of stroke. Furthermore, IL-1β was shown to have a contributing role in plaque rupture and thromboembolism (Packard et al., 2009).

Acute stroke has been showed to induce increased levels of IL-1β in blood and cerebrospinal fluid (Maas and Furie, 2009). Consequently, measurement of IL-1β levels may have an informative role serving as biomarker for improvement of diagnosis and prognosis (Jickling and Sharp, 2011; Sharp et al., 2011). In experimental animal models, IL-1β was able to modulate infarct evolution (the higher IL-1β the poorest the outcomes are), thus confirming its strong interest as putative marker of stroke severity and neurologic outcomes (Emsley et al., 2003; Jickling and Sharp, 2011).

d) Tumor Necrosis Factor alpha (TNFα)

TNFα is a glycoprotein produced mainly by macrophages and also by lymphoid cells, mast cells, endothelial cells, cardiomyocytes, adipose tissue, neurons and fibroblastes. It is an important cytokine involved in systemic inflammation and acute phase reaction. TNFα is released in response to

lipopolysaccharide, others bacterial products and IL-1. Among all its properties, TNFα stimulates the release of CRP by the liver, is a potent chemoattractant of neutrophils and promotes the expression of adhesion molecules on endothelial cells.

In atherosclerosis, TNFα was shown to increase proliferation of VSMCs (Rastogi et al., 2012), endothelial inflammation (Ouchi et al., 2010) and apoptosis (Csiszar et al., 2004) and plasmatic concentrations are positively correlated with carotid IMT (Skoog et al., 2002)**,** and increased in patients with premature coronary artery disease (Jovinge et al., 1997). Thus, TNFα can be considered as an important mediator for CVD development.

The use of TNFα as predictive biomarker of outcomes and infarct size is still debated. Actually, several studies showed increased seric and CSF levels of TNFα in stroke patients, correlated with worsening of neurological symptoms, increased infarct size and poor short-term outcomes (Mazzotta et al., 2004; Zaremba and Losy, 2001) while some others found that TNFα levels were not correlated with infarct size or outcomes (Intiso et al., 2003; Vila et al., 2000).

e) Monocyte chemoattractant protein 1 (MCP-1)

MCP-1 (also known as CCL2) is the major pro-inflammatory cytokine controlling the monocyte recruitment in the vessel, mediated through C-C chemokine receptor 2 (CCR2). This chemokine is expressed in macrophage-rich regions of atherosclerotic plaques (Namiki et al., 2002). MCP-1 has inflammatory and pro-atherogenic effects such as migration and proliferation of VSMCs, plaque neovascularization, thrombosis or induction of MMPs (Egashira, 2003)proven by gene deletion experiments (Inoue et al., 2002). Elevated plasmatic levels of MCP-1 were shown to be associated with future risk of major adverse events like MI or death (Kervinen et al., 2004; de Lemos et al., 2003) but its independent value as predictor of cardiovascular risk was not confirmed by the MONICA/KORA Augsburg study (Herder et al., 2006). Thus, to confirm the potential use of MCP-1 as clinical biomarker supplemental cohort studies are needed.

In stroke, the key post-ischemic event is leukocytes recruitment relying first on chemokines (Dirnagl et al., 1999). MCP-1 represents a crucial step for this infiltration and its expression in ischemic area exacerbates ischemic damages. An overexpression of this chemokine leads to an increased infarct size and monocytes/macrophages population in the injured area (Chen et al.,

2003). Moreover, an increase of MCP-1 levels has been showed in early stages of ischemic stroke in the CSF of patients (Garcia-Bonilla et al., 2014; Losy and Zaremba, 2001).

3. What about anti-inflammatory markers?

Anti-inflammatory markers can also be monitored, in order to refine the examination and stratification of the plaque stage. For example, IL-10 and IL-1 receptor antagonist (IL-1ra) plasmatic (and tissular when possible) levels can be measured and provide information on plaque characterization and status.

IL-10, produced by Th2 lymphocytes and monocytes/macrophages is known to inhibit the production of Th1-related cytokines (IFNγ, TNFα, IL-2) and macrophages-derived interleukins (IL-1, IL-6, IL-8, TNFα). Although protective effect of IL-10 was showed in different studies on advanced atherosclerosis plaque (Mallat et al., 1999; Tiret et al., 2005) and acute coronary syndrome (Anguera et al., 2002; Smith et al., 2001) and even in stroke (Ren et al., 2011) its status is still debated. Indeed, it is still unclear whether high plasmatic levels are a marker of anti-inflammatory pattern or counter-regulatory consequence of pro-inflammatory profiles observed in the atherosclerotic plaque. Moreover, TNFα/IL-10 ratio can be used to define the patient status, as it is increased in CAD patients compared to healthy ones (Goswami et al., 2009).

IL-1ra, produced by the same cells as IL-1, has the property to bind the IL-1 receptor and block the signaling cascade of inflammation. Its production is delayed after IL-1 secretion in order to avoid long-acting inflammation. In atherosclerosis, IL-1ra plasmatic level was found to be higher in diseased arteries than in normal and in this context IL-1ra behaves as an acute phase reactant (Gabay et al., 1997). Furthermore, measure of IL-1ra levels in unstable angina were shown to correlate with IL-6 levels, suggesting a prognostic role of IL-1ra (Biasucci et al., 1999).

Consequently, measurement of anti-inflammatory markers can be useful for a better accuracy of the patient's stratification.

B. Imaging biomarkers

The composition of the plaque is a critical factor determining risk of cerebral ischemia (Fisher et al., 2005). Rupture-prone plaque also called vulnerable plaque, present some characteristic features such as a large lipid necrotic core (Mono et al., 2012) covered by a thin fibrous cap (Li et al.,

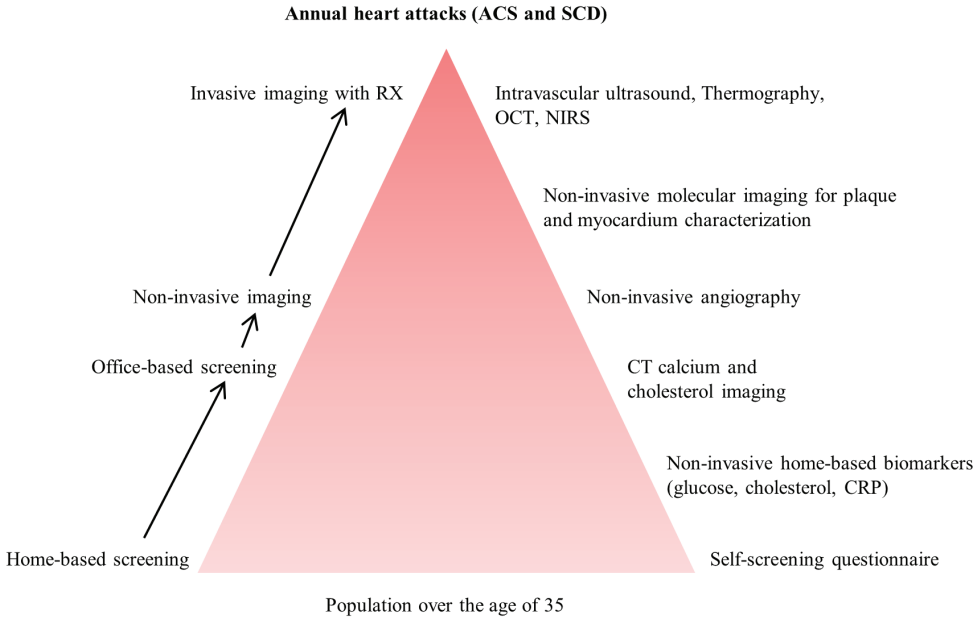

Figure 18: Importance of non-invasive imaging in vulnerable patient detection. The major need in cardiovascular clinic nowadays is to develop non-invasive, readily available and accurate screening/diagnostic tools allowing multistep screening of an apparently healthy population and for those with known atherosclerosis but with uncertain risk for acute event.
Adapted from Naghavi et al, Circulation, 2003

2006). Non-invasive imaging is a useful tool for atherosclerosis diagnosis, for cardiovascular risk stratification and vulnerable patient detection (**Figure 18)**.In this chapter we will discuss the different modalities available for atherosclerosis imaging and then focus more on the most used biomarkers imaged from these modalities.

1. Clinical-established imaging modalities for atherosclerosis

Numerous imaging modalities are now available for research and clinical purpose. Here we will briefly present what are those techniques to evaluate plaque morphology and function.

a) Ultrasound investigation of vascular territories

Medical ultrasound (also known as ultrasonography) is a diagnostic imaging based on the application of ultrasound.

The most used type of image is B-mode image, which displays the acoustic impedance of a two-dimensional cross-section of tissue. Other types of images can be used to analyses blood flow, location of blood, the stiffness of a tissue or anatomy of a three-dimensional region.

Ultrasound is a medical imaging modality presenting several advantages: real-time images, portability of the apparatus allowing the examination at the bedside of patient, low cost, and radiation-free. On the other hand, this technic can be limited by patient morphology, the difficulty of imaging structures behind bone or air and the critical dependence on the operator's skills.

Traditional ultrasound analysis provides information on the vessel wall, particularly on intima-media thickness (IMT) and on the severity of the stenosis. This technique also enables quantification of plaque tissue, including fibromuscular tissue, intraplaque hemorrhage, lipids and calcium (Lal et al., 2002)allowing identifying patients with vulnerable plaque (Salem et al., 2014). Several studies comparing histologic content of plaques and ultrasound plaque echogenicity showed that vulnerable and rupture-prone plaques have been characterized by low gray-scale values or echolucent on B-mode use (Grønholdt et al., 2001). Indeed, echolucent plaques revealed large lipid core, thin fibrous cap and numerous tissue factors for platelet deposition (Grønholdt et al., 2002; Nordestgaard et al., 2003). Furthermore, these plaques showed signs of ongoing inflammation and intraplaque neovascularization (Grønholdt et al., 2001; Partovi et al., 2012). On the contrary, high gray-scale or echogenic plaques were shown to contain denser fibrous tissues and calcification, being more stable (Grønholdt et al., 2002).

During the past years, emergence of computer-aided diagnostic method has improved the assessment of atherosclerosis plaque and in term of speed and accuracy, allowing the categorization of patients as symptomatic or asymptomatic and stratify the stroke (Acharya et al., 2012; Pedro et al., 2014; Steinl and Kaufmann, 2015) and cardiovascular disease events (Baldassarre et al., 2012; Polak et al., 2011; Weber et al., 2015).

The recent development of contrast agents for ultrasound improved the evaluation of IMT, irregularities or ulcerations on the plaque. Contrast agents are composed of gas microbubbles (<5µm) covered of substances (e.g. as albumin, lipids or polymers) and strongly reflects acoustic energy, increasing the return signal and behaving as a true intravascular tracer (Feinstein, 2004).

b) X-Ray imaging and Computed Tomography (CT) Scanner

The coronarography is an invasive imaging technique using X-Rays and iodine injection in order to visualize coronary arteries. It is the technique of reference for research of CAD such as atherosclerosis and its consequences (angor, myocardial infarction, and silent myocardial ischemia), and to treat culprit lesions by endovascular intervention. Modern CT scanner enables fast and non-invasive X-ray imaging of coronary arteries.

Calcification is an important factor in atherosclerosis burden and provides useful information regarding to the stage of the plaques. CT scan can be used to measure the amount of calcium in coronary arteries, it is called coronary artery calcium score (CACS). CACS is acquired with a non-contrast chest CT scan with a breath hold of 5 seconds and a low-dose radiation (<1mSv, similar as mammography) (Gerber et al., 2009). This enables to detect the presence of calcium through the whole epicardial coronary system. Coronary calcification is defined as a lesion observable on 3 or more adjacent pixels (~1mm²) and X-Ray attenuation superior to the threshold of 130 Hounsfield units (Agatston et al., 1990). CACS was characterized by a score determined by the product of the calcified plaque area and the maximal calcium lesion density. Nowadays, standardized categories for CACS are used from 0 (no calcified plaque) to >400 (severe plaque) (Agatston et al., 1990). In patients with asymptomatic CAD, CACS is the most robust predictor of coronary events and thus is important for primary prevention, especially in the intermediate-risk population, even surpassing the Framingham Risk Score (Hecht and Narula, 2012). CACS is also strongly associated with development of stroke or heart failure (Gibson et al., 2014; Hermann et al., 2013; Leening et al., 2012).

c) Optical imaging

Optical imaging includes various imaging techniques using visible, ultraviolet and infrared light for imaging. Molecular imaging involves inference of the deflection of light emitted from source to structure, texture or anatomic properties of materials. In the cardiovascular field, it includes near infrared luminescence (NIRF or spectroscopy (NIRS), optoacoustic imaging and several other imaging modalities.

Near infrared fluorescence (NIRF) is an optical imaging techniques using near-infrared fluorescence, mostly used in oncology. It displays high sensitivity and allows the *in vivo* visualization of a variety of molecular entities through versatile fluorescent probe design. NIR wavelengths permit relatively deep photon penetration into tissue, minimal autofluorescence and higher optical contrast. In vivo fluorescence with NIR possesses a huge potential for a numerous molecular diagnostic and therapeutic applications in atherosclerosis(Jaffer et al., 2008, 2011; Vinegoni et al., 2011; Yoo et al., 2011). Near infrared spectroscopy (NIRS) is a technique similar to that of NIRF and used for oxygen saturation detection and it is associated to Doppler for micro-emboli detection in cerebrovascular territories and detect high risk plaque (Goldstein et al., 2011; Igarashi et al., 2014; Liebig et al., 2015).

Optoacoustic imaging is a technique relied on absorption of pulsed laser light by an absorbing object within a tissue to create pressure waves that are detected at the tissue surface. It is used to visualize structures into a turbid environment combining spectroscopy accuracy and ultrasound resolution(Dima and Ntziachristos, 2012; Rosenthal et al., 2012).

d) Magnetic Resonance Imaging (MRI)

MRI is a medical imaging technique based on nuclear magnetic resonance (NMR) using quantic properties of atomic nucleus. Some atomic nuclei can absorb and emit radiofrequency energy when placed in an external magnetic field. For clinical and research use, hydrogen is the most used atom to generate radiofrequency signal due to its natural abundance in human and other biological organisms, especially in water and fat.

MRI acquisition parameters such as echo time (TE) and repetition time (TR) can be modified according to the feature or tissue analyzed. The setting of theses parameters allow the use of different ponderations allowing the analysis of the images from different point of view. T1 ponderation also called « anatomic ponderation » consists in short TR (400-600ms) and TE (10-20ms) in order to neutralize T2 bias. T1 ponderation makes white matter or fat appearing brighter than grey matter, bone or water. This sequence is also used with contrast agent injection for abnormalities characterization. On the contrary, T2 ponderation called “tissular” ponderation consists in long TR

(>2000ms) and TE (>80ms). Finally, the proton density ponderation is a mix between T1 and T2 ponderation with a short TE (10-20ms) and a long TR (>2000ms) allowing images with proton density contrast distinguishing liquids, tissues and fat. Other sequences permit the annulation of fat signal (short time of inversion recovery, STIR), of free water (FLAIR) for cerebral exploration without the CSF signal, gradient echo for visualization of heterogeneities on nervous system.

MRI is mostly used in diagnostic medicine and biomedical research allowing medical diagnosis, staging of disease and follow-up without ionizing radiation exposition. This is an imaging modality of major interest for acute ischemic stroke diagnosis (Nael and Kubal, 2016), measurement of myocardial infarction size (Rinta-Kiikka et al., 2014) and carotid plaque diagnosis (Brinjikji et al., 2016; Huibers et al., 2015).Studies even suggest that it is the new gold-standard for plaque composition assessment (Gupta et al., 2013). In this section, we will focus on the two most used classes of contrast agents, namely gadolinium chelates and ultrasmall superparamagnetic particles iron oxide (USPIOs) and their utility in clinical and research atherosclerosis.

i. Atherosclerosis fibrous cap thickness and neovascularization characterization with gadolinium-based contrast agents

Gadolinium (Gd) is a chemical component from the lanthanides group which is coupled to a chelator or a ligand in order to serve as contrast agent for MR imaging. Gd-based contrast agents (Gd-CAs) are administered intravenously and monitored via T1 MRI sequences, upon which it makes appear a hyperintense signal. Gd-CAs bind to albumin, forming a complex which extrasavates at sites of albumin leakage into the extraluminal space resulting in an enhancement of arterial wall. For imaging of atherosclerotic plaques, it penetrates into the lesions and will induce different signal intensities according to the tissue. When it enters in the plaque, Gd unbinds the albumin and accumulates in the extracellular matrix, but not in the lipid-rich necrotic core because of its lipophobic properties resulting in a preferential enhancement of fibrous tissue (Liu et al., 2012). On the same way, neovascularization areas, containing extensive microvessels, showed a strong enhancement of T1 signal (Calcagno et al., 2013; Yuan et al., 2002). The use of Gd-CAs is thus very helpful for further characterize the plaque constitution in patients candidating for endarterectomy (Sadat et al., 2014).

Likewise, Gd-CAs are well-known in the field of neuro-imaging for BBB leakage assessments (Runge et al., 1985). Indeed, Gd chelates cannot cross through an integer BBB, but in context of chronic or acute neuroinflammation such as multiple sclerosis, Alzheimer's disease or stroke, BBB presents more or less extended leakage, allowing Gd-CAs to pass through and accumulate in the brain (Essig et al., 2012; Merino et al., 2013). Gd-CAs can also be used for perfusion MR

imaging in brain after stroke or in context of brain vascular or inflammatory diseases (Cotton and Hermier, 2006).

ii. Phagocytosis imaging with Ultrasmall Superparamagnetic Particle Iron Oxide (USPIOs)

USPIOs consist of a small iron-oxide core embedded in dextran, citrate or polymer shell for a final size of 10 to 50 nm. These particles had large negative magnetic susceptibilities resulting in hypointensities (negative contrast) on T2-weighted sequences.

In this work, we will only discuss the use of USPIOs for monocytes/macrophages/microglia imaging as they are one of the contrast agents used during my thesis research. Indeed, these nanoparticles are phagocytized by macrophages, thus reflecting inflammation in the plaque. Some studies have shown that carotid plaque inflammation can be identified using USPIO-enhanced MRI and that these USPIOs accumulates mainly in macrophages of ruptured or rupture-prone carotid lesion in human (Kooi et al., 2003; Trivedi et al., 2006) confirming the fact that an important macrophage infiltration is an indicator of plaque vulnerability. Recent clinical trial also demonstrated the potential use of USPIOs for assessment of therapeutic response to anti-inflammatory drugs on atherosclerotic patients (Tang et al., 2009).

On cerebrovascular territories, USPIOs are used to image macrophage/microglia response to chronic (multiple sclerosis, glioma) (Brochet et al., 2006; Taschner et al., 2005) or acute inflammation (stroke) (Saleh et al., 2004). Several studies showed that phagocyte imaging was feasible in stroke patients and that they can provide additional information to infarct size (Nighoghossian et al., 2007).

iii. Other vulnerable plaque features imaged by MRI

Improvement of surface coils enabled accelerated acquisition and improvement of the signal-to-noise ratio. Moreover, development of multi-contrast sequences (i.e. post-Gd contrast enhanced black-blood imaging) resulted in an accurate identification of lipid-rich necrotic core (Trivedi et al., 2004), thrombus (Moody et al., 2003), fibrous cap and its rupture (Fayad and Fuster, 2000), arterial inflammation (Kerwin et al., 2006), intraplaque hemorrhage (Kampschulte et al., 2004)and neovascularization (Kerwin et al., 2003). A thin or ruptured fibrous cap, a larger necrotic core and intraplaque hemorrhage showed increased risk for stroke in clinical studies using MRI as prognostic tool (Singh et al., 2009; Takaya et al., 2006). Recently, new application was developed for MRI shear stress assessment (Canton et al., 2013)allowing an even more accurate evaluation of plaque composition and vulnerability.

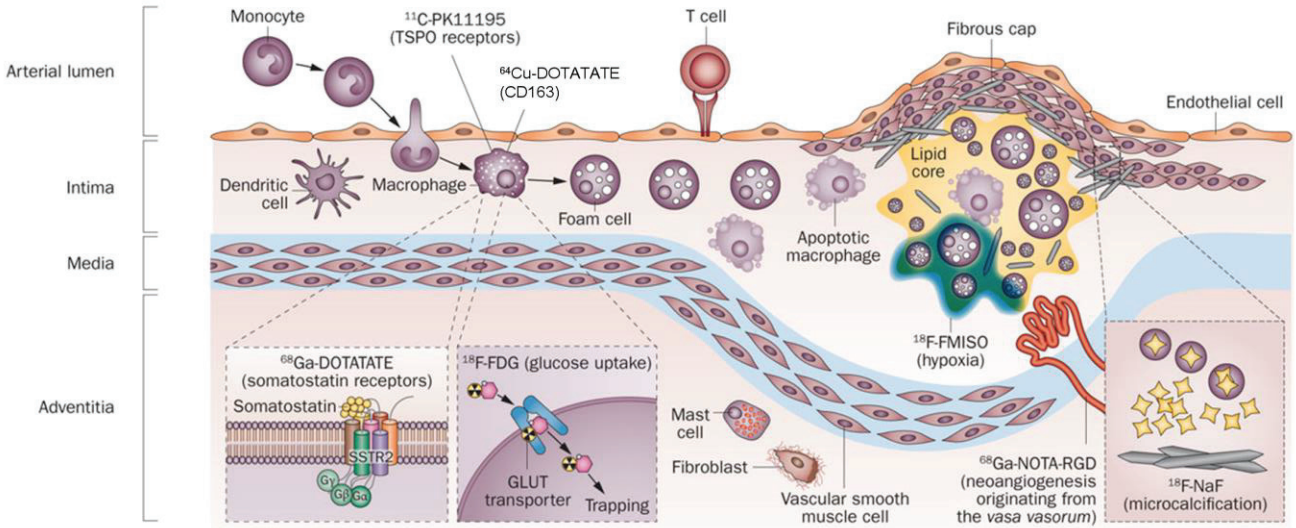

Figure 19: PET tracers for atherosclerosis. Inflammation and related pathogenic processes occurring within high-risk plaques can be imaged in vivo using specifically targeted radiolabelled PET tracers. ^{18}F-FDG is the most-widely studied and validated tracer, which is taken up by active macrophages where it is metabolically trapped and accumulates in proportion to intracellular demands. However, the ^{18}F-FDG arterial signal is also influenced by local hypoxia and uptake by other resident cell types. Alternative PET tracers, including ^{64}Cu-DOTATATE, ^{68}Ga-DOTATATE, and ^{11}C-PK11195 could be more-specific for macrophage activity (and, therefore, for inflammation) than ^{18}F-FDG. Within an inflamed plaque, hypoxia, neoangiogenesis, and microcalcification also contribute to plaque vulnerability; these processes can potentially be imaged with PET using novel tracers, such as ^{18}F-FMISO, ^{68}Ga-NOTA-RGD, and ^{18}F-NaF, respectively.

Adapted from Tarkin et al, Nat Rev Cardiol, 2014

2. Molecular imaging

In this section, we will focus more on the most used molecular imaging techniques and their tracers available for imaging the different features of atherosclerosis and neuroinflammation. We will base our discussion on clinically available tracers and probes.

a) Positron Emission tomodensitometry (PET/CT)

Positron Emission Tomography (PET) is a metabolic functional imaging modality used both in clinic and in research. It needs intravenous injection of a radiopharmaceutical positron emitter (called radiotracer), manufactured in a cyclotron. This production is divided into two steps: generation of the radioelement and radiosynthesis of the radiopharmaceutical. The PET imaging is most likely combined with a computerized tomography (CT) scan, to allow a more precise localization of the uptake region.

Injected tracer emits a positron, which after few millimeters in the tissue will meet an electron and result in an annihilation reaction namely the emission at 180° of two 511 keV photons. The PET camera detects those photons simultaneously, called coincidence detection.

The most used radioactive elements are the ^{18}F (half-life= 110 minutes), the ^{11}C (20 minutes), the ^{13}N (10 minutes) and the ^{15}O (2 minutes). The characteristics of ^{18}F and ^{11}C will be discussed in a following section.

Since few years, novel apparatus are available combining both TEP and MRI technique, enabling time saving and a more accurate registration of TEP images on anatomy due to the higher contrast of MR images versus CT. Moreover, the fact that both examinations are conducted in the same time relieves registration problems due to a different position of the patient in the bed.

PET tracers are increasingly used for atherosclerosis diagnosis and follow-up thanks to their high specificity. In the following section, we will discuss the use of the "gold standard" in atherosclerosis PET imaging (^{18}F-FDG), a well-used inflammation-targeting tracer (^{11}C-PK11195) and a rapid overview of other useful tracers in atherosclerosis field **(Figure 19)**.

i. ^{18}F-Fluorodesoxyglucose (^{18}F-FDG): the gold standard

^{18}F-FDG is a radionucleotide analog of glucose which accumulates intracellularly in proportion to cellular demand for glucose **(Figure 20)**. First used for imaging of tumor staging, this was found to be detected in arterial territories during whole-body scans suggesting its use in

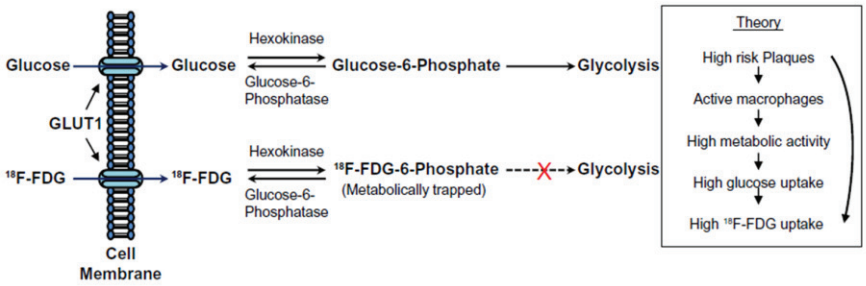

Figure 20: Pathway of uptake and utilization of ^{18}F-FDG versus glucose through the glucose transporter GLUT1 in a cell. ^{18}F-FDG can enter the cell via GLUT1 in a similar way than glucose but as the fluorure replace an OH group, it cannot be completely metabolized and is blocked in the cell at the ^{18}F-FDG-6-Phosphate state. The fact that 18F-FDG stay in the cell and cannot be metabolized enables imaging of cell metabolism.
Adapted from Alie et al, Clin Med Insight Cardiol, 2014

atherosclerosis imaging (Yun et al., 2001). FDG is now the most used radioligand in imaging studies of atherosclerosis. This tracer is taken up into cells via Glut 1 and 3 which are upregulated in atherogenesis due to hypoxia in the lipidic core. Once in the cytoplasm, it undergoes phosphorylation by hexokinase 1 but is unable to continue glycolysis cycle because of its conformation. Thus, FDG diffuse very slowly out of the cell, resulting in intracellular accumulation, which allows quantification. Consequently, it can be used as a sensitive measure of increased metabolic activity, particularly in tissues without baseline high metabolic activity such as physiologic vessel wall and blood. In the vulnerable plaque, a high concentration of pro-inflammatory macrophages induces a high metabolic activity (Davies et al., 2010; Liu et al., 2016; Tawakol et al., 2006).

FDG PET/CT is a useful technique for non-invasive imaging of plaque due to the variation of FDG uptake between symptomatic and non-symptomatic carotid plaque in humans (Rudd et al., 2002). It also allows the discrimination of non-stenotic symptomatic carotid plaque which is not possible with MRI (Davies et al., 2005). Lipidic-rich plaques are more prone to rupture than fibroatheroma or calcified plaque and present a higher FDG uptake (Silvera et al., 2009). Both LDL and TC have been shown to be independently associated with FDG uptake (Chróinín et al., 2014; Kaida et al., 2014).

Furthermore, higher FDG uptake has been shown to be correlated with an increased risk of cerebrovascular events such as microemboli, whatever the stenosis degree (Marnane et al., 2012; Moustafa et al., 2010). FDG uptake in aorta is higher in patients with recent myocardial infarction than those with stable angina and even higher in patient with ST elevation myocardial infarction (STEMI) versus non-STEMI showing a close correlation between neighboring arterial territories (Joshi et al., 2015; Rudd et al., 2009). Likewise, epidemiologic study showed that FDG uptake is higher in subjects with acute coronary syndrome than in those with stable angina (Kim et al., 2015).

In summary, carotid artery FDG uptake is correlated with age, clinical risk factors, inflammatory biomarkers (Noh et al., 2013; Rudd et al., 2009) and high-risk plaque features on imaging modalities such as CT, MRI and ultrasonography (Figueroa et al., 2012; Graebe et al., 2010; Silvera et al., 2009).

ii. TSPO: from a biological target to an imaging agent, ^{11}C-PK11195

Translocator protein (TSPO), formerly called PBR (peripheral benzodiazepine receptor) is a highly conservative 18kDa transmembrane protein, even found in bacteria. It is located on outer mitochondria membrane, mostly expressed in steroids-synthesizing tissues (e.g. brain, adrenal gland and gonads) and mature monocytes and characterized by its ability to bind a variety of

benzodiazepine-like drugs. It represents 5-10% of all proteins of outer mitochondria membrane in steroidogenic cells(Anholt et al., 1986). In case of high cholesterol handling, such as high cholesterol diet, TSPO expression is downregulated in aorta, testis and liver, not in brain (Dimitrova-Shumkovska et al., 2010). Inversely, in human macrophages, TSPO expression is increased when exposed to oxLDL as in atherosclerosis (Taylor et al., 2014).

TSPO is complexed with voltage-dependent anion channel (VDAC) and adenine nucleotide transporter (ANT) (McEnery et al., 1992), proteins involved in mitochondria permeability transition pore, and allows translocation of cholesterol from outer to inner mitochondria membrane. TSPO has long been associated with steroidogenesis and mitochondrial permeability transition pore (mPTP) (Azarashvili et al., 2014; Culty et al., 1999), some even hypothesize that a deletion of TSPO would lead to a lethal phenotype. TSPO seemed to be critical for mitochondrial processes but, in physiological situation, morphological adaptation and redundancy of functions in mitochondria could compensate for the loss of function of TSPO. Indeed, recent studies with TSPO knock-out mice showed that mice can have a normal phenotype despite of TSPO deletion (Banati et al., 2014; Morohaku et al., 2014; Sileikyte et al., 2014). We cantherefore think that TSPO may become phenotypically important when the mitochondria loses its compensation capacity as during aging or in response to metabolic challenges (Gut et al., 2015).

TSPO also interacts with cytosolic proteins and acts like a mitochondrial anchor allowing transduction of intracellular signals to mitochondria.

In central nervous system, TSPO is mostly expressed in microglia and reactive astrocytes and is now used as a biomarker of brain inflammation and reactive gliosis in PET/CT imaging. TSPO has a low brain expression level in physiological situation and up-regulates in pathological conditions (Alzheimer disease, Parkinson disease, and multiple sclerosis, brain trauma or stroke) (Batarseh and Papadopoulos, 2010; Chauveau et al., 2008). TSPO is a sensitive biomarker of neurodegeneration and brain damage (especially in neuroinflammation and reactive gliosis)(Batarseh and Papadopoulos, 2010; Janssen et al., 2016).

TSPO chemical ligands, as PK11195, were thus focused on diagnosis of numerous diseases such as traumatic brain injury, neuroinflammation and neurodegeneration (Selvaraj and Stocco, 2015). Although TSPO expression is upregulated in the brain at sites of injury and inflammation, as well asfollowing a number of neuropathological conditions including stroke, herpes and HIV encephalitis, and neurodegenerative disorders such as Alzheimer's disease, multiple sclerosis, amyotrophic lateral sclerosis, Parkinson's disease, and Huntington's disease (Batarseh et al., 2010), the molecular mechanisms underlying these diseases remain unclear.

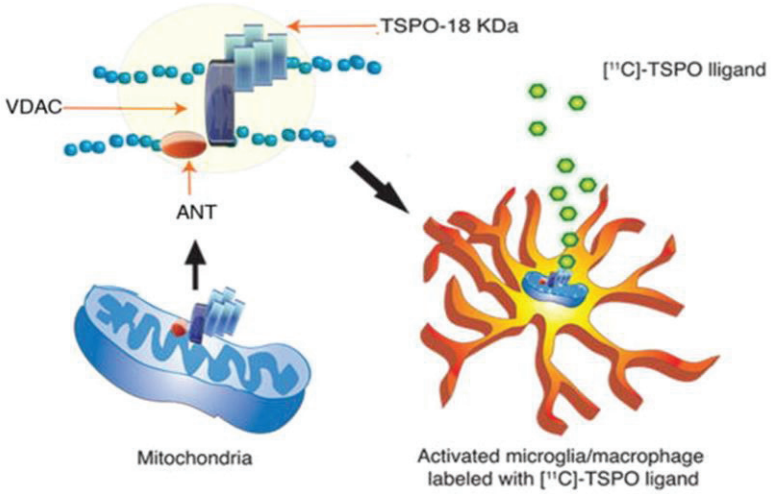

Figure 21: ^{11}C-PK11195 and TSPO. Translocator protein -18 kDa (TSPO) is located at the outer mitochondrial membrane and has a putative five transmembrane helical structure. It forms a hetero-oligomeric complex with the voltage dependent anion channel (VDAC) and the adenine nucleotide transporter (ANT) constituting the putative mitochondrial permeability transition pore. [^{11}C]-labeled TSPO ligands (green) bind to TSPO located in activated microglia/macrophages. The [^{11}C]-radionuclide decays by the emission of a positron enabling TSPO imaging via PET/CT. Adapted from Venneti et al, Glia, 2013

However, recent *in vivo* studies showed that TSPO also had a potential neuroprotective role. Indeed, upregulation of its expression level can enhance alternative M2 microglial activation, resulting in more phagocytic activity and upregulation of anti-inflammatory genes to promote recovery from tissue damages and resolve neuroinflammation (Kim and Yu, 2015).

Similar to what was observed in the brain, TSPO is also overexpressed in cardiac pathologies (Fairweather et al., 2014). Human clinical trials to diagnose carotid atherosclerosis have also been completed during the past few years (http://www.clinicaltrials.gov: NCT00547976), showing its utility in human clinic.

A second isoform of TSPO (TSPO2) exists, is expressed in hematopoietic tissues and is located on endoplasmic reticulum and nuclear membrane. It is involved in cholesterol redistribution during erythrocytes maturation. This isoform does not bind drugs (Rupprecht et al., 2010).

PK11195 is an isoquinoline carboxamide which is a potent and selective antagonist ligand for TSPO with an affinity in nanomolar range (Owen and Matthews, 2011)**(Figure 21)**. After monocyte activation, TSPO expression increase two to three-fold, resulting in more than 2 million of binding sites for PK11195 (Zavala and Lenfant, 1987). ^{11}C-PK11195 was showed to enable detection and quantification of inflammation in aorta of patients with vasculitis, showing a higher uptake of the tracer in patients compared to controls (Pugliese et al., 2010). Gaemperli et *al* demonstrated that carotid plaques associated with ipsilateral outcomes such as stroke or TIA had higher uptake of ^{11}C-PK11195(Gaemperli et al., 2012). Uptake of ^{11}C-PK11195 was showed to be more focal and localized than ^{18}F-FDG uptake, reflecting better the plaque composition (Gaemperli et al., 2012; Rudd et al., 2002).

^{11}C-PK11195 is the tracer of choice for neuroinflammation imaging *in vivo* as demonstrated in stroke (Ramsay et al., 1992), neurodegeneration (Banati et al., 2000; Edison et al., 2008; Okello et al., 2009) and braininjury(Ramlackhansingh et al., 2011). Some studies revealed that binding of ^{11}C-PK11195 correlated with the number of activated microglia/infiltrated monocytes in models of stroke (Myers et al., 1991; Raghavendra Rao et al., 2000). In rat model of induced stroke, ^{11}C-PK11195 imaging showed microglia/monocyte infiltration in the infarcted area (Cremer et al., 1992), and this finding was confirmed in human (Ramsay et al., 1992). Microglia was showed to be activated as early as day 3 post stroke, first at the external border of the infarct and then spreading to the core (Gerhard et al., 2005); and ^{11}C-PK11195 allowed the imaging of microglia activation as far as six months after stroke (Thiel et al., 2010).

iii. Others well-known PET tracers that can be used in atherosclerosis

^{68}Ga- and ^{64}Cu-DOTATATE

DOTATATE ([1,4,7,10-tetraazacyclododecane-*N,N',N'',N'''*-tetraacetic acid]-*d*-Phe1, Tyr3-octroate) is a radioligand binding somatostatin receptor subtype 2 (SST2) which is upregulated on macrophage membrane when they are activated (Armani et al., 2007). This radioligand can be labeled with ^{68}Ga or ^{64}Cu.

An uptake of ^{68}Ga-DOTATATE was shown in asymptomatic individuals with coronary calcification and CV risk factors (Mojtahedi et al., 2015; Rominger et al., 2010).

^{64}Cu-DOTATATE is also used in carotid imaging and its uptake is correlated with CD163 (and in a lower manner with CD68) mRNA expression suggesting the identification of a different component of the atherosclerotic inflammatory process (Pedersen et al., 2015). Furthermore, a recent retrospective study reported that a higher ^{64}Cu-DOTATATE uptake is associated with cardiovascular risk factors (Malmberg et al., 2015).

^{64}Cu has a longer half-life than ^{68}Ga (12,7h versus 68 min) but ^{68}Ga is more readily available due to its production by a generator when ^{64}Cu requires a cyclotron.

^{18}F-Sodium Fluoride (^{18}F-NaF)

Microcalcification is one of the features of vulnerable rupture-prone plaque. ^{18}F-NaF is taken up at mineralization sites allowing the identification of microcalcification areas in vivo (Hawkins et al., 1992). ^{18}F-NaF was first used in atherosclerosis imaging by Derlin et *al*, demonstrating that ^{18}F-NaF uptake in the plaque reflects the active mineralization process in microcalcification(Derlin et al., 2010). Carotid ^{18}F-NaF uptake correlates with cardiovascular risk factors in asymptomatic patients (Derlin et al., 2011) but not with stroke (Quirce et al., 2013).

^{18}F-Fluoromisonidazole (FMISO)

Hypoxia is often associated with atherosclerosis due to the high oxygen demand from foam cells. ^{18}F-FMISO imaging measures the effect of hypoxia directly within the necrotic core of the plaque. In a hypoxic environment ^{18}F-FMISO remains bound intracellularly, allowing a quantitative measure of its accumulation. ^{18}F-FMISO uptake was shown to be higher atheromatous regions rather than in normal tissue in rabbit (Mateo et al., 2014). In human, ^{18}F-FMISO uptake was found to be

higher in carotids of symptomatic versus asymptomatic patients and correlated with FDG uptake, suggesting a contribution of hypoxia to the uptake of FDG (Joshi, FR et al., 2013).

^{68}Ga-NOTA-RGD

Neoangiogenesis is another well-known vulnerable plaque feature due to the risk of intraplaque hemorrhage leading to plaque rupture. ^{68}Ga-1,4,7-triazaclyclononane-1,4,7-triacetic acid (NOTA)-Arg-Gly-Asp (RGD) (^{68}Ga-NOTA-RGD) target integrin αvβ3 expressed in angiogenic endothelial cells and macrophages. An increased uptake of this tracer was related to aortic atherosclerosis in ApoE null mice compared to atherosclerosis-free control animals and in a few patients with atherosclerosis (Paeng et al., 2013).

b) Adhesion molecules imaging

Migration of blood-borne leukocytes through the endothelium and/or the BBB if in the brain is a process consisting of chemoattraction, adhesion and transmigration. Chemoattraction is mediated via various cytokines and adhesion through the interaction of endothelial cell selectins (e.g. P-selectin), VCAM-1 or ICAM-1 with leukocytes integrins. Adhesion molecules are upregulated by inflammation and often represent the first hallmark of the inflammatory process making them interesting targets for imaging studies.

i. Vascular adhesion molecule (VCAM-1)

VCAM-1 (also called CD106) is and adhesion protein of the immunoglobulin superfamily expressed on endothelial cells. It is the most imaged adhesion molecule in atherosclerosis and neuroinflammation. VCAM-1 can be imaged using various tracers and techniques such as anti-VCAM-1 antibody conjugated to micron particles of iron oxide (MPIO) also named VCAM1-MPIO (McAteer et al., 2007) or A429 VCAM-1 antibody, which is more sensitive and allows imaging of subtle neuroinflammation on MRI (Montagne et al., 2012) both showing hypointensities on T2 weighted MRI. Monoclonal antibody A429 can also be coupled with microbubbles for ultrasound imaging enabling the visualizationof inflamed endothelium and *vasa vasorum*(Kaufmann et al., 2007; Wu et al., 2011). In nuclear imaging, ^{99m}Tc-cAbVCAM1-5nanobodies are available for SPECT (Broisat et al., 2012) and an in vivo phage display (VINP-28) labeled with ^{18}F for TEP/CT imaging of VCAM-1(Nahrendorf et al., 2009). This latter was for now only tested on mouse models of atherosclerosis and myocardial infarction but showed interesting properties.

ii. Intercellular adhesion molecule (ICAM-1)

ICAM-1 (also called CD54) is a member of immunoglobulin superfamily expressed by endothelial cells involved in leukocyte adhesion to endothelium. ICAM-1 can be imaged in systemic arteries using mostly anti-ICAM-1-conjugated bubbles for ultrasound (Villanueva et al., 1998). For neuroinflammation imaging, the MR tracer ICAM-MPIO which specifically bound brain endothelial cells in vitro after TNF stimulation and showsT2 hypointensities rapidly after induction of tMCAO stroke model in vivo(Deddens et al., 2013) is the most commonly used.

iii. P-selectin

P-selectin (also named CD62P) is an adhesion molecule expressed by platelets and activated endothelial cells. Several MRI probes exist for P-selectin imaging but most of them lack sensitivity. At these days, the most sensitive probe for P-selectin is a glyconanoparticle molecule (GNP-sLe^x) covered of a dextran-coated USPIO (van Kasteren et al., 2009)which is used for subclinical inflammatory foci imaging (Serres et al., 2009).

c) Myeloperoxidases imaging

As seen above, MPO is an important biomarker in cardiovascular diseases and its non-invasive detection can be performed by different imaging modalities. Indeed, MPO can be detected using a contrast agent, the MPO-activatable gadolinium chelate on MRI (Nahrendorf et al., 2008) or luminol on bioluminescence experiments (Gross et al., 2009). For SPECT modality, ^{111}In-bis-5HT-DTPA is used to visualize MPO in the arterial wall and plaques of humans and animals (Wu et al., 2012).

d) Matrix metalloproteinases (MMPs) imaging

MMPs are calcium-dependent zinc-containing endopeptidases capable of degrading all kinds of extracellular matrix proteins but also several bioactive molecules hence their role in the plaque rupture. They are known to be involved in cell surface receptors cleavage, release of apoptotic ligands and chemokine/cytokine inactivation (Van Lint and Libert, 2007). MMPs also play a role in cell behaviors such as proliferation, migration, differentiation, or apoptosis. MMPs can be imaged using ^{111}In-RP782 or ^{99m}Tc-RP05 on SPECT but also via MR imaging (P947) or NIRF (MMPsense) (Osborn and Jaffer, 2013).

This review of the literature highlights the importance of assessing in the same time inflammatory marker (especially hsCRP), lipidic profile (i.e. LDL-C) combined with plaque imaging is now acknowledged in human clinic as well as the relevance of exploring not one but multiple vascular territories for a better individual and global CV risk stratification and patient care.

In this second part, I have presented the different available biomarkers. Of note, as molecular imaging is still in development, we can easily imagine that new techniques and biomarkers will emerge in the near future. The next part of this manuscript focused on my research work, ultrasound and MRI were used for in vivo morphologic characterization of the arterial wall, and USPIO and ^{11}C-PK11195 for inflammation in large arteries and in brain.

AIMS AND OBJECTIVES

Atherosclerosis is a complex pathology combining a dyslipidemic context and a chronic low-grade inflammation resulting mainly in vascular lesions but also in cerebrovascular lesions still poorly explored. Indeed, inflammation combined with a lipotoxic context lead to a vicious circle of pernicious effects such as cerebrovascular unit disorganization. The high complexity of atherosclerosis process and outcomes requires the use of more accurate animal models, notably in taking account of the critical factor of age for cardiovascular risks, and capable of underwent translational explorations with both circulating and imaging biomarkers.

My PhD work was focused on atherosclerosis and its consecutive cerebrovascular lesions in term of inflammation and blood-brain barrier leakage. For this, I used different animal models of atherosclerosis, as aged ApoE$^{-/-}$ mice and non-human primates fed an atherogenic diet and focused on imaging and biological biomarkers to assess plaque-induced cerebrovascular inflammation.

First, we used aged ApoE$^{-/-}$ mice as they are a well-known atherosclerosis model and their predisposition to plaque development combined with a high cholesterol diet and an advanced age offered a maximal cardio-metabolic risk context. The aim of our first study was to assess the effect of voluntary regular exercise training on central and peripheral deleterious effects of a high cholesterol diet in aged ApoE$^{-/-}$ mice. For this study, mice were fed according to their metabolic needs (**article n°1**).

Then in a second time, as the results of the first study showed that when mice were fed with controlled high cholesterol diet the exercise training reduced the cerebrovascular lesions and the inflammatory and oxidative status, we wanted to assess whether the same protective effects of training can be observed when the high cholesterol diet is given *ad libitum* (**article n°2**).

The last part of my thesis was based on a non-human primate model of atherosclerosis. We used aged Cynomolgus monkeys (*Macaca fascicularis*) under atherogenic diet to assess if a combination of multi-modalities imaging (ultrasound, MRI and PET/CT) and biological analysis can allow an accurate stratification of the individual cardio and cerebrovascular risk (**article n°3**).

In summary, my PhD work focused on a biomarker approach of general inflammation and cerebrovascular integrity in atherosclerosis animal models to determine was is the most efficient and relevant combination of biomarkers, using translational imaging techniques, biological and genomic analysis.

RESULTS

ARTICLE n°1

MRI biomarkers of exercise-induced improvement of oxidative stress and inflammation in the brain of old high fat fed ApoE$^{-/-}$ mice

Erica N Chirico, **Vanessa Di Cataldo**, Fabien Chauveau, Alain Geloen, David Patsouris, Benoît Theze, Cyril Martin, Hubert Vidal, Jennifer Rieusset, Vincent Pialoux, and Emmanuelle Canet-Soulas

Journal of Physiology 2016. doi: 10.1113/JP271903

ARTICLE N°1:

Vascular brain lesions present in advanced atherosclerosis share pathological hallmarks with peripheral vascular lesions such as inflammation and oxidative stress. Physical activity was shown to reduce these peripheral risk factors, but few studies were published on its cerebrovascular effects. The aim of this study was to assess whether the beneficial effect of exercise training on inflammation and oxidative stress could be used as an intervention option in an aging atherosclerosis mouse model. The characterization of vascular brain damage in old ApoE$^{-/-}$ mice fed a high fat diet with dietary controlled intake was performed using a combination of in vivo imaging and post-mortem analysis.

ApoE$^{-/-}$ mice and C57Bl/6 (used as control) were divided into five groups: old untrained and exercise trained ApoE$^{-/-}$ (respectively O-ApoE-UT and O-ApoE-ExT; 60 weeks-old), young untrained ApoE$^{-/-}$ (Y-ApoE-UT; 10 weeks-old), old untrained and exercise trained C57BL/6 (respectively O-C57-UT and O-C57-ExT; 60 weeks-old). ApoE$^{-/-}$ mice were fed a high fat diet (0.15% cholesterol, 21% lard fat) since 8 weeks of age with a dietary controlled intake (20g per week per animal) when C57BL/6 were fed a standard diet. Exercise trained mice were housed separately and have free access to a running wheel in their cages, while untrained were housed in small groups in standard cages (see **Figure 22** for study design).

At the end of the 12-weeks training, insulin tolerance test was performed to assess the glucidic status of mice. *In vivo* MRI of brain and descending aorta was performed using contrast agents (Gadolinium and ultrasmall superparamgnetic iron oxide particle, USPIO) to quantify vascular permeability and macrophage accumulation in these two locations. After mice sacrifice, immunochemistry was realized on brain to confirm MRI observations (IgG for blood-brain barrier permeability and F4/80 for macrophages staining). Biological analysis were performed on heart, brain, aorta and liver to assess inflammation (IL-1β, TNFα) and oxidative stress (AOPP, catalase, FRAP, GPX, MDA, NOx, nitrotyrosine and SOD). Moreover, plasmatic cholesterol level was measured.

The training was effective as showed by the significantly increased citrate synthase activity and no weight variation was observed between trained and untrained ApoE$^{-/-}$ mice. O-ApoE-ExT showed an improvement of metabolic features (plasmatic cholesterol level and insulin sensitivity), and a reduced systemic and tissular (aorta, heart and liver) inflammation and oxidative stress, suggesting a protective effect of exercise on peripheral features. Furthermore, O-ApoE-ExT mice presented less aortic plaque with less macrophage accumulation and a better survival rate than the untrained (respectively 77% and 49%). Some hemi- and paraplegia events were observed in old ApoE$^{-/-}$ mice, especially in the untrained group. Brain abnormalities such as blood-brain barrier leakage and

macrophage accumulation were detected by MRI in periventricular areas of old ApoE$^{-/-}$ mice of both trained and untrained group. These abnormalities were significantly reduced by exercise training (observed in 14% of trained mice versus 71% of untrained), as well as inflammation and oxidative stress, suggesting that training also have a protective central effect.

Highly localized vascular brain damages are frequent in this aging atherosclerosis model and exercise is able to reduce this outcome and improve lifespan. *In vivo* MRI allowed evaluation of both neurovascular damage and protective effect of exercise.

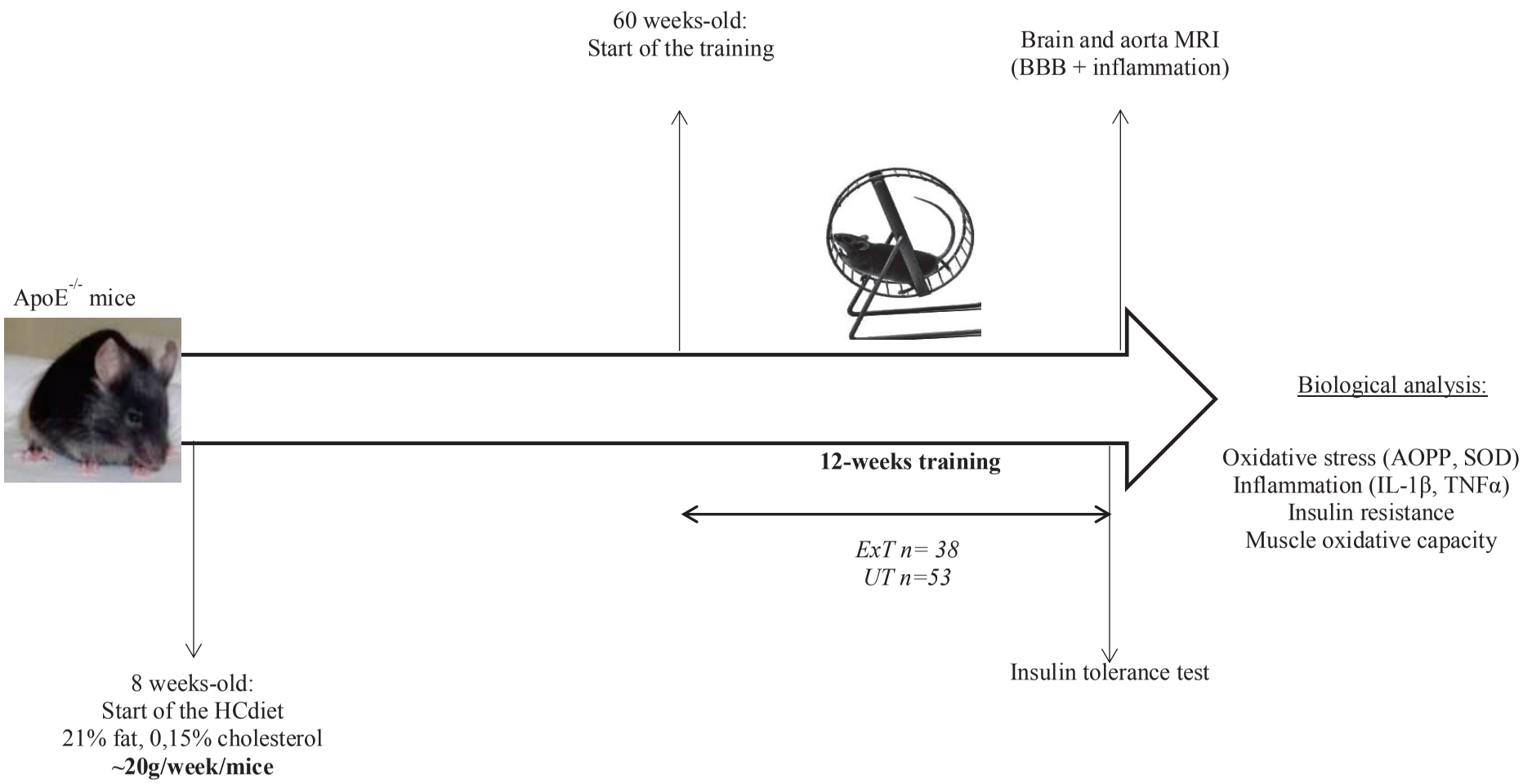

Figure 22: Study design J Physiol, 2016

J Physiol 594.23 (2016) pp 6969–6985

The Journal of Physiology

Magnetic resonance imaging biomarkers of exercise-induced improvement of oxidative stress and inflammation in the brain of old high-fat-fed ApoE$^{-/-}$ mice

Erica N. Chirico[1,2,3], Vanessa Di Cataldo[1], Fabien Chauveau[4], Alain Geloën[1], David Patsouris[1], Benoît Thézé[5], Cyril Martin[2], Hubert Vidal[1], Jennifer Rieusset[1], Vincent Pialoux[2] and Emmanuelle Canet-Soulas[1]

[1]*Cardiovascular, Metabolism, Diabetes and Nutrition (CarMeN INSERM U-1060), Faculty of Medicine Hospital Lyon Sud, University of Lyon, University Lyon 1, Oullins, France*
[2]*Laboratoire Inter-Universitaire de Biologie de la Motricité, University of Lyon, University Lyon 1, (LIBM EA7424), Villeurbanne, France*
[3]*Department of Biomedical Sciences, Cooper Medical School of Rowan University, Camden, NJ, USA*
[4]*Lyon Neuroscience Research Centre, Université de Lyon, Université Lyon 1, CNRS UMR5292; Inserm U1028, Lyon, France*
[5]*Laboratoire Réparation et Vieillissement, Institut de Radiobiologie Cellulaire et Moléculaire, CEA, Fontenay-aux-Roses, France*

Key points

- Vascular brain lesions and atherosclerosis are two similar conditions that are characterized by increased inflammation and oxidative stress.
- Non-invasive imaging in a murine model of atherosclerosis showed vascular brain damage and peripheral inflammation.
- In this study, exercise training reduced magnetic resonance imaging-detected abnormalities, insulin resistance and markers of oxidative stress and inflammation in old ApoE$^{-/-}$ mice.
- Our results demonstrate the protective effect of exercise on neurovascular damage in the ageing brain of ApoE$^{-/-}$ mice.

Abstract Vascular brain lesions, present in advanced atherosclerosis, share pathological hallmarks with peripheral vascular lesions, such as increased inflammation and oxidative stress. Physical activity reduces these peripheral risk factors, but its cerebrovascular effect is less documented, especially by non-invasive imaging. Through a combination of *in vivo* and post-mortem techniques, we aimed to characterize vascular brain damage in old ApoE$^{-/-}$ mice fed a high-cholesterol (HC) diet with dietary controlled intake. We then sought to determine the beneficial effects of exercise training on oxidative stress and inflammation in the brain as a treatment option in an ageing atherosclerosis mouse model. Using *in vivo* magnetic resonance imaging (MRI) and biological markers of oxidative stress and inflammation, we evaluated the occurrence of vascular abnormalities in the brain of HC-diet fed ApoE$^{-/-}$ mice >70 weeks old, its association with local and systemic oxidative stress and inflammation, and whether both can be modulated by exercise. Exercise training significantly reduced both MRI-detected abnormalities (present in 71% of untrained *vs.* 14% of trained mice) and oxidative stress (lipid peroxidation, 9.1 ± 1.4 *vs.* 5.2 ± 0.9 μmol mg^{-1}; $P < 0.01$) and inflammation (interleukin-1β, 226.8 ± 27.1 *vs.* 182.5 ± 21.5 pg mg^{-1}; $P < 0.05$) in the brain, and the mortality rate. Exercise also decreased peripheral insulin resistance, oxidative stress and inflammation, but significant associations were seen only within brain markers. Highly localized vascular brain damage is a frequent finding in

V. Pialoux and E. Canet-Soulas contributed equally to the supervision of this work.

DOI: 10.1113/JP271903

O-ApoE-ExT, respectively), young untrained ApoE$^{-/-}$ mice (Y-ApoE-UT) and old untrained and exercise-trained C57BL/6 (O-C57-UT and O-C57-ExT, respectively). Using *in vivo* MRI, the ascending aorta and brain were imaged, and contrast agents (iron oxide nanoparticles, P-904 and gadolinium Gd-DOTA; Guerbet, Aulnay-sous-Bois, France) were used to quantify macrophage infiltration and vascular permeability. At the end of the study, plasma measurements and tissue samples were taken. Total blood cholesterol, insulin, oxidative stress markers [advanced oxidation protein products (AOPP), malondialdehyde (MDA) and nitrotyrosine], antioxidant markers [catalase, glutathione peroxidase (GPX), superoxide dismutase (SOD), ferric reducing antioxidant power (FRAP) and nitric oxide metabolites (NOx)] and inflammatory markers [tumour necrosis factor-α (TNFα), interleukin-1β (IL-1β) and nuclear factor-κB (NF-κB)/p65] were measured. Brain samples were stained with standard Haematoxylin and Eosin, F4/80 immunostaining for macrophages and IgG immunostaining for BBB permeability.

Animals

Male and female ApoE$^{-/-}$ mice (C57BL/6 background; Charles-River, France) were fed a HF/HC diet (western diet; 21% fat, 0.15% cholesterol; U8220 version 153; SAFE, Augy, France) starting at 8 weeks of age, and control male and female C57BL/6 mice (Charles-River, France) were fed a normal diet (Teklad Global 16% Protein rodent diet with 12% fat; Harlan, Gannat, France). All animals were maintained on a 12 h–12 h light–dark cycle and were supplied with food (limited at 20 g week^{-1} per animal, equivalent to 955 kcal week^{-1} for ApoE$^{-/-}$ mice and 688 kcal week^{-1} for C57BL/6 mice) and water *ad libitum*. After careful maintenance of health conditions for 1 year (Guerbet, Animal Care Unit), at 60 $\pm$ 1 weeks old both ApoE$^{-/-}$ and C57 mice were randomly divided into two activity groups (untrained, UT; and exercise trained, ExT). Mice in the exercise-trained group (O-ApoE-ExT and O-C57-ExT) were individually housed in cages equipped with a 12.5 cm metal running wheel (HAGEN-61700, Montreal, QC, Canada) and digital magnetic counter (model BC906; Sigma Sport, Neustadt, Germany), whereas the untrained (O-ApoE-UT and O-C57-UT) groups had a standard cage. Male and female young-adult ApoE$^{-/-}$ mice (Y-ApoE-UT; aged 10 weeks) fed the same high-fat diet (starting at 8 weeks of age; fed the diet for 14 weeks in total) served as age controls. During the 12 weeks of training, the distance run and the general health (i.e. tumours, skin irritations) of the mice were noted three times a week. The exclusion criterion was overall poor health of the animal (i.e. tumours, skin irritations). A follow-up was performed daily by the technician in the animal facility to evaluate pain on the basis of external physical appearance, weight loss (with respect to food and water ingestion), assessable clinical signs (in particular, increase in respiratory frequency), change in behaviour (in particular, prostration) and non-response to external stimuli.

Magnetic resonance imaging protocol

Mice were randomly selected to undergo the imaging protocol. The mice were anaesthetized by inhalation of isoflurane (2% for induction and 1% to maintain anaesthesia; Tem Sega, Lormont, France). Cardiac and respiratory rates were monitored throughout the session, and body temperature was maintained using a circulating heated water blanket at 37 $\pm$ 1°C. Magnetic resonance image acquisition was performed on a 4.7 T Bruker magnet (Ettingen, Germany). The total duration of the MRI protocol was <2 h. The protocol was then repeated 48 h after the injection of ultrasmall iron oxide nanoparticles (USPIO; P904, 1 mmol Fe kg^{-1}; Guerbet) for vessel wall inflammation assessment, followed by the acquisition of brain images (Fig. 1).

Magnetic resonance imaging of the aorta. For imaging of the ascending aorta, double cardiac and respiratory gated acquisitions were obtained as previously described (Sigovan *et al.* 2012) with a homemade gating system developed in Matlab (The MathWorks Inc., Natick, MA. USA). Electrocardiographic signals were collected via three electrodes placed on the paws, and respiratory signals were collected via a pressure sensor placed on the abdomen.

The ascending and descending aorta was identified using reference axial slices. A bright-blood cine-mode FLASH sequence was used to locate the aortic arch. The reference slices were acquired with a gradient echo (GE) sequence with the following parameters: repetition time (TR) / echo time (TE) = one R–R interval/6.7 ms; field of view = 3.8 cm $\times$ 3.8 cm; matrix = 256 $\times$ 256; bandwidth, 25 kHz; and slice thickness = 1.1 mm. The oblique

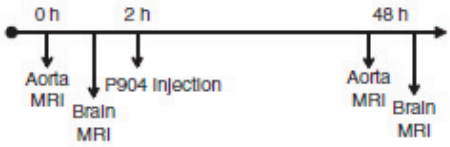

Figure 1. Magnetic resonance imaging (MRI) protocol
A pre-contrast imaging (0 h) protocol was performed on the aorta, followed immediately by brain imaging with gadolinium injection. An ultrasmall iron oxide nanoparticles (USPIO) contrast agent, P904 (Guerbet, Aulnay-sous-Bois, France), was then injected. Forty-eight hours later (48 h), an identical post-USPIO aortic imaging protocol was performed for assessment of inflammation. This was followed immediately by brain inflammation imaging.

Table 1. Visual lesion characteristics

Score	Pre-contrast image	Post-contrast image
1	No abnormality	No observable change from pre-contrast
2	Small lesions (>10 pixels) on ≤2 slices	Change in SNR and increase in dark region size from pre-contrast on ≤2 slices
3	>2 slices or medium-sized lesion (10 < pixels < 20) on ≤2 slices	Medium change in SNR and increase in dark region size from pre-contrast on ≤2 slices
4	Large lesion (>20 pixels) on >2 slices	Major change in SNR and increase in dark region size from pre-contrast on >2 slices

Abbreviations: SNR, signal-to-noise ratio

slice was placed perpendicular to the ascending aorta, directly above the sinus to avoid flow artifacts.

A black-blood multigradient echo sequence was used to image USPIO accumulation using the same slice number and positioning, spatial resolution, partial echo acquisition, and the following parameters: minimal repetition time, 742 ms (achieved by setting the gating system between three and five R–R intervals depending on the animal's heart rate); four echoes; bandwidth, 79.3 kHz; and number of averages, 2. The sequence was performed twice with two different values of TE: 3.1 ms, followed by 4.0 ms. The eight echo images acquired were interleaved to allow a better sampling of the T2* decay curve.

Magnetic resonance imaging of the brain. For brain imaging, a birdcage coil of 72 mm i.d. was used for radiofrequency transmission and a surface coil anatomically shaped to the mouse head for reception (Rapid Biomedical, Wurzburg, Germany).

Brain T2-weighted spin-echo images were acquired using a Rapid Imaging with Refocused Echoes (RARE) sequence in both axial and coronal planes. T2 RARE and T2* multi gradient echo (MGE) sequence positioned using standard MRI brain anatomical references for careful pre- and post-contrast registration were acquired. The RARE sequence was used with the following parameters: TR/TE = 4000 /69 ms; field of view = 2 cm × 2 cm; matrix = 256 × 256; slice thickness = 1 mm; RARE factor = 8; and number of slices = 15. The MGE sequence was used with the following parameters: TR/first TE = 1500/2.6 ms; flip angle = 75 deg; field of view = 2 cm × 2 cm; matrix = 256 × 192; slice thickness = 1 mm; 12 echoes and echo interval = 3.5 ms; and number of slices = 15.

In order to characterize the neurovascular lesions, an extended brain MRI protocol was performed in a separate set of old untrained ApoE$^{-/-}$ mice fed the HF/HC diet (n = 10) and old C57BL/6 mice. Neurovascular lesions and iron deposits were assessed respectively by baseline T2 and T2* imaging. T2* quantification was obtained using a multislice multi-echo gradient echo sequence. For BBB permeability assessment, a T1-weighted MGE sequence with identical geometrical parameters was acquired before and 10 min after injection of gadolinium chelate (Gd-DOTA, 0.1 mmol kg^{-1}; Guerbet, Aulnay-sous-Bois, France) with the following parameters: TR/TE = 124/2.8 ms; field of view = 2 cm × 2 cm; matrix = 256 × 192; slice thickness = 1 mm; and number of slices = 15. This was followed by USPIO injection and the 48 h post-USPIO T2/T2* imaging.

Analysis of MRI. For brain analysis, areas of interest on pre-USPIO T2/T2* images and post-gadolinium T1 images were first visually categorized based on the size of abnormal areas and the number of slices affected. The blinded investigators scored changes in pre- and post-contrast (48 h post-USPIO) T2/T2* images and gadolinium leakage on T1-weighted images. Briefly, a score of 1–4 was given for abnormalities seen on pre-contrast images and a score of 1–4 was given for changes seen on post-contrast images (see Table 1 for scoring assessment).

For analysis of the aortic arch, inner and outer vessel wall contours were delineated and vessel wall area calculated. T2* mapping of pre- and post-USPIO series was performed using Matlab (The MathWorks Inc.,) on interleaved multi-slice-multi-echo (MSME) images. The vessel wall regions of interest were used for the analysis of aortic T2* on both pre- and post-contrast images as described by Sigovan *et al.* (2010).

Dissections

After the second imaging session, mice were anaesthetized by an I.P. injection of pentobarbital (50 mg kg^{-1}; Dolethal; Vétoquinol, Lure, France) and blood was collected by cardiac puncture. Mice were killed by exsanguination with a 0.9% NaCl transcardial perfusion for 70 s. The brain, heart, ascending–descending aorta, liver and soleus were removed. Sections to be used for biological assays were stored at −80°C until assessment.

at 450 nm after excitation at 365 nm. Nitrates are converted to nitrite by nitrate reductase.

Nitrotyrosine. Concentrations of plasma nitrotyrosine, as the end-product of protein nitration by $ONOO^-$, were measured by a competitive enzyme-linked immunosorbent assay as previously described (Galiñanes & Matata, 2002) using precoated nitrated bovine serum albumin microplates and subsequent incubations and washings with anti-nitrotyrosine and anti-rabbit IgG–HRP conjugate. The concentration of nitrotyrosine was then calculated using nitrated bovin serum albumin as the standard.

Superoxide dismutase. The quantitative determination of SOD activity was performed on the plasma, aorta, heart, liver and brain using the method of Beauchamp & Fridovich (1971), slightly modified by Oberley & Spitz (1985). The SOD activity was determined by the degree of inhibition of the reaction between superoxide radicals, produced by a hypoxanthine–xanthine oxidase system, and nitroblue tetrazolium. The formazan blue subsequently formed was read at 560 nm for 5 min.

Cholesterol and metabolic measurements. Total blood cholesterol was assessed using an Amplex Red Cholesterol Assay Kit as instructed by Invitrogen (Carlsbad, CA, USA). One week before MRI, an intraperitoneal insulin tolerance test was performed on mice fasted for 6 h. Mice were injected I.P. with 0.75 mU (g body weight)$^{-1}$ of insulin. Blood was taken by tail puncture immediately before and at 15, 30, 45 and 60 min time points after injection for measurement of blood glucose.

All reagents used for biochemical assays were purchased from Sigma-Aldrich.

Inflammatory markers. Tumour necrosis factor-α (BD Biosciences, San Jose, CA, USA) and IL-1β (RayBiotech, Inc., Norcross, GA, USA) were assessed in plasma, aorta and brain supernatant, and interleukin-4 (IL-4; Abcam, Cambridge, UK) in brain supernatant using a commercially available mouse enzyme-linked immunosorbent assay kit, according to the manufacturer's instructions. The NF-κB/p65 activity (Imgenex, San Diego, CA, USA) was assessed in plasma according to the manufacturer's instructions.

Statistics

Statistical analyses were conducted using Statistica (version 8.0; Statsoft, Tulsa, OK, USA). Results are presented as means ± SD. For each parameter, a minimum of seven mice per group was used. Statistical comparisons between five groups (O-ApoE-UT, O-ApoE-ExT, Y-ApoE-UT, O-C57-UT and O-C57-ExT) were performed by one-way ANOVA followed by Bonferroni *post hoc* test. Pearson's coefficient correlations were used to determine the associations between plasma markers, brain markers and distance run. A logrank test was used for survival curve analysis. Statistical significance was determined by a P value of <0.05. All the animals that did not complete the study were excluded from all the analyses carried out except for the calculation of the survival rate.

Results

Animal characteristics and general effects of exercise

Ninety-one old ApoE$^{-/-}$, 20 young-adult ApoE$^{-/-}$ and 16 old C57BL/6 (O-C57) mice were originally included in the protocol. These animals were vulnerable to cerebrovascular disease, especially in the older cohorts, and a number of animals died prior to any biological assessment. The majority of these animals died spontaneously; however, seven mice died after signs of mono- or hemiplegia (all being old ApoE$^{-/-}$ mice, representing 13% of all deaths of this group), a possible symptom of cerebrovascular disease. Of the mice that died during the protocol, 29 were in the O-ApoE-UT group, 10 were in the O-ApoE-ExT group (Fig. 2), one in the O-C57-UT and one in the O-C57-ExT group. An additional six mice died during the insulin resistance test or MRI, and three mice were excluded at autopsy because of large tumours. After the induction and training period, 43 old ApoE$^{-/-}$ mice (19 O-ApoE-UT, 72.4 ± 2.4 weeks; and 24 O-ApoE-ExT, 71.8 ± 1.9 weeks) and 20 young-adult mice (Y-ApoE-UT, 20 ± 0 weeks) were used for biological assessment (Table 2). The O-ApoE-ExT mice ran 17.8 ± 15.3 km week^{-1}, whereas the O-C57-ExT mice ran 16.2 ± 8.8 km week^{-1}. The training effect was supported by higher CS activity in the soleus of both O-ApoE-ExT and O-C57-ExT mice compared with the

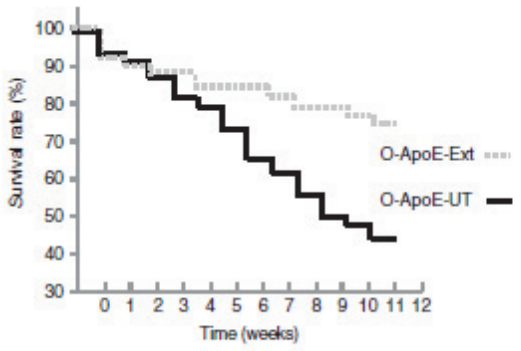

Figure 2. Survival rate for old untrained (O-ApoE-UT) and exercise-trained (O-ApoE-ExT) ApoE$^{-/-}$ mice ($P = 0.03$)

Table 2. Number of mice at inclusion, that died spontaneously, that died during experimental procedures, excluded after dissection for large tumours and used for biological assessments

	Y-ApoE-UT	O-ApoE-UT	O-ApoE-ExT	O-C57-UT	O-C57-ExT
Mice at inclusion (*n*)	20	53	38	8	8
Mice that died spontaneously (*n*)	0	29	10	1	1
Mice that died during ITT and MRI (*n*)	0	3	3	0	0
Mice excluded after dissection for large tumours (*n*)	0	2	1	0	0
Mice used for biological assessments (*n*)	20	19	24	7	7

Abbreviations: ITT, insulin tolerance test; MRI, magnetic resonance imaging; O-C57-ExT, old C57BL/6 exercise trained; O-C57-UT, old C57BL/6 untrained; O-ApoE-ExT, old ApoE$^{-/-}$ exercise trained; O-ApoE-UT, old ApoE$^{-/-}$ untrained; and Y-ApoE-UT, young-adult ApoE$^{-/-}$ untrained.

Table 3. Effect of age and exercise training on body weight, citrate synthase activity, cholesterol and insulin resistance

Parameter	Y-ApoE-UT	O-ApoE-UT	O-ApoE-ExT	O-C57-UT	O-C57-ExT
Body weight (g)	32.7 ± 1.5	40.2 ± 1.5*	38.5 ± 1.5*	27.2 ± 1.2	27.7 ± 1.1
Citrate synthase activity (nmol min^{-1} mg^{-1})	3.68 ± 0.2	6.76 ± 0.8*	8.50 ± 0.2*†	4.92 ± 0.42*	8.44 ± 0.86*†
Cholesterol (mmol l^{-1})	22.0 ± 4.1	18.2 ± 2.0	15.5 ± 1.2*†	6.2 ± 0.6‡	5.0 ± 0.4*‡
Insulin resistance (%)	−20.7 ± 8.1	−11.6 ± 2.2*	−22.3 ± 2.8†	−24.9 ± 2.4	−26.5 ± 1.9

Insulin resistance was estimated as the percentage change of glycaemia at 30 min (*vs.* baseline) during an insulin tolerance test. Groups are as in Table 2. *Significantly different ($P < 0.05$) from young. †Significantly different ($P < 0.05$) from corresponding untrained. ‡Significantly different ($P < 0.05$) from corresponding ApoE−/−.

corresponding UT mice (see Table 2). Despite higher plasma cholesterol concentrations in all ApoE$^{-/-}$ mice compared with old C57 mice (independently of training), Y-ApoE-UT mice had higher insulin sensitivity than O-ApoE-UT mice (Table 3). The training effect was also evident on both insulin sensitivity and plasma cholesterol concentrations in the O-ApoE-ExT *vs.* the corresponding untrained mice (see Table 2). Importantly, the O-ApoE-ExT mice had a significantly higher survival rate compared with the O-ApoE-UT mice (77 *vs.* 49%; $P = 0.03$; Fig. 2), Exercise training was therefore able to decrease the mortality rate of the old ApoE$^{-/-}$ mice. Both O-C57-UT and O-C57-ExT mice had a survival rate of 87%, which was significantly higher than the old ApoE$^{-/-}$ mice, confirming the pathological state of our old ApoE$^{-/-}$ mice.

Presence of multiple neurovascular lesions in old sedentary ApoE$^{-/-}$ mice on the HF/HC diet

As observed by *in vivo* MRI and histology, there were significant abnormalities in the brain vasculature of O-ApoE-UT mice (Fig. 3), whereas O-C57-UT mice did not show such abnormalities as indicated by significantly lower scoring between old O-ApoE-UT and O-C57-UT for both post-USPIO T2 and post-gadolinium T1 images (Fig. 3). On pre-contrast images, several dark areas on T2 images and T2* images indicated iron accumulation in a large number of O-ApoE-UT mice at the same periventricular location (71% of O-ApoE-UT *vs.* 0% for O-C57-UT). Post-gadolinium T1 images indicated the presence of periventricular BBB leakage and endothelial permeability in O-ApoE-UT mice (gadolinium score of 2.7 ± 0.80 for O-C57-UT mice *vs.* 1.42 ± 0.23 for O-C57-UT, $P < 0.05$; Fig. 3). Comparing the pre- and post-USPIO T2 images (Fig. 3), it was evident that there was also an accumulation of iron oxide nanoparticles. Given that circulating iron oxide nanoparticles would have been cleared from the circulation, this suggests the presence of macrophages and phagocytic activity in the same area. These signs of neuro-inflammation observed on both post-USPIO T2* and T2 images were confirmed by histology (Figs 4 and 6). Disorganized brain parenchyma was seen in the middle ventral zone, but was not related to an active apoptotic process (TUNEL negative on immunohistochemistry; data not shown). There was also an anatomical correspondence between this abnormal area in both T2/T2* images and post-gadolinium T1 images, which was histologically confirmed respectively by positive staining for IgG and F4/80. This would indicate BBB leakage (endothelial permeability). There was also some evidence of vesicular aggregates, which could indicate foam cell development (data not shown).

Brain MRI in trained *vs.* untrained old ApoE$^{-/-}$ mice

There were significantly more abnormalities in the brain vasculature of O-ApoE-UT ($n = 7$; 71% of mice) compared

with O-ApoE-ExT mice ($n = 7$, 14% of mice). Comparing the pre-USPIO images (respective scores, 1.71 ± 0.19 *vs.* 1.29 ± 0.19; $P = 0.12$) with post-USPIO images, there was more USPIO accumulation in O-ApoE-UT mice (*vs.* O-ApoE-ExT), suggesting phagocytic activity and inflammation (Figs 3 and 4) as indicated by the significantly higher post-USPIO T2* score in O-ApoE-UT mice compared with O-ApoE-ExT mice (2.92 ± 0.49 *vs.* 1.69 ± 0.44; $P < 0.05$).

Old ApoE$^{-/-}$ mice expressed higher brain oxidative stress and inflammation than old C57 and young ApoE$^{-/-}$ mice

Malondialdehyde, AOPP, Il-1β and TNFα were significantly lower and FRAP significantly higher in O-C57-UT than in O-ApoE-UT mice ($P < 0.01$), confirming the brain pathological state of our old ApoE$^{-/-}$ mice (Table 4). Superoxide dismutase and GPX were not different between O-C57-UT and O-ApoE-UT groups (Table 4). Brain concentrations of the oxidative stress marker MDA and the pro-inflammatory markers TNFα and IL-1β were significantly higher in both O-ApoE-UT and O-ApoE-ExT compared with Y-ApoE-UT mice ($P < 0.01$). On the contrary, SOD and GPX (see Table 4) and IL-4 (O-ApoE-UT, 2.34 ± 0.83 pg mg^{-1} *vs.* Y-ApoE-UT, 5.04 ± 3.26 pg mg^{-1}; $P < 0.05$) were decreased with age in ApoE$^{-/-}$ mice.

Exercise-induced changes in markers of oxidative stress and inflammation in the brain of old ApoE$^{-/-}$ mice (Table 4)

In the brain, MDA and AOPP were decreased in response to exercise training ($P < 0.01$ and $P < 0.05$, respectively). Moreover, there was an increase in brain catalase ($P < 0.05$) and a decrease in Il-1β and TNFα in O-ApoE-ExT compared with O-ApoE-UT mice ($P < 0.05$). Brain concentrations of IL-4 were significantly higher in O-ApoE-ExT compared with O-ApoE-UT mice (5.70 ± 3.87 *vs.* 2.34 ± 0.83 pg mg^{-1} for O-ApoE-ExT and O-ApoE-UT, respectively; $P < 0.05$). The FRAP, GPX and SOD were not significantly affected by exercise in old ApoE$^{-/-}$ mice.

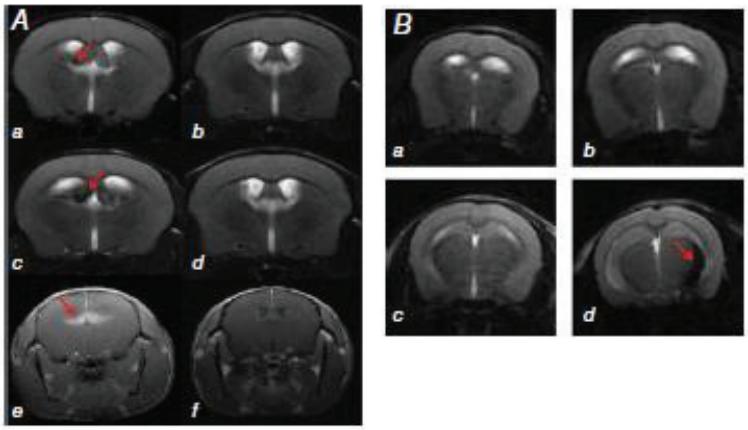

C	O-ApoE-UT	O-ApoE-ExT	O-C57-UT	O-C57-ExT
T2* Pre-Contrast Score	1.71 ± 0.2	1.29 ± 0.2	1.44 ± 0.2	1.30 ± 0.3
T2* Post-Contrast Score	2.92 ± 0.5‡†	1.69 ± 0.4‡*	1.50 ± 0.2	1.43 ± 0.2
Gadolinium Score	2.70 ± 0.8†	n.a.	1.42 ± 0.3	1.36 ± 0.2

Figure 3. Brain magnetic resonance imaging of old untrained C57 and trained and untrained ApoE$^{-/-}$ mice
A, brain MRI in old untrained ApoE$^{-/-}$ (O-ApoE-UT, left panel) *vs.* old untrained C57 mice (O-C57-UT, right panels; pre-USPIO T2 MRI, *a* and *b*; and 48 h post-USPIO T2 MRI, *c* and *d*; post-gadolinium T1 MRI, *e* and *f*). In O-ApoE-UT mice, red arrows indicate a hypointense region, suggesting inflammation, in *a* and *c*, and bright zone in *e*, suggesting BBB leakage. *B*, brain T2 MRI (pre-USPIO, *a* and *b*; and 48h-post-USPIO, *c* and *d*) in untrained (O-ApoE-UT, left panels) *vs.* trained old ApoE$^{-/-}$ mice (O-ApoE-Ext, right panels) showing a hypointense region (red arrow in *d*) demonstrating inflammation in the left periventricular fornix fimbria in the O-ApoE-UT mouse, and a normal image in the O-ApoE-ExT (*d*). *C*, brain pre- and post-USPIO T2* scores and post-gadolinium T1 score for old sedentary and trained ApoE$^{-/-}$ mice (O-ApoE-UT and O-ApoE-ExT, respectively) and old sedentary and trained C57 mice (O-C57-UT and O-C57-ExT, respectively). *Significantly different ($P < 0.05$) O-ApoE-ExT *vs.* O-ApoE-UT. †Significantly different ($P < 0.05$) O-C57-UT *vs.* O-ApoE-UT. ‡Significantly different ($P < 0.05$) from pre-contrast.

Magnetic resonance imaging of the aorta and biological vessel wall response

The O-ApoE-UT mice had a larger vessel wall area than the Y-ApoE-UT mice (4.02 ± 0.22 *vs.* 2.66 ± 0.03 mm^2; $P < 0.01$). In the O-ApoE-ExT mice, vessel wall area was reduced compared with O-ApoE-UT mice (see Fig. 5). Concerning T2* measurements, both pre- and post-USPIO values in O-ApoE-UT mice were lower than in Y-ApoE-UT mice, confirming more complex plaque composition and more inflammatory activity, respectively (Mihai *et al.* 2011). The O-ApoE-ExT mice had an increase in pre-USPIO T2* measurement compared with O-ApoE-UT mice, suggesting a less complex plaque composition (see Fig. 5). Post-USPIO T2* was lower than pre-contrast values for all the groups, indicating the presence of iron particles and phagocytic activity in the vessel wall. In the aorta, both O-ApoE-ExT and O-ApoE-UT mice had more TNFα, IL-1β and AOPP than Y-ApoE-UT mice, whereas only O-ApoE-UT mice had more SOD than Y-ApoE-UT mice. The O-ApoE-UT mice had more TNFα, IL-1β, AOPP and SOD in the aorta than O-ApoE-ExtT mice (see Table 5; $P < 0.05$). The AOPP, Il-1β and TNFα in the aorta were much lower in old C57 than in old ApoE$^{-/-}$ mice independent of exercise training ($P < 0.01$), which strengthens the atherosclerotic phenotype seen in the aorta of old ApoE$^{-/-}$ mice.

Heart markers

Heart concentrations of AOPP were higher in O-ApoE-UT compared with Y-ApoE-UT mice. The O-ApoE-UT

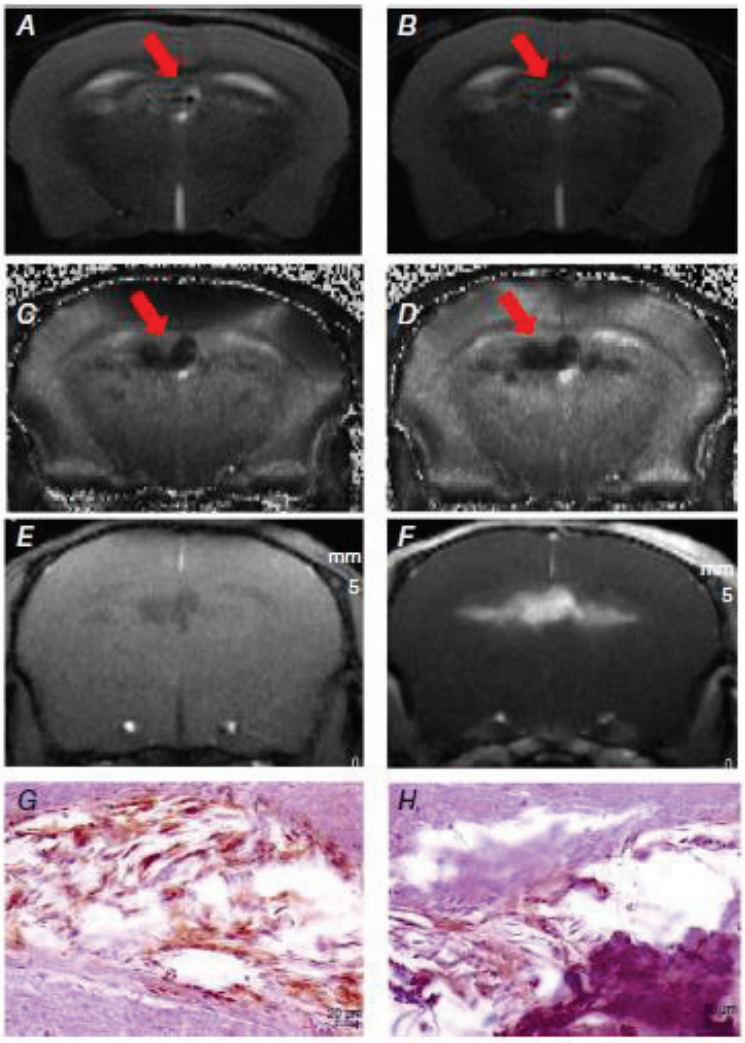

Figure 4. Brain magnetic resonance images of an old untrained ApoE$^{-/-}$ mouse
Pre- (*A*) and post-USPIO (*B*) T2 images, both showing hyposignal and heterogeneous regions around the choroid plexus representative of vascular sequelae (*A*, arrow) and inflammation (*B*, arrow). Pre- (*C*) and post-USPIO (*D*) T2* maps, with an increase of the hyposignal region on post-USPIO, suggesting iron deposits (*C*, arrow) and phagocytic activity (*D*, arrow). Pre- (*E*) and post-gadolinium (*F*) T1 images, the enhancing bright zone showing BBB leakage in the same area (*F*). *G*, positive F4/80 staining, confirming macrophages in this area. *H*, positive IgG staining in the same locations, confirming MRI findings of blood–brain barrier leakage.

Table 4. Effect of age and exercise training on brain markers of inflammation and oxidative stress

Marker	Y-ApoE-UT	O-ApoE-UT	O-ApoE-ExT	O-C57-UT	O-C57-ExT
MDA (μmol mg^{-1})	3.8 ± 0.6	9.1 ± 1.4*	5.2 ± 0.9*†	1.6 ± 1.3†	0.7 ± 0.3†
TNFα (pg mg^{-1})	47.4 ± 3.7	137.9 ± 20.8*	114.1 ± 8.9*†	36.6 ± 4.0†	31.2 ± 4.7*†
IL-1β (pg mg^{-1})	127.7 ± 18.7	226.8 ± 27.1*	182.5 ± 21.5*†	84.5 ± 19.7†	88.3 ± 13.2†
AOPP (μmol mg^{-1})	14.5 ± 1.1	16.1 ± 1.4	12.7 ± 1.2†	3.1 ± 1.1†‡	4.8 ± 2.5†‡
Catalase (μmol min^{-1} mg^{-1})	174.1 ± 14.6	65.5 ± 6.3*	90.2 ± 11.5*†	33.7 ± 10.4*‡	46.3.2 ± 29.3*‡
GPX (μmol min^{-1} mg^{-1})	168.0 ± 11.4	74.3 ± 1.5*	74.7 ± 12.0*	77.0 ± 13.9*	73.9 ± 10.1*
FRAP (μmol mg^{-1})	62.2 ± 4.1	56.9 ± 5.2	50.7 ± 4.3	70.1 ± 15.3*‡	65.4 ± 29.4
SOD (μmol min^{-1} mg^{-1})	9.56 ± 0.8	6.96 ± 1.1*	7.16 ± 0.9*	7.39 ± 3.20	6.33 ± 2.55*

Abbreviations: AOPP, protein oxidation; FRAP, ferric reducing antioxidant power; GPX, catalase and SOD, antioxidant enzymes activities; IL-1β, interleukin-1β; MDA, lipid peroxidation; and TNFα: tumour necrosis factor-α. Groups are as in Table 2. *Significantly different ($P < 0.05$) from young. †Significantly different ($P < 0.05$) from corresponding untrained. ‡Significantly different ($P < 0.05$) from corresponding ApoE$^{-/-}$.

mice had lower GPX and SOD than Y-ApoE-UT mice. Advanced oxidation protein products and antioxidant enzymes (SOD, GPX and catalase) were higher in old C57 compared with old ApoE$^{-/-}$ mice (Table 6). The O-ApoE-ExT mice had higher activities of SOD and lower AOPP than O-ApoE-UT mice (see Table 6).

Liver markers

Liver concentrations of AOPP and MDA were higher in O-ApoE-UT compared with both Y-ApoE-UT and O-C57-UT mice, whereas liver GPX activity was lower in O-ApoE-UT than in Y-ApoE-UT mice. In addition, O-ApoE-ExT mice had higher activities of SOD and GPX and lower AOPP and MDA than O-ApoE-UT mice (see Table 6).

Systemic oxidative stress and inflammation is higher in old ApoE$^{-/-}$ compared with old C57 mice

Nitrotyrosine and AOPP were higher ($P < 0.05$), whereas NOx ($P < 0.05$) was lower in old ApoE$^{-/-}$ compared with old C57 mice independently of training (Table 7). Glutathione peroxidase was higher in O-C57-ExT than in O-ApoE-UT mice ($P < 0.01$).

Exercise-induced changes in systemic oxidative stress and inflammation

Plasma MDA decreased in response to exercise training in the old ApoE$^{-/-}$ mice (23.3 ± 1.8 *vs.* 17.9 ± 1.7 μmol l^{-1} for O-ApoE-UT and O-ApoE-ExT, respectively; $P < 0.05$), whereas AOPP showed a trend to increase ($P = 0.09$;

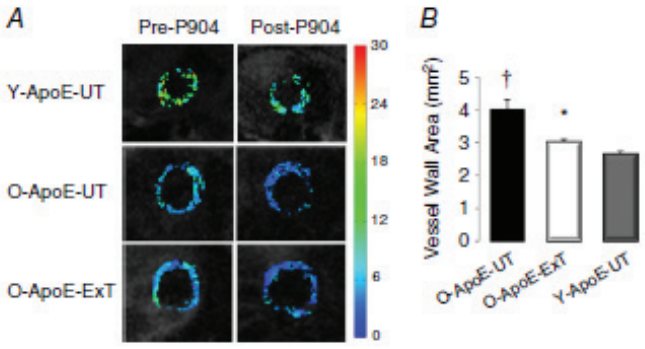

C	Y-ApoE-UT	O-ApoE-UT	O-ApoE-ExT
T2* Pre-Contrast	12.3 ± 0.1	10.9 ± 0.1*	11.5 ± 0.1*†
T2* Post-Contrast	9.9 ± 0.1‡	8.1 ± 0.1*‡	8.7 ± 0.1*†‡

Figure 5. Aorta magnetic resonance imaging of old and young untrained and old trained ApoE$^{-/-}$ mice
A, pre- and post-USPIO T2* maps of the ascending aorta in a young untrained (Y-ApoE-UT), an old untrained (O-ApoE-UT) and an old trained (O-ApoE-Ext) ApoE$^{-/-}$ mouse. *B*, ascending aorta vessel wall area measurements. *C*, vessel wall pre- and post-USPIO T2* measurements. In O-ApoE-UT mice, vessel wall area is significantly larger, and pre- and post-USPIO T2* significantly lower, representative of advanced and complex atherosclerotic lesions with inflammatory activity. *Significantly different ($P < 0.05$) from old ApoE$^{-/-}$ mice (O-ApoE-UT). †Significantly different ($P < 0.05$) from young ApoE$^{-/-}$ mice (Y-ApoE-UT). ‡Significantly different ($P < 0.05$) from pre-contrast.

Table 5. Effect of age and exercise training on aortic TNFα, IL-1β, AOPP and SOD

Marker	Y-ApoE-UT	O-ApoE-UT	O-ApoE-ExT	O-C57-UT	O-C57-ExT
TNFα (pg mg^{-1})	6.7 ± 1.7	11.8 ± 1.2*	9.6 ± 1.5*†	0.5 ± 0.3	2.5 ± 1.3
IL-1β (pg mg^{-1})	16.7 ± 4.9	47.8 ± 17.6*	28.0 ± 10.7*†	0.9 ± 0.2‡	1.0 ± 0.2‡
AOPP (μmol mg^{-1})	21.6 ± 1.4	159.5 ± 25.2*	122.3 ± 20.9*†	8.4 ± 2.7‡	9.1 ± 2.9‡
SOD (μmol min^{-1} mg^{-1})	9.27 ± 2.1	26.2 ± 1.7*	6.7 ± 2.0†	7.79 ± 1.7‡	5.59 ± 1.8

Abbreviations: AOPP, protein oxidation; IL-1β, interleukin-1β; SOD, superoxide dismutase activity; and TNFα, tumour necrosis factor-α. Groups are as in Table 2. *Significantly different ($P < 0.05$) from young. †Significantly different ($P < 0.05$) from corresponding untrained. ‡Significantly different ($P < 0.05$) from corresponding ApoE$^{-/-}$.

Table 6. Effect of age and exercise training on heart and liver markers of oxidative stress and antioxidants

Marker	Y-ApoE-UT	O-ApoE-UT	O-ApoE-ExT	O-C57-UT	O-C57-ExT
AOPP in heart (μmol mg^{-1})	28.5 ± 2.4	75.3 ± 5.8*	68.4 ± 5.6*†	152.7 ± 14.4‡	138.9 ± 6.1‡
Catalase in heart (μmol min^{-1} mg^{-1})	831 ± 76	2492 ± 436*	2033 ± 400*‡	4955 ± 508‡	4266 ± 449‡
GPX in heart (μmol min^{-1} mg^{-1})	451 ± 11	322.7 ± 7*	338 ± 7*	834 ± 87‡	781 ± 83‡
SOD in heart (μmol min^{-1} mg^{-1})	32.7 ± 4.5	24.1 ± 2.8*	32.2 ± 2.4†	48.0 ± 6.6‡	44.9 ± 7.9‡
AOPP in liver (μmol mg^{-1})	14.8 ± 5.3	41.4 ± 10.9*	36.0 ± 9.1*†	6.6 ± 2.0‡	9.3 ± 3.4‡
MDA in liver (μmol mg^{-1})	0.75 ± 0.42	4.11 ± 2.08*	2.37 ± 1.42*†	1.87 ± 0.45‡	2.37 ± 1.47
SOD in liver μmol min^{-1} mg^{-1})	0.92 ± 0.12	0.71 ± 0.26	0.83 ± 0.13†	0.75 ± 0.24	0.79 ± 0.21
GPX in liver μmol min^{-1} mg^{-1})	14.8 ± 12.9	6.0 ± 4.5*	27.4 ± 9.6*†	10.9 ± 1.5	22.7 ± 6.6

Abbreviations: AOPP, protein oxidation; FRAP, ferric reducing antioxidant power; GPX, catalase and SOD, antioxidant enzymes activities; and MDA, malondialdehyde. Groups are as in Table 2. *Significantly different ($P < 0.05$) from young. †Significantly different ($P < 0.05$) from corresponding untrained. ‡Significantly different ($P < 0.05$) from corresponding ApoE$^{-/-}$.

Table 7). The plasma volume collected from for O-C57-ExT and O-C57-U mice was insufficient to allow plasma MDA analysis for these two groups of mice. Antioxidant markers NOx and SOD were higher in O-ApoE-ExT than in O-ApoE-UT mice ($P < 0.05$ and $P = 0.11$, respectively; Table 7). Plasma AOPP were higher in O-ApoE-UT compared with Y-ApoE-UT mice ($P < 0.01$; see Table 7), whereas MDA was

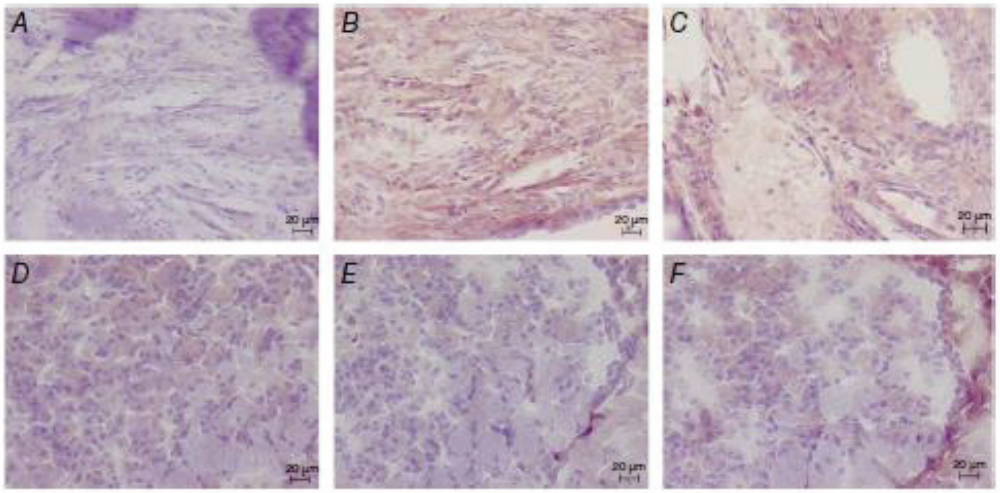

Figure 6. Histological staining of brain of old untrained ApoE$^{-/-}$ and C7 mice
Negative control (*A*), positive F4/80 (*B*) and positive IgG (*C*) for an old ApoE$^{-/-}$ untrained mouse (left side, at the level of the fornix fimbriae, original magification ×20). Negative control (*D*), positive F4/80 (*E*) and positive IgG (*F*) for an old C57 untrained mouse (left side, at the level of the fornix fimbriae, original magification ×20).

Table 7. Effect of age and exercise training on plasma markers of oxidative stress, antioxidants and inflammation

Marker	Y-ApoE-UT	O-ApoE-UT	O-ApoE-ExT	O-C57-UT	O-C57-ExT
AOPP (μmol l^{-1})	202.6 ± 9.1	152.4 ± 11.8*	131.0 ± 10.7*	15.3 ± 2.6‡	13.3 ± 2.7‡
GPX (μmol l^{-1} min^{-1})	123.0 ± 17.7	113.4 ± 14.5	102.4 ± 13.7	109.3 ± 15.2	227.0 ± 62.8†
Nitrotyrosine (nmol l^{-1})	25.6 ± 3.8	50.6 ± 11.0*	66.4 ± 8.9*	36.4 ± 4.0‡	26.4 ± 5.2‡
NOx (μmol l^{-1})	22.3 ± 1.3	22.6 ± 1.0	27.3 ± 1.1*†	28.3 ± 2.4‡	35.7 ± 3.2*†‡
SOD (μmol ml^{-1} min^{-1})	37.1 ± 1.0	32.3 ± 1.4*	36.7 ± 1.2	27.3 ± 1.8	33.3 ± 3.1†
TNFα (pg ml^{-1})	82.3 ± 7.9	42.3 ± 8.9*	40.8 ± 6.7*	46.3 ± 5.6	72.4 ± 16.4†
IL-1β (pg ml^{-1})	157.6 ± 14.7	118.2 ± 6.8*	114.2 ± 8.2*	111.5 ± 22.7	105.4 ± 12.8

Abbreviations: AOPP, protein oxidation; FRAP, ferric reducing antioxidant power; GPX and SOD, antioxidant enzymes activities; IL-1β, interleukin-1β; nitrotyrosine, protein nitration; NOx, nitric oxide metabolism (nitrites plus nitrates); and TNFα, tumour necrosis factor-α. Groups are as in Table 2. *Significantly different ($P < 0.05$) from young. †Significantly different ($P < 0.05$) from corresponding untrained. ‡Significantly different ($P < 0.05$) from corresponding ApoE$^{-/-}$.

lower (23.3 ± 1.8 *vs.* 8.8 ± 0.6 μmol l^{-1} for O-ApoE-UT and Y-ApoE-UT, respectively; $P < 0.01$). The pro-inflammatory markers TNFα and IL-1β were also significantly different in old ApoE$^{-/-}$ mice compared with young-adult mice ($P < 0.001$). Interestingly, NOx, SOD and GPX were improved in the trained old C57 mice (*vs.* untrained). On the contrary, in ApoE$^{-/-}$ mice fed the HF/HC diet, NF-κB was not significantly affected by age or exercise training (Y-ApoE-ExT, 97.4 ± 13.6 pg ml^{-1}; O-ApoE-UT, 102.3 ± 15.6 pg ml^{-1}; and O-ApoE-ExT, 84.1 ± 12.2 pg ml^{-1}).

Correlations

Inflammation and oxidative stress markers were correlated within the brain (see Table 8). However, none of the brain markers was correlated with corresponding plasma (see Table 9), aorta, heart or liver markers.

Discussion

Vascular brain lesions share similar pathological features with atherosclerosis, such as increased inflammation and oxidative stress (Dutta *et al.* 2012). In the present study, we found that compared with age-matched C57 mice fed a normal diet and with young ApoE$^{-/-}$ mice, old ApoE$^{-/-}$ mice fed a HF/HC diet exhibited increases in brain abnormalities and BBB permeability in specific periventricular areas, as confirmed by both MRI and histology. These results were associated with an increase of both inflammation and oxidative stress markers in the brain in the old ApoE$^{-/-}$ mice. All these phenotypic changes are likely to be responsible for the low survival (49% over 12 weeks) of sedentary ApoE$^{-/-}$ mice compared with C57BL6 mice (87%), which confirms the literature (Rowlatt *et al.* 1976; Blackwell *et al.* 1995; Moghadasian *et al.* 2001). More importantly, we found that in ageing ApoE$^{-/-}$ mice, exercise training, possibly via its ability to lower oxidative stress and inflammation, reduced brain macrophage infiltration, limited inflammation and oxidative stress in the brain, and improved metabolic conditions, thereby improving health status and life expectancy.

Inflammation and oxidative stress in old ApoE$^{-/-}$ mice fed HF/HC diet

Oxidative stress in the cerebral vasculature plays a crucial role in the pathogenesis of ischaemic brain injury [such as a compromised BBB (Hafezi-Moghadam *et al.* 2007; ElAli *et al.* 2011) and macrophage accumulation], especially in the aged ApoE$^{-/-}$ mouse model (Coyle & Puttfarcken, 1993). Disruption of the BBB, as measured here *in vivo* by the extent of gadolinium leakage in T1-weighted MRI, is a sign of endothelial permeability (Gloor *et al.* 2001). During conditions of inflammation, macrophages are able to cross the BBB and infiltrate the CNS parenchyma, as suggested by iron oxide nanoparticle-enhanced MRI in stroke patients and models (Nighoghossian *et al.* 2007; Wiart et al. 2007). In our study, the location of gadolinium leakage corresponded anatomically to the presence of macrophages detected *in vivo* after injection of iron nanoparticles by T2/T2*-weighted MRI and post mortem by histology. The iron accumulation observed on pre-contrast T2* in some old mice might have resulted from repeated microhaemorrhage, and could possibly explain the observed symptoms of hemi- and monoplegia. It should be acknowledged that non-invasive MRI with nanoparticles or gadolinium agents has previously demonstrated effectiveness in evaluation of endothelial permeability or in mapping atherosclerotic vascular territories in ApoE$^{-/-}$ mice fed with a high-fat diet (Phinikaridou *et al.* 2012), as well as in other experimental cerebral models (Wiart *et al.* 2007; Koffie *et al.* 2011). We have shown that combined brain and vascular inflammation imaging provides biomarkers of central and vascular metabolic dysfunction and inflammation in this mouse model. In addition, our study is also the first to demonstrate that such imaging is sufficiently sensitive to detect a beneficial effect of exercise training.

Table 8. Correlations between brain markers of oxidative stress and inflammation in young and old ApoE$^{-/-}$ mice

Variable	Correlated with variable	*n*	Pearson's correlation	*P* value
MDA in brain	IL-1β in brain	26	0.429	0.029
AOPP in brain	IL-1β in brain	26	0.764	0.000
Catalase in brain	FRAP in brain	27	0.453	0.018
	SOD in brain	27	0.573	0.002
	GPX in brain	26	0.505	0.009
TNFα in brain	IL-1β in brain	27	0.508	0.007
FRAP in brain	SOD in brain	27	0.552	0.003
	GPX in brain	26	0.515	0.007
SOD in brain	GPX in brain	26	0.683	0.000

Abbreviations: AOPP, protein oxidation; FRAP, ferric reducing antioxidant power; GPX and SOD, antioxidant enzyme activities; IL-1β, interleukin-1β; MDA, malondialdehyde; and TNFα, tumour necrosis factor-α.

Table 9. Lack of correlations between brain and plasma markers of oxidative stress and inflammation

Variable	Correlated with variable	*n*	Pearson's correlation	*P* value
TNFα in plasma	TNFα in brain	21	−0.1818	0.430
IL-1β in plasma	IL-1β in brain	22	0.1700	0.449
AOPP in plasma	AOPP in brain	42	0.1482	0.349
MDA in plasma	MDA in brain	27	−0.0811	0.688
SOD in plasma	SOD in brain	27	0.1836	0.359

Abbreviations: AOPP, protein oxidation; IL-1β, interleukin-1β; MDA, malondialdehyde; SOD, superoxide dismutase; and TNFα, tumour necrosis factor-α.

In this advanced atherosclerosis model, our study confirms the presence of multi-organ inflammation, as previously described in cardiovascular disease (Nahrendorf *et al.* 2015), as well as oxidative stress. Elevated marker concentrations were found in the aortic wall, brain, heart and liver. As they were not correlated, it can be hypothesized that local micro-environments drive specific pathological consequences. Indeed, brain inflammation was far more pronounced and was associated with severe functional impairments in periventricular areas, i.e. BBB damage and high phagocytic activity in the untrained ApoE$^{-/-}$ mice. Also, the observation of motor deficiency cases and the increased mortality rate in the untrained group are likely to be driven by these brain abnormalities shown by MRI. Local vicious circles of inflammation may be nourished further by systemic and distant inflammatory foci.

Effects of exercise training

We also showed that even in an advanced atherosclerotic mouse model, VWR was able to reduce risk factors for atherosclerosis and cerebrovascular damage by altering macrophage accumulation, oxidative stress, inflammation and metabolic parameters. Our mice ran 17.8 km week^{-1}, similar to the age-matched C57 mice (16.2 km week^{-1}). These weekly distances are also close to those reported by Soto *et al.* (2015; 23 km week^{-1}), who used voluntary wheel running in ApoE$^{-/-}$ mice receiving a standard diet. These distances are much greater than a forced treadmill running protocol, which is usually between 4 and 6 km week^{-1}. As mice are naturally active, VWR provides a stress-free way to exercise, as opposed to forced treadmill training and swimming, which may induce a stress response (Moraska *et al.* 2000). The total running distance with VWR is often superior to forced exercise, and it has been shown to produce cardiovascular adaptations, such as heart and left ventricular hypertrophy, and an increase in muscle oxidative capacity (Aufradet *et al.* 2012). Although the distance run by the mice in the present study was lower than healthy C57 mice (Aufradet *et al.* 2012), it was sufficient to increase muscle CS activity, a commonly used marker of an adaptation to habitual exercise (Sexton, 1995). Voluntary wheel running was also shown to be of moderate intensity rather than high intensity as can be seen in treadmill running.

In addition, VWR, regardless of exact distance, was able to induce a positive effect and reduced overall mortality compared with sedentary old animals. This is consistent with previous reports that physical inactivity is an independent predictor of mortality in animals (Laufs *et al.* 2005) and humans (Szostak & Laurant, 2011), whereas physical fitness is associated with preserved brain health (Weuve *et al.* 2004; Podewils *et al.* 2005). A

previous study found that VWR was sufficient to extend survival and decrease neuronal damage after a short episode of forebrain ischaemia (Stummer *et al.* 1994). In treadmill-trained rats, induced brain injury was also less severe as a consequence of improved brain integrity (Ding *et al.* 2006) and BBB function (Davis *et al.* 2007). On brain MRI, old trained ApoE$^{-/-}$ mice showed a significantly decreased score of BBB leakage at the locations where this dysfunction was observed in their untrained counterparts. Beneficial effects of exercise training on neurovascular damage to the brain via an increase in the number of pericytes has been reported recently in ApoE$^{-/-}$ mice (Soto *et al.* 2015). These adaptive effects may be the result of repetitive cerebrovascular shear stress induced by each bout of running training and a long-term increase in cerebral blood flow, both leading to a decrease in oxidative stress and endothelial dysfunction in the brain (Viboolvorakul & Patumraj, 2014). In this context, exercise training was also shown to restore the impaired nitric oxide synthase-dependent responses of cerebral arterioles in diabetic rats (Mayhan *et al.* 2011) and the impaired dilator responses of cerebral arterioles in rats submitted to chronic exposure to nicotine (Mayhan *et al.* 2010). In both studies, beneficial effects of exercise were associated with an increase in SOD and subsequent decrease in superoxide content. In our study, although we did not find any effect of exercise on the brain SOD and GPX activities, lipid peroxidation was reduced, suggesting that the content of reactive oxygen species might be reduced. Given that antioxidant therapies have been shown to reduce infarct volume and neurological impairment in different murine models of ischaemic stroke (Majid, 2014), it could be hypothesized that the beneficial effect of exercise that we observed in the brain could be drawn partly from a decrease in oxidative stress.

In contrast to a recent study by Soto *et al.* (2015), our mice were fed a HC/HF diet and were indeed more pathological than those fed a normal chow diet, as confirmed by the mortality of our old ApoE$^{-/-}$ mice (65% in 12 weeks at 70 weeks) compared with the 18- to 24-month-old mice used by Soto *et al.* (2015), which suggests a longer life expectancy. The HF/HC diet in ApoE$^{-/-}$ mice was previously shown to induce major changes at the level of the neurovascular unit (Badaut *et al.* 2012). Interestingly, this change included lipid droplet accumulation and BBB leakage at the same location as in our old ApoE$^{-/-}$ mice.

Additionally, exercise training reduced pro-inflammatory markers, which could be attributable to a concomitant increase in anti-inflammatory cascades (Pedersen, 2006; Szostak & Laurant, 2011), as we found for brain IL-4. Exercise was also shown to reduce brain IL-1β in a mouse model of Alzheimer's disease (Nichol *et al.* 2008) and brain inflammation in response to stroke (Ding *et al.* 2005), possibly through an increase in anti-inflammatory pathways at the level of the neurovascular unit.

Better brain health has been shown to be related to systemic improvement of cardiovascular health, lipid–cholesterol balance and inflammation (Pedersen, 2006). Here, beyond its effects on the brain, exercise training was able to improve the overall effects of atherosclerosis in the old ApoE$^{-/-}$ mice. More specifically, O-ApoE-ExT mice expressed lower oxidative stress and inflammation in the aorta than their sedentary counterparts. Magnetic resonance imaging revealed a decrease in vessel wall size in the mice that ran compared with sedentary mice, in agreement with others (Shimada *et al.* 2007; Pellegrin *et al.* 2009*b*; Kadoglou *et al.* 2011). In a study by Pellegrin *et al.* (2009*b*), swimming-trained ApoE$^{-/-}$ mice showed a decrease in macrophage accumulation, along with an increase in smooth muscle cell content, suggesting a more stable plaque. Exercise-trained mice had higher T2* values, suggesting a more stable plaque (Sigovan *et al.* 2010). Nevertheless, in future studies, measurement of biological markers of plaque stability in aortic tissue, such as metalloproteinases activity, should confirm this hypothesis.

In old ApoE$^{-/-}$ mice, training decreased oxidative stress markers in the plasma, heart and liver, in addition to the brain and aorta, suggesting that exercise may have a whole-body effect on oxidative stress in this model.

Compared with old ApoE$^{-/-}$ mice, oxidative stress is very low in the old C57 mice (between five and 10 times lower than in old ApoE$^{-/-}$ mice in the different organs). This suggests that C57 mice at the age of 70 weeks might have maintained their pro-oxidant–antioxidant balance. We also think that further reduction of oxidative stress could be more detrimental than beneficial. Indeed, reactive oxygen species and lipid peroxidation end-products (such as MDA) also have a role in the regulation and modulation of antioxidant cell signalling and gene expression, and a decrease of such products, when they are not in excess, might limit physiological adaptations (Niki, 2009).

Finally, although we report clear differences between O-ApoE-ExT and O-ApoE-UT mice regarding brain and aorta that suggest beneficial effects of exercise training, a longitudinal follow-up study of aortic and brain inflammation by MRI might be one of the perspectives of the present study to confirm our results.

In conclusion, we found that cardiovascular disease risk factors, which involve chronic systemic oxidative stress and inflammation, are associated with neuro-vascular lesions in old ApoE$^{-/-}$ mice at specific 'at-risk' locations. All together, our results demonstrate that 12 weeks of moderate-intensity physical activity was able to improve survival in aged ApoE$^{-/-}$ mice and decrease the extent of the neurovascular damage present in this dyslipidaemic aged mouse model. The VWR protocol decreased both brain disorders (BBB leakage

and macrophage accumulation) and aortic plaque size, and increased aortic plaque stabilization. The decrease in oxidative stress and inflammation directly at the brain level as a result of exercise training could be responsible for the neuroprotective effect and the reduced prevalence of lesions. Taken together, these results demonstrate the benefits of exercise training in a model of atherosclerosis. Finally, on the basis of the present study, non-invasive imaging, such as MRI, appears to be an essential tool, as follows: (i) to evaluate neurovascular risk in the brain of atherosclerotic patients; and (ii) to measure therapeutic intervention, such as physical exercise, with both a site-specific location and combined imaging biomarkers to evaluate the effect of exercise on BBB integrity and reduction of neuro-inflammation. More advanced hybrid molecular imaging techniques, such as positron emission tomography–MRI and targeted nanoparticles (Briley-Saebo *et al.* 2012), may provide longitudinal follow-up and new therapeutic options for these complex, high-risk cardiovascular profiles.

References

Aufradet E, Bessaad A, Alsaid H, Schäfer F, Sigovan M, De Souza G, Chirico E, Martin C & Canet-Soulas E (2012). *In vivo* cardiac anatomical and functional effects of wheel running in mice by magnetic resonance imaging. *Exp Biol Med (Maywood)* **237**, 263–270.

Badaut J, Copin J-C, Fukuda AM, Gasche Y, Schaller K & da Silva RF (2012). Increase of arginase activity in old apolipoprotein-E deficient mice under Western diet associated with changes in neurovascular unit. *J Neuroinflammation* **9**, 132.

Beauchamp C & Fridovich I (1971). Superoxide dismutase: improved assays and an assay applicable to acrylamide gels. *Anal Biochem* **44**, 276–287.

Benzie IF & Strain JJ (1996). The ferric reducing ability of plasma (FRAP) as a measure of "antioxidant power": the FRAP assay. *Anal Biochem* **239**, 70–76.

Blackwell BN, Bucci TJ, Hart RW & Turturro A (1995). Longevity, body weight, and neoplasia in *ad libitum*-fed and diet-restricted C57BL6 mice fed NIH-31 open formula diet. *Toxicol Pathol* **23**, 570–582.

Briley-Saebo KC, Nguyen TH, Saeboe AM, Cho Y-S, Ryu SK, Volkova ER, Volkava E, Dickson S, Leibundgut G, Wiesner P, Weisner P, Green S, Casanada F, Miller YI, Shaw W, Witztum JL, Fayad ZA & Tsimikas S (2012). In vivo detection of oxidation-specific epitopes in atherosclerotic lesions using biocompatible manganese molecular magnetic imaging probes. *J Am Coll Cardiol* **59**, 616–626.

Casserly I & Topol EJ (2004). Convergence of atherosclerosis and Alzheimer's disease: inflammation, cholesterol, and misfolded proteins. *Lancet* **363**, 1139–1146.

Chirico EN, Martin C, Faes C, Feasson L, Oyonno-Engelle S, Aufradet E, Dubouchaud H, Francina A, Canet-Soulas E, Thiriet P, Messonnier L & Pialoux V (2012). Exercise training blunts oxidative stress in sickle cell trait carriers. *J Appl Physiol* **112**, 1445–1453.

Coyle J & Puttfarcken P (1993). Oxidative stress, glutamate, and neurodegenerative disorders. *Science* **262**, 689–695.

Davis W, Mahale S, Carranza A, Cox B, Hayes K, Jimenez D & Ding Y (2007). Exercise pre-conditioning ameliorates blood–brain barrier dysfunction in stroke by enhancing basal lamina. *Neurol Res* **29**, 382–387.

Ding Y-H, Ding Y, Li J, Bessert DA & Rafols JA (2006). Exercise pre-conditioning strengthens brain microvascular integrity in a rat stroke model. *Neurol Res* **28**, 184–189.

Ding Y-H, Young CN, Luan X, Li J, Rafols JA, Clark JC, McAllister JP 2nd & Ding Y (2005). Exercise preconditioning ameliorates inflammatory injury in ischemic rats during reperfusion. *Acta Neuropathol* **109**, 237–246.

Drake C, Boutin H, Jones MS, Denes A, McColl BW, Selvarajah JR, Hulme S, Georgiou RF, Hinz R, Gerhard A, Vail A, Prenant C, Julyan P, Maroy R, Brown G, Smigova A, Herholz K, Kassiou M, Crossman D, Francis S, Proctor SD, Russell JC, Hopkins SJ, Tyrrell PJ, Rothwell NJ & Allan SM (2011). Brain inflammation is induced by co-morbidities and risk factors for stroke. *Brain Behav Immun* **25**, 1113–1122.

Dutta P, Courties G, Wei Y, Leuschner F, Gorbatov R, Robbins CS, Iwamoto Y, Thompson B, Carlson AL, Heidt T, Majmudar MD, Lasitschka F, Etzrodt M, Waterman P, Waring MT, Chicoine AT, van der Laan AM, Niessen HW, Piek JJ, Rubin BB, Butany J, Stone JR, Katus HA, Murphy SA, Morrow DA, Sabatine MS, Vinegoni C, Moskowitz MA, Pittet MJ, Libby P, Lin CP, Swirski FK, Weissleder R & Nahrendorf M (2012). Myocardial infarction accelerates atherosclerosis. *Nature* **487**, 325–329.

ElAli A, Doeppner TR, Zechariah A & Hermann DM (2011). Increased blood–brain barrier permeability and brain edema after focal cerebral ischemia induced by hyperlipidemia role of lipid peroxidation and calpain-1/2, matrix metalloproteinase-2/9, and RhoA overactivation. *Stroke* **42**, 3238–3244.

Galiñanes M & Matata BM (2002). Protein nitration is predominantly mediated by a peroxynitrite-dependent pathway in cultured human leucocytes. *Biochem J* **367**, 467–473.

Gloor SM, Wachtel M, Bolliger MF, Ishihara H, Landmann R & Frei K (2001). Molecular and cellular permeability control at the blood–brain barrier. *Brain Res Brain Res Rev* **36**, 258–264.

Hafezi-Moghadam A, Thomas KL & Wagner DD (2007). ApoE deficiency leads to a progressive age-dependent blood-brain barrier leakage. *Am J Physiol Cell Physiol* **292**, C1256–C1262.

Hebbel RP, Eaton JW, Balasingam M & Steinberg MH (1982). Spontaneous oxygen radical generation by sickle erythrocytes. *J Clin Invest* **70**, 1253–1259.

Johansson LH & Borg LA (1988). A spectrophotometric method for determination of catalase activity in small tissue samples. *Anal Biochem* **174**, 331–336.

Kadoglou NPE, Kostomitsopoulos N, Kapelouzou A, Moustardas P, Katsimpoulas M, Giagini A, Dede E, Boudoulas H, Konstantinides S, Karayannacos PE & Liapis CD (2011). Effects of exercise training on the severity and composition of atherosclerotic plaque in apoE-deficient mice. *J Vasc Res* **48**, 347–356.

Koffie RM, Farrar CT, Saidi L-J, William CM, Hyman BT & Spires-Jones TL (2011). Nanoparticles enhance brain delivery of blood–brain barrier-impermeable probes for in vivo optical and magnetic resonance imaging. *Proc Natl Acad Sci USA* **108**, 18837–18842.

Laufs U, Wassmann S, Czech T, Münzel T, Eisenhauer M, Böhm M & Nickenig G (2005). Physical inactivity increases oxidative stress, endothelial dysfunction, and atherosclerosis. *Arterioscler Thromb Vasc Biol* **25**, 809–814.

Lee S, Park Y, Zuidema MY, Hannink M & Zhang C (2011). Effects of interventions on oxidative stress and inflammation of cardiovascular diseases. *World J Cardiol* **3**, 18–24.

Lefèvre G, Beljean-Leymarie M, Beyerle F, Bonnefont-Rousselot D, Cristol JP, Thérond P & Torreilles J (1998). [Evaluation of lipid peroxidation by measuring thiobarbituric acid reactive substances]. *Ann Biol Clin (Paris)* **56**, 305–319.

Lesniewski LA, Durrant JR, Connell ML, Henson GD, Black AD, Donato AJ & Seals DR (2011). Aerobic exercise reverses arterial inflammation with aging in mice. *Am J Physiol Heart Circ Physiol* **301**, H1025–H1032.

Majid A (2014). Neuroprotection in stroke: past, present, and future. *Int Sch Res Notices* **2014**, e515716.

Mayhan WG, Arrick DM, Patel KP & Sun H (2011). Exercise training normalizes impaired NOS-dependent responses of cerebral arterioles in type 1 diabetic rats. *Am J Physiol Heart Circ Physiol* **300**, H1013–H1020.

Mayhan WG, Arrick DM, Sun H & Patel KP (2010). Exercise training restores impaired dilator responses of cerebral arterioles during chronic exposure to nicotine. *J Appl Physiol* **109**, 1109–1114.

Mihai G, He X, Zhang X, McCarthy B, Tran T, Pennell M, Blank J, Simonetti OP, Jackson RD & Raman SV (2011). Design and rationale for the study of changes in iron and atherosclerosis risk in perimenopause. *J Clin Exp Cardiolog* **2**, 152.

Misko TP, Schilling RJ, Salvemini D, Moore WM & Currie MG (1993). A fluorometric assay for the measurement of nitrite in biological samples. *Anal Biochem* **214**, 11–16.

Moghadasian MH, McManus BM, Nguyen LB, Shefer S, Nadji M, Godin DV, Green TJ, Hill J, Yang Y, Scudamore CH & Frohlich JJ (2001). Pathophysiology of apolipoprotein E deficiency in mice: relevance to apo E-related disorders in humans. *FASEB J* **15**, 2623–2630.

Moraska A, Deak T, Spencer RL, Roth D & Fleshner M (2000). Treadmill running produces both positive and negative physiological adaptations in Sprague-Dawley rats. *Am J Physiol Regul Integr Comp Physiol* **279**, R1321–R1329.

Nahrendorf M, Frantz S, Swirski FK, Mulder WJM, Randolph G, Ertl G, Ntziachristos V, Piek JJ, Stroes ES, Schwaiger M, Mann DL & Fayad ZA (2015). Imaging systemic inflammatory networks in ischemic heart disease. *J Am Coll Cardiol* **65**, 1583–1591.

Nichol KE, Poon WW, Parachikova AI, Cribbs DH, Glabe CG & Cotman CW (2008). Exercise alters the immune profile in Tg2576 Alzheimer mice toward a response coincident with improved cognitive performance and decreased amyloid. *J Neuroinflammation* **5**, 13.

Nighoghossian N, Wiart M, Cakmak S, Berthezène Y, Derex L, Cho T-H, Nemoz C, Chapuis F, Tisserand G-L, Pialat J-B, Trouillas P, Froment J-C & Hermier M (2007). Inflammatory response after ischemic stroke: a USPIO-enhanced MRI study in patients. *Stroke* **38**, 303–307.

Niki E (2009). Lipid peroxidation: physiological levels and dual biological effects. *Free Radic Biol Med* **47**, 469–484.

Oberley L & Spitz D (1985). Nitroblue tetrazolium. In *Handbook of Methods for Oxygen Radical Research*, ed Greenwald RA. CRC Press, Boca Raton.

Ohkawa H, Ohishi N & Yagi K (1979). Assay for lipid peroxides in animal tissues by thiobarbituric acid reaction. *Anal Biochem* **95**, 351–358.

Paglia DE & Valentine WN (1967). Studies on the quantitative and qualitative characterization of erythrocyte glutathione peroxidase. *J Lab Clin Med* **70**, 158–169.

Pedersen BK (2006). The anti-inflammatory effect of exercise: its role in diabetes and cardiovascular disease control. *Essays Biochem* **42**, 105–117.

Pellegrin M, Alonso F, Aubert J-F, Bouzourene K, Braunersreuther V, Mach F, Haefliger J-A, Hayoz D, Berthelot A, Nussberger J, Laurant P & Mazzolai L (2009*a*). Swimming prevents vulnerable atherosclerotic plaque development in hypertensive 2-kidney, 1-clip mice by modulating angiotensin II type 1 receptor expression independently from hemodynamic changes. *Hypertension* **53**, 782–789.

Pellegrin M, Miguet-Alfonsi C, Bouzourene K, Aubert J-F, Deckert V, Berthelot A, Mazzolai L & Laurant P (2009*b*). Long-term exercise stabilizes atherosclerotic plaque in ApoE knockout mice. *Med Sci Sports Exerc* **41**, 2128–2135.

Phinikaridou A, Andia ME, Protti A, Indermuehle A, Shah A, Smith A, Warley A & Botnar RM (2012). Noninvasive magnetic resonance imaging evaluation of endothelial permeability in murine atherosclerosis using an albumin-binding contrast agent. *Circulation* **126**, 707–719.

Pialoux V, Brown AD, Leigh R, Friedenreich CM & Poulin MJ (2009*a*). Effect of cardiorespiratory fitness on vascular regulation and oxidative stress in postmenopausal women. *Hypertension* **54**, 1014–1020.

Pialoux V, Mounier R, Brown AD, Steinback CD, Rawling JM & Poulin MJ (2009*b*). Relationship between oxidative stress and HIF-1α mRNA during sustained hypoxia in humans. *Free Radic Biol Med* **46**, 321–326.

Podewils LJ, Guallar E, Kuller LH, Fried LP, Lopez OL, Carlson M & Lyketsos CG (2005). Physical activity, *APOE* genotype, and dementia risk: findings from the Cardiovascular Health Cognition Study. *Am J Epidemiol* **161**, 639–651.

Rowlatt C, Chesterman FC & Sheriff MU (1976). Lifespan, age changes and tumour incidence in an ageing C57BL mouse colony. *Lab Anim* **10**, 419–442.

Saleh A, Schroeter M, Jonkmanns C, Hartung H, Mödder U & Jander S (2004). *In vivo* MRI of brain inflammation in human ischaemic stroke. *Brain* **127**, 1670–1677.

Sexton WL (1995). Vascular adaptations in rat hindlimb skeletal muscle after voluntary running-wheel exercise. *J Appl Physiol* **79**, 287–296.

Shepherd D & Garland PB (1969). The kinetic properties of citrate synthase from rat liver mitochondria. *Biochem J* **114**, 597–610.

Shimada K, Kishimoto C, Okabe T, Hattori M, Murayama T, Yokode M & Kita T (2007). Exercise training reduces severity of atherosclerosis in apolipoprotein E knockout mice via nitric oxide. *Circ J* **71**, 1147–1151.

Sigovan M, Bessaad A, Alsaid H, Lancelot E, Corot C, Neyran B, Provost N, Majd Z, Breisse M & Canet-Soulas E (2010). Assessment of age modulated vascular inflammation in ApoE−/− mice by USPIO-enhanced magnetic resonance imaging. *Invest Radiol* **45**, 702–707.

Sigovan M, Kaye E, Lancelot E, Corot C, Provost N, Majd Z, Breisse M & Canet-Soulas E (2012). Anti-inflammatory drug evaluation in ApoE−/− mice by ultrasmall superparamagnetic iron oxide-enhanced magnetic resonance imaging. *Invest Radiol* **47**, 546–552.

Soto I, Graham LC, Richter HJ, Simeone SN, Radell JE, Grabowska W, Funkhouser WK, Howell MC & Howell GR (2015). APOE stabilization by exercise prevents aging neurovascular dysfunction and complement induction. *PLoS Biol* **13**, e1002279.

Stummer W, Weber K, Tranmer B, Baethmann A & Kempski O (1994). Reduced mortality and brain damage after locomotor activity in gerbil forebrain ischemia. *Stroke* **25**, 1862–1869.

Szostak J & Laurant P (2011). The forgotten face of regular physical exercise: a 'natural' anti-atherogenic activity. *Clin Sci* **121**, 91–106.

Viboolvorakul S & Patumraj S (2014). Exercise training could improve age-related changes in cerebral blood flow and capillary vascularity through the upregulation of VEGF and eNOS. *Biomed Res Int* **2014**, 230791.

Weuve J, Kang JH, Manson JE, Breteler MMB, Ware JH & Grodstein F (2004). Physical activity, including walking, and cognitive function in older women. *JAMA* **292**, 1454–1461.

Wiart M, Davoust N, Pialat J-B, Desestret V, Moucharrafie S, Cho TH, Mutin M, Langlois JB, Beuf O, Honnorat J, Nighoghossian N & Berthezène Y (2007). MRI monitoring of neuroinflammation in mouse focal ischemia. *Stroke* **38**, 131–137.

Witko-Sarsat V1, Friedlander M, Capeillère-Blandin C, Nguyen-Khoa T, Nguyen AT, Zingraff J, Jungers P, Descamps-Latscha B (1996). Advanced oxidation protein products as a novel marker of oxidative stress in uremia. *Kidney Int* **49**, 1304–1313.

Zlokovic BV (2008). The blood-brain barrier in health and chronic neurodegenerative disorders. *Neuron* **57**, 178–201.

Additional information

Competing interests

None declared.

Author contributions

E.N.C., V.P. and E.C.-S. designed the study and drafted the manuscript. E.N.C., V.D.C., F.C., A.G., D.P., B.T., J.R., V.P. and E.C.-S. analysed the data. All authors interpreted the data and revised the manuscript critically for important intellectual content. All authors approved the final version of the manuscript and agree to be accountable for all aspects of the work in ensuring that questions related to the accuracy or integrity of any part of the work are appropriately investigated and resolved. All persons designated as authors qualify for authorship, and all those who qualify for authorship are listed.

Funding

This study was supported by the Institut Universitaire de France and the French Ministry of Research for PhD students.

Acknowledgements

Thanks to Guerbet for supplying the contrast agent and the old ApoE$^{-/-}$ mice; to Radu Bolbos and Jean-Baptiste Langlois at the Centre d'Exploration et de Recherche Médicale par Emission de Positons (CERMEP) imaging platform for brain acquisitions; to Andrew Fowler and Monica Sigovan for Matlab developments for MRI analysis; and to Charles Vilallonga for brain immunohistochemistry analyses.

Translational perspective

- Vascular brain lesions share pathological hallmarks with atherosclerosis, such as increased inflammation and oxidative stress.
- We showed that an ageing model of atherosclerosis (old ApoE$^{-/-}$ mice on a high-fat, high-cholesterol diet) presented with vascular brain damage and that these neurovascular disorders were associated with peripheral inflammation. Interestingly, exercise training was able to reduce these pathological outcomes.
- Our findings suggest that non-invasive imaging could be used to evaluate neurovascular risk in atherosclerosis and that regular physical activity might reduce these risks.

ARTICLE n°2

Exercise does not protect against peripheral and central effects of a high cholesterol diet given ad libitum in old ApoE$^{-/-}$ mice

Vanessa Di Cataldo, Alain Géloën, Jean-Baptiste Langlois, Fabien Chauveau, Benoît Thézé, Violaine Hubert, Marlène Wiart, Erica Chirico, Jennifer Rieusset, Hubert Vidal, Vincent Pialoux, Emmanuelle Canet-Soulas

Frontiers in Physiology, 06 October 2016 | http://dx.doi.org/10.3389/fphys.2016.00453

ARTICLE N°2:

Advanced atherosclerosis increases systemic and cerebrovascular inflammation and thereby the risk of stroke. Previous studies of us and others, exercise was shown to improve cardio-metabolic profiles when associated with caloric restriction but its efficiency in a context of non-restricted calories intake remains debated. The aim of this study was to determine the peripheral and central effect of exercise training in a context of unregulated consumption of high cholesterol diet in old $ApoE^{-/-}$ mice.

Forty-five weeks-old $ApoE^{-/-}$ mice (45 weeks-old) were fed a high cholesterol diet (0.15% cholesterol, 21% lard fat) *ad libitum* and divided into 2 groups: exercise trained (EX) and sedentary (SED). Exercise trained mice had free access to a running wheel in their housing while sedentary were in standard cages (see **Figure 23** for study design). In order to have a longitudinal follow-up, insulin tolerance test and brain MR imaging were performed before and after the twelve-weeks training. Brain MR imaging was realized with contrast agents for blood-brain barrier permeability assessment (Gadolinium) and macrophage accumulation (ultrasmall superparamagnetic iron oxide particles, USPIOs). After sacrifice, muscular insulin resistance was measured and oxidative stress and inflammation were assessed in plasma, aorta and brain. Histological analysis was also performed on brain to confirm MRI-detected lesions with macrophage and vascular permeability staining.

Aged $ApoE^{-/-}$ trained mice fed with ad libitum diet showed a significant weight gain (+18%, $p=0.027$) despite an effective training (citrate synthase activity $p<0.05$) compared to untrained mice. Exercise training showed no improvement on peripheral features such as plasmatic cholesterol level, systemic and aorta inflammation and oxidative stress. A worsening of insulin resistance was even observed in the trained mice after the twelve-weeks training. Brain imaging highlighted a worsening of blood-brain barrier leakage as showed by the longitudinal MRI follow-up (increase of $\Delta T1$ score, $r^2=0.87$, $p=0.049$) and higher USPIOs accumulation in periventricular areas in exercised mice compared to the sedentary, suggesting a worsening of central lesions in trained $ApoE^{-/-}$ mice under ad libitum high cholesterol diet.

In a context of high cardio-metabolic risk and of uncontrolled fat consumption exercise does not provide any protective effect in old ApoE-/- mice. No benefits of exercise training was observed on both peripheral (insulin sensitivity, oxidative stress and inflammation) and central features (vascular

permeability and inflammation). Furthermore, there was a fast induction of irreversible brain lesions in exercised-trained old ApoE-/- mice.

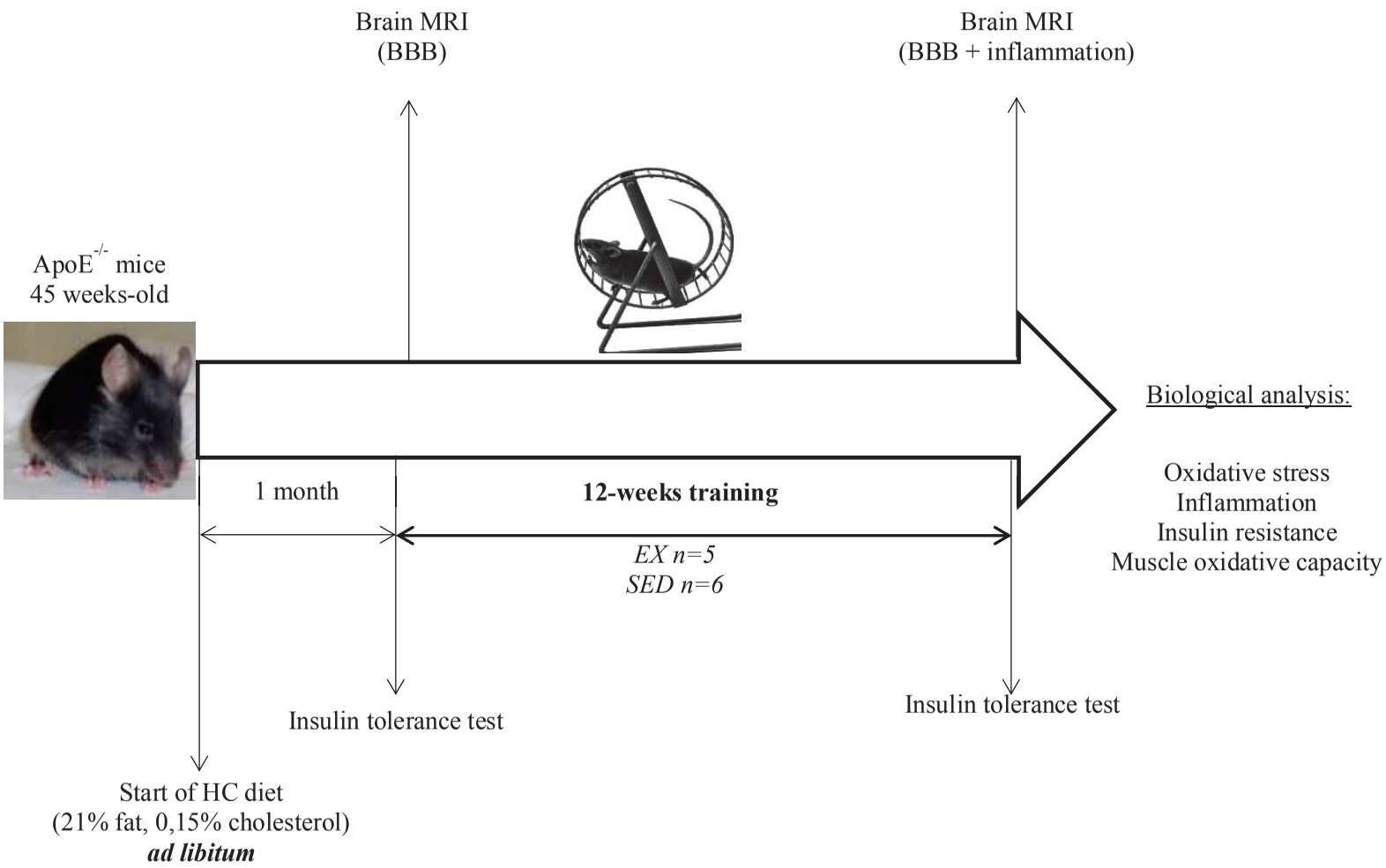

Figure 23: Study design Frontiers in Physiology, 2016

INTRODUCTION

Numerous studies have shown that regular physical activity had protective effects against chronic diseases, like in atherosclerosis (Szostak and Laurant, 1979; Laufs et al., 2005) by decreasing oxidative stress and inflammation. Through these protective effects, it is suggested that regular exercise training could decrease the risks of developing cardio and cerebrovascular complications (Pialoux et al., 2009). Overall, exercise training may create a favorable anti-inflammatory and antioxidant environment, counter-acting both local inflammatory burst, and systemic metabolic low-grade inflammation (Pialoux et al., 2009; Gleeson et al., 2011).

Central effects of exercise are less explored in the context of atherosclerosis. Advanced atherosclerosis increases the risk of stroke, inflammation, and oxidative stress in the cerebral vasculature. Aged ApoE$^{-/-}$ mice have a compromised blood-brain barrier (BBB), with an increased susceptibility to ischemic damage which is further altered by the high fat/high cholesterol diet (Hafezi-Moghadam et al., 2006; ElAli et al., 2011; Badaut et al., 2012). In addition to the vascular risk *per-se*, an increasing number of studies are reporting various locations of BBB permeability and hippocampal inflammation as a direct consequences of obesity and high fat consumption (Badaut et al., 2012; Thaler et al., 2012; Lee et al., 2013; Erion et al., 2014; Van der Donckt et al., 2015). In an atherosclerosis mouse model under high fat diet, we and others have recently shown that exercise can limit brain inflammation (Yi et al., 2012; Auer et al., 2015; Chirico et al., 2016).

On the other hand, whereas systemic benefits of physical activity on the cardio-metabolic profile are commonly recognized, there is a significant proportion of non-responders, showing no or even adverse exercise effect on glucose homeostasis in large clinical studies (Böhm et al., 2016). In some studies, it was found to be highly dependent on food intake and its effect on body weight (Bergouignan et al., 1985). Indeed, in obese subjects who had the same physical activity level, it was observed that those under food restriction presented reduced oxidative stress, inflammation, and insulin resistance compared to those with no food restriction and increased body weight (Bergouignan et al., 1985). This interplay between food intake and the peripheral response to physical training may also impact the central effects of training (Hicks et al., 2016), but has not been tested yet in a context of high cardiovascular risk.

Imaging biomarkers are increasingly used to evaluate progression of brain abnormalities. BBB damage is currently measured *in vivo* by the extent of gadolinium leakage in T1-weighted magnetic resonance imaging (MRI; Nighoghossian et al., 2007). Under conditions of acute or chronic inflammation, macrophages infiltrate the cerebral parenchyma, and exhibit an important phagocytic activity, that can be seen by ultrasmall superparamagnetic particles of iron oxide (USPIOs) enhanced MRI in stroke patients (Nighoghossian et al., 2007). In the cerebral parenchyma, several publications have reported that microbleeds (Akoudad et al., 2014) and brain accumulation of erythrocytes and iron (Schreiber et al., 2012) can also be detected *in vivo* using T2 and T2* MRI (Wardlaw et al., 2013).

Using imaging and insulin tolerance test for follow-up, the aim of the present study was to determine both the peripheral and central effects of exercise training in 45 weeks-old ApoE$^{-/-}$ mice fed *ad libitum* with a high fat/ high cholesterol (HC) diet.

Abbreviations: BBB, Blood-brain barrier; EX, Exercise-trained; HC, High cholesterol; MRI: Magnetic resonance imaging; SED, Sedentary; USPIO, Ultrasmall superparamagnetic particle of iron oxide; WT, Aged-matched C57Bl/6 Wild Type mice.

MATERIALS AND METHODS

Animals and Training

All procedures were in conformity with the European regulation for animal use and this study was approved by the local ethics committee of the institution (Comité d'éthique de l'INSA de Lyon Cetil *n*°102). ApoE$^{-/-}$ mice (C57Bl/6 background, Charles River, France $n = 14$) were fed a high cholesterol (HC) diet (Safe U8220 v.153: A04 + 21% fat, 0.15% cholesterol, SAFE, Augy, France) starting 1 month before the training and until the end of the study. Animals were males and females equally assigned in both groups and maintained on a 12 h light-dark cycle and were supplied with food and water *ad libitum*. After careful maintenance of health conditions during 1 year (Guerbet, Animal Care Unit, France), 45 weeks-old mice were randomly divided into 2 activity groups. Mice in the exercise-trained (EX) group individually housed in cages equipped with a 12.5 cm metal running wheel (HAGEN-61700, Montreal, Canada; Goh and Ladiges, 2015) and digital magnetic counter (model BC906 Sigma Sport, Neustadt, Germany), while the sedentary (SED) group had a standard cage (**Figure 1**). Sedentary mice were caged by 3–4 in order to avoid excessive stress due to loneliness (and not compensated by the possibility to exercise contrary to trained mice). During the 12 weeks of training, the distance ran and the general health of the mice were recorded one time a week. A regular check-up of mice was performed (twice a week) and the exclusion criterion was overall bad health of the animal (i.e., tumors, hemiparesis, large skin irritations). Before sacrifice for blood and tissue assessment, both exercise and sedentary mice were caged by 3–4, with no wheel access, and fasted for 12 h.

Wild type (WT) C57Bl/6 mice of matched age fed with a standard diet (12% fat, Teklad Global 16% protein, HARLAN, Gannat, France) and divided into EX and SED groups were also studied to provide reference values of metabolic and inflammatory markers in normal animals not at risk of vascular lesions.

Intraperitoneal Insulin Tolerance Test (ITT)

Glycaemia was measured over 45 min in 6 h-fasted mice using a glucometer (AccuCheck, Roche, Germany) after an initial tail puncture, corresponding to baseline glycaemia. Immediately after, all mice were sequentially injected by insulin (intraperitoneal injection, 0.75mU.g^{-1} of body weight). Fifteen minutes after insulin injection, glycaemia was assessed following the same sequence, and measurements were repeated at 30 and 45 min. ITT were performed before and after training, prior to

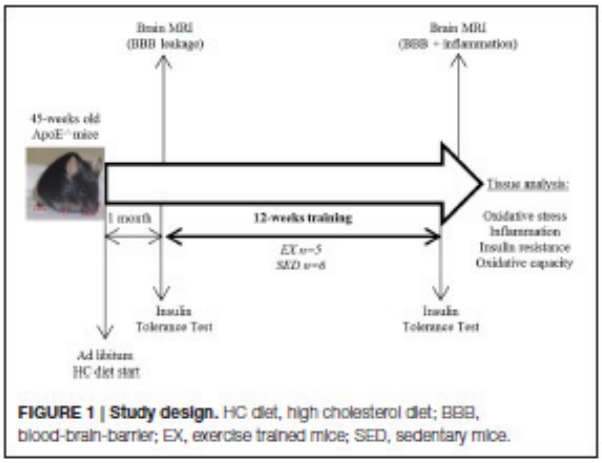

FIGURE 1 | Study design. HC diet, high cholesterol diet; BBB, blood-brain-barrier; EX, exercise trained mice; SED, sedentary mice.

MRI sessions. Insulin response was determined by area under curve (AUC).

Brain MRI

For the imaging protocol, mice were anesthetized by isoflurane (4% for induction, 1–2% for maintenance; TEM SEGA, Pessac, France). The scanning support bed used for the experiment was equipped with a warm water recirculation system and a respiratory sensor, which monitored the respiration rate throughout the scan. MRI acquisitions were performed on a Bruker BioSpec 7T system (Bruker Biospin, Ettlingen, Germany).

For brain imaging, a Bruker birdcage volume coil (outer diameter = 112 mm and inner diameter = 72 mm) was used for the signal transmission, and a Bruker single loop surface coil (15 mm diameter) positioned over the head was used for signal reception. Brain T2-weighted spin-echo images were acquired using a rapid acquisition with relaxation enhancement (RARE) sequence on axial plane. To further characterize the neurovascular lesions, an extended brain MRI protocol was performed (see supplemental methods in Supplementary Material). Vascular lesions and hemorrhage/erythrocytes/iron accumulation were assessed respectively by baseline T2 and T2* imaging (Schreiber et al., 2012; Akoudad et al., 2014). T2* mapping was obtained using a multi-slice multi-echo gradient echo sequence. Gadolinium chelate (Gd-DOTA, 0.1 mmol $Gd.kg^{-1}$, Guerbet, Aulnay-sous-Bois, France) was then retro-orbitally injected to observe possible BBB leakage. Macrophage imaging was performed using USPIO injection (P904, 1mmol $Fe.kg^{-1}$, Guerbet, Aulnay-sous-Bois, France) and the 48 h post-contrast T2/T2* for inflammation imaging, as previously described (Sigovan et al., 2012). The total duration of the MRI protocol was less than 2 h.

In addition, to assess body composition in both groups, whole body fat evaluation was performed in representative individuals of each group using 2D water/fat gradient echo acquisition and whole body nuclear magnetic resonance (NMR) spectrum at the end of the after-training MRI session (Naville et al., 2015). Results are presented as relative fat over water after analysis of corresponding peaks in the MR spectrum.

MRI Analysis

For brain analysis, pre-contrast T2/T2* images and post-gadolinium images were categorized based on the size of abnormal areas and the number of slices affected. Two observers scored anonymized data obtained before and after training, i.e., pre- and post- contrast (48 h post-P904, after-training MRI session) on T2/T2* images and gadolinium leakage on post-gadolinium T1-weighted images. Briefly, a score of 1–4 was given for abnormalities seen on pre-contrast images and a score of 1–4 was given for changes seen between pre and post-contrast images. A score of 1 is given when no abnormality was observed, 2 when small lesions (<10 pixels) appeared on one to two slices, 3 for medium size lesion (10<pixels<20) on one to two slices and finally a score of 4 represents a large lesion (>20 pixels) on at least two slices. In order to evaluate the evolution of BBB leakage, the delta of T1 (ΔT1) score was calculated by subtracting post-training to pre-training score.

Dissection

Following the second imaging session, mice were anesthetized by intraperitoneal injection of pentobarbital (50 $mg.kg^{-1}$, Dolethal®, Vétoquinol, Lure, France) and blood was collected by cardiac puncture. The heart was transcardially perfused for 70 s with 9% NaCl. The brain, ascending and abdominal aorta, gastrocnemius, soleus, and visceral and subcutaneous adipose tissue were removed. Sections to be used for biological assays were stored at −80°C until assessment.

Ex vivo Insulin Signalization Test

As previously described (Rieusset et al., 2012), immediately after sampling, gastrocnemius muscles were finely cut and incubated for 15 min at 37°C in 3 ml of low glucose Dulbecco's Modified Eagle's Medium (DMEM $1g.L^{-1}$) for the sample (−) and low glucose DMEM + 5% insulin 10^{-7}mol for the sample (+) and then quickly wiped and stored in liquid nitrogen. Samples (−) were used to study the expression of basal protein kinase B (PKB) and phosphorylated PKB (pPKB), while samples (+) to measure the quality of insulin signaling. Samples were kept at −80°C. Proteins of these muscles were then extracted by grinding with a Polytron in RIPA+ and centrifuged for 10 min at 3750 rpm at 4°C. The supernatant were recovered and diluted 1:5 in water in order to be assayed by the Bradford method. Then proteins (30 µg) were loaded on a precast gel (CRITERION TGX Stain-Free 10% acrylamide, BioRad, Hercules, CA, USA) to study muscle pPKB (#4060, Cell signaling, Danvers, MA, USA) and PKB (#9272, Cell signaling, Danvers, MA, USA) expression by Western Blot, and its response to insulin stimulation. Membranes are PVDF from BioRad Company (BioRad, Hercules, CA, USA).

Sample Preparation in Liquid Nitrogen

Tissue samples were stored at −80°C. Each one was weighed then put in a mortar placed in a polystyrene box filled with liquid nitrogen to be grounded into a powder. The powders obtained are divided into three equal parts of 80–120 mg, distributed separately to study ribonucleic acid (RNA), proteins and oxidative stress, and stored at −80°C.

Biological Analysis:

All tissues were kept frozen and homogenized with a 10% v/w buffer (PBS + 0.5mM EDTA). Homogenates were centrifuged at 4°C for 4 min at 1500 g for protein content and malondialdehyde (MDA) analysis, and again at 4°C for 10 min at 12,000 g for the remaining analyses. Supernatants were frozen at −80°C. Protein concentrations were determined spectrophotometrically (Biophotometer, Eppendorf, Germany) using a bicinchoninic acid (BCA) kit according to instructions (Sigma, St Louis, USA).

Citrate Synthase

Muscle adaptation to physical activity was determined by skeletal muscle citrate synthase activity measuring using soleus muscle homogenate according to the Shepherd and Garland method (Shepherd and Garland, 1969).

Cholesterol Assay

Total blood cholesterol was assessed using Amplex Red Cholesterol Assay Kit (Invitrogen, Carlsbad, CA) following manufacturer instructions.

Oxidative Stress

Oxidative stress markers (Advanced Oxidation Protein Products, AOPP and Malondialdehyde, MDA) and antioxidants markers (Superoxide dismutase, SOD and Glutathione peroxidase, GPx) were measured in plasma and brain as previously described (Chirico et al., 2012) using the method of Witko-Sarsat et al for AOPP (Witko-Sarsat et al., 1996), Ohkawa et al for MDA (Ohkawa et al., 1979), Oberley and Spitz for SOD (Oberley and Spitz, 1984), and Paglia and Valentine for GPx (Paglia and Valentine, 1967). All reagents used for biochemical assays were purchased from Sigma Aldrich. AOPP and SOD were also measured in descending aorta of ApoE$^{-/-}$ mice.

Inflammatory Markers

Inflammation status was assessed in plasma, brain, and descending aorta supernatant using a commercially available mouse enzyme-linked immunosorbent assay kit (IL-1β: ELM-IL1β-001, Raybiotech; TNFα: Mouse TNF BD OptEIA Kit, BD Biosciences) according to manufacturer's instructions.

Immunochemistry

Brain samples were harvested and fixed in a 4% paraformaldehyde solution during 1 h followed by sucrose for 24 h and preserved at −80°C until processing. Three successive 15 µm-thick sections for 3 MRI locations were assessed with DeadEnd™ Fluorometric TUNEL System kit (PROMEGA, San Luis Obispo, CA, USA) to detect DNA fragmentation (apoptosis), rat anti F4/80 antibody (MF48000, 1/200, CALTAG MEDSYSTEMS, Buckingham, UK) to detect macrophages and AlexaFluor 594 nm (AF594) goat anti-mouse IgG (A11032, Life Technologies, USA) for blood brain barrier (BBB) permeability. AF594 goat anti rat IgG (A11007, 1/1000, Life Technologies, USA) was used as secondary antibody for F4/80 labeling. Slides were mounted with Prolong gold anti-fade reagent (P36935, Life Technologies, USA) supplemented with DAPI for nuclear counterstain. Image acquisition was performed with an Axio Observer Z1 Zeiss microscope.

Statistics

Analyses were conducted using Statistica (version 8.0, Statsoft, Tulsa, OK, USA). As our study is based on longitudinal imaging features, in-house power analysis for assessing the brain effect of HC diet in ApoE$^{-/-}$ mice has shown that 6–7 mice per group are sufficient to reach the statistical potency with 80–90% power. Results are presented as mean ± standard error of the mean (SEM). A normality test (Kolgomorov-Smirnov test) has been applied and the distribution of our data is non-parametric. Statistical comparisons between ApoE$^{-/-}$SED vs. EX were performed by Mann-Whitney U test and comparisons between before and after-training were performed by Wilcoxon test. Linear regression was used for MR scores comparison and Spearman correlation coefficient was measured. Statistical significance was determined by a $p < 0.05$.

RESULTS

Three ApoE$^{-/-}$ mice on HC diet (1 SED and 2 EX) died during the training period. For the 11 animals (5 EX and 6 SED) that completed the entire protocol, weekly running distance and body weight before and after training are detailed in **Table 1**. Oxidative enzyme citrate synthase level in the soleus were higher in EX than in SED ApoE$^{-/-}$ mice ($p = 0.042$; **Figure 2A**). A similar EX to SED differences is observed in the aged-matched WT mice (**Figure 2B**), supporting the physiological efficiency of the exercise training.

Despite a substantial running distance, EX ApoE$^{-/-}$ significantly increased their body weight (+18%, $p = 0.027$) during the 12-weeks training (**Table 1**). Moreover, both EX

TABLE 1 | Training effect: running distances and weight of ApoE$^{-/-}$ (SED = 6; EX = 5) and WT mice (for reference values; SED = 7; EX = 6).

	Group	ApoE$^{-/-}$		WT	
		SED	EX	SED	EX
Before training	Weight (g)	44.7 ± 6.6	40.6 ± 2.5	27.3 ± 0.8	27.4 ± 0.8
After training	Weight (g)	44.3 ± 6.3	45 ± 3.1*	27.2 ± 0.5	27.7 ± 0.4
	Mean Δweight (%)	1%	18%	<1%	<1%
	Running distances (km/week)	N/A	12.5 ± 5.4	N/A	16.2 ± 3.6

*$p < 0.05$ Significantly different from before training.

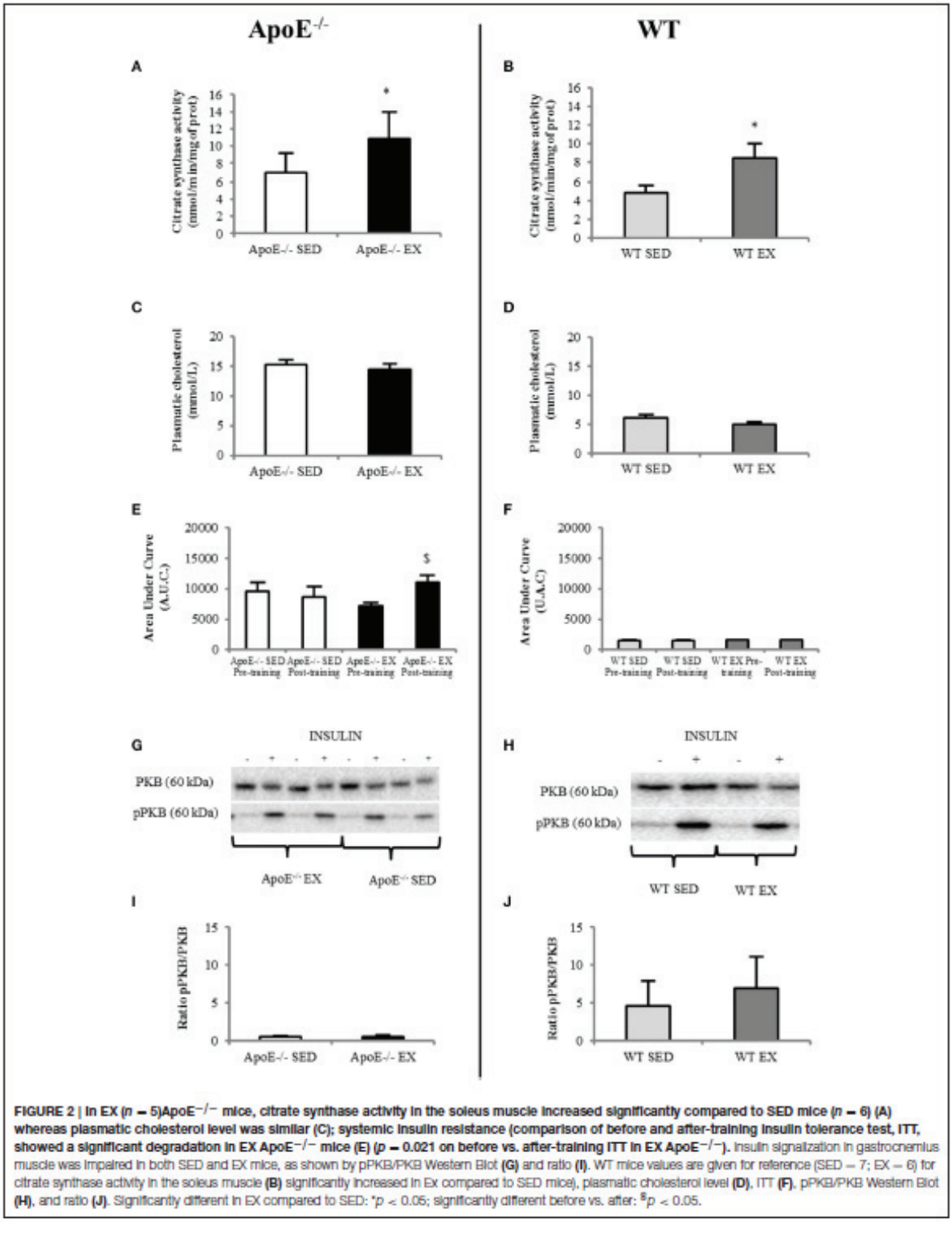

FIGURE 2 | In EX ($n = 5$)ApoE$^{-/-}$ mice, citrate synthase activity in the soleus muscle increased significantly compared to SED mice ($n = 6$) (A) whereas plasmatic cholesterol level was similar (C); systemic insulin resistance (comparison of before and after-training insulin tolerance test, ITT, showed a significant degradation in EX ApoE$^{-/-}$ mice (E) ($p = 0.021$ on before vs. after-training ITT in EX ApoE$^{-/-}$). Insulin signalization in gastrocnemius muscle was impaired in both SED and EX mice, as shown by pPKB/PKB Western Blot **(G)** and ratio **(I)**. WT mice values are given for reference (SED = 7; EX = 6) for citrate synthase activity in the soleus muscle **(B)** significantly increased in Ex compared to SED mice), plasmatic cholesterol level **(D)**, ITT **(F)**, pPKB/PKB Western Blot **(H)**, and ratio **(J)**. Significantly different in EX compared to SED: $^{*}p < 0.05$; significantly different before vs. after: $^{\$}p < 0.05$.

and SED ApoE$^{-/-}$ mice were already obese at the beginning of the study (**Table 1,** Figure S1).The fat index measured using MR spectroscopy showed no difference of fat content, and 3D fat MRI, no apparent difference of fat distribution in ApoE$^{-/-}$EX mice compared to their sedentary counterparts (Figure S1). Furthermore, visceral and subcutaneous adipose tissues had similar weight in both EX and SED ApoE$^{-/-}$ mice (Table S1).

Metabolic Parameters

Plasma cholesterol was high in ApoE$^{-/-}$ mice and was not modified by exercise training (i.e., no difference between EX and SED ApoE$^{-/-}$, **Figure 2C**). It was normal in both EX and SED WT mice, and not modified by exercise training (**Figure 2D**). Insulin tolerance test showed low insulin tolerance in ApoE$^{-/-}$ mice independently of training paradigm and time of the study as demonstrated by the large Area Under Curve of glucose concentration over time (AUC, **Figure 2E**). WT values are given in **Figure 2F**. It should also be pointed that ApoE$^{-/-}$ EX mice significantly further lowered their insulin tolerance after the training ($p = 0.027$) (**Figures 2C** and Figure S2).

Western blots of pPKB/PKB in gastrocnemius confirmed that both EX and SED ApoE$^{-/-}$ mice had muscle insulin resistance (**Figures 2G,I**).Values of aged-matched EX and SED WT mice are presented in **Figures 2H,J**. There was no beneficial effect of physical activity on muscle insulin sensitivity in ApoE$^{-/-}$ mice (**Figure 2I**).

Brain Imaging and Immunochemistry

Brain MRI performed at the beginning of the study showed that ApoE$^{-/-}$ mice brain have focal areas (periventricular area) of BBB leakage on post-gadolinium T1 images (**Figure 3**).

Analysis of longitudinal data showed that these features, present in old ApoE$^{-/-}$ mice (Chirico et al., 2016), evolved during the 12-weeks training in EX ApoE$^{-/-}$ mice, as confirmed by the significant increase in post-gadolinium T1 score ($p = 0.02$, **Figure 3A–B**), when there was no significant change in SED ApoE$^{-/-}$ mice. After-training, focal periventricular areas of signal loss were observed on T2* maps in both EX and SED ApoE$^{-/-}$ mice (Figure S3), but there were no significant T2 and T2* scores changes after the follow-up period. After-training post-USPIOs score showed more extended inflammation areas in EX ApoE$^{-/-}$ mice compared to SED ($p = 0.015$, **Table 2** and Figure S3). Inflammation areas co-localized with the periventricular BBB leakage and abnormalities on T2/T2* images (**Figure 3** and Figure S3). Post-USPIOs T2 score was significantly associated with the increased BBB leakage (ΔT1 score) in EX ApoE$^{-/-}$ mice ($p = 0.049$, **Figure 3C**).

There were no such features and no changes during follow-up in both EX and SED WT mice (data not shown, mean score of one for T1, T2, and T2* before and after training), and no periventricular post-USPIOs abnormalities on T2* maps (Figure S3).

To characterize brain lesions in ApoE$^{-/-}$ mice, WT mice served as negative control for the immunohistochemistry staining. In ApoE$^{-/-}$ mice disorganized brain parenchyma was seen in the middle ventral zone, but was not related to an active apoptotic process (TUNEL negative on immunohistochemistry; data not shown). F4/80 and IgG immunostaining indicated BBB leakage (endothelial permeability), and macrophage accumulation in the periventricular region and the fornix fimbria of the hippocampus (**Figure 4**). Visually, there was also some evidence of vesicular aggregates which could indicate foam cell development and cholesterol crystals, as already described (Walker et al., 1997).

Oxidative Stress/Inflammation in Brain

Imaging data were confirmed by assays that showed that ApoE$^{-/-}$ mice have high brain inflammation (IL-1β and TNFα; **Figures 5A–B**) and oxidative stress (MDA and AOPP were high, GPx had low activity; **Figures 5C–E** for ApoE$^{-/-}$) regarding to reference values of WT mice (**Figures 5G–L**). No beneficial effect of exercise was noted in ApoE$^{-/-}$ EX group.

Oxidative Stress/Inflammation in Plasma and Aorta

In aorta, ApoE$^{-/-}$ mice showed high concentration of the pro-inflammatory cytokines IL-1β and TNFα (Table S2). Oxidative stress was also present in ApoE$^{-/-}$ mice as shown by the high AOPP level (protein oxidization; Table S2).

Plasmatic IL-1β was high in both EX and SED ApoE$^{-/-}$ mice as well as oxidative stress (AOPP; Table S2). Reference values for WT mice are given in Table S2.

In these two tissues of interest, no beneficial effect of training was observed.

DISCUSSION

The aim of the present study was to determine both the peripheral and central effects of exercise training in 45 weeks-old ApoE$^{-/-}$ mice fed *ad libitum* with a high fat/ high cholesterol (HC) diet using imaging and insulin tolerance test for follow-up. This diet given *ad libitum* was initially used to describe for the first time in the ApoE$^{-/-}$ mouse the presence of vulnerable plaques, associated with a high mortality rate (Johnson and Jackson, 2001). We found that peripheral (insulin sensitivity and oxidative/inflammatory status) but also central features (BBB preservation and protection against inflammation) did not show any benefits of exercise. Indeed, there was a fast induction of irreversible brain damage that was more pronounced in exercise-trained ApoE$^{-/-}$ mice.

While it is already known from large clinical studies that exercise training may encounter non or even adverse response for glucose homeostasis (Böhm et al., 2016), this study is the first to show that the combination of physical training and *ad libitum* HC diet also impairs central mechanisms in a mouse model of advanced atherosclerosis. Indeed, mature ApoE$^{-/-}$ mice, i.e., with subsequent abnormal cholesterol handling, over-responded to the HC diet given *ad libitum*. *In vivo* MRI demonstrated the evolutive hippocampal consequences with an extremely fast induction of BBB leakiness that is correlated with an inflammatory burst with macrophage recruitment and high phagocytic activity (**Figure 3**). A parallel degradation of the systemic insulin response was measured (**Figure 2**).

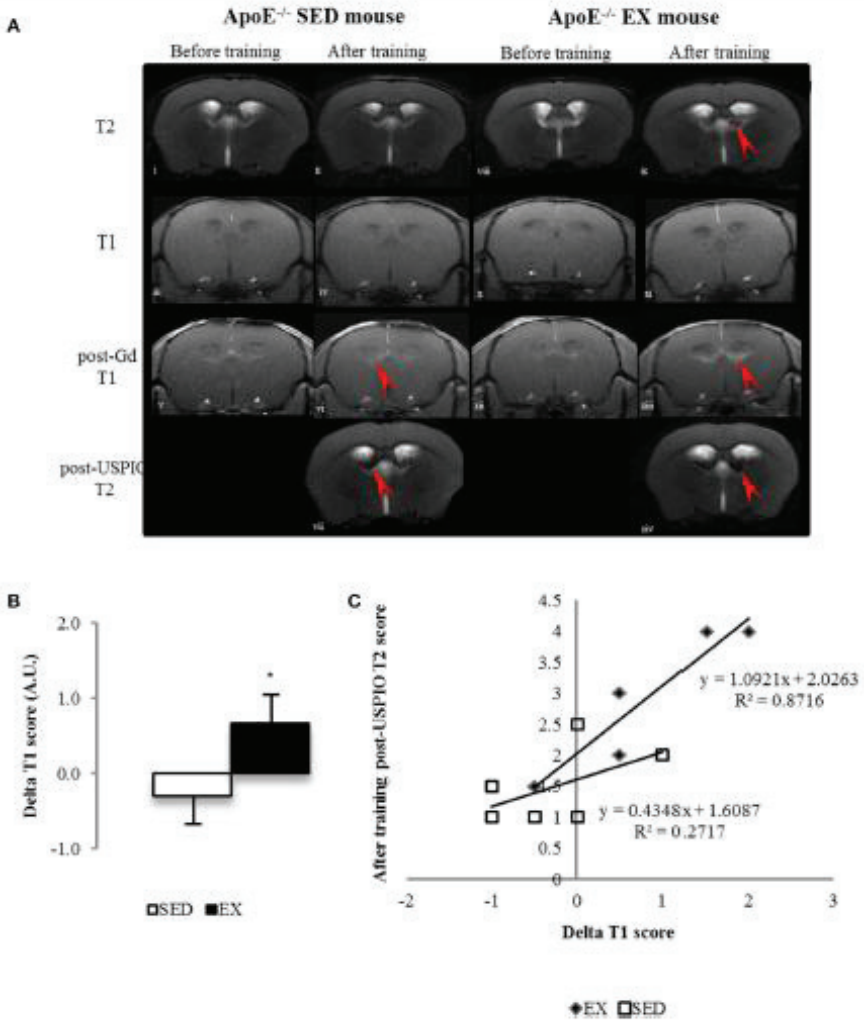

FIGURE 3 | Longitudinal brain MR images of a SED (i–vii) and an EX ApoE$^{-/-}$ mouse (viii–xiv). before (i, viii) and after training (ii, ix) native T2 image; native (iii, iv, x, xi) and Post-Gadolinium (Gd) T1 images (v, vi, xii, xiii), the enhancing bright zone after Gd showing BBB leakage in ApoE$^{-/-}$ mouse (vi, red arrow); Post-USPIO (vii, xiv) T2 images, the loss of signal showing USPIO phagocytosis by macrophages in ApoE$^{-/-}$ (vii, red arrow) **(A)** Delta score of longitudinal brain MR imaging before and after-training score of post-Gd T1 **(B)** in SED and EX ApoE$^{-/-}$ mice **(B)** ($p = 0.02$ compared to SED). Linear regression of Delta T1 (ΔT1) scores and after-training post-USPIOs T2 scores of EX and SED ApoE$^{-/-}$ mice showed a stronger correlation between increased BBB leakage and high phagocytic activity in EX mice **(C)** ($p = 0.049$). Significantly different from SED mice: *$p < 0.05$.

The observed consequences were neurological symptoms and mortality within the 12 weeks of follow-up (25 and 16% in EX and SED ApoE$^{-/-}$, respectively). This clinical aggravation was observed despite a regular physical activity, which was supposed to induce protection and counteract neuroinflammation and oxidative stress, as previously described when the food quantity was limited to 20 g/week in both sedentary and exercise mice (Chirico et al., 2016). In this context of limited access to the HC diet, exercise training, possibly via its oxidative stress and inflammation lowering capabilities, reduced brain macrophage infiltration, limited inflammation, and oxidative stress in the brain, and also improved insulin sensitivity. In a recent study, 50-weeks old C57Bl/6 mice on *ad libitum* high fat diet presented peripheral and central metabolic consequences, but as these mice were not in a high cardiovascular risk, there was no pathological damage (Gotthardt et al., 2016). Therefore, this amplification in ApoE$^{-/-}$ mice happened in a window where susceptibility to oxidative stress and hippocampal damage was high and was further aggravated by the abrupt HC diet exposure (HC diet starting 1 month before training), similar to what can be observed

TABLE 2 | After—training comparison of brain MR imaging scores of ApoE$^{-/-}$: vascular lesions (T2* score), USPIO's assessment of inflammation (post-USPIOs T2* score) and post-Gd BBB leakage (post-gadolinium T1-weighted sequence).

	ApoE$^{-/-}$ SED	ApoE$^{-/-}$ EX
T2* score	1.4 ± 0.3 (2)	1.2 ± 0.1 (4)
Post-USPIOs T2* score	1.6 ± 0.3 (2)	2.6 ± 1.0.5 (5)*
Post-Gd T1 score	2.4 ± 0.5 (4)	2.3 ± 0.4 (5)

*In brackets, number of mice with score > 1. *p < 0.05 Significantly different from ApoE$^{-/-}$ SED mice (mean ± SEM).*

in the human transition phases such as retirement, where eating, and physical habits are particularly evolving whereas there is a parallel decrease of insulin sensitivity with age. A previous paper with diet-induced obese mice proposed a model where a high fat diet rich in saturated fat given *ad libitum* induced an excessive consumption food behavior associated with hippocampal dysfunction (Kanoski and Davidson, 2011). Here, the diet contained 21% lard and 0.15% cholesterol and was given without restriction, with more weight gain in EX ApoE$^{-/-}$ mice compared to SED. Compared to other high cholesterol diets, this one is also richer in saturated fat (pork lard), which may have contributed to the insulin sensitivity degradation. In the early study of Johnson and Jackson, the high mortality rate was also attributed to this diet composition (Johnson and Jackson, 2001).

We also found that oxidative stress and inflammation were not decreased by exercise training in three tissues of interest (plasma, abdominal aorta, and brain). The measured markers presented similar (AOPP, SOD, and IL-1β) values in EX compared with SED ApoE$^{-/-}$ mice. Insulin response and cholesterol level were also not different between these 2 groups although EX mice showed a significant higher citrate synthase activity in their soleus muscle, supporting the muscular enzymatic effect of physical training. In term of metabolism, there was no beneficial effect of training on either insulin resistance (as shown both in plasma and muscle, with even an aggravation of systemic insulin resistance in EX ApoE$^{-/-}$ mice; **Figure 2**), or body composition (as assessed by the fat content measured by MRI) in old ApoE$^{-/-}$ mice. The weight gain was even more pronounced in EX ApoE$^{-/-}$ mice, and brain MRI clearly showed that ApoE$^{-/-}$ EX mice were more affected both in terms of focal BBB leakage and of microglia/macrophage accumulation. All these features (lack of changes, even worsening of the pathological parameters) of the EX group, which are contradictory with the usual beneficial impact of exercise training (Xu et al., 2011; Rao et al., 2013), have been possibly driven by the weight gain observed in the EX ApoE$^{-/-}$ mice when fed *ad libitum* with high HC diet.

In the present study, the ApoE$^{-/-}$ mice under HC diet can be considered obese with regards to their weight at the beginning of the study (1.5-fold higher than age-matched WT mice). Furthermore, EX ApoE$^{-/-}$ mice also had a decreased response to insulin during the 12 weeks of training, suggesting that their insulin resistance state was worsened instead of being improved as commonly assumed from an endurance training protocol (Roberts et al., 2013). It is also interesting to note that abdominal fat was primary subcutaneous and visceral (Figure S1), as typically observed in metabolic syndrome patients or animal model (Patel and Abate, 2013). In obese subjects, it was observed that for the same physical activity level, those under food restriction presented reduced oxidative stress, inflammation and insulin resistance while those without food restriction experienced increased body weight and no improvement of fat distribution (Bergouignan et al., 1985). Similarly, in animal model, both inflammation and insulin sensitivity worsened in trained obese mice with *ad libitum* diet whereas it was fully improved when the diet was controlled (Ringseis et al., 2015).

Previous studies have shown that there are also specific locations for the positive effect of exercise on brain inflammation (Yi et al., 2012). However, in rodents, there seems to be major differences depending on the nature of the exercise (forced versus voluntary) in response to both the food intake control and the central effect of exercise (Leasure and Jones, 2008; Copes et al., 2015). Nevertheless, MRI studies on diet interventions have shown that diet-induced inflammation and gliosis are mainly located in the hypothalamic region (Thaler et al., 2012; Berkseth et al., 2014). Recently, in the context of obesity, the central effect of exercise to decrease neuroinflammation was described in the hippocampus region (Erion et al., 2014; Koga et al., 2014; Spielman et al., 2014; Auer et al., 2015).

An emerging field of research focuses on the new major roles of inflammation in brain diseases, where both its balanced deleterious and beneficial effects are still under debate (Mori et al., 2014). The complex interactions between the nervous system and the immune system are now thought to occur at specific interfaces such as the choroid plexus. Indeed, the brain anomalies that we observed in the old ApoE$^{-/-}$ mice under HC diet are originally located in these areas and further extended from these periventricular areas (Leasure and Jones, 2008; Berkseth et al., 2014; Koga et al., 2014; Van der Donckt et al., 2015).

Due to the small number of animals, further studies would be needed to determine if there is any relationship between the activity level and brain inflammation. It would also be important to evaluate whether there is a difference of mortality rate between exercise and sedentary mice, or between male and female. Similar to the earlier study from Johnson and Jackson (2001), we did not observed any gender effect, but a larger animal group would be needed to further evaluate these possible differences.

Among the MRI biomarkers used in this study, the post-gadolinium T1 follow-up showed the unrevealed fast evolution of BBB leakiness in the ApoE$^{-/-}$ mice after HC diet exposure. The T2 and T2∗ scores were however unable to show a parallel evolution of tissue damage, which can be due to the small sample size. Yet, the change of T1 was strongly associated with the post-USPIO T2 score, and the two areas co-localized (**Figure 4** and Figure S2). The evaluation of inflammation was done on T2 images (post-USPIO T2 score) rather than on T2* maps because of technical issues. T2* images are very sensitive to slight changes of MR signal homogeneities, such as those observed when surface coils are used for signal reception or after retro-orbital injection of USPIO. Yet, it is noticeable that periventricular inflammation

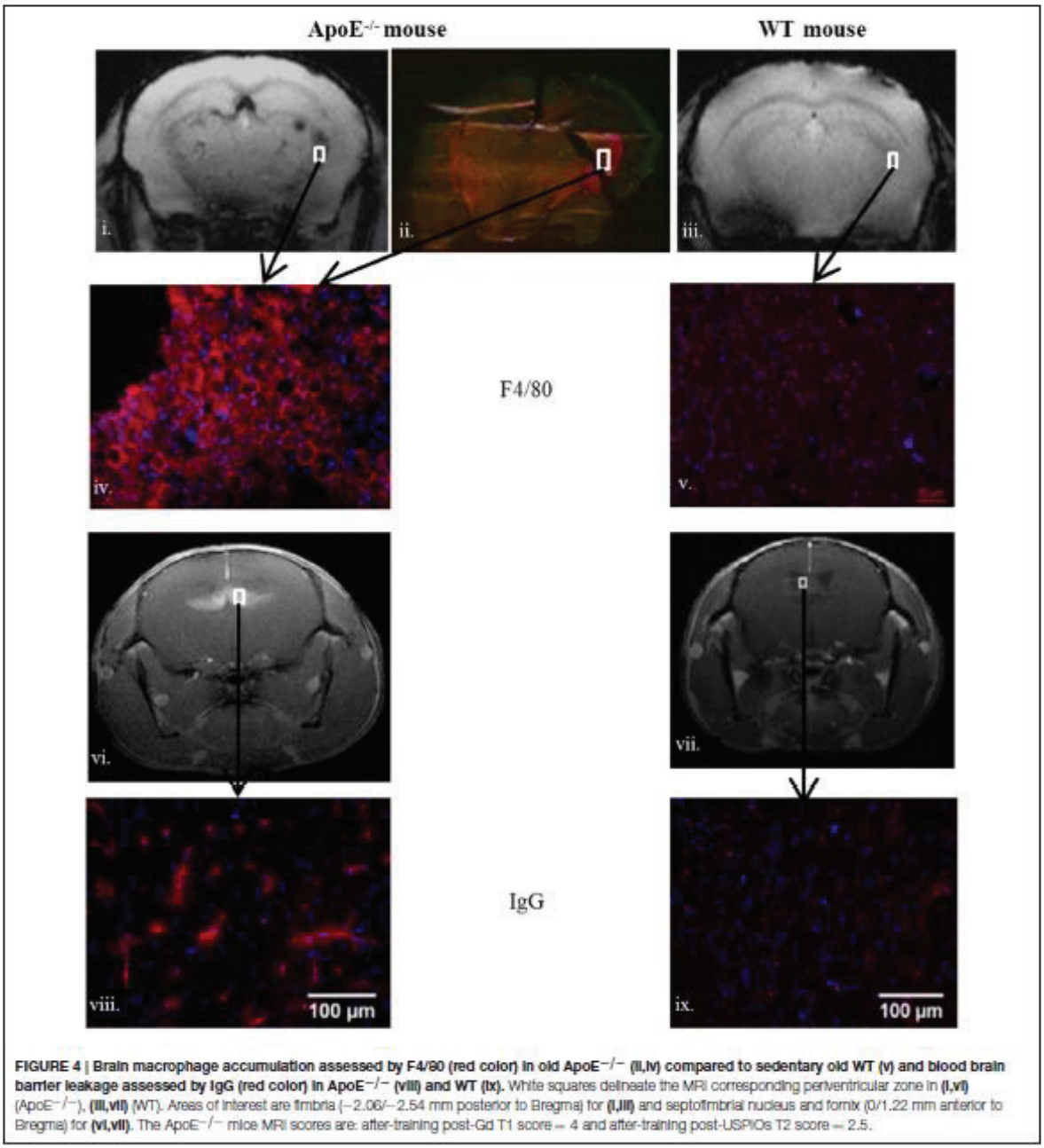

FIGURE 4 | Brain macrophage accumulation assessed by F4/80 (red color) in old ApoE$^{-/-}$ (II,IV) compared to sedentary old WT (v) and blood brain barrier leakage assessed by IgG (red color) in ApoE$^{-/-}$ (VIII) and WT (IX). White squares delineate the MRI corresponding periventricular zone in **(I,VI)** (ApoE$^{-/-}$), **(III,VII)** (WT). Areas of interest are fimbria (−2.06/−2.54 mm posterior to Bregma) for **(I,III)** and septofimbrial nucleus and fornix (0/1.22 mm anterior to Bregma) for **(VI,VII)**. The ApoE$^{-/-}$ mice MRI scores are: after-training post-Gd T1 score = 4 and after-training post-USPIOs T2 score = 2.5.

developed around small existing focal T2* lesions, as can be seen from T2* maps (baseline and post-USPIO, Figure S2). These lesions can either be vascular microbleeds or brain accumulation of erythrocytes and iron deposit (Yi et al., 2012; Erion et al., 2014; Van der Donckt et al., 2015), as previously shown in this model (Chirico et al., 2016). Using a high magnetic field and a high-sensitivity transmit/receive volume radio-frequency coil, it was recently shown that higher spatial resolution T2* mapping can detect very small quantity of iron or USPIO (Mori et al., 2014). In this specific study where neuro-inflammation was induced by a LPS challenge, there was no link between BBB leakage and inflammation. The new finding of rapid BBB

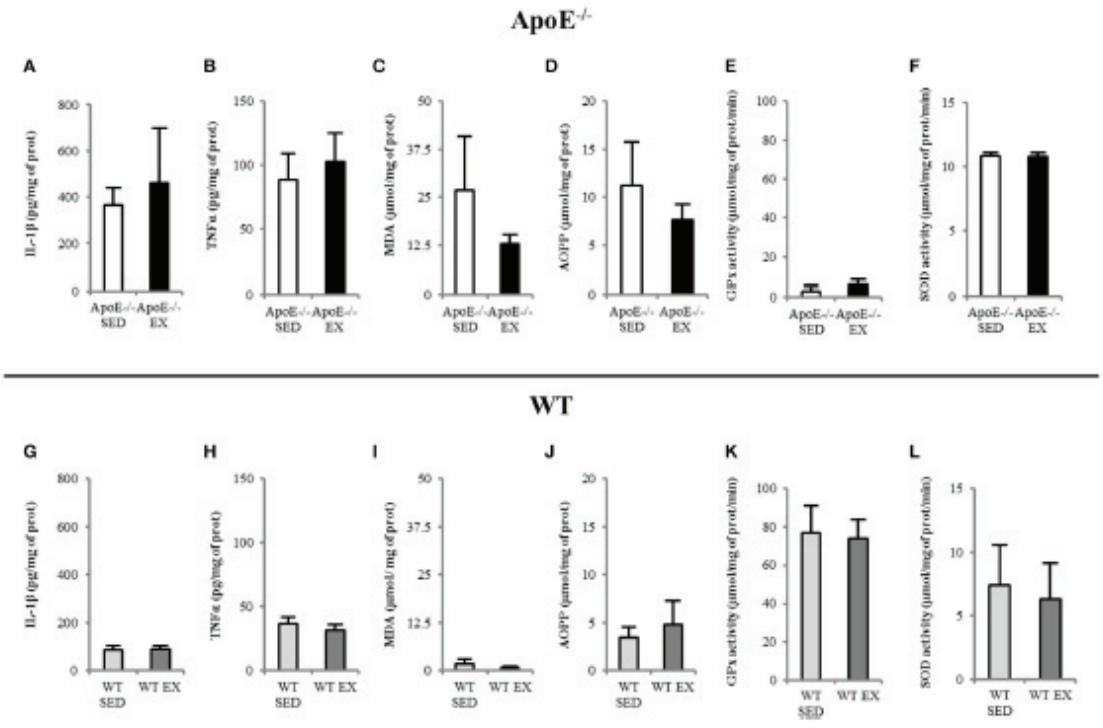

FIGURE 5 | EX and SED ApoE$^{-/-}$ mice showed high brain inflammation level (A,B) and oxidative stress (C–F) in both SED and EX ApoE$^{-/-}$ mice. WT values are given for reference in brain inflammation **(G–H)** and oxidative stress **(I–L)**. IL-1β (Interleukin 1β) and TNFα (Tumor Necrosis Factor alpha), MDA (Malondialdehyde), AOPP (Advanced Oxidization Proteins Products), GPx (GluthationPeroxydase) activity, SOD (Superoxide Dismutase) activity.

leakage evolution can be compared to previous mechanistic studies where abnormalities of both aquaporin 4 and tight junction proteins expression were found in the same mouse model (Thaler et al., 2012). In apparent contradiction with the present result in this ApoE$^{-/-}$ model, the destabilization of the neurovascular unit was partially modulated by exercise (Soto et al., 2015; Chirico et al., 2016). Yet, in our specific conditions of brutal HC diet exposure with no food consumption control, the imaging follow-up demonstrated aggravated BBB leakage that correlated with inflammation imaging, with high systemic, and brain inflammation and oxidative stress, and the brain status even worsened in exercise-trained mice. Future studies with higher spatial resolution MRI may provide deeper explanations of focal dynamic processes. An additional control group of ApoE$^{-/-}$ mice under chow diet could also be included to follow the effect of exercise without diet intervention. As previously shown in ApoE$^{-/-}$ mice under controlled diet intake (Chirico et al., 2016), they are likely to show a similar positive evolution if they have initial BBB lesion, or no evolution if they have normal BBB as our control group of age-matched WT mice.

In summary, we showed for the first time in this study that abrupt transition to HC diet with non-restricted consumption in old ApoE$^{-/-}$ mice impairs the expected central beneficial effect of exercise, leading to enhanced inflammation and BBB leakage in the areas involved in immune cells recruitments. Therefore, this work emphasizes the need for further longitudinal studies in order to evaluate the neuro-immune interactions and elucidate the central effect of the interventions.

AUTHOR CONTRIBUTIONS

VD, VP, and EC designed the study; VD, AG, JL, FC, BT, ENC, VP, and EC analyzed the data; VD, BT, FC, MW, HV, VP, and EC interpreted the data; VD, VP, and EC drafted the manuscript; VD, AG, FC, VH, MW, JR, HV, VP, and EC revised the manuscript critically for important intellectual content; VD, AG, JL, FC, BT, VH, MW, ENC, JR, HV, VP, and EC approved the final version of the manuscript submitted.

FUNDING

This study was supported by the Institut Universitaire de France and the University Claude Bernard Lyon 1 for Ph. D. students.

ACKNOWLEDGMENTS

We thank Caroline Gastebois for her helps on statistical analysis, Guerbet for providing animals, the INSA's animal facility for animal housing and caring and Emily Tubbs for editing.

SUPPLEMENTARY MATERIAL

The Supplementary Material for this article can be found online at: http://journal.frontiersin.org/article/10.3389/fphys.2016.00453

REFERENCES

Akoudad, S., Ikram, M. A., Koudstaal, P. J., Hofman, A., Niessen, W. J., Greenberg, S. M., et al. (2014). Cerebral microbleeds are associated with the progression of ischemic vascular lesions. *Cerebrovasc. Dis.* 37, 382–388. doi: 10.1159/000362590

Auer, M. K., Sack, M., Lenz, J. N., Jakovcevski, M., Biedermann, S. V., Falfán-Melgoza, C., et al. (2015). Effects of a high-caloric diet and physical exercise on brain metabolite levels: a combined proton MRS and histologic study. *J. Cereb. Blood Flow Metab.* 35, 554–564. doi: 10.1038/jcbfm.2014.231

Badaut, J., Copin, J.-C., Fukuda, A. M., Gasche, Y., Schaller, K., Da Silva, R. F., et al. (2012). Increase of arginase activity in old apolipoprotein-E deficient mice under Western diet associated with changes in neurovascular unit. *J. Neuroinflammation* 9, 132. doi: 10.1186/1742-2094-9-132

Bergouignan, A., Antoun, E., Momken, I., Schoeller, D. A., Gauquelin-Koch, G., Simon, C., et al. (1985). Effect of contrasted levels of habitual physical activity on metabolic flexibility. *J. Appl. Physiol.* 114, 371–379. doi: 10.1152/japplphysiol.00458.2012

Berkseth, K. E., Guyenet, S. J., Melhorn, S. J., Lee, D., Thaler, J. P., Schur, E. A., et al. (2014). Hypothalamic gliosis associated with high-fat diet feeding is reversible in mice: a combined immunohistochemical and magnetic resonance imaging study. *Endocrinology* 155, 2858–2867. doi: 10.1210/en.2014-1121

Böhm, A., Weigert, C., Staiger, H., and Häring, H.-U. (2016). Exercise and diabetes: relevance and causes for response variability. *Endocrine* 51, 390–401. doi: 10.1007/s12020-015-0792-6

Chirico, E. N., Martin, C., Faës, C., Féasson, L., Oyono-Enguéllé, S., Aufradet, E., et al. (2012). Exercise training blunts oxidative stress in sickle cell trait carriers. *J. Appl. Physiol.* 112, 1445–1453. doi: 10.1152/japplphysiol.01452.2011

Chirico, E. N., Di Cataldo, V., Chauveau, F., Geloën, A., Patsouris, D., Thézé, B., et al. (2016). MRI biomarkers of exercise-induced improvement of oxidative stress and inflammation in the brain of old high fat fed ApoE−/− mice. *J. Physiol.* doi: 10.1113/JP271903. [Epub ahead of print].

Copes, L. E., Schutz, H., Dlugosz, E. M., Acosta, W., Chappell, M. A., and Garland, T. (2015). Effects of voluntary exercise on spontaneous physical activity and food consumption in mice: results from an artificial selection experiment. *Physiol. Behav.* 149, 86–94. doi: 10.1016/j.physbeh.2015.05.025

ElAli, A., Doeppner, T. R., Zechariah, A., and Hermann, D. M. (2011). Increased blood-brain barrier permeability and brain edema after focal cerebral ischemia induced by hyperlipidemia: role of lipid peroxidation and calpain-1/2, matrix metalloproteinase-2/9, and RhoA overactivation. *Stroke* 42, 3238–3244. doi: 10.1161/STROKEAHA.111.615559

Erion, J. R., Wosiski-Kuhn, M., Dey, A., Hao, S., Davis, C. L., Pollock, N. K., et al. (2014). Obesity elicits interleukin 1-mediated deficits in hippocampal synaptic plasticity. *J. Neurosci.* 34, 2618–2631. doi: 10.1523/JNEUROSCI.4200-13.2014

Gleeson, M., Bishop, N. C., Stensel, D. J., Lindley, M. R., Mastana, S. S., and Nimmo, M. A. (2011). The anti-inflammatory effects of exercise: mechanisms and implications for the prevention and treatment of disease. *Nat. Rev. Immunol.* 11, 607–615. doi: 10.1038/nri3041

Goh, J., and Ladiges, W. (2015). Voluntary wheel running in mice. *Curr. Protoc. Mouse Biol.* 5, 283–290. doi: 10.1002/9780470942390.mo140295

Gotthardt, J. D., Verpeut, J. L., Yeomans, B. L., Yang, J. A., Yasrebi, A., Roepke, T. A., et al. (2016). Intermittent fasting promotes fat loss with lean mass retention, increased hypothalamic norepinephrine content, and increased neuropeptide y gene expression in diet-induced obese male mice. *Endocrinology* 157, 679–691. doi: 10.1210/en.2015-1622

Hafezi-Moghadam, A., Thomas, K. L., and Wagner, D. D. (2006). ApoE deficiency leads to a progressive age-dependent blood-brain barrier leakage. *AJP Cell Physiol.* 292, C1256–C1262. doi: 10.1152/ajpcell.00563.2005

Hicks, J. A., Hatzidis, A., Arruda, N. L., Gelineau, R. R., De Pina, I. M., Adams, K. W., et al. (2016). Voluntary wheel-running attenuates insulin and weight gain and affects anxiety-like behaviors in C57BL6/J mice exposed to a high-fat diet. *Behav. Brain Res.* 310, 1–10. doi: 10.1016/j.bbr.2016.04.051

Johnson, J. L., and Jackson, C. L. (2001). Atherosclerotic plaque rupture in the apolipoprotein E knockout mouse. *Atherosclerosis* 154, 399–406. doi: 10.1016/S0021-9150(00)00515-3

Kanoski, S. E., and Davidson, T. L. (2011). Western diet consumption and cognitive impairment: links to hippocampal dysfunction and obesity. *Physiol. Behav.* 103, 59–68. doi: 10.1016/j.physbeh.2010.12.003

Koga, S., Kojima, A., Ishikawa, C., Kuwabara, S., Arai, K., and Yoshiyama, Y. (2014). Effects of diet-induced obesity and voluntary exercise in a tauopathy mouse model: implications of persistent hyperleptinemia and enhanced astrocytic leptin receptor expression. *Neurobiol. Dis.* 71, 180–192. doi: 10.1016/j.nbd.2014.08.015

Laufs, U., Wassmann, S., Czech, T., Münzel, T., Eisenhauer, M., Böhm, M., et al. (2005). Physical inactivity increases oxidative stress, endothelial dysfunction, and atherosclerosis. *Arterioscler. Thromb. Vasc. Biol.* 25, 809–814. doi: 10.1161/01.ATV.0000158311.24443.af

Leasure, J. L., and Jones, M. (2008). Forced and voluntary exercise differentially affect brain and behavior. *Neuroscience* 156, 456–465. doi: 10.1016/j.neuroscience.2008.07.041

Lee, D., Thaler, J. P., Berkseth, K. E., Melhorn, S. J., Schwartz, M. W., and Schur, E. A. (2013). Longer T(2) relaxation time is a marker of hypothalamic gliosis in mice with diet-induced obesity. *Am. J. Physiol. Endocrinol. Metab.* 304, E1245–E1250. doi: 10.1152/ajpendo.00020.2013

Mori, Y., Chen, T., Fujisawa, T., Kobashi, S., Ohno, K., Yoshida, S., et al. (2014). From cartoon to real time MRI: *in vivo* monitoring of phagocyte migration in mouse brain. *Sci. Rep.* 4:6997. doi: 10.1038/srep06997

Naville, D., Labaronne, E., Vega, N., Pinteur, C., Canet-Soulas, E., Vidal, H., et al. (2015). Metabolic outcome of female mice exposed to a mixture of low-dose pollutants in a diet-induced obesity model. *PLoS ONE* 10:e0124015. doi: 10.1371/journal.pone.0124015

Nighoghossian, N., Wiart, M., Cakmak, S., Berthezène, Y., Derex, L., Cho, T.-H., et al. (2007). Inflammatory response after ischemic stroke: a USPIO-enhanced MRI study in patients. *Stroke* 38, 303–307. doi: 10.1161/01.STR.0000254548.30258.f2

Oberley, L. W., and Spitz, D. R. (1984). Assay of superoxide dismutase activity in tumor tissue. *Methods Enzymol.* 105, 457–464.

Ohkawa, H., Ohishi, N., and Yagi, K. (1979). Assay for lipid peroxides in animal tissues by thiobarbituric acid reaction. *Anal. Biochem.* 95, 351–358.

Paglia, D. E., and Valentine, W. N. (1967). Studies on the quantitative and qualitative characterization of erythrocyte glutathione peroxidase. *J. Lab. Clin. Med.* 70, 158–169.

Patel, P., and Abate, N. (2013). Body fat distribution and insulin resistance. *Nutrients* 5, 2019–2027. doi: 10.3390/nu5062019

Pialoux, V., Brown, A. D., Leigh, R., Friedenreich, C. M., and Poulin, M. J. (2009). Effect of cardiorespiratory fitness on vascular regulation and oxidative stress in postmenopausal women. *Hypertension* 54, 1014–1020. doi: 10.1161/HYPERTENSIONAHA.109.138917

Rao, X., Zhong, J., Xu, X., Jordan, B., Maurya, S., Braunstein, Z., et al. (2013). Exercise protects against diet-induced insulin resistance through downregulation of protein kinase Cβ in mice. *PLoS ONE* 8:e81364. doi: 10.1371/journal.pone.0081364

Rieusset, J., Chauvin, M.-A., Durand, A., Bravard, A., Laugerette, F., Michalski, M.-C., et al. (2012). Reduction of endoplasmic reticulum stress using chemical chaperones or Grp78 overexpression does not protect muscle cells from palmitate-induced insulin resistance. *Biochem. Biophys. Res. Commun.* 417, 439–445. doi: 10.1016/j.bbrc.2011.11.135

Ringseis, R., Eder, K., Mooren, F. C., and Krüger, K. (2015). Metabolic signals and innate immune activation in obesity and exercise. *Exerc. Immunol. Rev.* 21, 58–68.

SUPPLEMENTAL DATA

Material and Methods:

Brain imaging:

Using standard MRI brain coronal localizers and anatomical references for careful pre and post-contrast registration, T2 RARE and T2* multi-slice multi-echo gradient echo (MGE) sequence positioned were acquired in the axial plane. The RARE sequence was used with the following parameters: TR/TE = 4000 / 69 ms; field of view = 2 x 2 cm; matrix = 256 x 256; slice thickness = 1 mm; RARE factor= 8, number of slices = 15. The MGE sequence was used with the following parameters: TR / first TE = 1500 / 3.2 ms; flip angle = 75°; field of view = 2 x 2 cm; matrix = 192 x 192; slice thickness = 1 mm; 12 echoes and echo interval = 7.2 ms; number of slices = 15.

Neurovascular lesions and iron deposits were assessed respectively by baseline T2 and T2* imaging. T2* quantification was obtained using a MGE sequence. For BBB permeability assessment, the T1-weighted MGE sequence with identical geometrical parameters was acquired. The parameters are the following: TR/TE = 124 / 2.8 ms; field of view = 2 x 2 cm; matrix = 256 x 192; slice thickness = 1 mm; number of slices = 15.

Statistics:

Comparison between before and after-training glucose levels per each time point were performed using One-way ANOVA. Statistical significance was determined by a *p value* of less than 0.05.

FIGURES LEGENDS:

Table S1: Weight measurement of visceral and subcutaneous adipose tissues in sedentary (SED) and exercise trained (EX) ApoE$^{-/-}$ mice. SED and EX WT mice values are given for reference.

Table S2: Increased pro-inflammatory cytokines (IL-1β and TNFα) and oxidative stress markers (AOPP and SOD) concentration in aorta and plasma of both SED and EX ApoE$^{-/-}$ mice. SED and EX WT mice values are given for reference.

Figure S1: Abdominal MRI of fat mass of a SED (A) and an EX ApoE$^{-/-}$ mouse (B) and fat mass index (C) of ApoE$^{-/-}$ mice after the 12-weeks training. EX mice showed no apparent differences of fat distribution compared to SED mice (C). In both EX and SED ApoE$^{-/-}$ mice, localization of the fat depots was typical of the metabolic syndrome (A-B). Of note, the liver signal on the fat image was also higher than normal in both cases (A-B).

Figure S2: Impaired glucose time-course during insulin tolerance test of both SED and EX ApoE$^{-/-}$ mice before and after the twelve-weeks training (A). SED and EX WT mice values are given for reference, before and after the training (B). $ Significantly different from corresponding mice pre-training condition $p<0.05$; $$ $p<0.005$.

Figure S3: T2* map of SED and EX ApoE$^{-/-}$ mice before the twelve-weeks training (A for SED, D for EX) and after training (B for SED and E for EX), and after training post-USPIOs T2* in SED (C) and EX (F) ApoE$^{-/-}$ mice showing phagocytosis activity in periventricular areas. WT mice T2* maps under the same conditions are given for reference, before (G, J) and after training (H-I, K-L; I and L are after training post-USPIOs T2* maps). Display parameters (window width and contrast level) are identically set for all maps (respectively 5500 and 2500). After training, focal low T2* areas are visible in both SED and EX ApoE$^{-/-}$ (arrow, B and E). Inflammation is present around these areas, as shown by post-USPIOs maps (arrow, C and F).

TABLE S1:

	ApoE$^{-/-}$		WT	
	SED	EX	SED	EX
Visceral AT (g)	1.4 ± 0.5	1.5 ± 0.4	0.2 ± 0.0	0.1 ± 0.0
Subcutaneous AT (g)	1.9 ± 0.9	1.4 ± 0.4	0.4 ± 0.0	0.3 ± 0.0

TABLE S2:

		ApoE$^{-/-}$ SED	ApoE$^{-/-}$ EX	WT SED	WT EX
AORTA	IL-1β (pg/mg of prot)	610.0 ± 400	543.3 ± 216.0	0.9 ± 0.5	1.0 ± 0.4
	TNFα (pg/mg of prot)	607.4 ± 132.6	600.6 ± 216.6	0.5 ± 0.3	2.5 ± 3.2
	AOPP (µmol/mg of prot)	76.8 ± 17.3	74.3 ± 17.3	8.5 ± 6.8	9.1 ± 7.2
	SOD (µmol/mg of prot/min)	5.2 ± 0.2	4.7 ± 1.5	5.6 ± 1.8	7.8 ± 1.7
PLASMA	IL-1β (pg/mL)	376.7 ± 208.2	476.7 ± 378.6	111.6 ± 55.7	105.5 ± 31.5
	TNFα (pg/mL)	10.1 ± 13.6	6.5 ± 8.0	46.3 ± 5.6	72.4 ± 16.4
	AOPP (µmol/mL)	241.2 ± 31.8	210.3 ± 66.3	15.3 ± 2.6	13.4 ± 2.8

FIGURE S1:

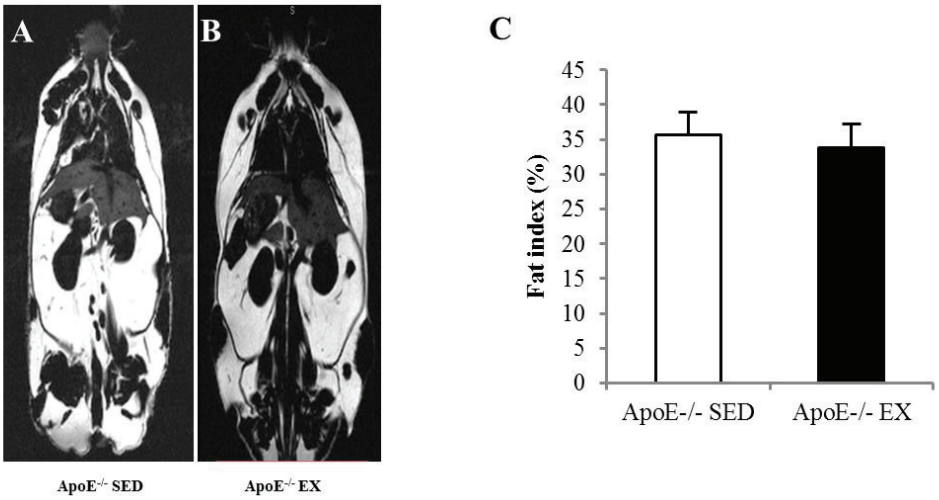
A
B
ApoE-/- SED
ApoE-/- EX
C
Fat index (%)
45
40
35
30
25
20
15
10
5
0
ApoE-/- SED
ApoE-/- EX

FIGURE S2:

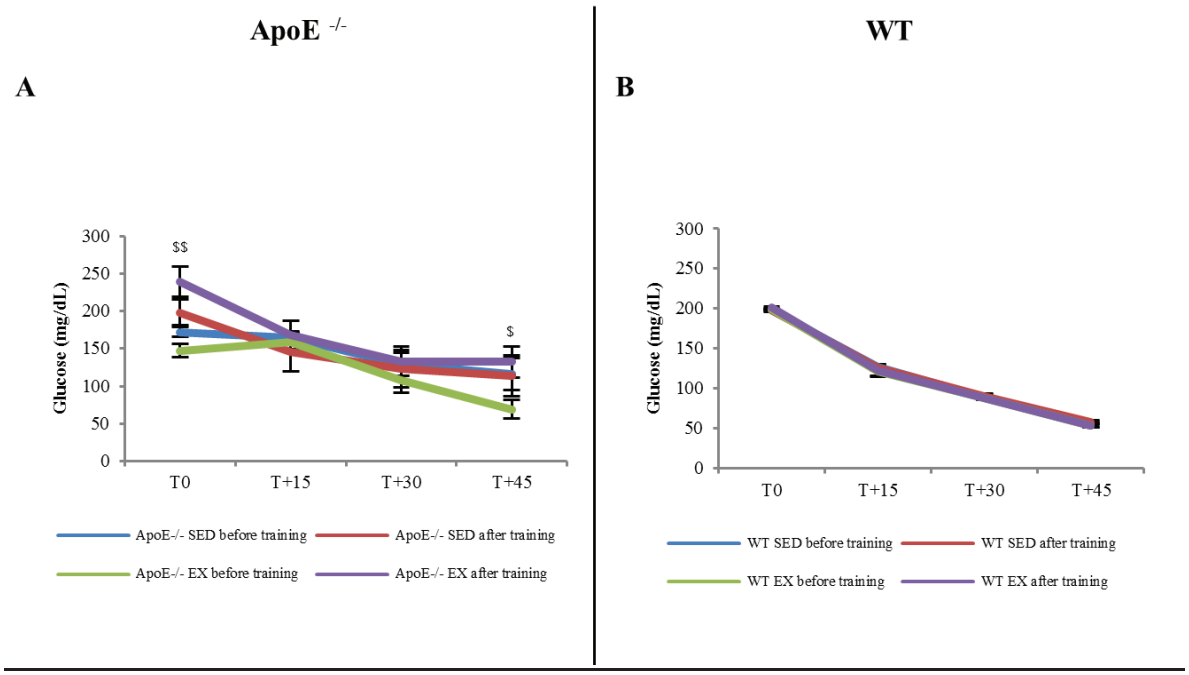
ApoE -/-
A
300
250
200
150
100
50
0
Glucose (mg/dL)
$$
$
T0
T+15
T+30
T+45
ApoE-/- SED before training
ApoE-/- SED after training
ApoE-/- EX before training
ApoE-/- EX after training
WT
B
300
250
200
150
100
50
0
Glucose (mg/dL)
T0
T+15
T+30
T+45
WT SED before training
WT SED after training
WT EX before training
WT EX after training

FIGURE S3:

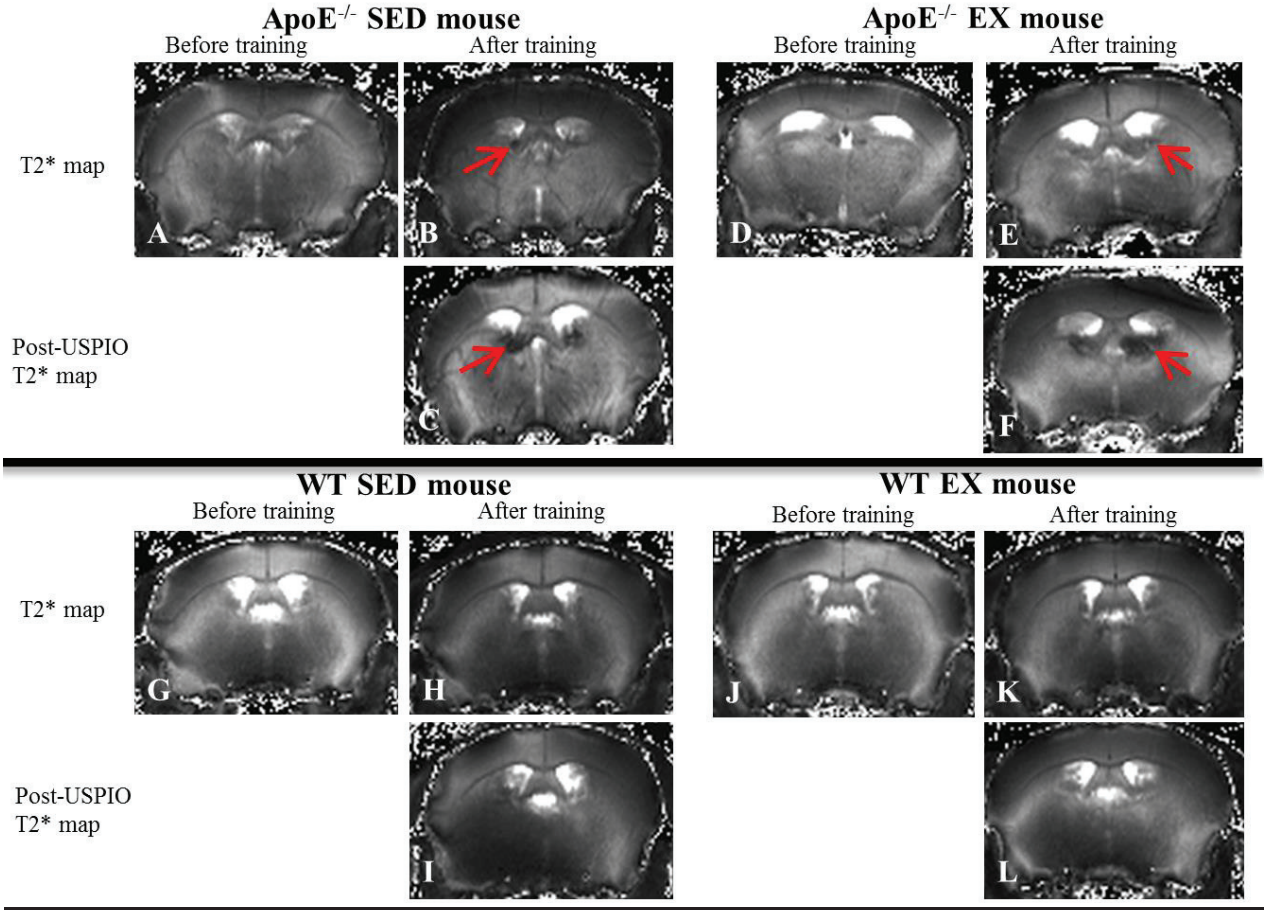
ApoE-/- SED mouse
Before training
After training
ApoE-/- EX mouse
Before training
After training
T2* map
Post-USPIO T2* map
A
B
C
D
E
F
WT SED mouse
Before training
After training
WT EX mouse
Before training
After training
T2* map
Post-USPIO T2* map
G
H
I
J
K
L

ARTICLE N°3

At-risk profiles from imaging and tissue biomarkerscombine inflammatory and anti-inflammatory features in non-human primates under cholesterol diet

Vanessa Di Cataldo, Joao Piraquive, Alain Geloën, Mickaël Verset, Adeline Paturet, Emmanuel Labaronne, Emmanuelle Loizon, André Serusclat, Franck Lamberton, Danièle Ibarrola, Franck Lavenne, Didier Le Bars, Hugues Contamin, Emmanuelle Canet-Soulas

In preparation

ARTICLE N°3:

Atherosclerosis is a complex pathology combining dyslipidemia and low-grade inflammation, leading to cardiovascular outcomes. Individual risk stratification is a real need in clinic as the efficiency of the clinical care depends on taking into account all individuals features of the patients. The aim of this study is to test the validity of multi-modal imaging focused on macrophage metabolism and phenotype associated with a biological analysis (lipidic profile, inflammatory cytokines and genomic analysis) in a non-human primate model (NHP) under atherogenic diet.

Sixteen Cynomolgus monkeys (13.1±4 years-old) were fed a high cholesterol diet (23% fat, 11.3% saturated fatty acids, 0.5% cholesterol, n=13 animals) or standard diet (11% fat, <1% saturated fatty acids, n=3 animals) during 24 months (see **Figure 24** for study design). Food ration was adapted to each animal according to their body weight. Longitudinal blood sampling was realized at 0, 1, 7, 12, 18 and 24 months for inflammatory cytokines, hsCRP and cholesterol/lipoprotein assessment. Ultrasound imaging of vascular territories was performed at T+12 and T+18 months to localize plaque and observe their potential progression within the 6-months interval. PET/CT imaging sessions were performed using dual tracers for measurement of metabolic and inflammatory cellular activity using [18F]-FDG and [11C]-PK11195 respectively. MR imaging was realized on carotids to assess the vessel wall thickness and on brain to visualize potential brain lesions. Inflammation and oxidative stress was assessed in carotids, aortic arch and abdominal aorta. Furthermore, tissular genomic analysis was performed on carotids, aortic arch, abdominal aorta, brain and adipose tissues, focused on metabolic, mitochondria , pan-macrophages, M1, M2 and lymphocytes markers.

NHPs fed atherogenic diet presented dyslipidemia (low HDL, high LDL and presence of at-risk LDL subfractions). Six-months ultrasound follow-up showed that most animals presented plaques in multiple location, with progressive lesions for some of them and at similar location than humans. Three animals showed downstream events (myocardial fibrosis, severe coronary or carotid plaque, lacunar stroke) confirming the relevance of this model and were the same than those presenting plaque progression on ultrasound follow-up. [18F]-FDG and [11C]-PK11195 presented similar uptake in high cholesterol animals (r^2=0.799, p=0.028) but an inverse in control diet animals (r^2=0.607). Analysis of gene expression of metabolic, inflammatory and anti-inflammatory markers in the carotids enabled the stratification of animals in three groups: low, medium and high cardiovascular risk. Of note, in high cardiovascular risk group, both M1 and M2 markers were highly expressed. Furthermore, the

three animals showing high CV risk in the carotids mRNA analysis are those that were highlighted by ultrasound and presence of downstream events.

Ultrasound follow-up as well as genomic analysis enabled the discrimination of animals with high cardiovascular risk. These animals being those presenting downstream events confirm the presence of vulnerable lesions in this model and the relevance of combination of inflammatory, metabolic and anti-inflammatory markers for individual stratification. This new biomarker combination offered possibilities for a better understanding of complex metabolic/inflammation interplay in the carotid plaque and adapted treatment in the clinical setting. The relevance of this association of gene expression was further evaluated in endarterectomy carotid samples of symptomatic and asymptomatic patients.

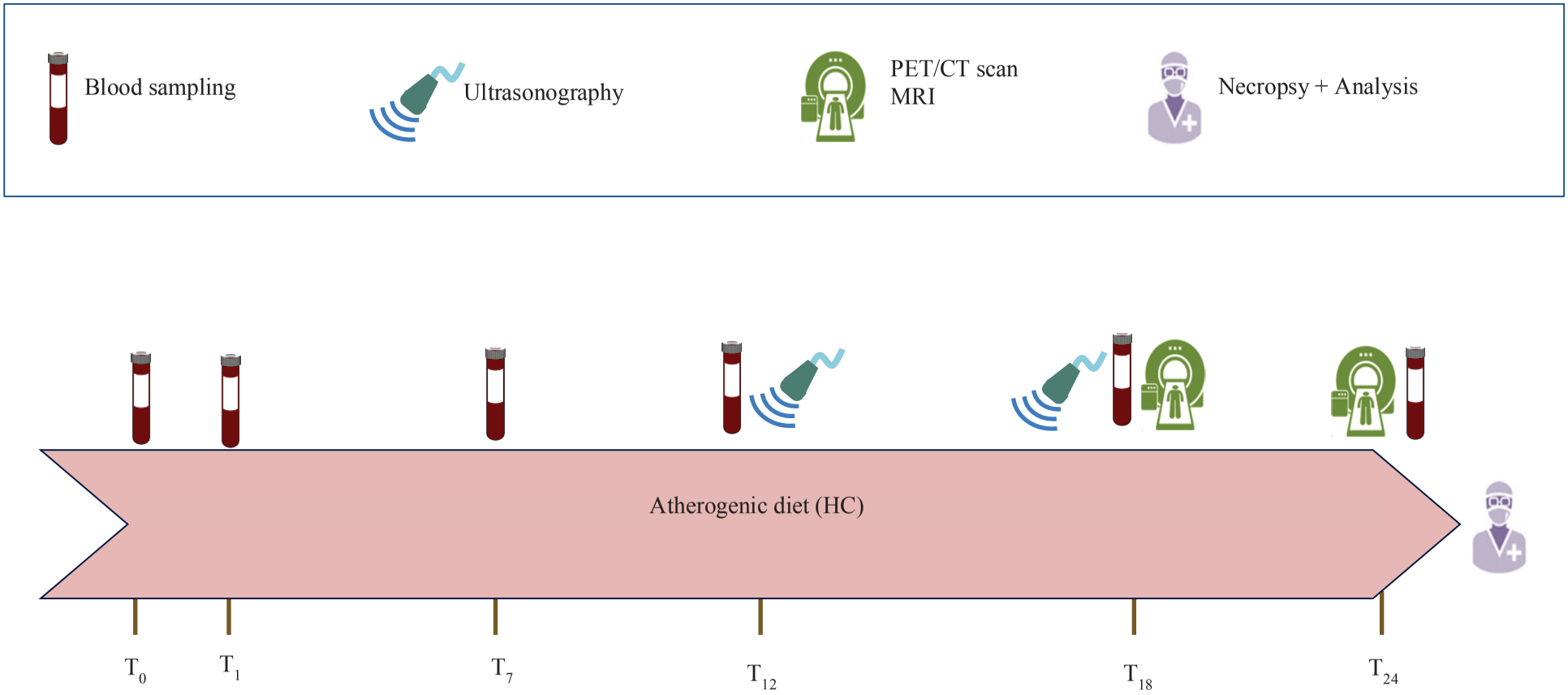

Figure 24: Study design non-human primate study

At-risk profiles from imaging and tissue biomarkers combine inflammatory and anti-inflammatory features in carotid atherosclerosis

DI CATALDO V.[1], PIRAQUIVE J.[2], GELOEN A.[1], VERSET M.[3], PATURET A.[3], LABARONNE E.[1], LOIZON, E.[1], MILLON, A.[1], SERUSCLAT A.[4], LAMBERTON F.[2], IBAROLLA D.[2], LAVENNE F.[2], TROALEN, T.[5], LE BARS D.[2], CONTAMIN H.[3], CANET-SOULAS E.[1]

[1]*Univ Lyon, CarMeN Laboratory, INSERM U1060, INRA U1397, Université Lyon 1, INSA Lyon, F-69600, Oullins, France*

[2]*CERMEP-Imagerie du Vivant, SFR East Lyon Health, CNRS UMS 3453, INSERM US7, Lyon 1 University, Lyon, France*

[3]*Cynbiose, VetAgroSup Campus, Marcy l'Etoile, France*

[4]*Departement of Radiology, Louis Pradel Hospital, Lyon, France*

[5]*Siemens Healthcare SAS, Saint-Denis, France*

Running title: At-risk profiles in carotid atherosclerosis

Address for correspondence:
Emmanuelle Canet-Soulas, DVM, PhD
Univ Lyon, CarMeNLaboratory, INSERM U1060, INRA U1397, Université Lyon 1, INSA Lyon, IHU OPERA Cardioprotection, U1060 CarMeN
bât. B13, Groupement Hospitalier Est
59 Boulevard Pinel
69 500 BRON, France
tel: (33) 4 72 68 49 09
emmanuelle.canet@univ-lyon1.fr

Word count for manuscript: 5060
Word count for abstract: 246
Total number of figures: 6
Total number of tables: 3

TOC category: translational
TOC subcategory:

ABSTRACT:

Atherosclerosis is a complex pathology, inducing cardiovascular events. Individual risk stratification remains difficult. The aim of the present study aim was to test the validity of multimodal imaging focused on macrophages combined with biological analysis in a non-human primate (NHP) model under atherogenic diet.

Sixteen Cynomolgus monkeys (mean age, 13.1±4 years) were fed high cholesterol (HC: 23% fat, 0.5% cholesterol) or standard diet for 24 months. Longitudinal blood sampling was performed for cholesterol and cytokine assessment. 6-month ultrasound follow-up of plaque progression and [^{18}F]-FDG, [^{11}C]-PK11195 PET/CT and MRI imaging were performed. Genomic analysis, focusing on metabolism, macrophage subsets and lymphocytes, was performed on NHP carotid, aorta and metabolic tissues and human endarterectomy samples from patients with symptomatic or asymptomatic carotid stenosis.

High-risk lipid profiles were noted at T+1 month. Ultrasound showed that most HC animals displayed lesions similar to humans. Three presented downstream events (myocardial fibrosis, small lacunar stroke), vessel wall inflammation and plaques, confirmed by PET/CT and MRI. Gene analysis further validated correlations between metabolic activity, inflammation and lymphocytes in carotids. Interestingly, anti-inflammatory M2 markers correlated with metabolic and M1 markers in both NHP and human carotids.

Animals graded high-risk on gene analysis presented downstream events, confirming our vulnerable plaque model and the validity of combining inflammatory, metabolic and anti-inflammatory markers for stratification. These results were confirmed in patients, and open the way for new combinations of biomarkers for better understanding of complex metabolism/inflammation interplay in carotid plaque and adapted treatment in the clinical setting.

INTRODUCTION:

Atherosclerosis is a complex inflammatory lipid pathology, leading to plaque development. The paradigm for atherosclerosis diagnosis has evolved from the detection of lesion-induced artery stenosis to the subtler notions of vulnerable plaque and vulnerable patient (Naghavi et al, 2006). However, as these concepts were originally defined from anatomopathology analysis, it remains challenging to stratify the cardiologic and cerebrovascular risk associated with atherosclerotic plaques in vivo in patients. Morphologic imaging (e.g.,. magnetic resonance imaging of carotids or ultrasound imaging of coronaries) demonstrated that plaque status may evolve in either direction, toward stability or vulnerability, depending on various local and systemic factors. In this dynamic situation, new biomarkers are therefore required, to enable the most appropriate treatment to be offered to each individual. More than a decade ago, [^{18}F]-fluorodeoxyglucose ([^{18}F]-FDG) PET/CT was first applied in patients to prospectively evaluate atherosclerosis inflammation and subsequent cerebrovascular risk (Rudd et al, 2002). Recently developed medical imaging methods have led to controversial results in various patient populations (Figueroa et al, 2013; Subramanian et al, 2012; Knudsen et al, 2015). Most novel imaging biomarkers target inflammation and macrophages, evaluating either macrophage phagocytic activity, glycolytic metabolism, macrophage mitochondrial proteins or M1/M2 receptors (Tarkin et al, 2014; Evans et al, 2016). But the debate is still open on the most useful association of circulating and imaging biomarkers to predict vulnerable plaque and future cardiovascular events, and to propose the best treatment in each specific situation (Duiveenvorden et al, 2013; Tarkin et al, 2016). For example, it is not known whether [^{11}C]-PK11195, a ligand targeting the mitochondrial translocator (18kDa) protein (TSPO) that is overexpressed in activated innate immune cells and was used for carotid imaging in patients (Gaemperli et al, 2012), enables better diagnosis of at-risk plaque than [^{18}F]-FDG.

There is no consensually accepted small-animal model of vulnerable plaque, and existing models are not fully relevant to establishing imaging biomarkers for translational purposes (Millon at al, 2012). The Cynomolgus macaque under atherogenic diet has been found to be invaluable in establishing the protective effect of estrogen against coronary plaque development (Adams et al, 1990). In this model, atherosclerosis develops with a lipidic blood profile and multi-site progression as in humans, and the carotid lesions reproduce the plaque morphology observed in clinical studies, as vessel geometry is very close to that found in humans (Shively et al, 1990). Moreover, the innate immune system is a key player in vulnerable plaque, and this non-human primate (NHP) atherosclerosis model is the only one to display the same chemokine and cytokine armamentarium as in human atherosclerosis. Vascular lesions and peripheral inflammation status in this NHP atherosclerosis model were characterized by immunohistochemistry and blood biomarkers (Register, 2009). Yet the model has never been explored using translational multimodal imaging techniques and inflammation imaging biomarkers.

The aim of the present study is to show the added value of inflammation imaging markers and blood biomarkers for stratifying cardiovascular risk in an NHP atherosclerosis model. To develop a tool for stratification of vulnerable profiles in NHPs, we used blood sampling (lipid profile, and inflammatory circulating biomarkers), PET/CT and MRI inflammation imaging using dual PET tracer imaging in NHPs under atherogenic diet. We then evaluated the gene expression risk profile from three vascular territories and compared this with the in-vivo biomarker risk assessment. The carotid gene expression pattern was also evaluated in human endarterectomy samples from symptomatic and asymptomatic carotid artery stenoses. The study hypothesis was that discrimination of cerebrovascular risk requires a combination of metabolic, inflammatory and anti-inflammatory biomarkers.

MATERIAL AND METHODS:

Animals:

All animal studies and experiments were approved by the French Ministry of Agriculture and carried out in accordance with its official regulations, after approval by the local institutional review board (n^{os} 1367 & 1239). Every effort was made to minimize animal suffering and reduce the number of animals used in the experiments. Animals were acclimated for at least 10 days prior to the first day of study, and were housed collectively with the following ambient parameters: aeration with > 10 air changes/hour and no air recirculation, 12-hour light/12-hour dark photoperiod, room temperature 22 ± 3°C, and humidity 55 ± 20%. The animal room and cages were cleaned daily. Sixteen Cynomolgus monkeys (*Macaca fascicularis*, Mauritius; mean age,13.1±4 years; 3 males, 13 ovariectomized females) received high cholesterol diet (HC: 23% fat (w/w), 0.5% cholesterol (w/w), 11.3% saturated fatty acids (w/w); E39126-34, Ssniff, Germany) (n=13) or standard diet (SD: 11% fat (w/w), saturated fatty acids < 1%; Pri V3944-000, Ssniff, Germany) (n=3: 2 female, 1 male) for 24 months. Food rations were adapted to each individual according to body weight (100g per day per animal under 5 kg; 200g per day per animal over 5 kg). One fruit was provided daily for each animal. Delicacies were also occasionally given to the animals at the end of the day as part of the test facility's environmental enrichment program. Study duration was 24 months.

Blood sampling:

For SD animals, 1 blood sample was taken at end of study. For lipid and cytokine plasma markers monitoring in HC animals, 6 blood samples were taken by venipuncture from the femoral vessel under anesthesia by ketamine (Imalgene® 1000, Merial, France) at 0, 1, 7, 12, 18 and 24 months (**see**

supplemental Figure S1 for study design). The animals were fasted prior to blood collection. Blood was collected in EDTA tubes for plasma harvesting and inflammatory cytokine assay, and in citrate tubes for cholesterol/lipoprotein assay. The EDTA and citrate tubes were centrifuged at 1,500 g for 10 minutes; then supernatant was removed and stored at -80°C until further assays.

At the last time point, serum was used for high-sensitivity C-reactive protein (hs-CRP) measurement.

Cholesterol/lipoprotein and triglyceride assay:

Total plasma cholesterol was measured using the Accutrend Plus kit (Roche, France), and lipoprotein fractions in plasma were assessed using the Lipoprint® LDL subfractions kit (Quantimetrix, California, USA) according to the manufacturer's instructions.

Peripheral inflammation:

Hs-CRP was assessed in serum using a commercial kit (CSB-E10035Mo, CUSABIO, Baltimore, MD, USA).

Multimodal imaging in NHP

Ultrasonography:

Ultrasonography of vascular territories was performed jointly by a veterinarian and a cardiologist, both experts in ultrasound imaging, using a Philips CX 50 apparatus with a C8-5 microconvex probe according to a standardized imaging protocol: aorta, iliac bifurcation and carotid arteries. Results were expressed as presence or absence of lesion, and vessel wall thickness, and intima-media thickness (=IMT, when possible) (otherwise, in patients, IMT>0.7 mm can be assumed). For longitudinal assessment of disease progression, a score was given at each ultrasound session: 1 for small lesion in a single location, 2 for multi-site small lesions, and 3 for multi-site lesions with at least 1 large plaque.

PET/CT Scan:

Images were acquired on a 64-multidetector PET/CT scanner Biograph mCT (Siemens, Erlangen, Germany) with an axial field of view of 22 cm. The scanner is checked every day using established calibration procedures.

FDG imaging was performed in all animals 60 minutes after intravenous [^{18}F]-FDG injection of a target dose of 5 MBq/kg (mean dose, 86.24 ± 22.72 MBq). Animals were placed in a supine position. 60 minutes after injection of the radiotracer, a whole-body low-dose CT scan (80kV, 20mAs, 1 mm slice thickness and 0.5 sec pitch) was acquired for attenuation correction. The CT scan dose was adjusted using the Care Dose 4D software (Siemens), with the animal body centered in the scanner to enable the whole-body coverage.

Three bed positions were used: the first one centered on the carotids encompassing the aortic arch and its branches, and the others 2 distally to cover the upper and lower part of the abdomen. Prior to FDG PET, fasting blood glucose concentration was recorded to check for a level less than 200 mg/dL. For each bed position, acquisition duration was 5 minutes.

After the PET examination, a CT angiography was acquired with the same field of view (FOV). A bolus of 20ml Iomeron 400 (Guerbet, Aulnay-sous-Bois, France) was injected at a rate of 3.5ml/sec in the antecubital vein, followed by saline flush at the same rate. Acquisition parameters were: 80kV, 20mAs, FOV 500 mm, 30 sec B filter, slice thickness 1 mm, and pitch 0.5 sec.

A subgroup of 8 animals was also explored using the [^{11}C]-PK11195 PET tracer (mean dose, 123.70 ± 30.96 MBq) targeting TSPO of activated macrophages. This [^{11}C]-PK11195 examination was performed before the FDG examination. PET emission data of [11C]-PK11195 centered on the carotids were acquired over 60 min in list-mode format and rebinned into 18 temporal frames (background 56.42 ± 11.16 s, 6x10s, 4x60s, 6x300s and 2x600s).

MRI:

MRI was performed on a 3-Testla MR scanner (MAGNETOM Prisma, Siemens). Animals were installed in supine position, with the head in the center of the posterior part of the 64-channels Head/Neck coil.

For carotid imaging, a 4-channel phased array receiver coil was combined with head coil to optimize the signal-to-noise ratio and with cardiac triggering and breathing monitoring. The carotid was located with time of flight (TOF) sequences. MRI images were centered on the bifurcation and acquired using turbo spin echo (TSE). Proton density weighted (PDW) and T1-weighted (T1W) images were used. Imaging parameters were: 9 slices thickness of 2 mm, Field of View (FOV) = 205 mm, Echo Train Length (ETL) = 29, Repetition Time (TR) = 262 ms / 260 ms (PDW/ T1W), Echo Time (TE) = 23.0 ms/ 5.8 ms (PDW/ T1W), Echo Spacing (ES) = 5.79 ms and Receiver Bandwidth (BW) = 868 Hz/Px.

Dynamic images were acquired with the TWIST (Time resolved angiography With Interleaved Stochastic Trajectories) pulse sequences and using all channels of MR coils. TWIST sequences were

applied in the coronal orientation and acquired with a separation of 5 seconds between frames, interpolated to 2.46 ms. A 10 ml bolus of DOTAREM® (Guerbet, Aulnay-sous-Bois, France) was administered intravenously at 0.1 mL/s. Imaging parameters were: voxel size 0.8x0.8x1 mm, FOV = 280x228x88 mm, TR/TE = 3.0/1.12 ms and FA = 25º.

Brain imaging was performed with the following sequences:

3D T1W MPRAGE used in pre- and post-injection: voxel size = 0.6x0.6x0.8 mm, FOV 180x180x102 mm, TR/TI/TE = 2100/1000/ 2.77 ms, FA = 8º, ES = 8 ms, BW = 210 Hz/Px

2D T2*W multi-gradient echo: 20 slices, voxel size = 0.7x0.7x2 mm, FOV 180x146x42 mm, ,TR = 1200, 12 echos times from 3.04 ms upto 49.68 ms (ΔTE = 4.24 ms), FA = 70º, bandwidth 270 Hz/Px.

3D T2W-FLAIR (Fluid Attenuation Inversion Recovery) voxel size = 0.6x0.6x0.8 mm, FOV = 180x180x102 mm, TR/TI/TE = 5000/1800/346 ms, ETL = 314, Echo Train Duration (ETD) = 926 ms, ES = 3.81 ms, BW = 744 Hz/Px.

Tissue analysis

NHP vascular and non-vascular tissus preparations:

At end of study, the animals were deeply anesthetized before lethal injection of pentobarbital. Carotids, aortic arch, abdominal aorta, and non vascular tissues (heart, pericardial and pericoronary, visceral and subcutaneous fat, brain) were collected and prepared for further analysis (i.e. pathological examination, gene expression or biochemistry measurements).

Human carotid endarterectomy samples:

Human carotid samples (n=19) were obtained from asymptomatic and symptomatic patients undergoing carotid endarterectomy in vascular surgery department of Edouard Herriot Hospital (Lyon, France). Written informed consent for analysis of blood and tissue samples was obtained from all patients before surgery. Patients were considered symptomatic when an ipsilateral carotid-related neurological event was reported in the previous 6 months. Samples were prepared and gene expression was performed with the same methods as NHP samples.

Inflammation and oxidative stress:

Vascular samples from the imaging location (carotids, aortic arch, and abdominal aorta) were kept frozen at -80°C and ground into powder using a mortar. Proteins were extracted from the powder using a PBS/EDTA (5mM) solution. Protein extracts were then used to assess inflammatory cytokines and oxidative stress markers (IL-1 β, IL-6, TNFα and MDA), in the same way than in plasma.

Gene expression study:

mRNA were extracted from NHP carotids, aortic arch, abdominal aorta, adipose tissues (visceral, pericardial and periarterial) and frontal brain and from human carotid samples using the TRIZOL reagent procedure. Expression was assessed for 20 genes corresponding to glycolytic metabolism (*Hk1*), mitochondria metabolism (*Ppif, Tspo*), pan-macrophages (*Cd14, Cd68*), M1 (*Il-1β, Tlr4, Ccl2, Il-6, Tnfα, Cxcl9, Il-17ra, IL-22ra*) and M2 (*Il-1ra, Ccr2, Il-10, Clec7a, Irf4, Cd163*) markers and lymphocyte infiltration (*Cd3ε*) (list of primers on demand: vdicataldo@hotmail.fr), using the qPCR method. Actine β was used as the reference gene.

Histopathology of vessel wall and heart

The left carotid and parts of aortic arch and heart (apical area) were removed and stored in a 4% paraformaldehyde solution for 24 hours and then in 15% sucrose for 48h, and placed in a histology cassette and frozen in liquid nitrogen, except for heart samples which were embedded in paraffin.

These samples were cut in 10µm slices by cryostat (LEICA CM3050S), then stained with Hematoxilin/Eosin (MHS32-1L & HT110232-1L, Sigma-Aldrich), Oil Red O (841K04010169, MERK) and Masson's trichoma (ab150686, AbCam) in order to visualize respectively section morphology, lipids and fibrosis. Photographs were acquired using the ZEISS Scope A1 microscope (ZEISS).

A researcher experienced in vascular pathology and blind to the imaging results examined all histology sections of each specimen. The following features were graded on a simple semi-quantitative scale previously published by Lovett et al (Lovett et al, 2004): thrombus area, thick, thin (<200 µm) or ruptured fibrous cap, intraplaque hemorrhage, neovascularization, and macrophage infiltration. Loose fibrosis, defined as fibrous tissue rich in non-fibrillar extracellular matrix with thin and non-condensed collagen fibers, was graded as <30% or >30% of total fibrous tissue.

Plaques were classified according to the American Heart Association classification of coronary atherosclerosis and according to the Lovett and Redgrave classification (Lovett et al, 2004; Stary et al, 1995).

Data analysis:

Blood kinetics:

To estimate overall risk in the plasma profile over time for each animal, lipid and hs-CRP levels were summarized by the maximal, median and final (at imaging time point) values.

Image analysis:

MRI: vessel wall area was measured (in mm²) in the right and left carotids (3 slices / per artery) by manual delineation of the inner and outer contours. MR angiography and CT angiography acquisitions then registered the region of interest (ROI) on the PET/CT data (**supplemental Figure S2**).

[^{18}F]-FDG image post-processing: All emission images were normalized using an inhomogeneity detector and corrected for dead time, random coincidences, diffusion and attenuation. Image reconstruction was performed with iterative Ordered-Subset Expectation Maximization (iterative OSEM method, TrueX + TOF UltraHD-PET) with 12 iterations and 21 subsets (effective number of iterations, ENI of 252), non-filtered in line with recent recommendations for FDG analysis in atherosclerosis (Huet et al, 2015).

Spatial resolution at reconstruction was: voxel size 0.82 x 0.91 x 0.4mm. Standardized Uptake Value (SUVmean and max, Bq/mL) and Target-to-background ratio (TBR: SUVmax normalized by SUVmean of the superior vena cavae) were measured at 3 vascular locations (right and left carotids, aortic arch and abdominal aorta at the level of renal bifurcations) and in visceral adipose tissue in ROIs at the various location. MR angiography and PDW images (for the carotids) were used to generate regions-of-interest at the different locations. For brain images, SUVmax was evaluated for the ROIs defined using the NHP atlas (Ballanger et al, 2013) (see below).

[^{11}C]-PK11195 analysis: Levels of translocator protein (18 KDa) expressed in active macrophages were assessed using [^{11}C]-PK11195 kinetic analysis with an image arterial input function (descending aorta) and a 2-compartment reversible model (2TC-rev) or an equivalent graphical analysis (Logan).

2TC-rev allows identification of the following kinetic rate constants: K1, k2 between vascular volume and non-specific tissue, and association (k3) and dissociation rate constants (k4) for receptor-specific

(Kropholler et al, 2005). Rate constants depend on local concentration in the region of interest (ROI), in arterial plasma and in tissue. The relationship between micro-parameters (K1, k2, k3 and k4) enabled estimation of a macro-parameter: volume distribution (Vt).

Logan plot is a linear method, enabling estimation of Vt regardless of the number of compartments (Logan et al, 1990). This graphical method is based on observation of the portion of the reversible model, which approaches a steady state after a certain time following, a linear trend the slope of which can be related to Vt. As performed in Gaemperli's clinical carotid study (Gaemperli et al, 2012), a simplified TBR (PK) was also calculated using a static image reconstructed from the 20-35 minutes frames.

Vt, SUVmax (PK) and TBR (PK) (calculated using a static image reconstructed from the 20-35 minutes frames) were then compared to FDG uptake levels (SUVmax [^{18}F]-FDG) and TBR [^{18}F]-FDG) at the same locations (right and left carotids).

Brain PET/CT analysis

Based on anatomical-MRI and a maximum probability atlas (Ballanger et al., 2013), 88 ROIs were defined and used to measure [^{11}C]-PK11195 binding potential (BP, with the Simplified Reference Tissue Model, SRTM), using the caudate nucleus as reference region with minimal uptake on PET-scans for these regions; here we focused on the frontal cortex (7 ROIs) and limbic system (6 ROIs).

Statistical analysis

All values are expressed as mean ± standard deviation or median with percentile ranges. Differences were tested on t test. Regression analysis was used for comparison between MR and PET parameters. A p level <0.05 was considered significant. Heat-maps for genomic risk profile were generated by hierarchical clustering of samples, using the ward.2 algorithm. Statistical analysis for longitudinal follow-up and for comparison between HC and SD measurements was performed with $p<0.05$ considered as significant. All statistical analyses were performed using R software.

RESULTS:

During the 24 months of the study, 5 HC animals died: 2 early and abruptly after diet onset, 2 euthanized because of acute kidney failure, and 1 prematurely from acute pancreatitis (severe pancreas autolysis found on necropsy). In these animals, large atherosclerotic lesions were also observed in various vascular beds (data not shown).

High-risk lipid profiles

Plasma cholesterol levels were normal in all HC animals at the beginning of the study and showed a brutal increase after the first month of diet (1 month on HC diet, compared to baseline: $p=4.5.10^{-4}$) and stayed at high levels throughout the 24 months (**Figure 1A**). The HDL/LDL ratio showed a parallel sudden decrease during the first month and remained low thereafter (1-month compared to baseline ratio; $p=1.2.10^{-5}$**; Figure 1B**).

Lipoprotein profiles further exhibited the differences between HC and SD animals: a lower HDL concentration and "at-risk" LDL subfractions (dense LDL subfractions are associated with coronary artery disease and risk of myocardial infarction; Austin et al., 1988; Campos et al., 1992) in HC animals, corroborating lipid dysregulation (**Figure 1C-D**). Triglyceride levels did not significantly differ between HC and SD animals, although individual differences were observed (data not shown).

Multi-site active lesions on multimodal imaging in HC animals

Numerous atherosclerotic plaques in HC animals were visible on ultrasound imaging; at T+18 months' diet, 9 of the 10 HC monkeys showed atherosclerotic lesions at locations similar to those found in humans (common carotid and bulb, aortic arch, iliac arteries), confirmed by vessel histology. Plaque burden in the carotid was also shown by MRI measurements (**Figure 2A-C**). PET/CT imaging showed both [^{18}F]-FDG (**Figure 2D-E**) and [^{11}C]-PK11195 (**Figure 2F-G**) uptake in carotids in HC animals, suggesting low-grade inflammation. Carotid MRI showed vessel wall thickening in the carotids (median wall area, 0.11 cm^2 (interquartile 0.09 – 0.12) in HC versus 0.04 cm^2 in SD animals; $p<0.001$; **Figure 2A, and Supplemental Figure S3**) and gadolinium enhancement characteristic of advanced carotid plaques (**Figure 2B-C and Figure S3**), confirming pathological status.

Longitudinal follow-up of inflammatory biomarkers and ultrasound for diagnosis of high-risk animals

Longitudinal ultrasound study showed lesions at various locations at 12 months (score of 2 in 4 animals; **Figures 3 and S4**) with progression of atherosclerosis in 3 out of 8 animals at 18 months (**Figure S4).** Hs-CRP levels confirmed chronic low-grade inflammation persisting over time (**Figure 3B and S4**). LDL-C levels were also high in the same time interval, but with no significant increase (**Figure 3C**). The animals with increasing ultrasound scores also showed increased hs-CRP or maintained a high level during follow-up (**Figure S4**).

Animals that did not complete the study showed a burst of circulating inflammation biomarkers in the blood sample prior to death (data not shown). Finally, downstream consequences found in the heart (fibrosis on histology) and brain (lacunar stroke on FLAIR MRI) in animals with advanced lesions (**Figure 4**) confirmed overall vulnerable status with high-risk HC animals. Interestingly, the 3 animals exhibiting myocardial fibrosis on histology were those with increased ultrasound score at T+18 months, and either elevated hs-CRP at baseline or stronger increase at T+18 months (**Figures S4 and 4)**.

For HC animals, PET and MR inflammation marker levels did not correlate with MR plaque burden (data not shown; p=0.3 plaque with Gd, p=0.9 plaque with [^{18}F]-FDG, p=0.18 plaque with [^{11}C]-PK11195), or between each other except for Gd and [^{18}F]-FDG (p=0.03). Of note, in HC animals with dual tracer injection, [^{11}C]-PK11195 imaging correlated positively with [^{18}F]-FDG findings (y=0.65x+0.15, r=0.89; p=<0.001) in HC animals, and negatively in SD animals (y=0.29x+2.26, r=-0.78, p=0.036), and there was a trend between Gd and [^{11}C]-PK11195 in HC animals (p=0.07). Left/right uptake difference was similar between MR and PET inflammation markers in HC and not in SD animals (**Figure S3**).

SD animals presented relatively elevated hs-CRP levels (18 and 35 µg/ml respectively) and their corresponding inflammation imaging was also above normal values for both gadolinium signal intensity enhancement, [^{18}F]-FDG SUV and [^{11}C]-PK11195 TBR (**Figure 2B, D, F**). On histology, myocarditis with diffuse myocardial fibrosis was discovered in 1 animal (SD#2), confirming the in-vivo inflammation findings.

Carotid high-risk profiles combine overexpression of metabolic, inflammatory and anti-inflammatory genes

Genomic analysis of carotid arteries showed strong correlations between genes related to imaging biomarkers (*Hk1* for [^{18}F]-FDG and *Tspo* for [^{11}C]-PK11195) in carotid arteries and vulnerable plaque markers such as *Ccl2* (p=0.009 and 0.001 respectively), *Il-1β* (p=0.001 and 0.006 respectively) and *Il-6* (p=0.044 for *Hk1*) (**Table 1**). These three markers were also intercorrelated and correlated with other inflammatory markers such as *Tlr4* (p=0.001 with *Ccl2*; p=0.002 with *Il-1β*), *Clec7a* (p<0.001 with *Ccl2*; p<0.001 with *Il-1β*), with *Cd3ε* (marker of lymphocyte infiltration: p=0.003 with *Ccl2*; p=0.044 with *Il-1β* and p=0.007 with *Il-6*). Interestingly, markers of vulnerable plaque were also associated with expression of anti-inflammatory markers such as *Il-1ra* (p=0.003 with *Ccl2*, p=0.001 with *Il-1β* and p=0.009 with *Il-6*), *Il-10* (p=0.027 with *Il-6*), *Irf4* (p=0.001 with *Ccl2*) and *Cd163* (p=0.001 with *Ccl2*) (**Table 1**). Heat-maps of gene expression in carotids highlighted 3 distinct groups of NHP according to level expression (**Figure 5A**). Of note, the 3 NHPs presenting downstream events (HC#1, 9 and 13)

were all grouped as high-risk by this analysis, confirming the stratification using ultrasound and circulating biomarkers such as LDL-C and hs-CRP (**Figure 5A-B and supplemental S4**).

Analysis of patients' carotid endarterectomy samples showed that this high-risk profile was more frequent in symptomatic than asymptomatic patients, with the same macrophage pattern with both inflammatory and anti-inflammatory markers expressed (**Figure 6**). These results confirmed the pattern already observed in NHPs, and strengthened the concept of a combination of metabolic, M1 and M2 markers in high-risk subjects (**Tables 2 and 3**).

Other vascular trees, brain, and adipose and immune tissues

HC animals with carotid [^{18}F]-FDG uptake also showed increased signal in the aortic arch, and in hematopoietic organs (spleen and bone marrow) (**Figure S5**). Tissue analysis of 3 arterial walls (carotid, aortic arch and abdominal aorta) confirmed the high-risk status of the NHPs, as they were the only cases presenting higher values for more than 1 inflammatory/oxidative marker (out of the 4 selected) (data not shown). Gene expression in the 2 aortic locations did not provide a completely similar stratification. However, the association between inflammatory/metabolic and anti-inflammatory gene expression was maintained (**Figure S6**).

Interestingly, brown fat activity was significantly decreased in HC compared to SD animals, whereas the increased activity of visceral and subcutaneous fat did not reach significance (**Figure S7**). In both perivascular and visceral adipose tissue, the association between inflammatory and anti-inflammatory gene expression was also strong (**Figure S7**).

Finally, brain image analysis with the dedicated NHP atlas segmentation showed higher [^{11}C]-PK11195 uptake in regions of the limbic system and frontal cortex in HD than SD animals, and a correspondingly lower [^{18}F]-FDG uptake (**Figure S8**). Gene expression in the frontal brain showed correlation between TSPO and HK1 genes (related to imaging biomarkers) and inflammatory genes CCL2, CD3ε and IL-6, and strikingly a negative correlation between IL-1β and IL-1ra (**Figure S9**).

DISCUSSION:

Severe diffuse plaques with large lipid core were observed in NHPs, and were associated with myocardial fibrosis and lacunar stroke in the corresponding territories, validating our NHP model of vulnerable plaque. Both metabolic and mitochondrial macrophage activity imaging markers were closely associated, as demonstrated by the correlation between [^{18}F]-FDG and [^{11}C]-PK11195 carotid measurements. Carotid gene analysis confirmed this finding, but also found a strong association with

anti-inflammatory markers in both the NHP model and the endarterectomy samples. This relationship was further used to stratify the high-risk profiles, and diagnosed the same NHPs presenting progressive lesions at follow-up and pathological downstream consequences of plaque rupture. The two aortic locations (arch and abdomen) confirmed the association of inflammatory/anti-inflammatory gene expression. As in patients, [^{18}F]-FDG whole-body inflammation imaging in the NHP model of advanced atherosclerosis confirmed abnormal uptake in hematopoietic organs and white adipose tissue, and a decrease in the metabolic activity of brown fat. Finally, metabolic activity ([^{18}F]-FDG uptake) was lower in the limbic system in HC than in SD animals,, in parallel with increased TSPO mitochondrial activity in the same regions (i.e., increased [^{11}C]-PK11195 binding).

In the last year or two, the classical dichotomy of M1 (inflammatory) and M2 (anti-inflammatory/repair) macrophages has been seriously reconsidered (Tabas et al, 2016). A more comprehensive vision is emerging in the immunology community. Innate immune cell priming has been shown to be essential for future monocyte/macrophage response in cardiovascular diseases, and has also recently been postulated in resident macrophages, even in the brain (Holtmann et al, 2015). This priming promotes very different phenotypes that combine a delicate mixture of conventional M1 and M2 markers. For clinical translation to atherosclerosis, this was very recently demonstrated by pathological analysis of abdominal aorta from a tissue bank (van Dijk et al, 2016), showing macrophages of both phenotypes intricately associated in lesions with vulnerable features. Analysis of carotid endarterectomy specimens has so far led to somewhat controversial results (de Gaetano et al, 2016; Jager et al, 2016), perhaps because the external part of the media and the adventitia, which is missing in endarterectomy samples, is an important supplier of macrophages in atherosclerosis (van Dijk, 2016).

M2 markers for atherosclerosis imaging have also already been evaluated. The mannose receptor CD206 was imaged by direct targeting (Blykers et al, 2015, Cope et al, 2016) or using its carboxylate ligand by FDM PET imaging (Tahara et al, 2014), and indirect CD163 imaging was performed by targeting the somatostatin receptor with its ligand [^{64}Cu]-DOTATATE, which correlated with CD163 macrophages and symptomatic plaques (Pedersen et al, 2015). The present gene analysis confirmed that M2 markers (IL-10, CD163, IRF4, IL-1ra) were closely associated with both metabolic and inflammatory markers (IL6, IL1β, CCL2) in the 3 vascular beds studied; IL-1ra was the anti-inflammatory marker more frequently associated with inflammatory markers in vascular tissues (with CCL2 and IL-1β in carotid and aortic arch and with IL-6 in carotid).

In-vivo imaging in the carotids showed that [^{11}C]-PK11195 and [^{18}F]-FDG were correlated in HC animals. Therefore, these two tracers appeared equivalent in carotid and aortic arch atheroma, but were negatively correlated in the vessel wall and perivascular tissues of SD animals. Genomic analysis of metabolic and mitochondrial gene expression confirmed this association in the carotids and in the two

aortic sites, but only in pericardial adipose tissue and not in the other depots. Yet, in all adipose tissues, inflammatory and anti-inflammatory gene expressions were still closely associated, confirming the strength of this association in different microenvironments in this context of chronic low-grade chronic inflammation.

Conversely, [^{18}F]-FDG and [^{11}C]-PK11195 gave contrasting results in the brain: in the limbic system and frontal cortex. Lower [^{18}F]-FDG uptake in the limbic system may be related to lower neuronal activity, as observed in Alzheimer's disease (Kato et al, 2016), and increased [^{11}C]-PK11195 uptake may represent neuroinflammation induced by HC diet, as previously demonstrated in mice (Mao et al, 2015).

In hypercholesterolemia, the central role of TSPO in mitochondrial cholesterol trafficking may be disturbed, and could be a therapeutic target (Lecanu et al, 2013). It plays a major role in cholesterol trafficking and astrocyte homeostasis (Da Pozzo et al, 2016). In the brain, increased TSPO expression is also linked to astrocyte and microglial activation and/or macrophage recruitment in acute and chronic inflammation (stroke, epilepsy) (Chauveau et al, 2011; Yankam Njiwa et al, 2016).

Further studies in this advanced atherosclerosis model would be necessary to confirm these TSPO/FDG imaging findings in the brain, combining inflammation and neuron damage, particularly in the limbic system. These mechanisms have already been explored in the ApoE$^{-/-}$ mouse model (Fullerton et al, 2001; Schwartz et al, 2013). In primates, TSPO imaging was recently performed in the context of acute neuro-inflammation progressing to neurodegeneration (Lavisse et al, 2015), further confirming the relevance of the NHP model for translational neuro-inflammation imaging studies.

Compared to mouse models, the present NHP model is unique, as vulnerable plaque phenotypes were observed in both the carotid and coronary arteries, with pathological downstream events. Longitudinal follow-up using imaging of plaque progression in multiple sites and inflammation biomarkers provided a first read-out of at-risk profiles, very similar to the clinical pattern. In terms of translation, the at-risk signature in the vessel wall combined metabolic, inflammatory and anti-inflammatory gene expression, which was further confirmed in endarterectomy samples. Moreover, this gene association in the carotids was able to stratify higher-risk animals. This finding is very relevant for patient care after endarterectomy, but needs to be confirmed.

Another limitation of the present study was the single inflammation imaging session. [^{18}F]-FDG imaging has been successfully performed in phase II and III clinical trial, where changes in carotid and aorta [^{18}F]-FDG uptake were essential to showing inflammation modulation with treatment and the globally more stable phenotype in the treatment group (Tawakol et al, 2013; Tarkin et al, 2014).

In conclusion, the present NHP vulnerable plaque model demonstrated that the 2 imaging markers of inflammation used for carotid examination in patients, [^{18}F]-FDG and [^{11}C]-PK11195, are closely linked in the context of atherosclerosis. In the brain, they may provide additional information about locally impaired brain activity in the case of [^{18}F]-FDG and abnormal glial and/or macrophage mitochondria activity in the case of [^{11}C]-PK11195.

More importantly, we demonstrated for the first time in a translational model that vulnerable plaque shows increased expression of metabolic, inflammatory and anti-inflammatory genes and that, in carotid plaque, this association enables high-risk subjects to be stratified. Further studies in NHPs and patients are needed to evaluate how this can impact care and future treatments.

ACKNOWLEDGEMENTS:

Sources of funding: This study was supported by the Institut Universitaire de France and the French Ministry of Research for PhD students.

Disclosures: None

REFERENCES:

1. Naghavi, M., Falk, E., Hecht, H.S., et al, SHAPE Task Force. From vulnerable plaque to vulnerable patient—Part III: Executive summary of the Screening for Heart Attack Prevention and Education (SHAPE) Task Force report. Am J Cardiol. 2006 : 98: 2H–15H.
2. Rudd, J.H., Warburton, E.A., Fryer, T.D., et al. Imaging atherosclerotic plaque inflammation with [18F]-fluorodeoxyglucose positron emission tomography. Circulation. 2002 : 105(23):2708-11.
3. Figueroa, A.L., Abdelbaky, A., Truong, Q.A., et al. Measurement of arterial activity on routine FDG PET/CT images improves prediction of risk of future CV events. JACC Cardiovasc Imaging. 2013 : 6(12):1250-9.
4. Subramanian, S., Tawakol, A., Burdo, T.H., et al. Arterial inflammation in patients with HIV. JAMA. 2012 : 308:379-86.
5. Knudsen, A., Hag, A.M., Loft, A., et al. HIV infection and arterial inflammation assessed by (18)F-fluorodeoxyglucose (FDG) positron emission tomography (PET): a prospective cross-sectional study. J NuclCardiol. 2015 : 22(2):372-80.
6. Tarkin, J.M., Joshi. F.R., Rudd, J.H.. PET imaging of inflammation in atherosclerosis. Nat Rev Cardiol. 2014 : 11:443-57.
7. Evans, N.R., Tarkin, J.M., Chowdhury, M.M., et al. PET Imaging of Atherosclerotic Disease: Advancing Plaque Assessment from Anatomy to Pathophysiology. Curr Atheroscler Rep. 2016 : 18(6):30.
8. Duivenvoorden, R., Mani, V., Woodward, M., et al. Relationship of serum inflammatory biomarkers with plaque inflammation assessed by FDG PET/CT: the dal-PLAQUE study. JACC Cardiovasc Imaging. 2013 : 6(10):1087-94.
9. Tarkin, J.M., Dweck, M.R., Evans, N.R., et al. Imaging Atherosclerosis. Circ Res. 2016 : 118(4):750-69.
10. Gaemperli, O. Shalhoub, J., Owen, D.R., and al. Imaging intraplaque inflammation in carotid atherosclerosis with 11C-PK11195 positron emission tomography/computed tomography. Eur Heart J. 2012 : 33:1902-10.
11. Millon, A., Canet-Soulas, E., Boussel, L., et al. Animal models of atherosclerosis and magnetic resonance imaging for monitoring plaque progression. Vascular. 2014 : 22(3):221-37.
12. Adams, M.R., Kaplan, J.R., Manuck. S.B., et al. Inhibition of coronary artery atherosclerosis by 17-beta estradiol in ovariectomized monkeys. Lack of an effect of added progesterone. Arteriosclerosis. 1990 : 10(6):1051-7
13. Shively, C.A., Kaplan, J.R., Clarkson, T.B. Carotid artery atherosclerosis in cholesterol-fed female cynomolgus monkeys. Effects of oral contraceptive treatment, social factors, and regional adiposity. Arteriosclerosis. 1990 : 10(3):358-66.

14. Register, T.C. Primate models in women's health: inflammation and atherogenesis in female cynomolgus macaques (Macaca fascicularis). Am J Primatol. 2009 : 71:766-775.
15. Lovett, J.K., Gallagher, P.J., Hands, L.J., et al. Histological correlates of carotid plaque surface morphology on lumen contrast imaging. Circulation. 2004 : 110:2190-2197.
16. Stary, H.C., Chandler, A.B., Dinsmore, R.E., et al. A definition of advanced types of atherosclerotic lesions and a histological classification of atherosclerosis. A report from the Committee on Vascular Lesions of the Council on Arteriosclerosis, American Heart Association. Arterioscler Thromb Vasc Biol. 1995 : 15:1512-1531.
17. Huet P[1], Burg S[2], Le Guludec D[2], et al. Variability and uncertainty of 18F-FDG PET imaging protocols for assessing inflammation in atherosclerosis : suggestions for improvement. J Nucl Med. 2015 : 56(4):552-9. doi: 10.2967/jnumed.114.142596. Epub 2015 Feb 26.
18. Ballanger, B., Tremblay, L., Sgambato-Faure, V., et al. A multi-atlas based method for automated anatomical Macaca fascicularis brain MRI segmentation and PET kinetic extraction. Neuroimage. 2013 : 77:26-43. doi: 10.1016/j.neuroimage.2013.03.029. Epub 2013 Mar 26.
19. Kropholler, M.A., Boellaard, R., Schuitemaker, A., et al. Development of a tracer kinetic plasma input model for (R)-[^{11}C]PK11195 brain studies. J Cereb Blood Flow Metab. 2005 : 25:842–851.
20. Logan, J., Fowler, J.S., Volkow, N.D., et al. Graphical analysis of reversible radioligand binding from time-activity measurements applied to [N-11C-methyl]-(−)-cocaine PET studies in human subjects. J Cereb.Blood Flow Metab. 1990 : 10:740–747.
21. Austin, M.A., Breslow. J.L., Hennekens, C.H., et al. Low density lipoprotein subclass patterns and risk of myocardial infarction. *JAMA*. 1988 : 260 : 1917-21.
22. Campos, H., Genest, J.J. Jr, Blijlevens, E., et al. Low density lipoprotein particle size and coronary artery disease. *Arterioscler Thromb* 1992 : 12 : 187-95.
23. Tabas, I., Bornfeldt, K.E. Macrophage Phenotype and Function in Different Stages of Atherosclerosis. Circ Res. 2016 : 118(4):653-67.
24. Holtman, I.R., Raj, D.D., Miller, J.A., et al. Induction of a common microglia gene expression signature by aging and neurodegenerative conditions: a co-expression meta-analysis. Acta Neuropathologica Communications. 2015. Doi.10.1186/s40478-015-0203-5
25. van Dijk, R.A., Rijs, K., Wezel, A., et al. Systematic Evaluation of the Cellular Innate Immune Response During the Process of Human Atherosclerosis. J Am Heart Assoc. 2016 : 5(6). pii: e002860. doi: 10.1161/JAHA.115.002860.
26. de Gaetano, M., Crean, D., Barry, M., et al. M1- and M2-Type Macrophage Responses Are Predictive of Adverse Outcomes in Human Atherosclerosis. Front Immunol. 2016 : 7:275. doi: 10.3389/fimmu.2016.00275. eCollection 2016.
27. Jager, N.A., Wallis de Vries, B.M., Hillebrands, J.L., et al. Distribution of Matrix Metalloproteinases in Human Atherosclerotic Carotid Plaques and Their Production by Smooth

Muscle Cells and Macrophage Subsets. Mol Imaging Biol. 2016 : 18(2):283-91. doi: 10.1007/s11307-015-0882-0.

28. Blykers, A., Schoonooghe, S., Xavier, C., et al. PET Imaging of Macrophage Mannose Receptor-Expressing Macrophages in Tumor Stroma Using 18F-Radiolabeled Camelid Single-Domain Antibody Fragments. J Nucl Med. 2015 : 56(8):1265-71. doi: 10.2967/jnumed.115.156828.
29. Cope, F.O., Abbruzzese, B., Sanders, J., et al. The inextricable axis of targeted diagnostic imaging and therapy: An immunological natural history approach. Nucl Med Biol. 2016 : 43(3):215-25.
30. Tahara, N., Mukherjee, J., de Haas, H.J., et al. 2-deoxy-2-[18F]fluoro-D-mannose positron emission tomography imaging in atherosclerosis. Nat Med. 2014 : 20(2):215-9.
31. Pedersen, S.F., Sandholt, B.V., Keller, S.H., et al. 64Cu-DOTATATE PET/MRI for Detection of Activated Macrophages in Carotid Atherosclerotic Plaques: Studies in Patients Undergoing Endarterectomy. Arterioscler Thromb Vasc Biol. 2015 : 35(7):1696-703.
32. Kato T[1], Inui Y[2], Nakamura A., et al. Brain fluorodesoxyglucose (FDG) PET in dementia. Ageing Res Rev. 2016 : 30:73-84. doi: 10.1016/j.arr.2016.02.003. Epub 2016 Feb 11.
33. Mao, J.W., Tang, H.Y., Zhao, T., Tan, X.Y., Bi, J., Wang, B.Y., Wang, Y.D. Intestinal mucosal barrier dysfunction participates in the progress of nonalcoholic fatty liver disease. Int J Clin Exp Pathol. 2015 : 8(4): 3648-3658.
34. Lecanu, L., Yao, Z.X., McCourty, A., et al. Control of hypercholesterolemia and atherosclerosis using the cholesterol recognition/interaction amino acid sequence of the translocator protein TSPO. Steroids. 2013 : 78(2):137-46. doi: 10.1016/j.steroids.2012.10.018. Epub 2012 Nov 23.
35. Da Pozzo, E., Giacomelli, C., Costa, B., et al. TSPO PIGA Ligands Promote Neurosteroidogenesis and Human Astrocyte Well-Being. Int J Mol Sci. 2016 : 17(7). doi: 10.3390/ijms17071028.
36. Chauveau, F., Boutin, H., Van Camp, N., et al. In vivo imaging of neuroinflammation in the rodent brain with [11C]SSR180575, a novel indoleacetamide radioligand of the translocator protein (18kDa). Eur J Nucl Med Mol Imaging. 2011 : 38(3):509-14. doi: 10.1007/s00259-010-1628-5. Epub 2010 Oct 9.
37. Yankam Njiwa, J., Costes, N., Bouillot, C. et al. Quantitative longitudinal imaging of activated microglia as a marker of inflammation in the pilocarpine rat model of epilepsy using [11C]-(R)-PK11195 PET and MRI. J Cereb Blood Flow Metab. 2016 : 271678X16653615. doi: 10.1177/0271678X16653615.
38. Fullerton, S.M., Shirman, G.A., Strittmatter, W.J., et al. Impairment of the blood-nerve and blood-brain barriers in apolipoprotein e knockout mice. Exp Neurol. 2001: 169(1): 13-22.
39. Schwartz, M., Baruch, K. The resolution of neuroinflammation in neurodegeneration: leukocyte recruitment via the choroid plexus. EMBO J. 2014 : 33(1): 7-22.

40. Lavisse, S., Inoue, K., Jan, C., et al. [18F]DPA-714 PET imaging of translocator protein TSPO (18 kDa) in the normal and excitotoxically-lesioned nonhuman primate brain. Eur J Nucl Med Mol Imaging. 2015 : 42(3):478-94. doi: 10.1007/s00259-014-2962-9. Epub 2014 Dec 9.
41. Tawakol, A., Fayad, Z.A., Mogg, R., et al. Intensification of statin therapy results in a rapid reduction in atherosclerotic inflammation : results of a multicenter fluorodesoxyglucose-positron emission tomography/computed tomography feasability study. J Am Coll Cardiol. 2013 : 62(10):909-17. doi: 10.1016/j.jacc.2013.04.066. Epub 2013 May 30.

TABLES:

Table 1: Correlations between RNA vulnerable markers in carotid artery.* genes related to imaging (*Hk1* for [^{18}F]-FDG and *Tspo* for [^{11}C]-PK11195), ** anti-inflammatory markers

	Correlated with	r	p
Ccl2	*Il-1β*	0.9	0.001
	Tlr4	0.9	0.001
	Il-1ra **	0.9	0.003
	Tspo *	0.89	0.001
	Cd163 **	0.88	0.001
	Clec7a **	0.87	<0.001
	Cd3ε	0.86	0.003
	Cd68	0.86	0.002
	Cd14	0.85	0.001
	Ppif (CyD)	0.81	0.006
	Hk1 *	0.79	0.009
	Il-6	0.71	0.027
	Irf4 **	0.7	0.001
Il-1β	*Cd14*	0.95	<0.001
	Clec7a **	0.95	<0.001
	Ccl2	0.9	0.001
	Il-1ra **	0.9	0.001
	Hk1 *	0.89	0.001
	Tlr4	0.86	0.002
	Tspo *	0.82	0.006
	Ppif (CyD)	0.8	0.009
	Il-6	0.69	0.031
	Cd3ε	0.66	0.044
Il-6	*Cd3ε*	0,81	0,007
	Il-1ra **	0.75	0.009
	Ccl2	0,71	0,027
	Cd14	0.71	0.01
	Il-1β	0,69	0,031
	Il-10 **	0.69	0.027
	Hk1 *	0,66	0,044

Table 2: Correlations between RNA vulnerable markers in carotid endarterectomy of symptomatic patients (n=9).* genes related to imaging (*Hk1* for [^{18}F]-FDG and *Tspo* for [^{11}C]-PK11195), ** anti-inflammatory markers

	Correlated with	r	p
IL-1β	*Irf4* **	0.91	0.001
Ccl2	*Hk1* *	0.9	0.001
	Tspo *	0.97	<0.001
	Ppif	0.93	<0.001
	Cd14	0.96	<0.001
	Cd68	0.82	0.007
	Tlr4	0.98	<0.001
	Il-6	0.92	<0.001
	Tnfα	0.88	0.002
	Cxcl9	0.71	0.032
	Il1-7ra	0.81	0.009
	Ccr2	0.87	0.003
	Il-10 **	0.88	0.002
	Clec7a **	0.93	<0.001
	Cd163 **	0.91	0.001
Il-6	*Hk1* *	0.87	0.002
	Tspo *	0.83	0.005
	Ppif	0.92	<0.001
	Cd14	0.86	0.003
	Tlr4	0.97	<0.001
	Ccl2	0.92	0.000
	Tnfα	0.75	0.019
	Cxcl9	0.72	0.029
	Ccr2	0.77	0.014
	Il-10 **	0.84	0.005
	Clec7a **	0.80	0.011
	Cd163 **	0.81	0.008
	Cd3ε	0.78	0.014

Table 3: Correlations between RNA vulnerable markers in carotid endarterectomy of asymptomatic patients (n=10).* genes related to imaging (*Hk1* for [^{18}F]-FDG and *Tspo* for [^{11}C]-PK11195), ** anti-inflammatory markers

	Correlated with	r	p
Il-1ß	*Tspo* *	0.72	0.020
	Cd14	0.80	0.006
	Cd68	0.86	0.001
	Tlr4	0.76	0.011
	Ccl2	0.82	0.004
	Il-6	0.83	0.003
	Tnfα	0.72	0.014
	Cxcl9	0.78	0.008
	Il1-7ra	0.85	0.002
	Ccr2	0.83	0.003
	Clec7a **	0.84	0.002
	Cd163 **	0.84	0.002
Ccl2	*Tspo* *	0.66	0.036
	Cd14	0.71	0.008
	Cd68	0.90	0.000
	Il1ß	0.82	0.004
	Tlr4	0.67	0.034
	Il-6	0.97	<0.001
	Tnfα	0.97	<0.001
	Cxcl9	0.76	0.011
	Il1-7ra	0.98	<0.001
	Ccr2	0.99	<0.001
	Clec7a **	0.98	<0.001
	Cd163 **	0.90	<0.001
Il-6	*Tspo* *	0.76	0.011
	Cd14	0.86	0.002
	Cd68	0.94	<0.001
	Il-1ß	0.83	0.003
	Tlr4	0.75	0.013
	Ccl2	0.97	<0.001
	Tnfα	0.96	<0.001
	Cxcl9	0.84	0.003
	Il1-7ra	0.98	<0.001
	Ccr2	0.99	<0.001
	Clec7a **	0.97	<0.001
	Cd163 **	0.95	<0.001

FIGURES LEGENDS:

Figure 1: Lipid profiles. Plasmatic cholesterol level (A) and HDL/LDL ratio (B) in HC diet animals at 0, 1, 7, 12, 18 and 24 months after start of diet. Lipoprotein profile of 1 HC (C) and 1 control (D) NHP at T+24 months.

*** Significantly different from T0 $p<0.001$; HC and SD: high cholesterol and standard diet

Figure2: MRI carotid plaque area (A) and gadolinium signal intensity (SI) enhancement (B) of HC and SD animals. MRI carotid plaque measurement showed thicker vessel wall in HC than SD animals (A, $p<0.001$), but no difference in gadolinium SI measurement. Differential right/left enhancement was observed in HC NHPs (C, arrow for the right enhanced carotid). [^{18}F]-FDG SUV of right and left carotid of HC NHPs (D) showed no difference between HC and SD animals. For the same HC NHP as in C, [^{18}F]-FDG uptake was also observed in the right carotid (E, arrow). There was also no difference between HC and SD animals for [^{11}C]-PK1195 TBR of carotid arteries (F), but right/left asymmetry was also observed for the same HD animal as in C and E (G, arrow).

*** Significantly different from SD $p<0.001$; HC and SD: high cholesterol and standard diet; TBR: target-to-background ratio

Figure 3: Longitudinal ultrasound and systemic biomarkers. Ultrasound score in the carotid arteries (A), hs-CRP (B) and plasma LDL-C level (C) at T+12 and T+18 months.

Figure 4: At-risk NHPs with downstream events. Histological evidences of coronary stenosis (A, C), myocardial fibrosis (B) and severe and diffuse plaque (D) in 3 NHPs. These animals also presented severe and diffuse plaque visible in the left carotid (E,H, J). MRI (F) showed a lacunar stroke in 1 of these 2 animals, and PET/CT imaging showed high binding potential for [^{11}C]-PK11195 in the left carotid (G). The left carotid of this NHP showed multifocal plaque on histology (I).

Figure 5: RNA expression of gene of vulnerable plaque markers in the carotid arteries enabled NHPs to be divided into 3 groups according to cardiovascular risk (A). To be noted: the three animals with downstream events were classified in the high cardiovascular risk group on the RNA expression analysis alone. PCA analysis confirmed the 3 groups of animals (B).

Figure 6: RNA expression of gene of vulnerable plaque markers in the carotid arteries confirmed the pattern of significant co-expression of inflammatory and anti-inflammatory macrophages in both symptomatic (A) and asymptomatic (B) inflammatory patients.

FIGURE 1

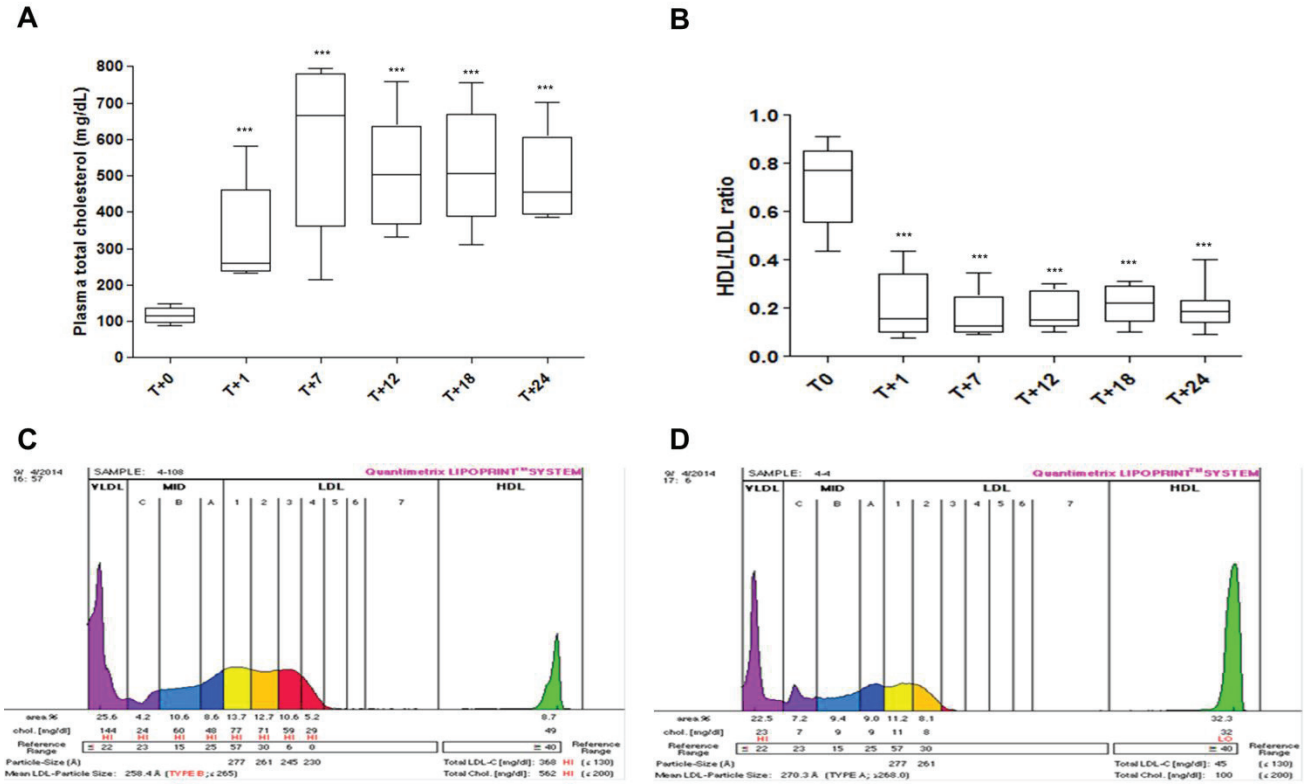
A
Plasma a total cholesterol (mg/dL)
800
700
600
500
400
300
200
100
0
***
T+0
T+1
T+7
T+12
T+18
T+24
B
HDL/LDL ratio
1.0
0.8
0.6
0.4
0.2
0.0
T0
T+1
T+7
T+12
T+18
T+24
C
SAMPLE: 4-108
Quantimetrix LIPOPRINT™SYSTEM
VLDL
MID
LDL
HDL
D
SAMPLE: 4-4
Quantimetrix LIPOPRINT™SYSTEM
VLDL
MID
LDL
HDL

FIGURE 2

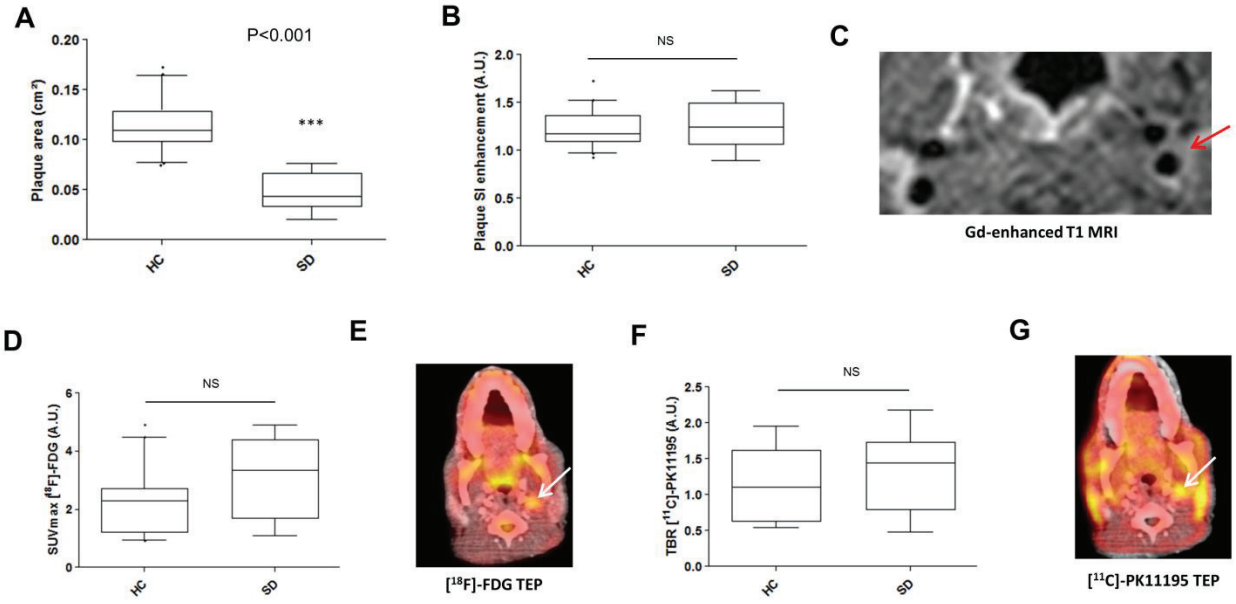
A
P<0.001
***
Plaque area (cm²)
0.20
0.15
0.10
0.05
0.00
HC
SD
B
NS
Plaque SI enhancement (A.U.)
2.0
1.5
1.0
0.5
0.0
HC
SD
C
Gd-enhanced T1 MRI
D
NS
SUVmax [18F]-FDG (A.U.)
6
4
2
0
HC
SD
E
[18F]-FDG TEP
F
NS
TBR [11C]-PK11195 (A.U.)
2.5
2.0
1.5
1.0
0.5
0.0
HC
SD
G
[11C]-PK11195 TEP

FIGURE 3

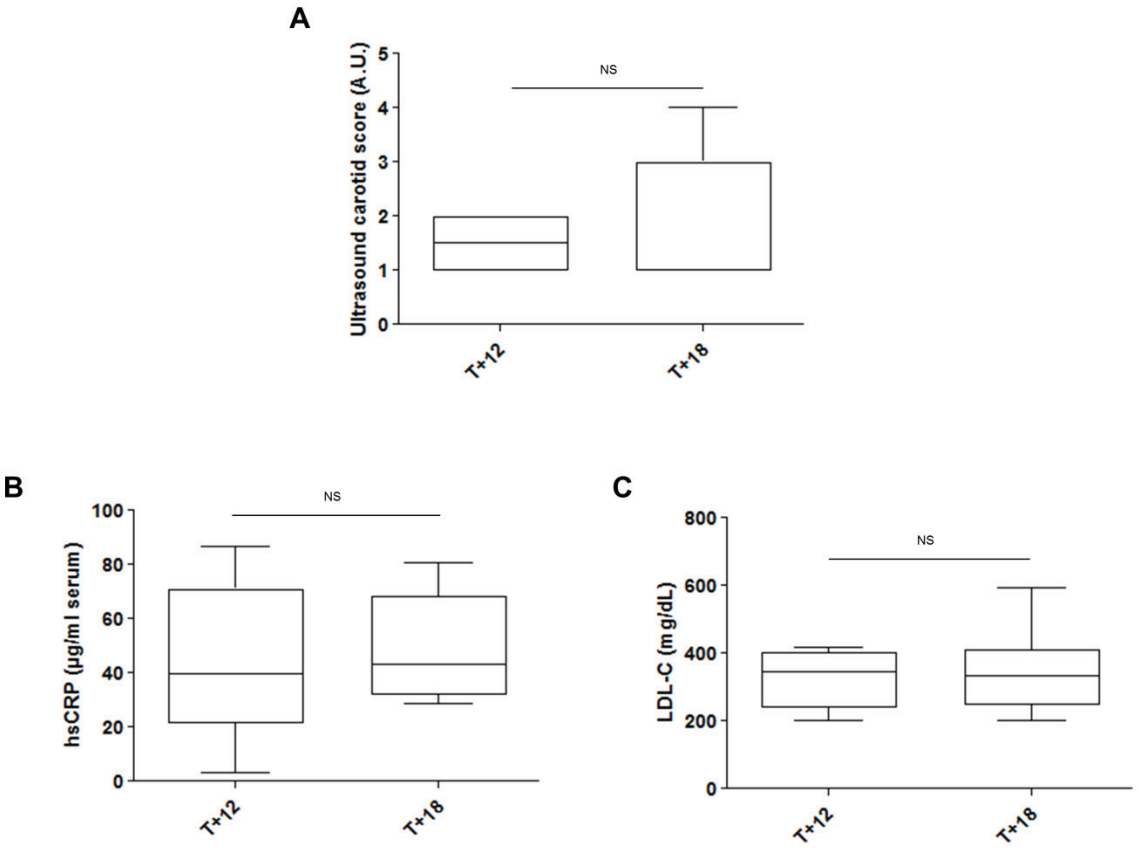
A
Ultrasound carotid score (A.U.)
0
1
2
3
4
5
NS
T+12
T+18
B
hsCRP (µg/ml serum)
0
20
40
60
80
100
NS
T+12
T+18
C
LDL-C (mg/dL)
0
200
400
600
800
NS
T+12
T+18

FIGURE 4

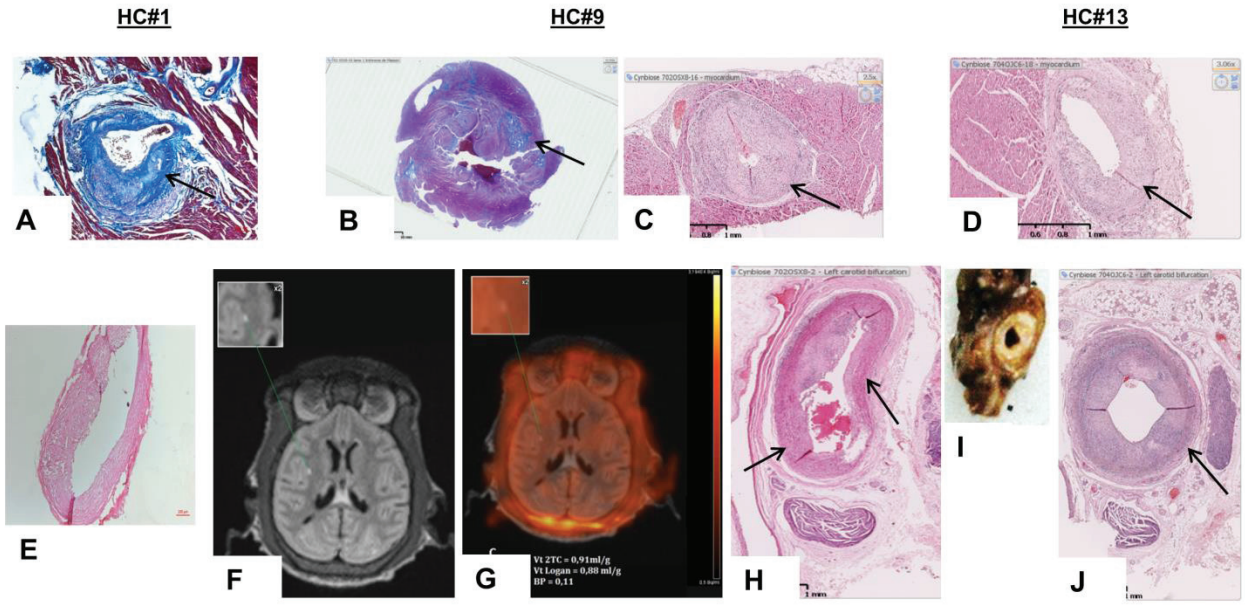

FIGURE 5

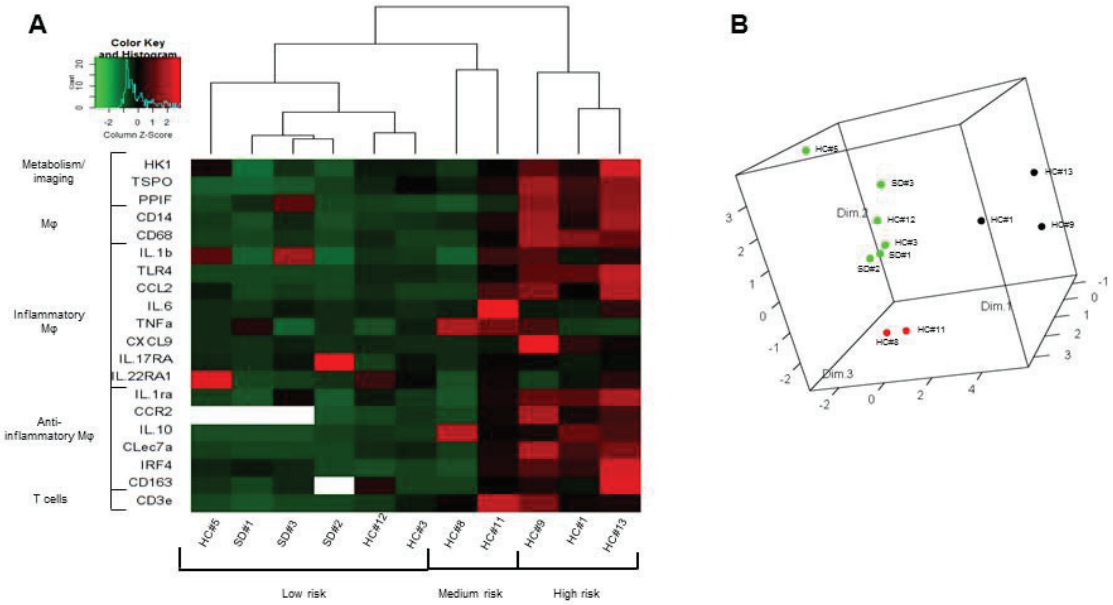
A
Color Key and Histogram
Count
Column Z-Score
Metabolism/ imaging
HK1
TSPO
PPIF
Mφ
CD14
CD68
IL.1b
TLR4
CCL2
Inflammatory Mφ
IL.6
TNFa
CXCL9
IL.17RA
IL.22RA1
IL.1ra
CCR2
Anti-inflammatory Mφ
IL.10
CLec7a
IRF4
CD163
T cells
CD3e
HC#5
SD#1
SD#3
SD#2
HC#12
HC#3
HC#8
HC#11
HC#9
HC#1
HC#13
Low risk
Medium risk
High risk
B
Dim.1
Dim.2
Dim.3

FIGURE 6

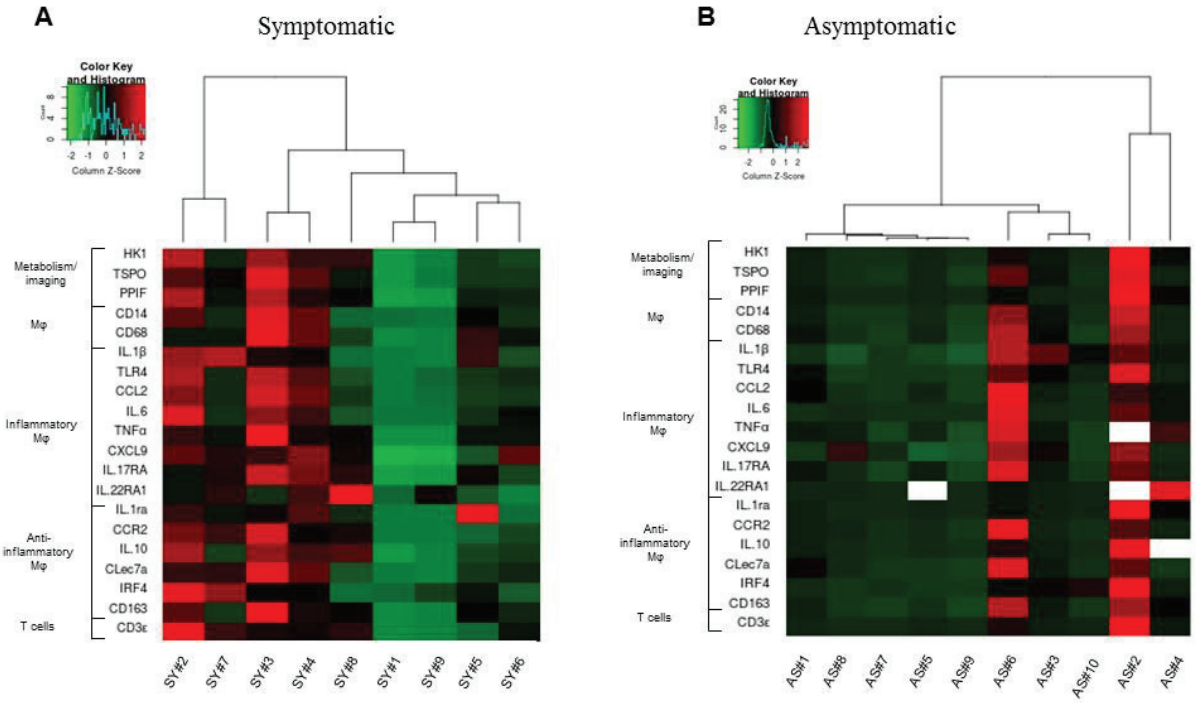
A
Symptomatic
Color Key and Histogram
Column Z-Score
Metabolism/ imaging
Mφ
Inflammatory Mφ
Anti-inflammatory Mφ
T cells
HK1
TSPO
PPIF
CD14
CD68
IL.1β
TLR4
CCL2
IL.6
TNFα
CXCL9
IL.17RA
IL.22RA1
IL.1ra
CCR2
IL.10
CLec7a
IRF4
CD163
CD3ε
SY#2
SY#7
SY#3
SY#4
SY#8
SY#1
SY#9
SY#5
SY#6
B
Asymptomatic
Color Key and Histogram
Column Z-Score
Metabolism/ imaging
Mφ
Inflammatory Mφ
Anti-inflammatory Mφ
T cells
HK1
TSPO
PPIF
CD14
CD68
IL.1β
TLR4
CCL2
IL.6
TNFα
CXCL9
IL.17RA
IL.22RA1
IL.1ra
CCR2
IL.10
CLec7a
IRF4
CD163
CD3ε
AS#1
AS#8
AS#7
AS#5
AS#9
AS#6
AS#3
AS#10
AS#2
AS#4

SUPPLEMENTAL DATA

Figure S1: Experimental study design over the 24 months.

Figure S2: MR and CT angiographies used for MR and PET/CT images registration for an accurate placing of ROI for carotid wall measurement.

Figure S3: Right and left carotid individual values for MRI plaque surface (A, B), for gadolinium plaque SI enhancement (C, D), for SUVmax [^{18}F]-FDG (E, F), [^{11}C]-PK11195 (G, H) in HC and SD animals, respectively. Though PET inflammation biomarkers and gadolinium MRI permeability marker levels are not directly correlated, there is a corresponding left/right difference in HC animals with the three imaging markers. In old SD animals, there was also elevated inflammation at the measurement time-point, illustrating the importance of longitudinal inflammation evaluation to discriminate between chronic atherosclerosis inflammation and acute unrelated inflammatory status.

Figure S4: Individual values for ultrasound carotid scores (A), hsCRP (B) and LDL-C levels (C) at T+12 and T+18 months in HC animals. At-risk cholesterol profile (low HDL, high LDL-C), chronic inflammation (hsCRP high or increasing) and lesion progression by US were found in 3 NHP (#1, #9, #13).

Figure S5: Multi-site inflammation showing corresponding higher uptake in aortic arch and hematopoietic organs (bone marrow and spleenin in an at-risk HC animal compared to a lower risk SD subject.

Figure S6: RNA expression of genes of vulnerable plaque markers and correlation between them in aortic arch (left) and abdominal aorta (right).

Figure S7: Adipose tissue imaging of white subcutaneuous (SAT) and visceral fat (VAT) (A-B), and brown fat (BAT) (C-D). HC animals presented a higher [^{18}F]-FDG uptaje in visceral adipose tissue and a lower in brown adipose tissue compared to SD. Correlations from gene analysis in pericardic (E), periarterial (F) and visceral (G) adipose tissues showed positive correlations between pro and anti-inflammatory markers.

Figure S8: Brain PET/CT imaging. Higher uptake of [^{11}C]-PK11195 in the frontal cortex (A) and limbic system (B) in HC animals. Lower metabolic activity (lower [^{18}F]-FDG uptake) in the limbic system in HC animals (C).

Figure S9: RNA expression of genes of vulnerable plaque markers in the brain.

FIGURE S1

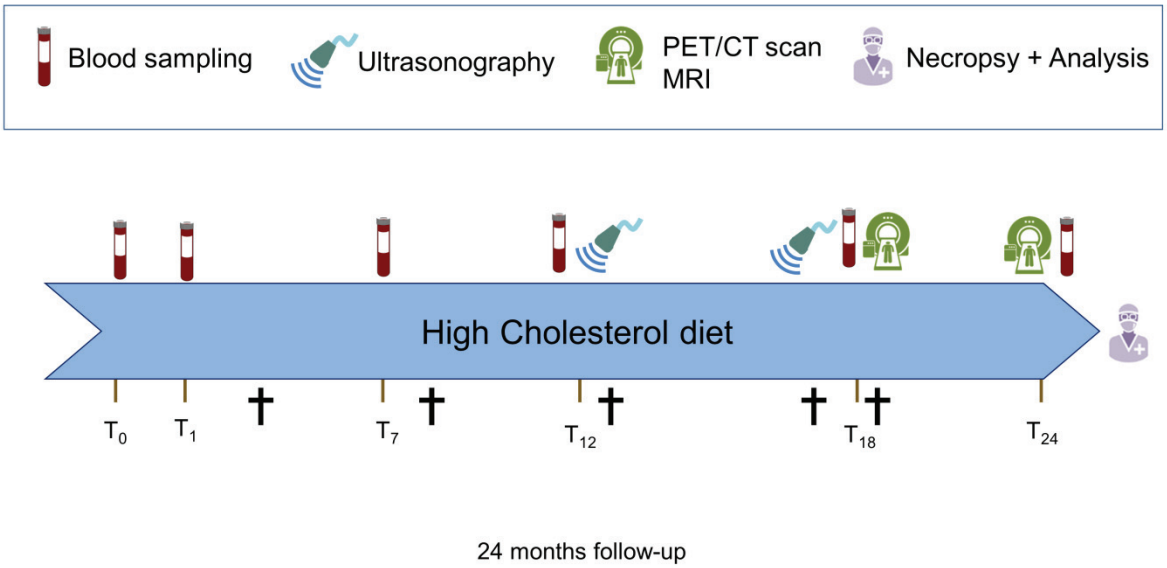
Blood sampling
Ultrasonography
PET/CT scan
MRI
Necropsy + Analysis
High Cholesterol diet
T0
T1
T7
T12
T18
T24
24 months follow-up

FIGURE S2

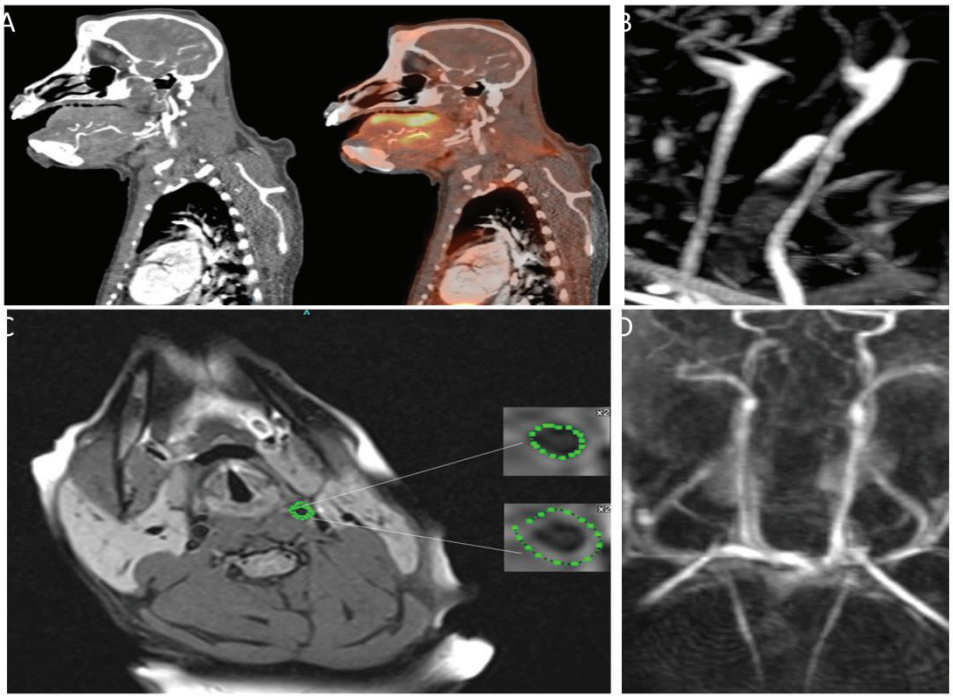

FIGURE S3

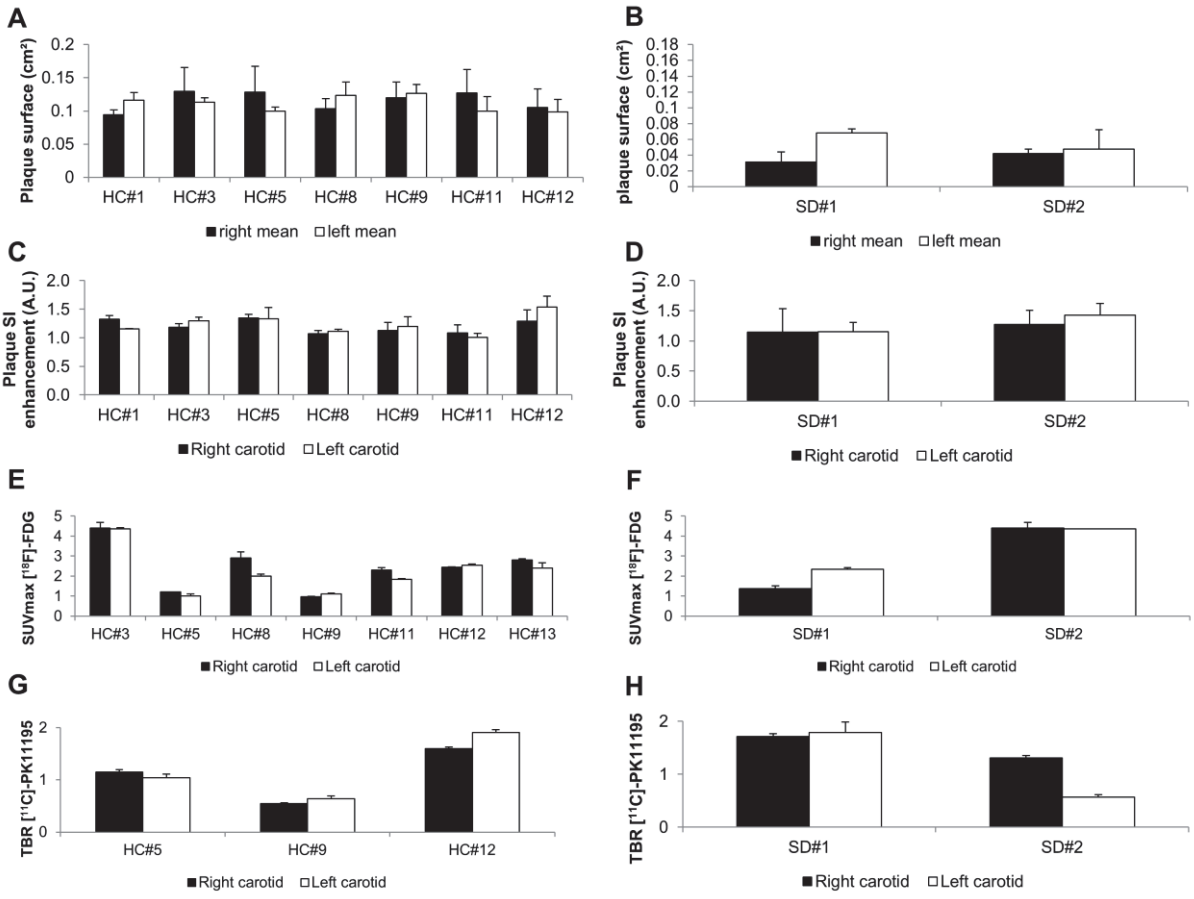
A
Plaque surface (cm²)
0.2
0.15
0.1
0.05
0
HC#1 HC#3 HC#5 HC#8 HC#9 HC#11 HC#12
right mean left mean
B
plaque surface (cm²)
0.18
0.16
0.14
0.12
0.1
0.08
0.06
0.04
0.02
0
SD#1 SD#2
right mean left mean
C
Plaque SI enhancement (A.U.)
2.0
1.5
1.0
0.5
0.0
HC#1 HC#3 HC#5 HC#8 HC#9 HC#11 HC#12
Right carotid Left carotid
D
Plaque SI enhancement (A.U.)
2.0
1.5
1.0
0.5
0.0
SD#1 SD#2
Right carotid Left carotid
E
SUVmax [18F]-FDG
5
4
3
2
1
0
HC#3 HC#5 HC#8 HC#9 HC#11 HC#12 HC#13
Right carotid Left carotid
F
SUVmax [18F]-FDG
5
4
3
2
1
0
SD#1 SD#2
Right carotid Left carotid
G
TBR [11C]-PK11195
2
1
0
HC#5 HC#9 HC#12
Right carotid Left carotid
H
TBR [11C]-PK11195
2
1
0
SD#1 SD#2
Right carotid Left carotid

FIGURE S4

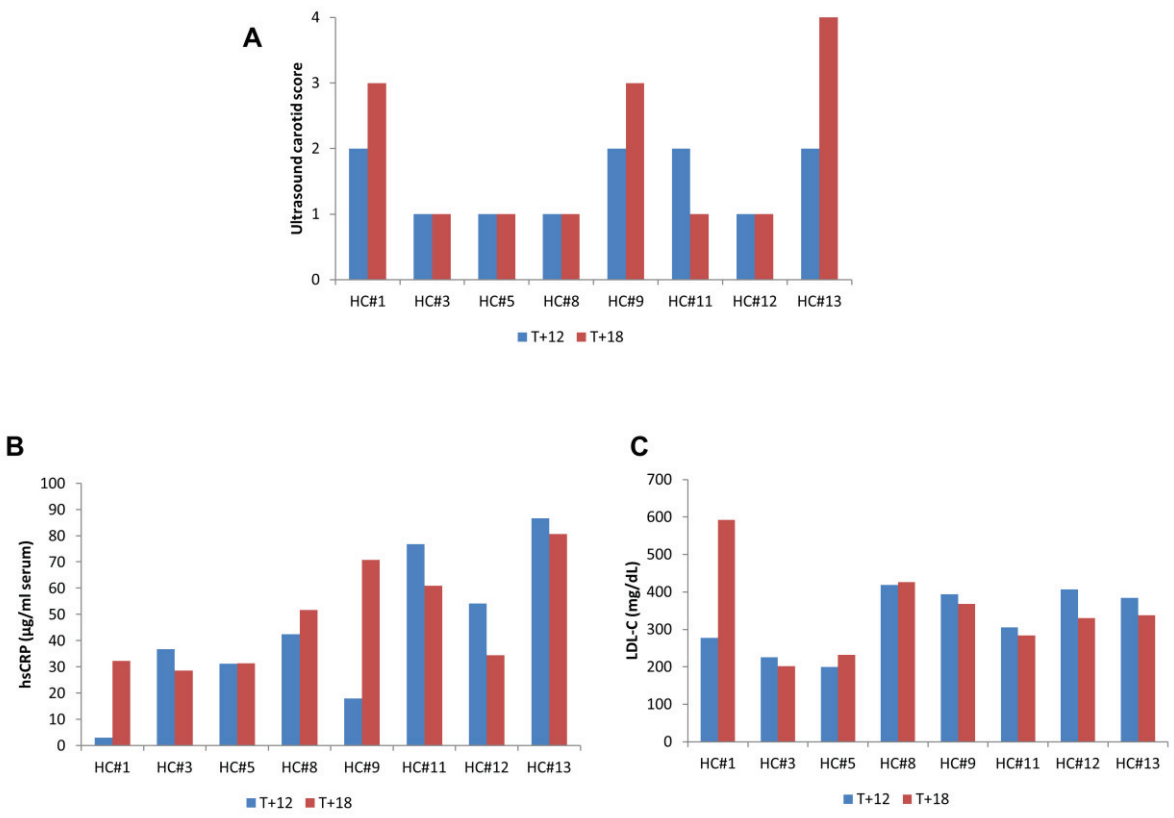
A
Ultrasound carotid score
0
1
2
3
4
HC#1
HC#3
HC#5
HC#8
HC#9
HC#11
HC#12
HC#13
T+12
T+18
B
hsCRP (µg/ml serum)
0
10
20
30
40
50
60
70
80
90
100
HC#1
HC#3
HC#5
HC#8
HC#9
HC#11
HC#12
HC#13
T+12
T+18
C
LDL-C (mg/dL)
0
100
200
300
400
500
600
700
HC#1
HC#3
HC#5
HC#8
HC#9
HC#11
HC#12
HC#13
T+12
T+18

FIGURE S5

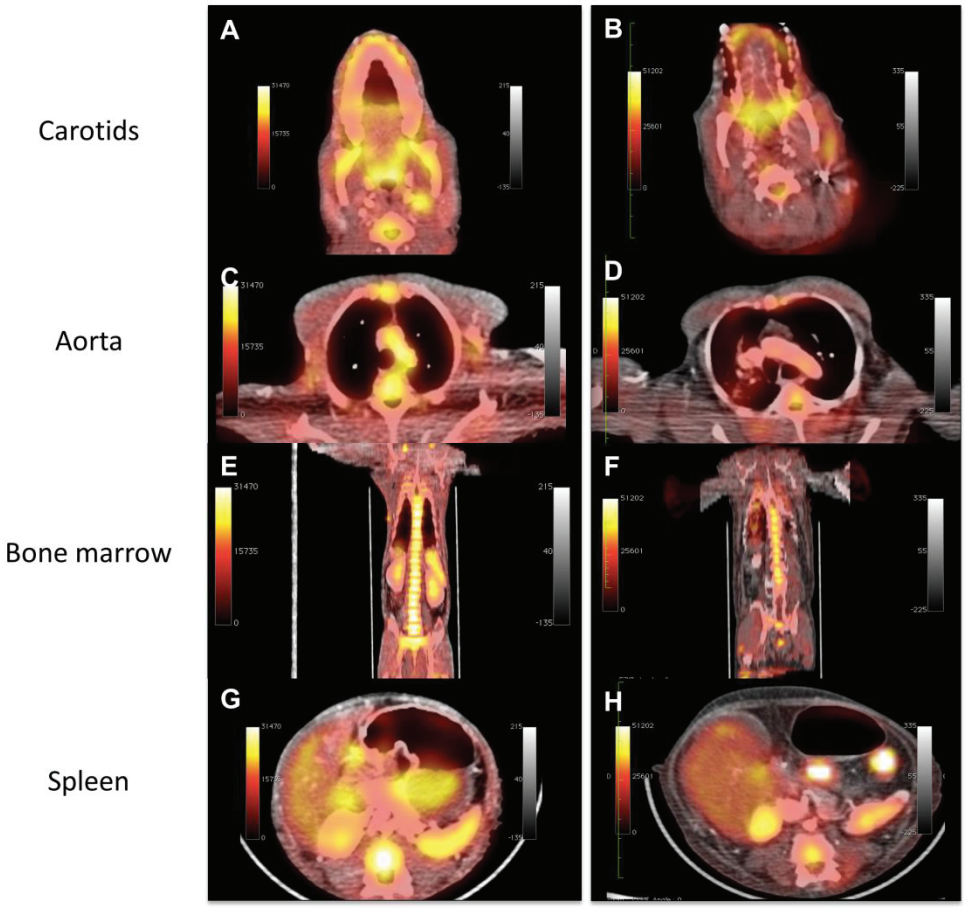

FIGURE S6

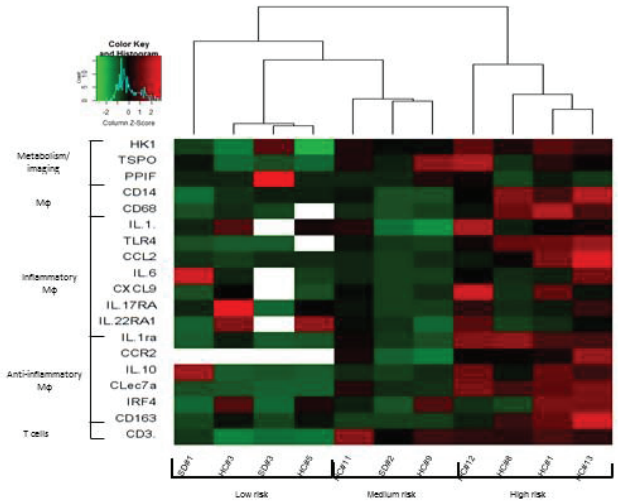

	Correlated with	r	p
Col3	Cd14	0.95	<0.001
	Cd68	0.82	0.002
	Tlr4	0.95	<0.001
	Clec7a	0.79	0.004
	Cd163 **	0.92	<0.001
	Irf4 **	0.87	<0.001
	Hk1 *	0.65	0.03
	Il-1ra **	0.64	0.034
	Ccr2	0.67	0.024
	Cd3e	0.61	0.046

	Correlated with	r	p
Il-1β	Hk1 *	0.82	0.002
	Tspo *	0.72	0.012
	Il-1ra **	0.76	0.005
	Clec7a	0.76	0.007
	Il-17ra	0.85	<0.001
	Cd14	0.66	0.027
	Cxcl9	0.65	0.038
	Ccr2	0.67	0.024
	Il-10 **	0.64	0.034
	Cd3e	0.74	0.009
Il-6	Il-10 **	0.77	0.006

Aortic arch

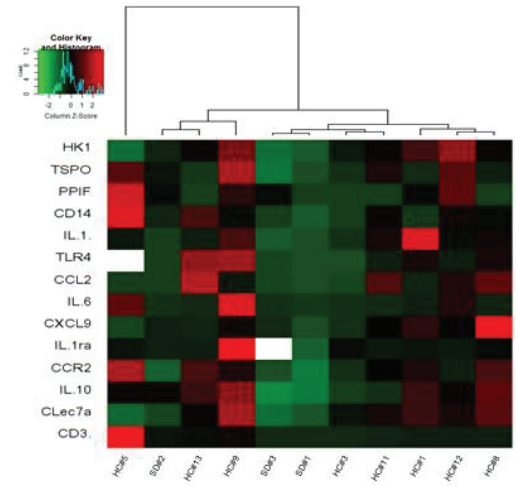

	Correlated with	r	p
Col3	Hk1 *	0.65	0.03
	Tlr4	0.72	0.012
	Ccr2	0.68	0.021
	Cd14	0.78	0.005
	Il-10 **	0.87	<0.001
	Clec7a	0.8	0.005
	Cd3e	0.92	<0.001
Il-1β	Tspo *	0.64	0.034
	Il-6	0.93	<0.001
	Cd14	0.75	0.008
	Clec7a	0.63	0.038
Il-6	Cd14	0.68	0.021

Abdo aorta

FIGURE S7

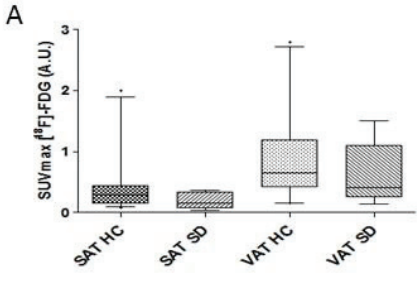

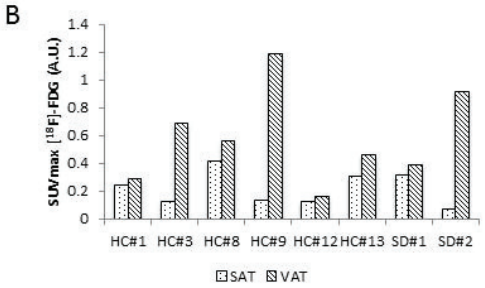

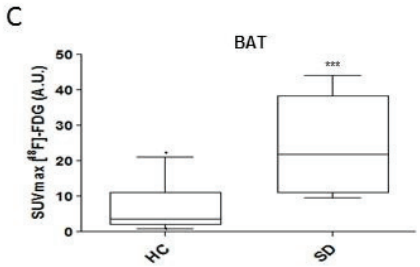

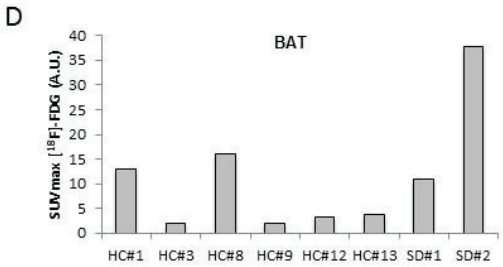

E

Pericardic AT

	Correlate w/	r
MCP1 (CCL2)	IL-1b	0.674
	TLR4	0.677
	IL-6	0.644
	IL-10	0.761
	CD3e	0.652
IL-6	IL-1b	0.807
CD3e	TLR4	-0.645
	MCP1	-0.652
	CD163	0.691
	IL-17RA	0.743

F

Periarterial AT

	Correlate w/	r
IL-1b	IL-6	0.776
	CXCL9	0.831
	CCR2	0.861
	CLec7a	0.958
IL-6	CD3e	0.776
CD3e	PPIF	0.976

G

VAT

	Correlate w/	r
MCP1	CD14	0.723
	TLR4	0.691
	IL-6	0.906
	IL-1ra	0.98
	IL-10	0.655
	CD163	0.85
IL-1b	CCR2	0.677
	IL-10	0.739
	CD163	0.633
IL-6	CD68	0.841
	IL-1ra	0.894
	CD163	0.856
CD3e	PPIF	0.865
	CXCL9	0.739

FIGURE S8

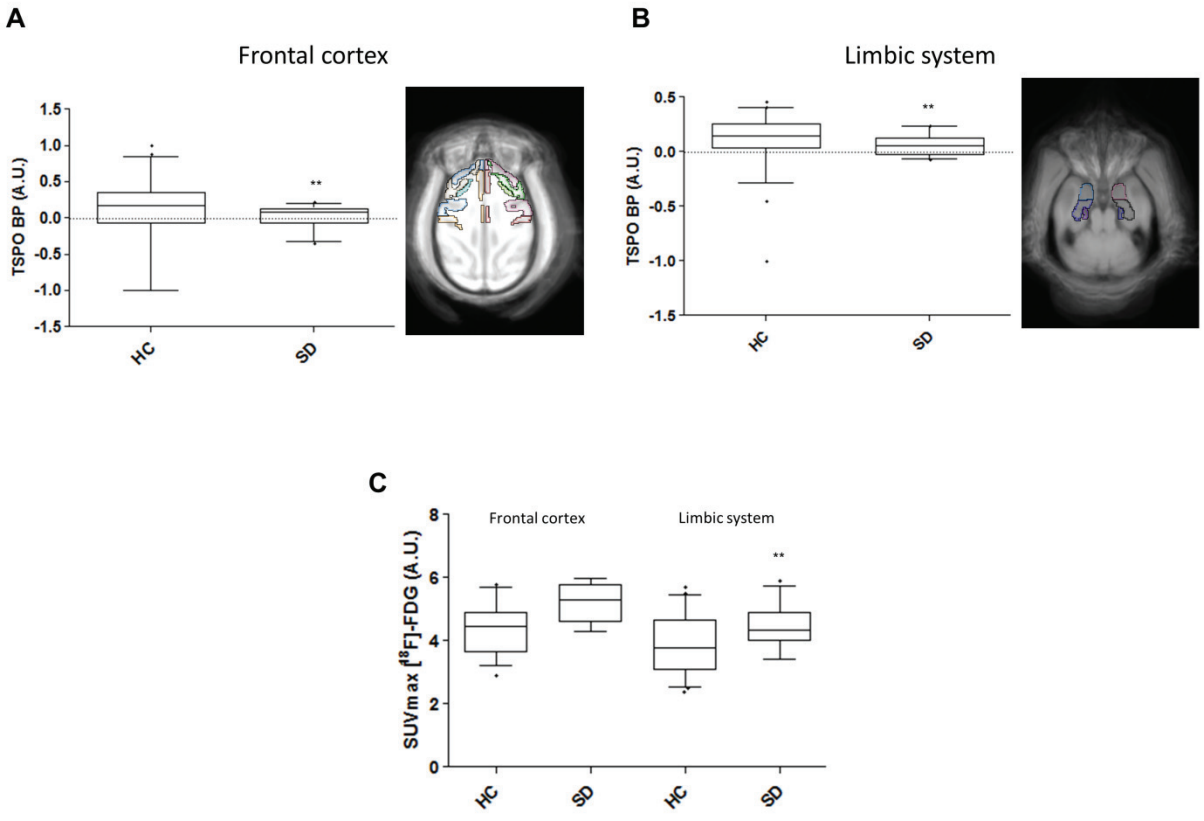
A
Frontal cortex
TSPO BP (A.U.)
1.5
1.0
0.5
0.0
-0.5
-1.0
-1.5
**
HC
SD
B
Limbic system
TSPO BP (A.U.)
0.5
0.0
-0.5
-1.0
-1.5
**
HC
SD
C
Frontal cortex
Limbic system
SUVmax [18F]-FDG (A.U.)
8
6
4
2
0
**
HC
SD
HC
SD

FIGURE S9

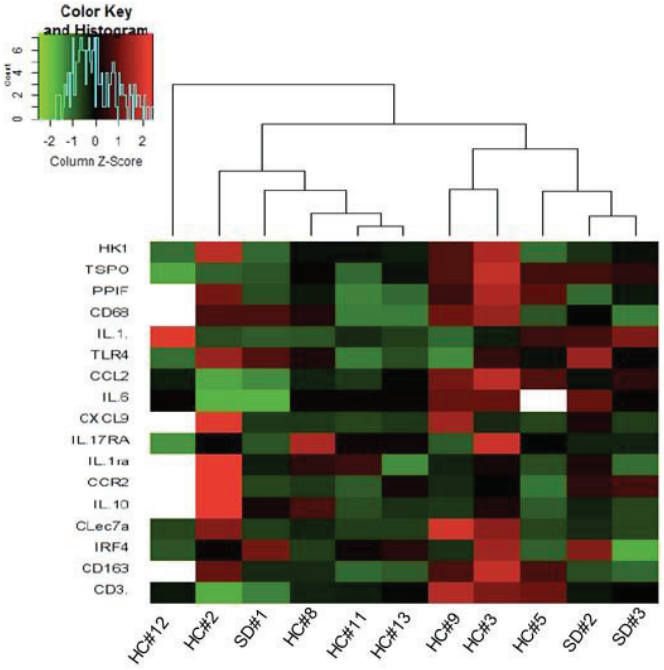

	Correlate with	r
MCP1	TSPO *	0.824
	CD3e	0.952
IL-1b	IL-1ra	-0.617
IL-6	HK1 *	0.675
CD3e	TSPO *	0.718

DISCUSSION

DISCUSSION

Atherosclerosis is a complex multifactorial pathology characterized by dyslipidemia and low-grade inflammation leading to plaque formation. Over time, the plaques develop and can lead to vessel lumen stenosis or rupture and form thrombus or emboli resulting in clinical outcomes such as angina, myocardial infarction or stroke. Although atherosclerosis has been well studied during the last decades using different animal models and clinical studies, the cerebrovascular impacts of this pathology are still poorly investigated. Another issue is the lack of accurate biomarkers or combination of biomarkers available for accurate individual risk stratification.

I demonstrated that regular exercise training was able to counteract peripheral and central damaging effects of a HC diet in old ApoE$^{-/-}$ mice when food rations were controlled, and that MRI enabled visualization of the cerebral damages (**article n°1**). My second study with longitudinal follow-up based on insulin resistance and brain MR imaging showed that exercise training was no longer beneficial in old ApoE-/- mice when fed with *ad libitum* HC diet (**article n°2**). HC consumption, when unregulated or not counterbalanced by physical exercise, leads to cerebrovascular unit disorganization characterized by BBB permeability and increased inflammatory activity in periventricular areas and in the hippocampus (**article n°1 and 2**). Lastly, my work on non-human primates fed an atherogenic diet emphasized the usefulness of multimodal imaging and a combination of biomarkers including not only metabolic and inflammatory markers but also anti-inflammatory markers for individual stratification of cardiovascular risk (**article n°3**). Overall, my work highlights the relevance of controlling calories intakes to benefit the protective effects of exercise on the progression of atherosclerosis and its outcomes as well as the significance of having a global view of the individual for an accurate stratification of CV risk.

In the following section, I will discuss more precisely the results obtained during my PhD on the lights of the literature and the perspectives opened by this work.

A. Protective effect of exercise depends on the control of HC diet consumption

The beneficial effects of exercise training are well-known and regular moderate intensity exercise is recommended for patients with chronic cardiovascular or metabolic diseases, as well as in all populations, for health preservation. Although some studies show improvement of patients' health status with exercise only (Hambrecht et al., 2000), others studies show that a controlled food intake and/or a careful diet is necessary to obtain these beneficial effects (Bergouignan et al., 2013). Others

publications have even shown that regular exercise can lead to plaque regression or to a reduction of necrotic core area in at-risk patients (Kurose et al., 2016; Madssen et al., 2015).

1. Peripheral effects

In **article n°1** we showed that exercise training had positive effects on systemic and peripheral organs (aorta, heart and liver) in old ApoE$^{-/-}$ mice under controlled calorie intake. First, exercise decreased cholesterol level and improved insulin sensitivity in old ApoE$^{-/-}$ mice. A decrease of oxidative stress characterized by a decrease of oxidative products (lower AOPP in the heart, aorta and liver and lower MDA in plasma), and an increase of antioxidant enzymes (increase of SOD in aorta, heart, plasma and liver and of GPx in liver) was observed in mice that underwent regular voluntary exercise training compared to sedentary ones. Similarly, a lower level of inflammatory cytokines (IL-1β and TNFα) in aorta confirmed a decrease in inflammation in the exercised mice. Of note, although old ApoE$^{-/-}$ mice were obese at the beginning of the study due to their exposure to a HC diet beginning at 8 weeks of age, no significant weight gain was observed in either trained or sedentary mice due to the controlled calories intake.

In the context of *ad libitum* access to HC diet (**article n°2**), no beneficial effect of exercise was observed. Indeed, plasmatic cholesterol levels were similarly high in exercised and sedentary mice, as were oxidative stress and inflammation in the plasma and the aorta. A significant weight gain and a worsening of insulin resistance were even noted in trained mice at the end of the study.

The only difference between these two studies is the free/controlled HC diet access. This suggests that the differences observed on the impact of exercise in these two studies are related to fat/cholesterol consumption. Indeed, although our HC diet was not the maximally-enriched in cholesterol (0.5% when diet with 1.25% are available), it contained 21% fat mainly from pork lard (saturated fatty acid) which is known to play a role in the development of insulin resistance (Putti et al., 2015). Another suggestion is that, as mentioned in **article n°2** and presented in several publications, some individuals were recognized as "non-responders" to exercise (Böhm et al., 2016). However, other recent studies highlighted the fact that maybe "non-responders" are just individuals who need more exercise (i.e. larger amount of exercise and especially high intensity exercise) than the majority of people to present the same beneficial effects of training (Ross et al., 2015). Indeed, they showed that after 24 weeks of high-amount + high-intensity resistance training, there were no non-responders, while there was still 38% in the low-amount + low-intensity group. In a similar way, Bourdier et *al* showed that high-intensity exercise reduced size of myocardial infarction (Bourdier et al., 2016). These are really interesting findings, but I do not think that they can explain the more severe lesions found in our ApoE$^{-/-}$ mice under ad libitum HC diet compared to those of under controlled caloric intake. Indeed, ApoE$^{-/-}$

mice of both **articles 1 and 2** ran similar distances per week, but showed completely opposite metabolic effects. Furthermore, it would be a huge coincidence if all of the 7 trained mice of **article n°2** were non-responders. In my opinion, the main difference is that *ad libitum*-fed mice consumed a lot more "lipotoxic" food than controlled ones, and this food behavior can be due to their regular exercising. Indeed, if the mice in both articles exercised in a similar manner, the fact that those in **article n°2** had *ad libitum* access to high fat diet resulted in a blunting of positive metabolic effects of exercise.

2. *Central effects*

Exercise impacted the brain differently in our two studies. While exercise presented a beneficial impact on cerebrovascular lesion with maintenance of BBB integrity and a low macrophage accumulation in periventricular areas in old ApoE$^{-/-}$ mice fed a controlled ration of HC diet, in a context of unregulated consumption of HC diet, exercise exhibited effects that are more deleterious. In **article n°2**, we observed a significant increase of BBB leakage and macrophage accumulation in the brain in exercised mice compared to sedentary mice. This discovery is strengthened by the longitudinal imaging follow-up which enabled us to observe the changes between pre and post-training images on both gadolinium-enhanced and T2/T2* sequences.

As shown recently, a daily ingestion of large amounts of high fat or HC diet in mice could lead to a chronic increase of LPS concentration in the gut by the microbiota, which can then be transferred to plasma, and to metabolic organs as well as to the brain (Mao et al., 2015). Therefore, this nutritional condition could lead to both chronic low-grade metabolic inflammation and neuroinflammation as showed in our old ApoE$^{-/-}$ mice under HC diet. In the brain, LPS is also known to affect permeability of the BBB through the release of cytokines (Xaio et al., 2001).

In old ApoE$^{-/-}$ mice consuming an atherogenic diet, inflammation and BBB leakage are located in first-line responding regions in terms of BBB influx and immune cell recruitment, such as the hippocampus and circumventricular organs (Fullerton et al., 2001; Schwartz and Baruch, 2014). These specific areas have also been found to respond after a simple intraperitoneal LPS challenge (Mori et al., 2014). The fact that these locations are impacted supports the hypothesis that the continuous ingestion of HC diet by our obese mice increased LPS influx. These areas are also functionally involved in the regulation of food intake and central response to specific endocrine signals, such as leptin and others linked to obesity and metabolic diseases (Erion et al., 2014; Hsu and Kanoski, 2014; Kanoski et al., 2015; Wang et al., 2015).

In old animals with advanced metabolic diseases, such as our ApoE$^{-/-}$ mice, the central beneficial effects of exercise appear to be impeded by the combined deleterious effects of the HC diet and age. This would lead to a vicious circle of central inflammation, promoted by overfeeding of

atherogenic diet and eventually a constant influx of LPS, in turn worsening the central endocrine dysregulation of food intake.

It is now acknowledged that unhealthy diets can cause dysbiosis leading to gut inflammation (Chistiakov et al., 2015) and numerous studies have shown that chronically inflamed gut may upregulate barrier breakdown, LPS permeability, generation of proinflammatory cytokines, systemic inflammation and neuroinflammation (Denes et al., 2010; Macrez et al., 2011). Indeed, a wide range of inflammation-related proteins (LPS, CRP, and inflammatory cytokines) were found to be increased in Alzheimer's disease (AD) patients, promoting systemic and neuroinflammation (Zhang et al., 2009). Numerous recent studies have pointed out the link between peripheral inflammation and neuroinflammation and/or cognitive defects such as in AD, Parkinson's disease (PD), and Crohn's disease (CD) (Denes et al., 2010; Herrera et al., 2015; van Langenberg, 2016). Atherosclerosis has a significant impact on AD progression, and although the mechanisms are still unclear (Takeda et al., 2008) we can hypothesize that circulating proinflammatory cytokines are part of the link between these two pathologies. Interestingly, the hippocampus is the most cited brain region impacted by systemic inflammation (Hall et al., 2013; Rodríguez et al., 2013).

These studies highlighted the different routes by which systemic inflammation can access the brain, such as the vagus nerve, leaked BBB or by circumventricular organs (CVOs) (Daulatzai, 2014; Roth et al., 2004). CVOs border the hippocampus and the cerebellum possibly explaining why these regions are the first affected by the neuroinflammation induced by systemic inflammation. In our $ApoE^{-/-}$ mice, we can hypothesize that BBB leakage observed by MRI might be the result of the release of LPS from HC diet absorption. Interestingly, the regions affected in our study are the hippocampus and the periventricular areas (CVOs) giving evidence that the gut-brain axis plays a role in the lesions observed.

B. <u>What imaging modality or combination of imaging modalities is the most relevant for CV risk assessment?</u>

In our non-human primate study, we used multimodal imaging to determine the cardiovascular risk of each animal (**article n°3**). We demonstrated that ultrasound follow-up of multiple vascular territories was useful and allowed the detection of plaque progression and the more accurate stratification of animals according to the number of territories impacted and the progression or regression of the plaque during the follow-up. This single observation, combined with LDL-C and

hsCRP level variations during the same period was sufficient to distinguish the three animals exhibiting evident downstream events at the time of sacrifice. As said above, ultrasound imaging was performed on multiple arteries in order to evaluate the most relevant localizations for further examinations. Then, MRI and molecular imaging was focused on the carotids as the most frequently lesioned territory in our animals and also the most studied in human clinical studies. MRI provided morphologic information of vessel wall volume and plaque area while PET/CT imaging with [^{18}F]-FDG and [^{11}C]-PK11195 was used to detect high metabolic activity and inflammation in the plaque, respectively. These two features are important to take into account because they indicate plaque activity and enable the differentiation of active and vulnerable plaques from silent plaques, which are less dangerous, even if they can be more stenotic than others.

Ultrasound and especially carotid intima-media thickness (cIMT) and X-ray tomography coronary calcium scores (CCS) have been considered to be standard measurements for CV risk assessment in asymptomatic patient for decades (Beere et al., 1992; Naqvi and Lee, 2014; Spence, 2006) and are even part of the AHA/ACC guidelines (Greenland et al., 2010). However, their usefulness is still debated as some studies showed that it might not be accurate (Finn et al., 2010; Meershoek et al., 2016). Indeed, cIMT and CCS are relevant measurements for early stage plaques, but showed no longer correlation with advanced plaques, showing that cIMT and CCS do not provide any supplemental benefit to prediction algorithms such as the Framingham Risk Score (Polak et al., 2011). Interestingly, if cIMT was not correlated to the plaque severity as observed post-mortem in the study of the Johnsen's team, it was demonstrated that the location where the measure is performed is of major importance. Indeed, cIMT of the common carotid showed no association with cardiovascular event (CVE) occurrence while cIMT of the carotid bulb showed a positive association (Johnsen et al., 2007).

It is worth noting that the fact that plaques extend faster in length along the carotid than in thickness (Barnett et al., 1997) might explain the non-accuracy of cIMT measurements. Moreover, it is now known that the real danger in the plaque is its constitution (mainly lipidic, fibrotic, calcified, vascularized, etc) more than its thickness (Naghavi, 2003). Thus ultrasound using microbubbles also is an interesting modality especially for treatment follow-up as some agents are very sensitive and able to detect changes in endothelial phenotype as increase of adhesion molecules in endothelial cell surface (Khanicheh et al., 2013).

More importantly, we found that [^{18}F]-FDG and [^{11}C]-PK11195 uptake were positively correlated in high cholesterol animals but negatively in the standard diet animals, suggesting that atherosclerosis pathology induced the uptake of these two markers in similar ways (**article n°3**). On the contrary, standard diet animals showed high uptake of [^{18}F]-FDG and low uptake of [^{11}C]-PK11195 or

the inverse thus demonstrating the relevance of the dual tracer imaging for cardiovascular risk assessment.

As interesting as our imaging finding in this NHP study are, one important limitation is the fact that PET/CT and MRI imaging were only performed once, respectively at T+18 and T+24 months, thus providing incomplete information regarding lesion evolutivity. Indeed gene analysis is representative of the physiopathologic state of the animals at the end time point. Thus, [^{18}F]-FDG and [^{11}C]-PK11195 uptake at T+24 months would have enabled a direct comparison to gene expression and MRI findings. In the same way, a combined PET/ MRI examination would have been useful to analyze the progression of the inflammation in the studied vessels and to better situate the onset of the lacunar stroke observed in HC#9.

C. CV risk stratification: are M2 markers signals of healing or alarm?

In our **article n°3**, we analyzed M2 markers expression in the carotid and aortic arch in non-human primates under atherogenic diet or standard diet. We showed that M1 markers were more highly expressed in animals presenting large and severe plaques as well as downstream events (i.e. myocardial fibrosis or stroke), confirming the literature. Strikingly, we demonstrated that M2 markers (IL-1ra, CCR2, IL-10, Dectin-1 (CLec7a), IRF4 and CD163) were also highly expressed in these same animals. Indeed, in our study, mRNA expression analysis in the carotids grouped together animals presenting the most expressed M1 and M2 markers and these three NHPs are the ones that exhibited myocardial fibrosis and lacunar stroke at the autopsy, confirming the classification based on mRNA expression. These results are challenging the M1/M2 dichotomy paradigm that is largely accepted with M1 being predominant in vulnerable plaque and/or in symptomatic patients and M2 mostly in asymptomatic patients/stable plaque (de Gaetano et al., 2016; Mosser and Edwards, 2008). Thus it confirms the observations of several studies exhibiting that human macrophages subtype are extremely plastic and dynamic and are largely more complex than the M1/M2 dichotomy (Chinetti-Gbaguidi et al., 2015; van Dijk et al., 2016).

In their study, van Dijk et al, demonstrated in an abdominal aorta tissue bank that multiplex staining for M1/M2 macrophages failed to show a significant predominance of M1 macrophages in the foam cell-rich areas in humans' abdominal aorta plaques. Moreover, in this study, ~20 to 30% of macrophages from plaque at early to advanced stages are double positive for both M1 and M2 markers, challenging even more the paradigm of a clear M1 to M2 dichotomy. This is consistent with our results in **article n°3** showing that animals with high M2 markers expression also have high expression of M1 markers. Furthermore, in our NHP study, animals for which M1 and M2 macrophage marker were most

expressed were those presenting downstream events, suggesting that in late advanced stages of atherosclerosis or rupture-prone plaque, M2 markers are more likely a signal of danger than a sign of healing in progress as we used to see them.

Although macrophages' plasticity has been well documented *in vitro* as *in vivo* strongly suggesting a functional adaptivity of these cells (Shnyra et al., 1998; Stout et al., 2005), this might not be systematic and may depend not only of the microenvironment but also of the state of differentiation of the macrophage (Bouhlel et al., 2007; Gleissner et al., 2010). Nonetheless, if M2 macrophages may exhibit mostly anti-atherogenic functions, they still have some properties that may promote plaque progression such as increased sensitivity to oxLDL, which may lead to enlargement of the lipidic core. Furthermore, this plasticity can even lead to undesired functions and switch healing-prone macrophages to deleterious-prone ones without completely changing their phenotype.

D. Is combination of inflammatory with anti-inflammatory biomarker the answer for accurate individual stratification in atherosclerosis-induced CV risk?

As stated above, in our non-human primate study (**article n°3**), we observed an interesting correlation in the carotids between the mRNA expression of M1 (mainly TLR4, MCP-1, IL-6, IL-1β) and M2 (CD163, IRF4, IL-1ra, CLec7a) markers, with an increased expression in the most affected animals. It is worth noting that these markers were also positively correlated to metabolic (HK1), macrophage activation (TSPO) (both of them being related to the PET/CT imaging tracers used in this study) and lymphocyte (CD3ε) markers. Indeed, metabolic and inflammatory activity of cells contained in, or in the neighborhood of the plaque are essential features to take into account, not to mention lymphocyte infiltration into the plaque, which is a known marker of vulnerable/rupture-prone plaque in humans (van Dijk et al., 2015; Sakakura et al., 2013).

Based on these markers, gene analysis enabled to divide animals in three groups, the ones presenting the higher expression of these markers being the same as those exhibiting severe plaques, myocardial fibrosis, and for one of them even a lacunar stroke, suggesting that this combination of tissular markers is relevant for an individual stratification of cardiovascular risk. Furthermore, these three animals (called "at-risk") highlighted by the genomic analysis are those presenting an increase of their ultrasound score, i.e. presenting an aggravation and/or a development of their plaques during the 6 months between the two ultrasound sessions confirming the recent highlightening of the high value of combining molecular tools (transcriptomics, proteomics and lipidomics) with imaging techniques to improve the individual CV risk stratification (Calcagno et al., 2016).

Interestingly, in the aortic arch, the classification of the animals is slightly different, but *in fine*, all animals grouped in the "medium" and "high-risk" groups showed up. The NHP HC#9 went from the high-risk group in the carotids to medium risk group in the aortic arch, confirming that not all plaques represent the same CV risk in one subject.

In at-risk animals, a high TSPO expression was observed in the carotids, which seems to be correlated with TLR4 and with macrophages (CD68). In the brain, it appears to be different, it is not correlated with macrophages (CD68 is negatively correlated to IL1β, and positively to M2 markers) but still with TLR4 and CD3ε. However, in this study, only the frontal part of the brain was used for gene expression analysis while on images we can see that the area presenting a lacunar stroke is close to the ventricles and more in a ventrotemporal localization, which might be part of the differences in gene expression between the carotid and the brain (**article n°3**).

Nonetheless, we had to notice that in our NHPs, as well as in our ApoE$^{-/-}$ mice, the brain regions exhibiting a high [^{11}C]-PK11195 uptake are periventricular areas, related to limbic system (hippocampus, amygdala, etc) and circumventricular organs (**articles n°1, 2 and 3**). Indeed, in our ApoE$^{-/-}$ mice studies, USPIOs MR imaging showed the same most affected regions, confirming the deleterious impact of high cholesterol diet on cerebrovascular units and circumventricular organs. Mice are a well-used animal model for atherosclerosis research thanks to their technical advantages (small size, easy breeding) and mostly because of the abundance of genetic modifications available enabling mechanistic studies and so importance advances in comprehension of atherosclerosis physiopathology (Badaut et al., 2012; Millon et al., 2014). However, translation from mice to humans is really difficult as showed by an abundant literature displaying large amounts of evidences of negative results obtained in clinical studies on neuroprotection despite a large body of evidence in mouse models of stroke (Cho et al., 2013; Kohler et al., 2013; Nighoghossian et al., 2015). On the other hand, although non-human primates' studies are performed on a small animal number and do not enable such genetic modifications as mice, they present such physiological and even pathophysiological similarities with humans. Moreover, their large size allows the use of the same imaging methods that they can be considered as an accurate and relevant animal model for phase II and III trial in such complex context as atherosclerosis and its outcomes.

CONCLUSION AND PERSPECTIVES

We showed in our **article n°1** that low-intensity exercise effectively protects the brain from high fat diet-induced cerebrovascular lesions and for the first time in our second study on ApoE-/- mice (**article n°2**) that the non-restricted consumption of an atherogenic diet in old ApoE$^{-/-}$ mice blunts these central beneficial effects, leading to inflammation and BBB leakage in areas that are both involved in food intake regulation and immune cell recruitment. This work suggest that exercise-induced modulation depends on the amount of food intake. Indeed, when food intake was regulated, exercise showed a positive modulation of atherosclerosis (decrease of inflammation, oxidative stress, and plaque progression), while exercise induced deleterious effects when associated with unregulated food intake. These results emphasizes the need for further gut-brain axis studies, including diet and exercise combined with neuroimaging biomarkers of inflammation and BBB permeability in order to evaluate the neuro-immune interactions and elucidate the central effect of the interventions.

The first thing to note on our **article n°3** is that non-human primates under atherogenic diet is a relevant model of vulnerable plaque. Our results suggest that for an accurate stratification of the individual cardiovascular risk, it would be useful to perform an ultrasound follow-up of multiple arterial territories to observe global plaque progression, and of systemic inflammation marker such as hsCRP combined with imaging evaluation of M1 and M2 markers expression in the plaque. To note that in non-human primates as well as in humans, increased expression of both M1 and M2 markers in the plaque of at-risk subjects, challenges the M1/M2 paradigm. Thus, further studies on the macrophage phenotype in vulnerable atherosclerotic plaque are needed.

To summarize, atherosclerosis risk factors induce a local vascular inflammation, promoting the development of the plaque, which results in an increase of the local inflammation. This spreads into the systemic circulation leading to a systemic inflammation, which induces chronic cerebrovascular inflammation in the periventricular areas and favors the occurrence of ischemic accidents such as TIA and stroke that contribute to the systemic inflammation leading to plaque progression. This vicious circle between local, systemic and cerebrovascular inflammation and their component is still unexplained. Imaging modalities enable the visualization and the study of both systemic circulation and brain and specific imaging markers can be used to characterize the plaques (e.g. morphology, activity, and metabolism) (**Figure 25**). Further studies are needed to reveal the role of each actors of the vicious circle.

To go further, analysis of peripheral blood mononuclear cells (PBMCs) is in progress in our NHP model, focused on their function and metabolic pathways involved in it (glycolytic, oxidative,

mitochondrial markers) and their translational potential for CV risk stratification in atherosclerosis animals and in NHP acute stroke model.

Human's analysis of differences in M1/M2 and metabolic markers expression in symptomatic and asymptomatic human carotids is ongoing, with the objective to make the link with the impact of oxidative stress and sedentary (and even ultra-sedentary) behavior on these markers.

In parallel, a NHP study between a phase II and phase III trial of neuroprotective strategies targeting mitochondria with PET/MRI and PBMC longitudinal evaluation is in progress, as well as clinical studies using PET/MRI in stroke. A better selection of inclusion and exclusion criteria can be performed using translational imaging biomarkers (PET/MRI) and translational results from NHPs models (TSPO expression via PET imaging and BBB functional PET/MR in the cerebro-vasculature).

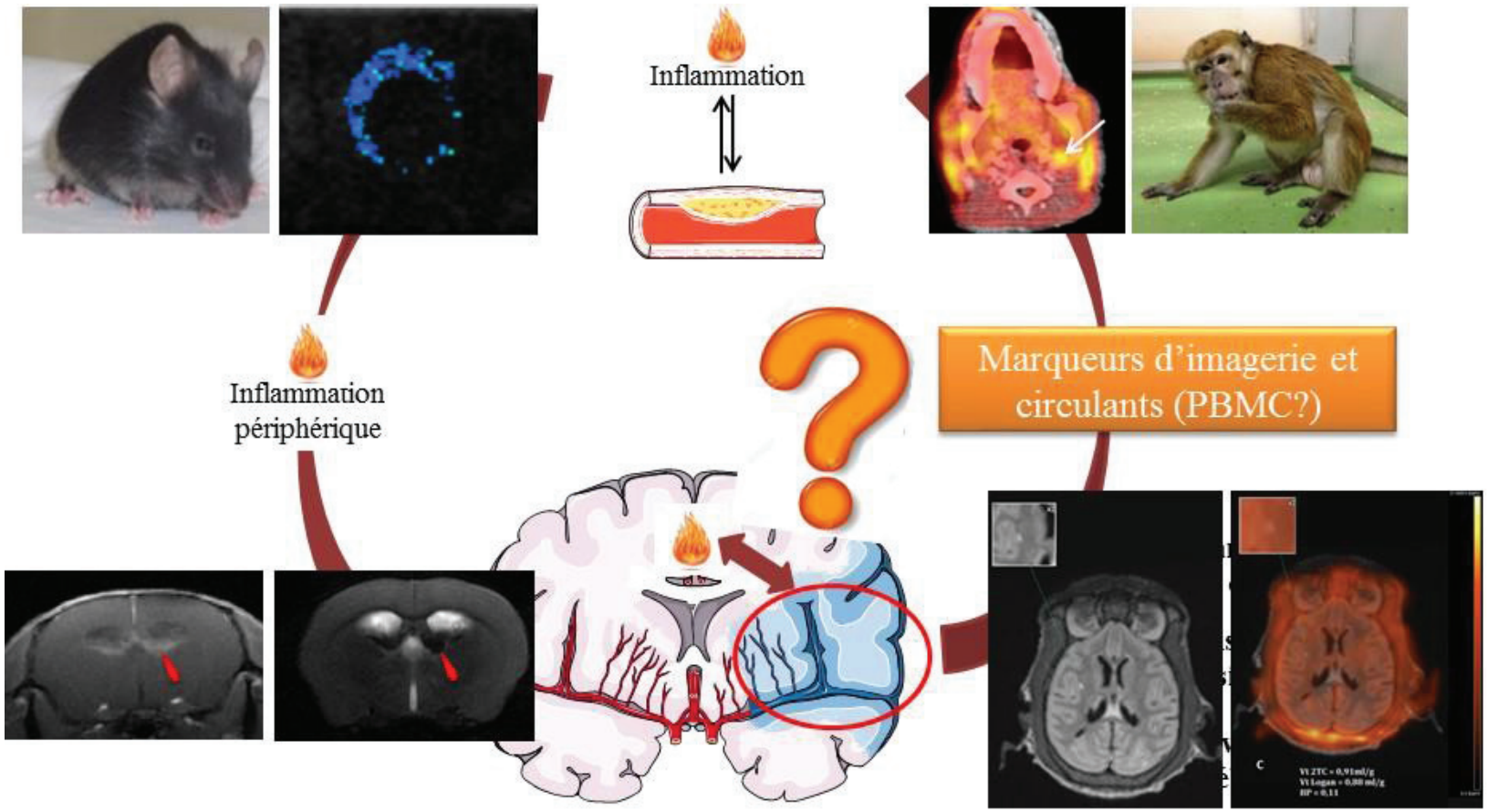

Figure 25: General conclusion and perspectives. Local vascular inflammation induced by dyslipidemia and endothelial dysfunction promotes plaque progression, which results in an increase of the local inflammation. This leads to a systemic inflammation inducing chronic neuroinflammation, mainly localized in the ventricle neighborhood, and favors the occurrence of transient ischemic accident and stroke, which also contribute to the systemic inflammation leading to plaque progression. This suggests a vicious circle between local vascular inflammation and neuroinflammation. Imaging modalities enable the visualization and the study of both territories, and specific tracers/contrast agents can be used to characterize the plaques. Now, there is a need of development of new specific imaging and circulating markers (why not peripheral blood mononuclear cells, PBMC?) to study this implication of each actor of this vicious circle.

REFERENCES

Aaron, K.J., and Sanders, P.W. (2013). Role of dietary salt and potassium intake in cardiovascular health and disease: a review of the evidence. Mayo Clin. Proc. *88*, 987–995.

Abbate, A., Kontos, M.C., Abouzaki, N.A., Melchior, R.D., Thomas, C., Van Tassell, B.W., Oddi, C., Carbone, S., Trankle, C.R., Roberts, C.S., et al. (2015). Comparative safety of interleukin-1 blockade with anakinra in patients with ST-segment elevation acute myocardial infarction (from the VCU-ART and VCU-ART2 pilot studies). Am. J. Cardiol. *115*, 288–292.

Acalovschi, D., Wiest, T., Hartmann, M., Farahmi, M., Mansmann, U., Auffarth, G.U., Grau, A.J., Green, F.R., Grond-Ginsbach, C., and Schwaninger, M. (2003). Multiple levels of regulation of the interleukin-6 system in stroke. Stroke J. Cereb. Circ. *34*, 1864–1869.

Acharya, U.R., Sree, S.V., Krishnan, M.M.R., Molinari, F., Saba, L., Ho, S.Y.S., Ahuja, A.T., Ho, S.C., Nicolaides, A., and Suri, J.S. (2012). Atherosclerotic risk stratification strategy for carotid arteries using texture-based features. Ultrasound Med. Biol. *38*, 899–915.

Agatston, A.S., Janowitz, W.R., Hildner, F.J., Zusmer, N.R., Viamonte, M., and Detrano, R. (1990). Quantification of coronary artery calcium using ultrafast computed tomography. J. Am. Coll. Cardiol. *15*, 827–832.

Ajami, B., Bennett, J.L., Krieger, C., Tetzlaff, W., and Rossi, F.M.V. (2007). Local self-renewal can sustain CNS microglia maintenance and function throughout adult life. Nat. Neurosci. *10*, 1538–1543.

Al Rifai, M., Silverman, M.G., Nasir, K., Budoff, M.J., Blankstein, R., Szklo, M., Katz, R., Blumenthal, R.S., and Blaha, M.J. (2015). The association of nonalcoholic fatty liver disease, obesity, and metabolic syndrome, with systemic inflammation and subclinical atherosclerosis: the Multi-Ethnic Study of Atherosclerosis (MESA). Atherosclerosis *239*, 629–633.

Alberts, A.W. (1988). Discovery, biochemistry and biology of lovastatin. Am. J. Cardiol. *62*, 10J–15J.

Alexander, R.W. (2003). The Jeremiah Metzger Lecture. Pathogenesis of atherosclerosis: redox as a unifying mechanism. Trans. Am. Clin. Climatol. Assoc. *114*, 273–304.

Alexander, M.R., Moehle, C.W., Johnson, J.L., Yang, Z., Lee, J.K., Jackson, C.L., and Owens, G.K. (2012). Genetic inactivation of IL-1 signaling enhances atherosclerotic plaque instability and reduces outward vessel remodeling in advanced atherosclerosis in mice. J. Clin. Invest. *122*, 70–79.

Aliev, G., and Burnstock, G. (1998). Watanabe rabbits with heritable hypercholesterolaemia: a model of atherosclerosis. Histol. Histopathol. *13*, 797–817.

Amarenco, P., and Labreuche, J. (2009). Lipid management in the prevention of stroke: review and updated meta-analysis of statins for stroke prevention. Lancet Neurol. *8*, 453–463.

Amarenco, P., Labreuche, J., Elbaz, A., Touboul, P.-J., Driss, F., Jaillard, A., Bruckert, E., and GENIC Investigators (2006). Blood lipids in brain infarction subtypes. Cerebrovasc. Dis. Basel Switz. *22*, 101–108.

American Heart Association The American Heart Association's Diet and Lifestyle Recommendations.

Anand, S.S., and Yusuf, S. (2010). C-reactive protein is a bystander of cardiovascular disease. Eur. Heart J. *31*, 2092–2096.

Anatoliotakis, N., Deftereos, S., Bouras, G., Giannopoulos, G., Tsounis, D., Angelidis, C., Kaoukis, A., and Stefanadis, C. (2013). Myeloperoxidase: expressing inflammation and oxidative stress in cardiovascular disease. Curr. Top. Med. Chem. *13*, 115–138.

Anber, V., Griffin, B.A., McConnell, M., Packard, C.J., and Shepherd, J. (1996). Influence of plasma lipid and LDL-subfraction profile on the interaction between low density lipoprotein with human arterial wall proteoglycans. Atherosclerosis *124*, 261–271.

Anguera, I., Miranda-Guardiola, F., Bosch, X., Filella, X., Sitges, M., Marín, J.L., Betriu, A., and Sanz, G. (2002). Elevation of serum levels of the anti-inflammatory cytokine interleukin-10 and decreased risk of coronary events in patients with unstable angina. Am. Heart J. *144*, 811–817.

Anholt, R.R., Pedersen, P.L., De Souza, E.B., and Snyder, S.H. (1986). The peripheral-type benzodiazepine receptor. Localization to the mitochondrial outer membrane. J. Biol. Chem. *261*, 576–583.

ANICHKOV, Nikolai Nikolaevich, and CHALATOV, Semen Sergeevich (1913). Ueber experimentelle Cholesterinsteatose und ihre Bedeutung für die Entstehung einiger pathologischer Prozesse. Zbl Allg Path Path Anat *24*, 1–9.

Appleton, S.L., Seaborn, C.J., Visvanathan, R., Hill, C.L., Gill, T.K., Taylor, A.W., Adams, R.J., and North West Adelaide Health Study Team (2013). Diabetes and cardiovascular disease outcomes in the metabolically healthy obese phenotype: a cohort study. Diabetes Care *36*, 2388–2394.

Arauz, A., Murillo, L., Cantú, C., Barinagarrementeria, F., and Higuera, J. (2003). Prospective study of single and multiple lacunar infarcts using magnetic resonance imaging: risk factors, recurrence, and outcome in 175 consecutive cases. Stroke J. Cereb. Circ. *34*, 2453–2458.

Armani, C., Catalani, E., Balbarini, A., Bagnoli, P., and Cervia, D. (2007). Expression, pharmacology, and functional role of somatostatin receptor subtypes 1 and 2 in human macrophages. J. Leukoc. Biol. *81*, 845–855.

Arsenault, B.J., Lemieux, I., Després, J.-P., Wareham, N.J., Luben, R., Kastelein, J.J.P., Khaw, K.-T., and Boekholdt, S.M. (2007). Cholesterol levels in small LDL particles predict the risk of coronary heart disease in the EPIC-Norfolk prospective population study. Eur. Heart J. *28*, 2770–2777.

Assmann, G., and Schulte, H. (1992). The importance of triglycerides: results from the Prospective Cardiovascular Münster (PROCAM) Study. Eur. J. Epidemiol. *8 Suppl 1*, 99–103.

Audebert, H.J., Rott, M.M., Eck, T., and Haberl, R.L. (2004). Systemic inflammatory response depends on initial stroke severity but is attenuated by successful thrombolysis. Stroke J. Cereb. Circ. *35*, 2128–2133.

Aung, H.H., Lame, M.W., Gohil, K., An, C.-I., Wilson, D.W., and Rutledge, J.C. (2013). Induction of ATF3 gene network by triglyceride-rich lipoprotein lipolysis products increases vascular apoptosis and inflammation. Arterioscler. Thromb. Vasc. Biol. *33*, 2088–2096.

Austin, M.A., King, M.C., Vranizan, K.M., and Krauss, R.M. (1990). Atherogenic lipoprotein phenotype. A proposed genetic marker for coronary heart disease risk. Circulation *82*, 495–506.

Azarashvili, T., Baburina, Y., Grachev, D., Krestinina, O., Papadopoulos, V., Lemasters, J.J., Odinokova, I., and Reiser, G. (2014). Carbenoxolone induces permeability transition pore opening in rat mitochondria via the translocator protein TSPO and connexin43. Arch. Biochem. Biophys. *558*, 87–94.

Badaut, J., Copin, J.-C., Fukuda, A.M., Gasche, Y., Schaller, K., Da Silva, R.F., and others (2012). Increase of arginase activity in old apolipoprotein-E deficient mice under Western diet associated with changes in neurovascular unit. J Neuroinflammation *9*, 132.

Baigent, C., Keech, A., Kearney, P.M., Blackwell, L., Buck, G., Pollicino, C., Kirby, A., Sourjina, T., Peto, R., Collins, R., et al. (2005). Efficacy and safety of cholesterol-lowering treatment: prospective meta-analysis of data from 90,056 participants in 14 randomised trials of statins. Lancet Lond. Engl. *366*, 1267–1278.

Baigent, C., Landray, M.J., Reith, C., Emberson, J., Wheeler, D.C., Tomson, C., Wanner, C., Krane, V., Cass, A., Craig, J., et al. (2011). The effects of lowering LDL cholesterol with simvastatin plus ezetimibe in patients with chronic kidney disease (Study of Heart and Renal Protection): a randomised placebo-controlled trial. Lancet Lond. Engl. *377*, 2181–2192.

Baldassarre, D., Hamsten, A., Veglia, F., de Faire, U., Humphries, S.E., Smit, A.J., Giral, P., Kurl, S., Rauramaa, R., Mannarino, E., et al. (2012). Measurements of carotid intima-media thickness and of interadventitia common carotid diameter improve prediction of cardiovascular events: results of the IMPROVE (Carotid Intima Media Thickness [IMT] and IMT-Progression as Predictors of Vascular Events in a High Risk European Population) study. J. Am. Coll. Cardiol. *60*, 1489–1499.

Banati, R.B., Newcombe, J., Gunn, R.N., Cagnin, A., Turkheimer, F., Heppner, F., Price, G., Wegner, F., Giovannoni, G., Miller, D.H., et al. (2000). The peripheral benzodiazepine binding site in the brain in multiple sclerosis: quantitative in vivo imaging of microglia as a measure of disease activity. Brain J. Neurol. *123 (Pt 11)*, 2321–2337.

Banati, R.B., Middleton, R.J., Chan, R., Hatty, C.R., Kam, W.W.-Y., Quin, C., Graeber, M.B., Parmar, A., Zahra, D., Callaghan, P., et al. (2014). Positron emission tomography and functional characterization of a complete PBR/TSPO knockout. Nat. Commun. *5*, 5452.

Barcat, D., Amadio, A., Palos-Pinto, A., Daret, D., Benlian, P., Darmon, M., and Bérard, A.M. (2006). Combined hyperlipidemia/hyperalphalipoproteinemia associated with premature spontaneous atherosclerosis in mice lacking hepatic lipase and low density lipoprotein receptor. Atherosclerosis *188*, 347–355.

Barnett, P.A., Spence, J.D., Manuck, S.B., and Jennings, J.R. (1997). Psychological stress and the progression of carotid artery disease. J. Hypertens. *15*, 49–55.

Batarseh, A., and Papadopoulos, V. (2010). Regulation of translocator protein 18 kDa (TSPO) expression in health and disease states. Mol. Cell. Endocrinol. *327*, 1–12.

Batarseh, A., Li, J., and Papadopoulos, V. (2010). Protein kinase C epsilon regulation of translocator protein (18 kDa) Tspo gene expression is mediated through a MAPK pathway targeting STAT3 and c-Jun transcription factors. Biochemistry (Mosc.) *49*, 4766–4778.

Bauer, S., Kerr, B.J., and Patterson, P.H. (2007). The neuropoietic cytokine family in development, plasticity, disease and injury. Nat. Rev. Neurosci. *8*, 221–232.

Beamer, N.B., Coull, B.M., Clark, W.M., Hazel, J.S., and Silberger, J.R. (1995). Interleukin-6 and interleukin-1 receptor antagonist in acute stroke. Ann. Neurol. *37*, 800–805.

Beaty, T.H., Prenger, V.L., Virgil, D.G., Lewis, B., Kwiterovich, P.O., and Bachorik, P.S. (1992). A genetic model for control of hypertriglyceridemia and apolipoprotein B levels in the Johns Hopkins colony of St. Thomas Hospital rabbits. Genetics *132*, 1095–1104.

Beere, P.A., Glagov, S., and Zarins, C.K. (1992). Experimental atherosclerosis at the carotid bifurcation of the cynomolgus monkey. Localization, compensatory enlargement, and the sparing effect of lowered heart rate. Arterioscler. Thromb. J. Vasc. Biol. Am. Heart Assoc. *12*, 1245–1253.

Berg, A.H., and Scherer, P.E. (2005). Adipose tissue, inflammation, and cardiovascular disease. Circ. Res. *96*, 939–949.

Berglund, L., Lefevre, M., Ginsberg, H.N., Kris-Etherton, P.M., Elmer, P.J., Stewart, P.W., Ershow, A., Pearson, T.A., Dennis, B.H., Roheim, P.S., et al. (2007). Comparison of monounsaturated fat with carbohydrates as a replacement for saturated fat in subjects with a high metabolic risk profile: studies in the fasting and postprandial states. Am. J. Clin. Nutr. *86*, 1611–1620.

Bergouignan, A., Antoun, E., Momken, I., Schoeller, D.A., Gauquelin-Koch, G., Simon, C., and Blanc, S. (2013). Effect of contrasted levels of habitual physical activity on metabolic flexibility. J. Appl. Physiol. Bethesda Md 1985 *114*, 371–379.

Biasillo, G., Leo, M., Della Bona, R., and Biasucci, L.M. (2010). Inflammatory biomarkers and coronary heart disease: from bench to bedside and back. Intern. Emerg. Med. *5*, 225–233.

Biasucci, L.M., Liuzzo, G., Fantuzzi, G., Caligiuri, G., Rebuzzi, A.G., Ginnetti, F., Dinarello, C.A., and Maseri, A. (1999). Increasing levels of interleukin (IL)-1Ra and IL-6 during the first 2 days of hospitalization in unstable angina are associated with increased risk of in-hospital coronary events. Circulation *99*, 2079–2084.

Biomarkers Definitions Working Group. (2001). Biomarkers and surrogate endpoints: preferred definitions and conceptual framework. Clin. Pharmacol. Ther. *69*, 89–95.

Bisoendial, R.J., Boekholdt, S.M., Vergeer, M., Stroes, E.S.G., and Kastelein, J.J.P. (2010). C-reactive protein is a mediator of cardiovascular disease. Eur. Heart J. *31*, 2087–2091.

Björkhem, I., and Meaney, S. (2004). Brain cholesterol: long secret life behind a barrier. Arterioscler. Thromb. Vasc. Biol. *24*, 806–815.

Björkhem, I., Heverin, M., Leoni, V., Meaney, S., and Diczfalusy, U. (2006). Oxysterols and Alzheimer's disease. Acta Neurol. Scand. Suppl. *185*, 43–49.

Björnheden, T., Babyi, A., Bondjers, G., and Wiklund, O. (1996). Accumulation of lipoprotein fractions and subfractions in the arterial wall, determined in an in vitro perfusion system. Atherosclerosis *123*, 43–56.

Block, R.C., Dorsey, E.R., Beck, C.A., Brenna, J.T., and Shoulson, I. (2010). Altered cholesterol and fatty acid metabolism in Huntington disease. J. Clin. Lipidol. *4*, 17–23.

Bloomer, R.J., and Fisher-Wellman, K.H. (2008). Blood oxidative stress biomarkers: influence of sex, exercise training status, and dietary intake. Gend. Med. *5*, 218–228.

Boekholdt, S.M., Arsenault, B.J., Mora, S., Pedersen, T.R., LaRosa, J.C., Nestel, P.J., Simes, R.J., Durrington, P., Hitman, G.A., Welch, K.M.A., et al. (2012). Association of LDL cholesterol, non-HDL cholesterol, and apolipoprotein B levels with risk of cardiovascular events among patients treated with statins: a meta-analysis. JAMA *307*, 1302–1309.

Böhm, A., Weigert, C., Staiger, H., and Häring, H.-U. (2016). Exercise and diabetes: relevance and causes for response variability. Endocrine *51*, 390–401.

Bohula, E.A., Giugliano, R.P., Cannon, C.P., Zhou, J., Murphy, S.A., White, J.A., Tershakovec, A.M., Blazing, M.A., and Braunwald, E. (2015). Achievement of dual low-density lipoprotein cholesterol and high-sensitivity C-reactive protein targets more frequent with the addition of ezetimibe to simvastatin and associated with better outcomes in IMPROVE-IT. Circulation *132*, 1224–1233.

Bonetti, P.O., Lerman, L.O., and Lerman, A. (2003). Endothelial dysfunction: a marker of atherosclerotic risk. Arterioscler. Thromb. Vasc. Biol. *23*, 168–175.

Bots, M.L., Visseren, F.L., Evans, G.W., Riley, W.A., Revkin, J.H., Tegeler, C.H., Shear, C.L., Duggan, W.T., Vicari, R.M., Grobbee, D.E., et al. (2007). Torcetrapib and carotid intima-media thickness in mixed dyslipidaemia (RADIANCE 2 study): a randomised, double-blind trial. Lancet Lond. Engl. *370*, 153–160.

Bouhlel, M.A., Derudas, B., Rigamonti, E., Dièvart, R., Brozek, J., Haulon, S., Zawadzki, C., Jude, B., Torpier, G., Marx, N., et al. (2007). PPARgamma activation primes human monocytes into alternative M2 macrophages with anti-inflammatory properties. Cell Metab. *6*, 137–143.

Bourdier, G., Flore, P., Sanchez, H., Pepin, J.-L., Belaidi, E., and Arnaud, C. (2016). High-intensity training reduces intermittent hypoxia-induced ER stress and myocardial infarct size. Am. J. Physiol. Heart Circ. Physiol. *310*, H279-289.

Boyle, J.J., Weissberg, P.L., and Bennett, M.R. (2003). Tumor necrosis factor-alpha promotes macrophage-induced vascular smooth muscle cell apoptosis by direct and autocrine mechanisms. Arterioscler. Thromb. Vasc. Biol. *23*, 1553–1558.

Boyle, J.J., Harrington, H.A., Piper, E., Elderfield, K., Stark, J., Landis, R.C., and Haskard, D.O. (2009). Coronary intraplaque hemorrhage evokes a novel atheroprotective macrophage phenotype. Am. J. Pathol. *174*, 1097–1108.

Brinjikji, W., Huston, J., Rabinstein, A.A., Kim, G.-M., Lerman, A., and Lanzino, G. (2016). Contemporary carotid imaging: from degree of stenosis to plaque vulnerability. J. Neurosurg. *124*, 27–42.

Brochet, B., Deloire, M.S.A., Touil, T., Anne, O., Caillé, J.M., Dousset, V., and Petry, K.G. (2006). Early macrophage MRI of inflammatory lesions predicts lesion severity and disease development in relapsing EAE. NeuroImage *32*, 266–274.

Broisat, A., Hernot, S., Toczek, J., De Vos, J., Riou, L.M., Martin, S., Ahmadi, M., Thielens, N., Wernery, U., Caveliers, V., et al. (2012). Nanobodies targeting mouse/human VCAM1 for the nuclear imaging of atherosclerotic lesions. Circ. Res. *110*, 927–937.

Brown, M.S., and Goldstein, J.L. (1979). Receptor-mediated endocytosis: insights from the lipoprotein receptor system. Proc. Natl. Acad. Sci. U. S. A. *76*, 3330–3337.

Brown, M.S., and Goldstein, J.L. (1983). Lipoprotein metabolism in the macrophage: implications for cholesterol deposition in atherosclerosis. Annu. Rev. Biochem. *52*, 223–261.

Bullock, B.C., Lehner, N.D., Clarkson, T.B., Feldner, M.A., Wagner, W.D., and Lofland, H.B. (1975). Comparative primate atherosclerosis. I. Tissue cholesterol concentration and pathologic anatomy. Exp. Mol. Pathol. *22*, 151–175.

Calcagno, C., Ramachandran, S., Millon, A., Robson, P.M., Mani, V., and Fayad, Z. (2013). Gadolinium-Based Contrast Agents for Vessel Wall Magnetic Resonance Imaging (MRI) of Atherosclerosis. Curr. Cardiovasc. Imaging Rep. *6*, 11–24.

Calcagno, C., Mulder, W.J.M., Nahrendorf, M., and Fayad, Z.A. (2016). Systems Biology and Noninvasive Imaging of Atherosclerosis. Arterioscler. Thromb. Vasc. Biol. *36*, e1-8.

Campos, H., Arnold, K.S., Balestra, M.E., Innerarity, T.L., and Krauss, R.M. (1996). Differences in receptor binding of LDL subfractions. Arterioscler. Thromb. Vasc. Biol. *16*, 794–801.

Cannon, C.P., Braunwald, E., McCabe, C.H., Rader, D.J., Rouleau, J.L., Belder, R., Joyal, S.V., Hill, K.A., Pfeffer, M.A., Skene, A.M., et al. (2004). Intensive versus moderate lipid lowering with statins after acute coronary syndromes. N. Engl. J. Med. *350*, 1495–1504.

Cannon, C.P., Blazing, M.A., Giugliano, R.P., McCagg, A., White, J.A., Theroux, P., Darius, H., Lewis, B.S., Ophuis, T.O., Jukema, J.W., et al. (2015). Ezetimibe Added to Statin Therapy after Acute Coronary Syndromes. N. Engl. J. Med. *372*, 2387–2397.

Canton, G., Chiu, B., Chen, H., Chen, Y., Hatsukami, T.S., Kerwin, W.S., and Yuan, C. (2013). A framework for the co-registration of hemodynamic forces and atherosclerotic plaque components. Physiol. Meas. *34*, 977–990.

Cardilo-Reis, L., Gruber, S., Schreier, S.M., Drechsler, M., Papac-Milicevic, N., Weber, C., Wagner, O., Stangl, H., Soehnlein, O., and Binder, C.J. (2012). Interleukin-13 protects from atherosclerosis and modulates plaque composition by skewing the macrophage phenotype. EMBO Mol. Med. *4*, 1072–1086.

Cardinot, T.M., Lima, T.M., Moretti, A.I.S., Koike, M.K., Nunes, V.S., Cazita, P.M., Krieger, M.H., Brum, P.C., and Souza, H.P. (2016). Preventive and therapeutic moderate aerobic exercise programs convert atherosclerotic plaques into a more stable phenotype. Life Sci. *153*, 163–170.

Carobbio, S., Rodriguez-Cuenca, S., and Vidal-Puig, A. (2011). Origins of metabolic complications in obesity: ectopic fat accumulation. The importance of the qualitative aspect of lipotoxicity. Curr. Opin. Clin. Nutr. Metab. Care *14*, 520–526.

Carter, C.P., Howles, P.N., and Hui, D.Y. (1997). Genetic variation in cholesterol absorption efficiency among inbred strains of mice. J. Nutr. *127*, 1344–1348.

Castelli, W.P., Garrison, R.J., Wilson, P.W., Abbott, R.D., Kalousdian, S., and Kannel, W.B. (1986). Incidence of coronary heart disease and lipoprotein cholesterol levels. The Framingham Study. JAMA *256*, 2835–2838.

Chait, A., Brazg, R.L., Tribble, D.L., and Krauss, R.M. (1993). Susceptibility of small, dense, low-density lipoproteins to oxidative modification in subjects with the atherogenic lipoprotein phenotype, pattern B. Am. J. Med. *94*, 350–356.

Chauveau, F., Boutin, H., Van Camp, N., Dollé, F., and Tavitian, B. (2008). Nuclear imaging of neuroinflammation: a comprehensive review of [11C]PK11195 challengers. Eur. J. Nucl. Med. Mol. Imaging *35*, 2304–2319.

de Chaves, E.I., Bussière, M., Vance, D.E., Campenot, R.B., and Vance, J.E. (1997). Elevation of ceramide within distal neurites inhibits neurite growth in cultured rat sympathetic neurons. J. Biol. Chem. *272*, 3028–3035.

Chen, D., Ding, Y., Schröppel, B., Zhang, N., Fu, S., Chen, D., Zhang, H., and Bromberg, J.S. (2003). Differential chemokine and chemokine receptor gene induction by ischemia, alloantigen, and gene transfer in cardiac grafts. Am. J. Transplant. Off. J. Am. Soc. Transplant. Am. Soc. Transpl. Surg. *3*, 1216–1229.

Chinetti-Gbaguidi, G., Colin, S., and Staels, B. (2015). Macrophage subsets in atherosclerosis. Nat. Rev. Cardiol. *12*, 10–17.

Chiplunkar, A.R., Curtis, B.C., Eades, G.L., Kane, M.S., Fox, S.J., Haar, J.L., and Lloyd, J.A. (2013). The Krüppel-like factor 2 and Krüppel-like factor 4 genes interact to maintain endothelial integrity in mouse embryonic vasculogenesis. BMC Dev. Biol. *13*, 40.

Chistiakov, D.A., Bobryshev, Y.V., Kozarov, E., Sobenin, I.A., and Orekhov, A.N. (2015). Role of gut microbiota in the modulation of atherosclerosis-associated immune response. Front. Microbiol. *6*, 671.

Cho, T.-H., Aguettaz, P., Campuzano, O., Charriaut-Marlangue, C., Riou, A., Berthezène, Y., Nighoghossian, N., Ovize, M., Wiart, M., and Chauveau, F. (2013). Pre- and post-treatment with

cyclosporine A in a rat model of transient focal cerebral ischaemia with multimodal MRI screening. Int. J. Stroke Off. J. Int. Stroke Soc. *8*, 669–674.

Choi, H.K., Hernán, M.A., Seeger, J.D., Robins, J.M., and Wolfe, F. (2002). Methotrexate and mortality in patients with rheumatoid arthritis: a prospective study. Lancet Lond. Engl. *359*, 1173–1177.

Cholesterol Treatment Trialists' (CTT) Collaboration, Baigent, C., Blackwell, L., Emberson, J., Holland, L.E., Reith, C., Bhala, N., Peto, R., Barnes, E.H., Keech, A., et al. (2010). Efficacy and safety of more intensive lowering of LDL cholesterol: a meta-analysis of data from 170,000 participants in 26 randomised trials. Lancet Lond. Engl. *376*, 1670–1681.

Chróinín, D.N., Marnane, M., Akijian, L., Merwick, A., Fallon, E., Horgan, G., Dolan, E., Murphy, S., O'Rourke, K., O'Malley, K., et al. (2014). Serum lipids associated with inflammation-related PET-FDG uptake in symptomatic carotid plaque. Neurology *82*, 1693–1699.

Cinti, S. (2001). The adipose organ: morphological perspectives of adipose tissues. Proc. Nutr. Soc. *60*, 319–328.

Clarkson, T.B., Lofland, H.B., Bullock, B.C., and Goodman, H.O. (1971). Genetic control of plasma cholesterol. Studies on squirrel monkeys. Arch. Pathol. *92*, 37–45.

Coccia, E.M. (1999). STAT1 activation during monocyte to macrophage maturation: role of adhesion molecules. Int. Immunol. *11*, 1075–1083.

Colberg, S.R., Sigal, R.J., Fernhall, B., Regensteiner, J.G., Blissmer, B.J., Rubin, R.R., Chasan-Taber, L., Albright, A.L., Braun, B., American College of Sports Medicine, et al. (2010). Exercise and type 2 diabetes: the American College of Sports Medicine and the American Diabetes Association: joint position statement executive summary. Diabetes Care *33*, 2692–2696.

Cook, N.R., Paynter, N.P., Eaton, C.B., Manson, J.E., Martin, L.W., Robinson, J.G., Rossouw, J.E., Wassertheil-Smoller, S., and Ridker, P.M. (2012). Comparison of the Framingham and Reynolds Risk scores for global cardiovascular risk prediction in the multiethnic Women's Health Initiative. Circulation *125*, 1748–1756, S1-11.

Cornelissen, V.A., and Smart, N.A. (2013). Exercise training for blood pressure: a systematic review and meta-analysis. J. Am. Heart Assoc. *2*, e004473.

Costanzo, P., Perrone-Filardi, P., Petretta, M., Marciano, C., Vassallo, E., Gargiulo, P., Paolillo, S., Petretta, A., and Chiariello, M. (2009). Calcium channel blockers and cardiovascular outcomes: a meta-analysis of 175,634 patients. J. Hypertens. *27*, 1136–1151.

Cotton, F., and Hermier, M. (2006). The advantage of high relaxivity contrast agents in brain perfusion. Eur. Radiol. *16 Suppl 7*, M16-26.

Coutinho, T., Goel, K., Corrêa de Sá, D., Carter, R.E., Hodge, D.O., Kragelund, C., Kanaya, A.M., Zeller, M., Park, J.S., Kober, L., et al. (2013). Combining body mass index with measures of central obesity in the assessment of mortality in subjects with coronary disease: role of "normal weight central obesity." J. Am. Coll. Cardiol. *61*, 553–560.

Coyle, J.T., and Puttfarcken, P. (1993). Oxidative stress, glutamate, and neurodegenerative disorders. Science *262*, 689–695.

Cremer, J.E., Hume, S.P., Cullen, B.M., Myers, R., Manjil, L.G., Turton, D.R., Luthra, S.K., Bateman, D.M., and Pike, V.W. (1992). The distribution of radioactivity in brains of rats given [N-methyl-11C]PK 11195 in vivo after induction of a cortical ischaemic lesion. Int. J. Rad. Appl. Instrum. B *19*, 159–166.

Crossey, E., Amar, M.J.A., Sampson, M., Peabody, J., Schiller, J.T., Chackerian, B., and Remaley, A.T. (2015). A cholesterol-lowering VLP vaccine that targets PCSK9. Vaccine *33*, 5747–5755.

Cruz-Leal, Y., Lucatelli Laurindo, M.F., Osugui, L., Luzardo, M.D.C., López-Requena, A., Alonso, M.E., Álvarez, C., Popi, A.F., Mariano, M., Pérez, R., et al. (2014). Liposomes of phosphatidylcholine and cholesterol induce an M2-like macrophage phenotype reprogrammable to M1 pattern with the involvement of B-1 cells. Immunobiology *219*, 403–415.

Csiszar, A., Ungvari, Z., Koller, A., Edwards, J.G., and Kaley, G. (2004). Proinflammatory phenotype of coronary arteries promotes endothelial apoptosis in aging. Physiol. Genomics *17*, 21–30.

Cui, R., Iso, H., Yamagishi, K., Saito, I., Kokubo, Y., Inoue, M., Tsugane, S., and JPHC Study Group (2012). High serum total cholesterol levels is a risk factor of ischemic stroke for general Japanese population: the JPHC study. Atherosclerosis *221*, 565–569.

Culty, M., Li, H., Boujrad, N., Amri, H., Vidic, B., Bernassau, J.M., Reversat, J.L., and Papadopoulos, V. (1999). In vitro studies on the role of the peripheral-type benzodiazepine receptor in steroidogenesis. J. Steroid Biochem. Mol. Biol. *69*, 123–130.

Cunha, T.F., Bacurau, A.V.N., Moreira, J.B.N., Paixão, N.A., Campos, J.C., Ferreira, J.C.B., Leal, M.L., Negrão, C.E., Moriscot, A.S., Wisløff, U., et al. (2012). Exercise training prevents oxidative stress and ubiquitin-proteasome system overactivity and reverse skeletal muscle atrophy in heart failure. PloS One *7*, e41701.

Cunningham, K.S., and Gotlieb, A.I. (2005). The role of shear stress in the pathogenesis of atherosclerosis. Lab. Investig. J. Tech. Methods Pathol. *85*, 9–23.

Czernuszewicz, T.J., Homeister, J.W., Caughey, M.C., Farber, M.A., Fulton, J.J., Ford, P.F., Marston, W.A., Vallabhaneni, R., Nichols, T.C., and Gallippi, C.M. (2015). Non-invasive in vivo characterization of human carotid plaques with acoustic radiation force impulse ultrasound: comparison with histology after endarterectomy. Ultrasound Med. Biol. *41*, 685–697.

Dahlbäck, B. (2000). Blood coagulation. The Lancet *355*, 1627–1632.

Daulatzai, M.A. (2014). Chronic functional bowel syndrome enhances gut-brain axis dysfunction, neuroinflammation, cognitive impairment, and vulnerability to dementia. Neurochem. Res. *39*, 624–644.

Davidson, W.S., Silva, R.A.G.D., Chantepie, S., Lagor, W.R., Chapman, M.J., and Kontush, A. (2009). Proteomic analysis of defined HDL subpopulations reveals particle-specific protein clusters: relevance to antioxidative function. Arterioscler. Thromb. Vasc. Biol. *29*, 870–876.

Davies, J.R., Rudd, J.H.F., Fryer, T.D., Graves, M.J., Clark, J.C., Kirkpatrick, P.J., Gillard, J.H., Warburton, E.A., and Weissberg, P.L. (2005). Identification of culprit lesions after transient ischemic attack by combined 18F fluorodeoxyglucose positron-emission tomography and high-resolution magnetic resonance imaging. Stroke J. Cereb. Circ. *36*, 2642–2647.

Davies, J.R., Izquierdo-Garcia, D., Rudd, J.H.F., Figg, N., Richards, H.K., Bird, J.L.E., Aigbirhio, F.I., Davenport, A.P., Weissberg, P.L., Fryer, T.D., et al. (2010). FDG-PET can distinguish inflamed from non-inflamed plaque in an animal model of atherosclerosis. Int. J. Cardiovasc. Imaging *26*, 41–48.

Davignon, J. (2004). Beneficial cardiovascular pleiotropic effects of statins. Circulation *109*, III39-43.

Davis, H.R., Vesselinovitch, D., and Wissler, R.W. (1984a). Histochemical detection and quantification of macrophages in rhesus and cynomolgus monkey atherosclerotic lesions. J. Histochem. Cytochem. Off. J. Histochem. Soc. *32*, 1319–1327.

Davis, H.R., Vesselinovitch, D., and Wissler, R.W. (1984b). Reticuloendothelial system response to hyperlipidemia in rhesus and cynomolgus monkeys. J. Leukoc. Biol. *36*, 63–80.

De Caterina, R., Scarano, M., Marfisi, R., Lucisano, G., Palma, F., Tatasciore, A., and Marchioli, R. (2010). Cholesterol-lowering interventions and stroke: insights from a meta-analysis of randomized controlled trials. J. Am. Coll. Cardiol. *55*, 198–211.

Deddens, L.H., van Tilborg, G.A.F., van der Toorn, A., van der Marel, K., Paulis, L.E.M., van Bloois, L., Storm, G., Strijkers, G.J., Mulder, W.J.M., de Vries, H.E., et al. (2013). MRI of ICAM-1 upregulation after stroke: the importance of choosing the appropriate target-specific particulate contrast agent. Mol. Imaging Biol. MIB Off. Publ. Acad. Mol. Imaging *15*, 411–422.

Dehghan, A., Dupuis, J., Barbalic, M., Bis, J.C., Eiriksdottir, G., Lu, C., Pellikka, N., Wallaschofski, H., Kettunen, J., Henneman, P., et al. (2011). Meta-analysis of genome-wide association studies in >80 000 subjects identifies multiple loci for C-reactive protein levels. Circulation *123*, 731–738.

Del Rio, D., Stewart, A.J., and Pellegrini, N. (2005). A review of recent studies on malondialdehyde as toxic molecule and biological marker of oxidative stress. Nutr. Metab. Cardiovasc. Dis. NMCD *15*, 316–328.

Denes, A., Thornton, P., Rothwell, N.J., and Allan, S.M. (2010). Inflammation and brain injury: acute cerebral ischaemia, peripheral and central inflammation. Brain. Behav. Immun. *24*, 708–723.

Derlin, T., Richter, U., Bannas, P., Begemann, P., Buchert, R., Mester, J., and Klutmann, S. (2010). Feasibility of 18F-sodium fluoride PET/CT for imaging of atherosclerotic plaque. J. Nucl. Med. Off. Publ. Soc. Nucl. Med. *51*, 862–865.

Derlin, T., Wisotzki, C., Richter, U., Apostolova, I., Bannas, P., Weber, C., Mester, J., and Klutmann, S. (2011). In vivo imaging of mineral deposition in carotid plaque using 18F-sodium fluoride PET/CT: correlation with atherogenic risk factors. J. Nucl. Med. Off. Publ. Soc. Nucl. Med. *52*, 362–368.

Di Iorio, A., Ferrucci, L., Sparvieri, E., Cherubini, A., Volpato, S., Corsi, A., Bonafè, M., Franceschi, C., Abate, G., and Paganelli, R. (2003). Serum IL-1beta levels in health and disease: a population-based study. "The InCHIANTI study." Cytokine *22*, 198–205.

Di Napoli, M., Papa, F., and Bocola, V. (2001). C-reactive protein in ischemic stroke: an independent prognostic factor. Stroke J. Cereb. Circ. *32*, 917–924.

Di Paolo, G., and Kim, T.-W. (2011). Linking lipids to Alzheimer's disease: cholesterol and beyond. Nat. Rev. Neurosci. *12*, 284–296.

Dietschy, J.M., and Turley, S.D. (2004). Thematic review series: brain Lipids. Cholesterol metabolism in the central nervous system during early development and in the mature animal. J. Lipid Res. *45*, 1375–1397.

van Dijk, R.A., Duinisveld, A.J.F., Schaapherder, A.F., Mulder-Stapel, A., Hamming, J.F., Kuiper, J., de Boer, O.J., van der Wal, A.C., Kolodgie, F.D., Virmani, R., et al. (2015). A change in inflammatory footprint precedes plaque instability: a systematic evaluation of cellular aspects of the adaptive immune response in human atherosclerosis. J. Am. Heart Assoc. *4*.

van Dijk, R.A., Rijs, K., Wezel, A., Hamming, J.F., Kolodgie, F.D., Virmani, R., Schaapherder, A.F., and Lindeman, J.H.N. (2016). Systematic Evaluation of the Cellular Innate Immune Response During the Process of Human Atherosclerosis. J. Am. Heart Assoc. *5*.

Dima, A., and Ntziachristos, V. (2012). Non-invasive carotid imaging using optoacoustic tomography. Opt. Express *20*, 25044–25057.

Dimitrova-Shumkovska, J., Veenman, L., Ristoski, T., Leschiner, S., and Gavish, M. (2010). Chronic high fat, high cholesterol supplementation decreases 18 kDa Translocator Protein binding capacity in association with increased oxidative stress in rat liver and aorta. Food Chem. Toxicol. Int. J. Publ. Br. Ind. Biol. Res. Assoc. *48*, 910–921.

Dinarello, C.A. (2010). Anti-inflammatory Agents: Present and Future. Cell *140*, 935–950.

Dinarello, C.A. (2011). A clinical perspective of IL-1β as the gatekeeper of inflammation. Eur. J. Immunol. *41*, 1203–1217.

Dirnagl, U., Iadecola, C., and Moskowitz, M.A. (1999). Pathobiology of ischaemic stroke: an integrated view. Trends Neurosci. *22*, 391–397.

Downs, J.R., Clearfield, M., Weis, S., Whitney, E., Shapiro, D.R., Beere, P.A., Langendorfer, A., Stein, E.A., Kruyer, W., and Gotto, A.M. (1998). Primary prevention of acute coronary events with lovastatin in men and women with average cholesterol levels: results of AFCAPS/TexCAPS. Air Force/Texas Coronary Atherosclerosis Prevention Study. JAMA *279*, 1615–1622.

Drake, C., Boutin, H., Jones, M.S., Denes, A., McColl, B.W., Selvarajah, J.R., Hulme, S., Georgiou, R.F., Hinz, R., Gerhard, A., et al. (2011). Brain inflammation is induced by co-morbidities and risk factors for stroke. Brain. Behav. Immun. *25*, 1113–1122.

Duff, GL (1935). Experimental cholesterol arteriosclerosis and its relationship to human atherosclerosis. Arch Pathol *20*, 81–123.

Dutta, P., and Nahrendorf, M. (2014). Regulation and consequences of monocytosis. Immunol. Rev. *262*, 167–178.

Dutta, P., Courties, G., Wei, Y., Leuschner, F., Gorbatov, R., Robbins, C.S., Iwamoto, Y., Thompson, B., Carlson, A.L., Heidt, T., et al. (2012). Myocardial infarction accelerates atherosclerosis. Nature *487*, 325–329.

Duverger, N., Kruth, H., Emmanuel, F., Caillaud, J.M., Viglietta, C., Castro, G., Tailleux, A., Fievet, C., Fruchart, J.C., Houdebine, L.M., et al. (1996). Inhibition of atherosclerosis development in cholesterol-fed human apolipoprotein A-I-transgenic rabbits. Circulation *94*, 713–717.

Eckel, R.H., Jakicic, J.M., Ard, J.D., de Jesus, J.M., Houston Miller, N., Hubbard, V.S., Lee, I.-M., Lichtenstein, A.H., Loria, C.M., Millen, B.E., et al. (2014). 2013 AHA/ACC guideline on lifestyle management to reduce cardiovascular risk: a report of the American College of Cardiology/American Heart Association Task Force on Practice Guidelines. J. Am. Coll. Cardiol. *63*, 2960–2984.

Edison, P., Archer, H.A., Gerhard, A., Hinz, R., Pavese, N., Turkheimer, F.E., Hammers, A., Tai, Y.F., Fox, N., Kennedy, A., et al. (2008). Microglia, amyloid, and cognition in Alzheimer's disease: An [11C](R)PK11195-PET and [11C]PIB-PET study. Neurobiol. Dis. *32*, 412–419.

Egashira, K. (2003). Molecular mechanisms mediating inflammation in vascular disease: special reference to monocyte chemoattractant protein-1. Hypertens. Dallas Tex 1979 *41*, 834–841.

Eijsvogels, T.M.H., Fernandez, A.B., and Thompson, P.D. (2016). Are There Deleterious Cardiac Effects of Acute and Chronic Endurance Exercise? Physiol. Rev. *96*, 99–125.

Eisenhardt, S.U., Habersberger, J., Murphy, A., Chen, Y.-C., Woollard, K.J., Bassler, N., Qian, H., von Zur Muhlen, C., Hagemeyer, C.E., Ahrens, I., et al. (2009). Dissociation of pentameric to monomeric C-reactive protein on activated platelets localizes inflammation to atherosclerotic plaques. Circ. Res. *105*, 128–137.

Ekdahl, C.T., Claasen, J.-H., Bonde, S., Kokaia, Z., and Lindvall, O. (2003). Inflammation is detrimental for neurogenesis in adult brain. Proc. Natl. Acad. Sci. U. S. A. *100*, 13632–13637.

Ekmekcioglu, C., Elmadfa, I., Meyer, A.L., and Moeslinger, T. (2016). The role of dietary potassium in hypertension and diabetes. J. Physiol. Biochem. *72*, 93–106.

Emerging Risk Factors Collaboration, Di Angelantonio, E., Sarwar, N., Perry, P., Kaptoge, S., Ray, K.K., Thompson, A., Wood, A.M., Lewington, S., Sattar, N., et al. (2009). Major lipids, apolipoproteins, and risk of vascular disease. JAMA *302*, 1993–2000.

Emerging Risk Factors Collaboration, Kaptoge, S., Di Angelantonio, E., Lowe, G., Pepys, M.B., Thompson, S.G., Collins, R., and Danesh, J. (2010). C-reactive protein concentration and risk of coronary heart disease, stroke, and mortality: an individual participant meta-analysis. Lancet Lond. Engl. *375*, 132–140.

Emsley, H.C.A., Smith, C.J., Gavin, C.M., Georgiou, R.F., Vail, A., Barberan, E.M., Hallenbeck, J.M., del Zoppo, G.J., Rothwell, N.J., Tyrrell, P.J., et al. (2003). An early and sustained peripheral inflammatory response in acute ischaemic stroke: relationships with infection and atherosclerosis. J. Neuroimmunol. *139*, 93–101.

Erbel, C., Akhavanpoor, M., Okuyucu, D., Wangler, S., Dietz, A., Zhao, L., Stellos, K., Little, K.M., Lasitschka, F., Doesch, A., et al. (2014). IL-17A influences essential functions of the monocyte/macrophage lineage and is involved in advanced murine and human atherosclerosis. J. Immunol. Baltim. Md 1950 *193*, 4344–4355.

Erion, J.R., Wosiski-Kuhn, M., Dey, A., Hao, S., Davis, C.L., Pollock, N.K., and Stranahan, A.M. (2014). Obesity elicits interleukin 1-mediated deficits in hippocampal synaptic plasticity. J. Neurosci. Off. J. Soc. Neurosci. *34*, 2618–2631.

Essig, M., Dinkel, J., and Gutierrez, J.E. (2012). Use of contrast media in neuroimaging. Magn. Reson. Imaging Clin. N. Am. *20*, 633–648.

Esteve, E., Castro, A., López-Bermejo, A., Vendrell, J., Ricart, W., and Fernández-Real, J.-M. (2007). Serum interleukin-6 correlates with endothelial dysfunction in healthy men independently of insulin sensitivity. Diabetes Care *30*, 939–945.

Fabbrini, E., Magkos, F., Mohammed, B.S., Pietka, T., Abumrad, N.A., Patterson, B.W., Okunade, A., and Klein, S. (2009). Intrahepatic fat, not visceral fat, is linked with metabolic complications of obesity. Proc. Natl. Acad. Sci. U. S. A. *106*, 15430–15435.

Faergeman, O., Holme, I., Fayyad, R., Bhatia, S., Grundy, S.M., Kastelein, J.J.P., LaRosa, J.C., Larsen, M.L., Lindahl, C., Olsson, A.G., et al. (2009). Plasma triglycerides and cardiovascular events in the Treating to New Targets and Incremental Decrease in End-Points through Aggressive Lipid Lowering trials of statins in patients with coronary artery disease. Am. J. Cardiol. *104*, 459–463.

Fairweather, D., Coronado, M.J., Garton, A.E., Dziedzic, J.L., Bucek, A., Cooper, L.T., Brandt, J.E., Alikhan, F.S., Wang, H., Endres, C.J., et al. (2014). Sex differences in translocator protein 18 kDa (TSPO) in the heart: implications for imaging myocardial inflammation. J Cardiovasc. Transl. Res. *7*, 192–202.

Fan, J., McCormick, S.P., Krauss, R.M., Taylor, S., Quan, R., Taylor, J.M., and Young, S.G. (1995). Overexpression of human apolipoprotein B-100 in transgenic rabbits results in increased levels of LDL and decreased levels of HDL. Arterioscler. Thromb. Vasc. Biol. *15*, 1889–1899.

Fayad, Z.A., and Fuster, V. (2000). Characterization of atherosclerotic plaques by magnetic resonance imaging. Ann. N. Y. Acad. Sci. *902*, 173–186.

Fazio, S., Babaev, V.R., Murray, A.B., Hasty, A.H., Carter, K.J., Gleaves, L.A., Atkinson, J.B., and Linton, M.F. (1997). Increased atherosclerosis in mice reconstituted with apolipoprotein E null macrophages. Proc. Natl. Acad. Sci. U. S. A. *94*, 4647–4652.

Feig, J.E., Parathath, S., Rong, J.X., Mick, S.L., Vengrenyuk, Y., Grauer, L., Young, S.G., and Fisher, E.A. (2011a). Reversal of hyperlipidemia with a genetic switch favorably affects the content and inflammatory state of macrophages in atherosclerotic plaques. Circulation *123*, 989–998.

Feig, J.E., Rong, J.X., Shamir, R., Sanson, M., Vengrenyuk, Y., Liu, J., Rayner, K., Moore, K., Garabedian, M., and Fisher, E.A. (2011b). HDL promotes rapid atherosclerosis regression in mice and alters inflammatory properties of plaque monocyte-derived cells. Proc. Natl. Acad. Sci. U. S. A. *108*, 7166–7171.

Feinstein, S.B. (2004). The powerful microbubble: from bench to bedside, from intravascular indicator to therapeutic delivery system, and beyond. Am. J. Physiol. Heart Circ. Physiol. *287*, H450-457.

Fester, L., Zhou, L., Bütow, A., Huber, C., von Lossow, R., Prange-Kiel, J., Jarry, H., and Rune, G.M. (2009). Cholesterol-promoted synaptogenesis requires the conversion of cholesterol to estradiol in the hippocampus. Hippocampus *19*, 692–705.

Figueroa, A.L., Subramanian, S.S., Cury, R.C., Truong, Q.A., Gardecki, J.A., Tearney, G.J., Hoffmann, U., Brady, T.J., and Tawakol, A. (2012). Distribution of inflammation within carotid atherosclerotic plaques with high-risk morphological features: a comparison between positron emission tomography activity, plaque morphology, and histopathology. Circ. Cardiovasc. Imaging *5*, 69–77.

Finn, A.V., Kolodgie, F.D., and Virmani, R. (2010). Correlation between carotid intimal/medial thickness and atherosclerosis: a point of view from pathology. Arterioscler. Thromb. Vasc. Biol. *30*, 177–181.

Fisher, M., Paganini-Hill, A., Martin, A., Cosgrove, M., Toole, J.F., Barnett, H.J.M., and Norris, J. (2005). Carotid plaque pathology: thrombosis, ulceration, and stroke pathogenesis. Stroke J. Cereb. Circ. *36*, 253–257.

Freiberg, J.J., Tybjaerg-Hansen, A., Jensen, J.S., and Nordestgaard, B.G. (2008). Nonfasting triglycerides and risk of ischemic stroke in the general population. JAMA *300*, 2142–2152.

Frostegård, J., Ulfgren, A.K., Nyberg, P., Hedin, U., Swedenborg, J., Andersson, U., and Hansson, G.K. (1999). Cytokine expression in advanced human atherosclerotic plaques: dominance of pro-inflammatory (Th1) and macrophage-stimulating cytokines. Atherosclerosis *145*, 33–43.

Frøyshov, H.M., Bjørnerem, Å., Engstad, T., and Halvorsen, D.S. (2016). Elevated inflammatory markers predict mortality in long-term ischemic stroke-survivors: a population-based prospective study. Aging Clin. Exp. Res.

Fruhwirth, G.O., Moumtzi, A., Loidl, A., Ingolic, E., and Hermetter, A. (2006). The oxidized phospholipids POVPC and PGPC inhibit growth and induce apoptosis in vascular smooth muscle cells. Biochim. Biophys. Acta *1761*, 1060–1069.

Fullerton, S.M., Shirman, G.A., Strittmatter, W.J., and Matthew, W.D. (2001). Impairment of the blood-nerve and blood-brain barriers in apolipoprotein e knockout mice. Exp. Neurol. *169*, 13–22.

Gabay, C., Smith, M.F., Eidlen, D., and Arend, W.P. (1997). Interleukin 1 receptor antagonist (IL-1Ra) is an acute-phase protein. J. Clin. Invest. *99*, 2930–2940.

Gaborit, B., Venteclef, N., Ancel, P., Pelloux, V., Gariboldi, V., Leprince, P., Amour, J., Hatem, S.N., Jouve, E., Dutour, A., et al. (2015). Human epicardial adipose tissue has a specific transcriptomic

signature depending on its anatomical peri-atrial, peri-ventricular, or peri-coronary location. Cardiovasc. Res. *108*, 62–73.

Gaemperli, O., Shalhoub, J., Owen, D.R.J., Lamare, F., Johansson, S., Fouladi, N., Davies, A.H., Rimoldi, O.E., and Camici, P.G. (2012). Imaging intraplaque inflammation in carotid atherosclerosis with 11C-PK11195 positron emission tomography/computed tomography. Eur. Heart J. *33*, 1902–1910.

de Gaetano, M., Crean, D., Barry, M., and Belton, O. (2016). M1- and M2-Type Macrophage Responses Are Predictive of Adverse Outcomes in Human Atherosclerosis. Front. Immunol. *7*, 275.

Galeano, N.F., Milne, R., Marcel, Y.L., Walsh, M.T., Levy, E., Ngu'yen, T.D., Gleeson, A., Arad, Y., Witte, L., Al-Haideri, M., et al. (1994). Apoprotein B structure and receptor recognition of triglyceride-rich low density lipoprotein (LDL) is modified in small LDL but not in triglyceride-rich LDL of normal size. J. Biol. Chem. *269*, 511–519.

Galis, Z.S., and Khatri, J.J. (2002). Matrix metalloproteinases in vascular remodeling and atherogenesis: the good, the bad, and the ugly. Circ. Res. *90*, 251–262.

Galkina, E., and Ley, K. (2007). Vascular adhesion molecules in atherosclerosis. Arterioscler. Thromb. Vasc. Biol. *27*, 2292–2301.

Galkina, E., and Ley, K. (2009). Immune and inflammatory mechanisms of atherosclerosis (*). Annu. Rev. Immunol. *27*, 165–197.

Garcia-Bonilla, L., Benakis, C., Moore, J., Iadecola, C., and Anrather, J. (2014). Immune mechanisms in cerebral ischemic tolerance. Front. Neurosci. *8*, 44.

Geissmann, F., Jung, S., and Littman, D.R. (2003). Blood monocytes consist of two principal subsets with distinct migratory properties. Immunity *19*, 71–82.

Genest, J.J., Bard, J.M., Fruchart, J.C., Ordovas, J.M., Wilson, P.F., and Schaefer, E.J. (1991). Plasma apolipoprotein A-I, A-II, B, E and C-III containing particles in men with premature coronary artery disease. Atherosclerosis *90*, 149–157.

Geng, Y.J., Henderson, L.E., Levesque, E.B., Muszynski, M., and Libby, P. (1997). Fas is expressed in human atherosclerotic intima and promotes apoptosis of cytokine-primed human vascular smooth muscle cells. Arterioscler. Thromb. Vasc. Biol. *17*, 2200–2208.

Gerber, T.C., Carr, J.J., Arai, A.E., Dixon, R.L., Ferrari, V.A., Gomes, A.S., Heller, G.V., McCollough, C.H., McNitt-Gray, M.F., Mettler, F.A., et al. (2009). Ionizing radiation in cardiac imaging: a science advisory from the American Heart Association Committee on Cardiac Imaging of the Council on Clinical Cardiology and Committee on Cardiovascular Imaging and Intervention of the Council on Cardiovascular Radiology and Intervention. Circulation *119*, 1056–1065.

Gerhard, A., Schwarz, J., Myers, R., Wise, R., and Banati, R.B. (2005). Evolution of microglial activation in patients after ischemic stroke: a [11C](R)-PK11195 PET study. NeuroImage *24*, 591–595.

Gerhardt, T., and Ley, K. (2015). Monocyte trafficking across the vessel wall. Cardiovasc. Res. *107*, 321–330.

Gerszten, R.E., Garcia-Zepeda, E.A., Lim, Y.C., Yoshida, M., Ding, H.A., Gimbrone, M.A., Luster, A.D., Luscinskas, F.W., and Rosenzweig, A. (1999). MCP-1 and IL-8 trigger firm adhesion of monocytes to vascular endothelium under flow conditions. Nature *398*, 718–723.

Gertz, K., Kronenberg, G., Kälin, R.E., Baldinger, T., Werner, C., Balkaya, M., Eom, G.D., Hellmann-Regen, J., Kröber, J., Miller, K.R., et al. (2012). Essential role of interleukin-6 in post-stroke angiogenesis. Brain J. Neurol. *135*, 1964–1980.

Getz, G.S., and Reardon, C.A. (2009). Apoprotein E as a lipid transport and signaling protein in the blood, liver, and artery wall. J. Lipid Res. *50 Suppl*, S156-161.

Gibson, A.O., Blaha, M.J., Arnan, M.K., Sacco, R.L., Szklo, M., Herrington, D.M., and Yeboah, J. (2014). Coronary artery calcium and incident cerebrovascular events in an asymptomatic cohort. The MESA Study. JACC Cardiovasc. Imaging *7*, 1108–1115.

Gill, D., Sivakumaran, P., Wilding, P., Love, M., Veltkamp, R., and Kar, A. (2016). Trends in C-Reactive Protein Levels Are Associated with Neurological Change Twenty-Four Hours after Thrombolysis for Acute Ischemic Stroke. J. Stroke Cerebrovasc. Dis. Off. J. Natl. Stroke Assoc. *25*, 1966–1969.

Gimbrone, M.A., and García-Cardeña, G. (2013). Vascular endothelium, hemodynamics, and the pathobiology of atherosclerosis. Cardiovasc. Pathol. Off. J. Soc. Cardiovasc. Pathol. *22*, 9–15.

Gimbrone, M.A., Topper, J.N., Nagel, T., Anderson, K.R., and Garcia-Cardeña, G. (2000). Endothelial dysfunction, hemodynamic forces, and atherogenesis. Ann. N. Y. Acad. Sci. *902*, 230-239-240.

Ginsberg, H.N. (2002). New perspectives on atherogenesis: role of abnormal triglyceride-rich lipoprotein metabolism. Circulation *106*, 2137–2142.

Ginsberg, H.N., Kris-Etherton, P., Dennis, B., Elmer, P.J., Ershow, A., Lefevre, M., Pearson, T., Roheim, P., Ramakrishnan, R., Reed, R., et al. (1998). Effects of reducing dietary saturated fatty acids on plasma lipids and lipoproteins in healthy subjects: the DELTA Study, protocol 1. Arterioscler. Thromb. Vasc. Biol. *18*, 441–449.

Gleissner, C.A., Shaked, I., Erbel, C., Böckler, D., Katus, H.A., and Ley, K. (2010). CXCL4 downregulates the atheroprotective hemoglobin receptor CD163 in human macrophages. Circ. Res. *106*, 203–211.

Goldhammer, E., Tanchilevitch, A., Maor, I., Beniamini, Y., Rosenschein, U., and Sagiv, M. (2005). Exercise training modulates cytokines activity in coronary heart disease patients. Int. J. Cardiol. *100*, 93–99.

Goldstein, J.L., and Brown, M.S. (2009). The LDL receptor. Arterioscler. Thromb. Vasc. Biol. *29*, 431–438.

Goldstein, J.A., Maini, B., Dixon, S.R., Brilakis, E.S., Grines, C.L., Rizik, D.G., Powers, E.R., Steinberg, D.H., Shunk, K.A., Weisz, G., et al. (2011). Detection of lipid-core plaques by intracoronary near-infrared spectroscopy identifies high risk of periprocedural myocardial infarction. Circ. Cardiovasc. Interv. *4*, 429–437.

Gordon, S., and Taylor, P.R. (2005). Monocyte and macrophage heterogeneity. Nat. Rev. Immunol. *5*, 953–964.

Gordon, T., Castelli, W.P., Hjortland, M.C., Kannel, W.B., and Dawber, T.R. (1977). High density lipoprotein as a protective factor against coronary heart disease. The Framingham Study. Am. J. Med. *62*, 707–714.

Goritz, C., Mauch, D.H., and Pfrieger, F.W. (2005). Multiple mechanisms mediate cholesterol-induced synaptogenesis in a CNS neuron. Mol. Cell. Neurosci. *29*, 190–201.

Goswami, B., Rajappa, M., Mallika, V., Shukla, D.K., and Kumar, S. (2009). TNF-alpha/IL-10 ratio and C-reactive protein as markers of the inflammatory response in CAD-prone North Indian patients with acute myocardial infarction. Clin. Chim. Acta Int. J. Clin. Chem. *408*, 14–18.

Graebe, M., Pedersen, S.F., Højgaard, L., Kjaer, A., and Sillesen, H. (2010). 18FDG PET and ultrasound echolucency in carotid artery plaques. JACC Cardiovasc. Imaging *3*, 289–295.

Grammer, T.B., Kleber, M.E., März, W., Silbernagel, G., Siekmeier, R., Wieland, H., Pilz, S., Tomaschitz, A., Koenig, W., and Scharnagl, H. (2015). Low-density lipoprotein particle diameter and mortality: the Ludwigshafen Risk and Cardiovascular Health Study. Eur. Heart J. *36*, 31–38.

Greaves, D.R., and Gordon, S. (2009). The macrophage scavenger receptor at 30 years of age: current knowledge and future challenges. J. Lipid Res. *50 Suppl*, S282-286.

Greenland, P., Alpert, J.S., Beller, G.A., Benjamin, E.J., Budoff, M.J., Fayad, Z.A., Foster, E., Hlatky, M.A., Hodgson, J.M., Kushner, F.G., et al. (2010). 2010 ACCF/AHA guideline for assessment of cardiovascular risk in asymptomatic adults: a report of the American College of Cardiology Foundation/American Heart Association Task Force on Practice Guidelines. J. Am. Coll. Cardiol. *56*, e50-103.

Griendling, K.K., Sorescu, D., and Ushio-Fukai, M. (2000). NAD(P)H oxidase: role in cardiovascular biology and disease. Circ. Res. *86*, 494–501.

Grønholdt, M.L., Wagner, A., Wiebe, B.M., Hansen, J.U., Schroeder, T.V., Wilhjelm, J.E., Nowak, M., and Sillesen, H. (2001). Spiral computed tomographic imaging related to computerized ultrasonographic images of carotid plaque morphology and histology. J. Ultrasound Med. Off. J. Am. Inst. Ultrasound Med. *20*, 451–458.

Grønholdt, M.-L.M., Nordestgaard, B.G., Bentzon, J., Wiebe, B.M., Zhou, J., Falk, E., and Sillesen, H. (2002). Macrophages are associated with lipid-rich carotid artery plaques, echolucency on B-mode imaging, and elevated plasma lipid levels. J. Vasc. Surg. *35*, 137–145.

Gross, S., Gammon, S.T., Moss, B.L., Rauch, D., Harding, J., Heinecke, J.W., Ratner, L., and Piwnica-Worms, D. (2009). Bioluminescence imaging of myeloperoxidase activity in vivo. Nat. Med. *15*, 455–461.

Gu, L., Okada, Y., Clinton, S.K., Gerard, C., Sukhova, G.K., Libby, P., and Rollins, B.J. (1998). Absence of monocyte chemoattractant protein-1 reduces atherosclerosis in low density lipoprotein receptor-deficient mice. Mol. Cell *2*, 275–281.

Guo, F., Dong, M., Ren, F., Zhang, C., Li, J., Tao, Z., Yang, J., and Li, G. (2014). Association between local interleukin-6 levels and slow flow/microvascular dysfunction. J. Thromb. Thrombolysis *37*, 475–482.

Gupta, A., Baradaran, H., Schweitzer, A.D., Kamel, H., Pandya, A., Delgado, D., Dunning, A., Mushlin, A.I., and Sanelli, P.C. (2013). Carotid plaque MRI and stroke risk: a systematic review and meta-analysis. Stroke J. Cereb. Circ. *44*, 3071–3077.

Gupta, S., Sodhi, S., and Mahajan, V. (2009). Correlation of antioxidants with lipid peroxidation and lipid profile in patients suffering from coronary artery disease. Expert Opin. Ther. Targets *13*, 889–894.

Gut, P., Zweckstetter, M., and Banati, R.B. (2015). Lost in translocation: the functions of the 18-kD translocator protein. Trends Endocrinol. Metab. *26*, 349–356.

Gwechenberger, M., Mendoza, L.H., Youker, K.A., Frangogiannis, N.G., Smith, C.W., Michael, L.H., and Entman, M.L. (1999). Cardiac myocytes produce interleukin-6 in culture and in viable border zone of reperfused infarctions. Circulation *99*, 546–551.

Haase, C.L., Tybjærg-Hansen, A., Qayyum, A.A., Schou, J., Nordestgaard, B.G., and Frikke-Schmidt, R. (2012). LCAT, HDL cholesterol and ischemic cardiovascular disease: a Mendelian randomization study of HDL cholesterol in 54,500 individuals. J. Clin. Endocrinol. Metab. *97*, E248-256.

Hajra, L., Evans, A.I., Chen, M., Hyduk, S.J., Collins, T., and Cybulsky, M.I. (2000). The NF-kappa B signal transduction pathway in aortic endothelial cells is primed for activation in regions predisposed to atherosclerotic lesion formation. Proc. Natl. Acad. Sci. U. S. A. *97*, 9052–9057.

Hall, J.R., Wiechmann, A.R., Johnson, L.A., Edwards, M., Barber, R.C., Winter, A.S., Singh, M., and O'Bryant, S.E. (2013). Biomarkers of vascular risk, systemic inflammation, and microvascular pathology and neuropsychiatric symptoms in Alzheimer's disease. J. Alzheimers Dis. JAD *35*, 363–371.

Hamaguchi, M., Kojima, T., Takeda, N., Nagata, C., Takeda, J., Sarui, H., Kawahito, Y., Yoshida, N., Suetsugu, A., Kato, T., et al. (2007). Nonalcoholic fatty liver disease is a novel predictor of cardiovascular disease. World J. Gastroenterol. *13*, 1579–1584.

Hambrecht, R., Wolf, A., Gielen, S., Linke, A., Hofer, J., Erbs, S., Schoene, N., and Schuler, G. (2000). Effect of exercise on coronary endothelial function in patients with coronary artery disease. N. Engl. J. Med. *342*, 454–460.

Hamik, A., Lin, Z., Kumar, A., Balcells, M., Sinha, S., Katz, J., Feinberg, M.W., Gerzsten, R.E., Edelman, E.R., and Jain, M.K. (2007). Kruppel-like factor 4 regulates endothelial inflammation. J. Biol. Chem. *282*, 13769–13779.

Hansson, G.K., and Jonasson, L. (2009). The discovery of cellular immunity in the atherosclerotic plaque. Arterioscler. Thromb. Vasc. Biol. *29*, 1714–1717.

Hansson, G.K., Chao, S., Schwartz, S.M., and Reidy, M.A. (1985). Aortic endothelial cell death and replication in normal and lipopolysaccharide-treated rats. Am. J. Pathol. *121*, 123–127.

Hawkins, R.A., Choi, Y., Huang, S.C., Messa, C., Hoh, C.K., and Phelps, M.E. (1992). Quantitating tumor glucose metabolism with FDG and PET. J. Nucl. Med. Off. Publ. Soc. Nucl. Med. *33*, 339–344.

Hayashi, H., Campenot, R.B., Vance, D.E., and Vance, J.E. (2009). Protection of Neurons from Apoptosis by Apolipoprotein E-containing Lipoproteins Does Not Require Lipoprotein Uptake and Involves Activation of Phospholipase Cγ1 and Inhibition of Calcineurin. J. Biol. Chem. *284*, 29605–29613.

Hazen, S.L., Zhang, R., Shen, Z., Wu, W., Podrez, E.A., MacPherson, J.C., Schmitt, D., Mitra, S.N., Mukhopadhyay, C., Chen, Y., et al. (1999). Formation of nitric oxide-derived oxidants by myeloperoxidase in monocytes: pathways for monocyte-mediated protein nitration and lipid peroxidation In vivo. Circ. Res. *85*, 950–958.

Heart Protection Study Collaborative Group (2002). MRC/BHF Heart Protection Study of cholesterol lowering with simvastatin in 20,536 high-risk individuals: a randomised placebo-controlled trial. Lancet Lond. Engl. *360*, 7–22.

Hecht, H.S., and Narula, J. (2012). Coronary artery calcium scanning in asymptomatic patients with diabetes mellitus: a paradigm shift. J. Diabetes *4*, 342–350.

Hegele, R.A., Ginsberg, H.N., Chapman, M.J., Nordestgaard, B.G., Kuivenhoven, J.A., Averna, M., Borén, J., Bruckert, E., Catapano, A.L., Descamps, O.S., et al. (2014). The polygenic nature of

hypertriglyceridaemia: implications for definition, diagnosis, and management. Lancet Diabetes Endocrinol. *2*, 655–666.

Heistad, D.D., and Armstrong, M.L. (1986). Blood flow through vasa vasorum of coronary arteries in atherosclerotic monkeys. Arterioscler. Dallas Tex *6*, 326–331.

Herder, C., Baumert, J., Thorand, B., Martin, S., Löwel, H., Kolb, H., and Koenig, W. (2006). Chemokines and incident coronary heart disease: results from the MONICA/KORA Augsburg case-cohort study, 1984-2002. Arterioscler. Thromb. Vasc. Biol. *26*, 2147–2152.

Hermann, D.M., Gronewold, J., Lehmann, N., Moebus, S., Jöckel, K.-H., Bauer, M., Erbel, R., and Heinz Nixdorf Recall Study Investigative Group (2013). Coronary artery calcification is an independent stroke predictor in the general population. Stroke J. Cereb. Circ. *44*, 1008–1013.

Hernández, R.H., Armas-Hernández, M.J., Velasco, M., Israili, Z.H., and Armas-Padilla, M.C. (2003). Calcium antagonists and atherosclerosis protection in hypertension. Am. J. Ther. *10*, 409–414.

Herrera, A.J., Espinosa-Oliva, A.M., Oliva-Martin, M.J., Carrillo-Jimenez, A., Venero, J.L., and de Pablos, R.M. (2015). Collateral Damage: Contribution of Peripheral Inflammation to Neurodegenerative Diseases. Curr. Top. Med. Chem. *15*, 2193–2210.

Heusch, G., Libby, P., Gersh, B., Yellon, D., Böhm, M., Lopaschuk, G., and Opie, L. (2014). Cardiovascular remodelling in coronary artery disease and heart failure. Lancet Lond. Engl. *383*, 1933–1943.

Higashi, Y., Noma, K., Yoshizumi, M., and Kihara, Y. (2009). Endothelial function and oxidative stress in cardiovascular diseases. Circ. J. Off. J. Jpn. Circ. Soc. *73*, 411–418.

Hodis, H.N. (1999). Triglyceride-rich lipoprotein remnant particles and risk of atherosclerosis. Circulation *99*, 2852–2854.

Hoeg, J.M., Santamarina-Fojo, S., Bérard, A.M., Cornhill, J.F., Herderick, E.E., Feldman, S.H., Haudenschild, C.C., Vaisman, B.L., Hoyt, R.F., Demosky, S.J., et al. (1996). Overexpression of lecithin:cholesterol acyltransferase in transgenic rabbits prevents diet-induced atherosclerosis. Proc. Natl. Acad. Sci. U. S. A. *93*, 11448–11453.

Holmström, K.M., and Finkel, T. (2014). Cellular mechanisms and physiological consequences of redox-dependent signalling. Nat. Rev. Mol. Cell Biol. *15*, 411–421.

Horenstein, R.B., Smith, D.E., and Mosca, L. (2002). Cholesterol predicts stroke mortality in the Women's Pooling Project. Stroke J. Cereb. Circ. *33*, 1863–1868.

Hsu, T.M., and Kanoski, S.E. (2014). Blood-brain barrier disruption: mechanistic links between Western diet consumption and dementia. Front. Aging Neurosci. *6*, 88.

Huibers, A., de Borst, G.J., Wan, S., Kennedy, F., Giannopoulos, A., Moll, F.L., and Richards, T. (2015). Non-invasive Carotid Artery Imaging to Identify the Vulnerable Plaque: Current Status and Future Goals. Eur. J. Vasc. Endovasc. Surg. Off. J. Eur. Soc. Vasc. Surg. *50*, 563–572.

Hwang, J., Saha, A., Boo, Y.C., Sorescu, G.P., McNally, J.S., Holland, S.M., Dikalov, S., Giddens, D.P., Griendling, K.K., Harrison, D.G., et al. (2003). Oscillatory shear stress stimulates endothelial production of O2- from p47phox-dependent NAD(P)H oxidases, leading to monocyte adhesion. J. Biol. Chem. *278*, 47291–47298.

Iacobellis, G., Lonn, E., Lamy, A., Singh, N., and Sharma, A.M. (2011). Epicardial fat thickness and coronary artery disease correlate independently of obesity. Int. J. Cardiol. *146*, 452–454.

Igarashi, T., Sakatani, K., Shibuya, T., Hirayama, T., Yoshino, A., and Katayama, Y. (2014). Monitoring of filter patency during carotid artery stenting using near-infrared spectroscopy with high time-resolution. Adv. Exp. Med. Biol. *812*, 325–331.

IL6R Genetics Consortium Emerging Risk Factors Collaboration, Sarwar, N., Butterworth, A.S., Freitag, D.F., Gregson, J., Willeit, P., Gorman, D.N., Gao, P., Saleheen, D., Rendon, A., et al. (2012). Interleukin-6 receptor pathways in coronary heart disease: a collaborative meta-analysis of 82 studies. Lancet Lond. Engl. *379*, 1205–1213.

Imamura, T., Doi, Y., Arima, H., Yonemoto, K., Hata, J., Kubo, M., Tanizaki, Y., Ibayashi, S., Iida, M., and Kiyohara, Y. (2009). LDL cholesterol and the development of stroke subtypes and coronary heart disease in a general Japanese population: the Hisayama study. Stroke J. Cereb. Circ. *40*, 382–388.

Inoue, S., Egashira, K., Ni, W., Kitamoto, S., Usui, M., Otani, K., Ishibashi, M., Hiasa, K., Nishida, K., and Takeshita, A. (2002). Anti-monocyte chemoattractant protein-1 gene therapy limits progression and destabilization of established atherosclerosis in apolipoprotein E-knockout mice. Circulation *106*, 2700–2706.

Intiso, D., Stampatore, P., Zarrelli, M.M., Guerra, G.L., Arpaia, G., Simone, P., Tonali, P., and Beghi, E. (2003). Incidence of first-ever ischemic and hemorrhagic stroke in a well-defined community of southern Italy, 1993-1995. Eur. J. Neurol. *10*, 559–565.

Iwata, A., Browne, K.D., Chen, X.-H., Yuguchi, T., and Smith, D.H. (2005). Traumatic brain injury induces biphasic upregulation of ApoE and ApoJ protein in rats. J. Neurosci. Res. *82*, 103–114.

Jaffer, F.A., Vinegoni, C., John, M.C., Aikawa, E., Gold, H.K., Finn, A.V., Ntziachristos, V., Libby, P., and Weissleder, R. (2008). Real-time catheter molecular sensing of inflammation in proteolytically active atherosclerosis. Circulation *118*, 1802–1809.

Jaffer, F.A., Calfon, M.A., Rosenthal, A., Mallas, G., Razansky, R.N., Mauskapf, A., Weissleder, R., Libby, P., and Ntziachristos, V. (2011). Two-dimensional intravascular near-infrared fluorescence molecular imaging of inflammation in atherosclerosis and stent-induced vascular injury. J. Am. Coll. Cardiol. *57*, 2516–2526.

Janssen, B., Vugts, D.J., Funke, U., Molenaar, G.T., Kruijer, P.S., van Berckel, B.N.M., Lammertsma, A.A., and Windhorst, A.D. (2016). Imaging of neuroinflammation in Alzheimer's disease, multiple sclerosis and stroke: Recent developments in positron emission tomography. Biochim. Biophys. Acta *1862*, 425–441.

Jayalath, V.H., de Souza, R.J., Ha, V., Mirrahimi, A., Blanco-Mejia, S., Di Buono, M., Jenkins, A.L., Leiter, L.A., Wolever, T.M., Beyene, J., et al. (2015). Sugar-sweetened beverage consumption and incident hypertension: a systematic review and meta-analysis of prospective cohorts. Am. J. Clin. Nutr. *102*, 914–921.

Jerome, W.G. (2006). Advanced atherosclerotic foam cell formation has features of an acquired lysosomal storage disorder. Rejuvenation Res. *9*, 245–255.

Jerome, W.G., Minor, L.K., Glick, J.M., Rothblat, G.H., and Lewis, J.C. (1991). Lysosomal lipid accumulation in vascular smooth muscle cells. Exp. Mol. Pathol. *54*, 144–158.

Jeske, D.J., and Dietschy, J.M. (1980). Regulation of rates of cholesterol synthesis in vivo in the liver and carcass of the rat measured using [3H]water. J. Lipid Res. *21*, 364–376.

Jickling, G.C., and Sharp, F.R. (2011). Blood biomarkers of ischemic stroke. Neurother. J. Am. Soc. Exp. Neurother. *8*, 349–360.

Johnsen, S.H., Mathiesen, E.B., Joakimsen, O., Stensland, E., Wilsgaard, T., Løchen, M.-L., Njølstad, I., and Arnesen, E. (2007). Carotid atherosclerosis is a stronger predictor of myocardial infarction in women than in men: a 6-year follow-up study of 6226 persons: the Tromsø Study. Stroke J. Cereb. Circ. *38*, 2873–2880.

Johnson, J.L. (2007). Matrix metalloproteinases: influence on smooth muscle cells and atherosclerotic plaque stability. Expert Rev. Cardiovasc. Ther. *5*, 265–282.

Josephson RA Exercise Prescription: The Devil Is in the Details - American College of Cardiology.

Joshi, N.V., Toor, I., Shah, A.S.V., Carruthers, K., Vesey, A.T., Alam, S.R., Sills, A., Hoo, T.Y., Melville, A.J., Langlands, S.P., et al. (2015). Systemic Atherosclerotic Inflammation Following Acute Myocardial Infarction: Myocardial Infarction Begets Myocardial Infarction. J. Am. Heart Assoc. *4*, e001956.

Joshi, FR, Manavaki, R, and Fryer, TD (2013). Imaging of hypoxia and inflammation in carotid atherosclerosis with 18F-fluoromisonidazole and 18F-fluorodeoxyglucose positron emission tomography. Circulation *128 (suppl 22)*.

Jovinge, S., Hultgårdh-Nilsson, A., Regnström, J., and Nilsson, J. (1997). Tumor necrosis factor-alpha activates smooth muscle cell migration in culture and is expressed in the balloon-injured rat aorta. Arterioscler. Thromb. Vasc. Biol. *17*, 490–497.

Jung, J.E., Kim, G.S., and Chan, P.H. (2011). Neuroprotection by interleukin-6 is mediated by signal transducer and activator of transcription 3 and antioxidative signaling in ischemic stroke. Stroke J. Cereb. Circ. *42*, 3574–3579.

Kabir, M., Catalano, K.J., Ananthnarayan, S., Kim, S.P., Van Citters, G.W., Dea, M.K., and Bergman, R.N. (2005). Molecular evidence supporting the portal theory: a causative link between visceral adiposity and hepatic insulin resistance. Am. J. Physiol. Endocrinol. Metab. *288*, E454-461.

Kadl, A., Meher, A.K., Sharma, P.R., Lee, M.Y., Doran, A.C., Johnstone, S.R., Elliott, M.R., Gruber, F., Han, J., Chen, W., et al. (2010). Identification of a novel macrophage phenotype that develops in response to atherogenic phospholipids via Nrf2. Circ. Res. *107*, 737–746.

Kaida, H., Tahara, N., Tahara, A., Honda, A., Nitta, Y., Igata, S., Ishibashi, M., Yamagishi, S., and Fukumoto, Y. (2014). Positive correlation between malondialdehyde-modified low-density lipoprotein cholesterol and vascular inflammation evaluated by 18F-FDG PET/CT. Atherosclerosis *237*, 404–409.

Kalousová, M., Zima, T., Tesar, V., Sulková, S., and Fialová, L. (2003). Relationship between advanced glycoxidation end products, inflammatory markers/acute-phase reactants, and some autoantibodies in chronic hemodialysis patients. Kidney Int. Suppl. S62-64.

Kampschulte, A., Ferguson, M.S., Kerwin, W.S., Polissar, N.L., Chu, B., Saam, T., Hatsukami, T.S., and Yuan, C. (2004). Differentiation of intraplaque versus juxtaluminal hemorrhage/thrombus in advanced human carotid atherosclerotic lesions by in vivo magnetic resonance imaging. Circulation *110*, 3239–3244.

Kaneda, H., Taguchi, J., Ogasawara, K., Aizawa, T., and Ohno, M. (2002). Increased level of advanced oxidation protein products in patients with coronary artery disease. Atherosclerosis *162*, 221–225.

Kannel, W.B., Dawber, T.R., Kagan, A., Revotskie, N., and Stokes, J. (1961). Factors of risk in the development of coronary heart disease--six year follow-up experience. The Framingham Study. Ann. Intern. Med. *55*, 33–50.

Kanoski, S.E., Ong, Z.Y., Fortin, S.M., Schlessinger, E.S., and Grill, H.J. (2015). Liraglutide, leptin and their combined effects on feeding: additive intake reduction through common intracellular signalling mechanisms. Diabetes Obes. Metab. *17*, 285–293.

Kaplan, J.R., Chen, H., and Manuck, S.B. (2009). The relationship between social status and atherosclerosis in male and female monkeys as revealed by meta-analysis. Am. J. Primatol. *71*, 732–741.

Kaptoge, S., Seshasai, S.R.K., Gao, P., Freitag, D.F., Butterworth, A.S., Borglykke, A., Di Angelantonio, E., Gudnason, V., Rumley, A., Lowe, G.D.O., et al. (2014). Inflammatory cytokines and risk of coronary heart disease: new prospective study and updated meta-analysis. Eur. Heart J. *35*, 578–589.

Kastelein, J.J.P., Sager, P.T., de Groot, E., and Veltri, E. (2005). Comparison of ezetimibe plus simvastatin versus simvastatin monotherapy on atherosclerosis progression in familial hypercholesterolemia. Design and rationale of the Ezetimibe and Simvastatin in Hypercholesterolemia Enhances Atherosclerosis Regression (ENHANCE) trial. Am. Heart J. *149*, 234–239.

van Kasteren, S.I., Campbell, S.J., Serres, S., Anthony, D.C., Sibson, N.R., and Davis, B.G. (2009). Glyconanoparticles allow pre-symptomatic in vivo imaging of brain disease. Proc. Natl. Acad. Sci. U. S. A. *106*, 18–23.

Kaufmann, B.A., Sanders, J.M., Davis, C., Xie, A., Aldred, P., Sarembock, I.J., and Lindner, J.R. (2007). Molecular imaging of inflammation in atherosclerosis with targeted ultrasound detection of vascular cell adhesion molecule-1. Circulation *116*, 276–284.

Kervinen, H., Mänttäri, M., Kaartinen, M., Mäkynen, H., Palosuo, T., Pulkki, K., and Kovanen, P.T. (2004). Prognostic usefulness of plasma monocyte/macrophage and T-lymphocyte activation markers in patients with acute coronary syndromes. Am. J. Cardiol. *94*, 993–996.

Kerwin, W., Hooker, A., Spilker, M., Vicini, P., Ferguson, M., Hatsukami, T., and Yuan, C. (2003). Quantitative magnetic resonance imaging analysis of neovasculature volume in carotid atherosclerotic plaque. Circulation *107*, 851–856.

Kerwin, W.S., O'Brien, K.D., Ferguson, M.S., Polissar, N., Hatsukami, T.S., and Yuan, C. (2006). Inflammation in carotid atherosclerotic plaque: a dynamic contrast-enhanced MR imaging study. Radiology *241*, 459–468.

Khan, U., Porteous, L., Hassan, A., and Markus, H.S. (2007). Risk factor profile of cerebral small vessel disease and its subtypes. J. Neurol. Neurosurg. Psychiatry *78*, 702–706.

Khanicheh, E., Qi, Y., Xie, A., Mitterhuber, M., Xu, L., Mochizuki, M., Daali, Y., Jaquet, V., Krause, K.-H., Ruggeri, Z.M., et al. (2013). Molecular imaging reveals rapid reduction of endothelial activation in early atherosclerosis with apocynin independent of antioxidative properties. Arterioscler. Thromb. Vasc. Biol. *33*, 2187–2192.

Khera, A.V., Cuchel, M., de la Llera-Moya, M., Rodrigues, A., Burke, M.F., Jafri, K., French, B.C., Phillips, J.A., Mucksavage, M.L., Wilensky, R.L., et al. (2011). Cholesterol efflux capacity, high-density lipoprotein function, and atherosclerosis. N. Engl. J. Med. *364*, 127–135.

Khoury, H., Lavoie, L., Welner, S., and Folkerts, K. (2016). The Burden of Major Adverse Cardiac Events and Antiplatelet Prevention in Patients with Coronary or Peripheral Arterial Disease. Cardiovasc. Ther. *34*, 115–124.

Kim, E.-J., and Yu, S.-W. (2015). Translocator protein 18 kDa (TSPO): old dogma, new mice, new structure, and new questions for neuroprotection. Neural Regen. Res. *10*, 878–880.

Kim, J.H., Malhotra, R., Chiampas, G., d'Hemecourt, P., Troyanos, C., Cianca, J., Smith, R.N., Wang, T.J., Roberts, W.O., Thompson, P.D., et al. (2012). Cardiac arrest during long-distance running races. N. Engl. J. Med. *366*, 130–140.

Kim, S., Lee, S., Kim, J.B., Na, J.O., Choi, C.U., Lim, H.-E., Rha, S.-W., Park, C.G., Oh, D.J., Yoo, H., et al. (2015). Concurrent Carotid Inflammation in Acute Coronary Syndrome as Assessed by (18)F-FDG PET/CT: A Possible Mechanistic Link for Ischemic Stroke. J. Stroke Cerebrovasc. Dis. Off. J. Natl. Stroke Assoc. *24*, 2547–2554.

Kim, T.H., Yu, S.H., Choi, S.H., Yoon, J.W., Kang, S.M., Chun, E.J., Choi, S.I., Shin, H., Lee, H.K., Park, K.S., et al. (2011). Pericardial fat amount is an independent risk factor of coronary artery stenosis assessed by multidetector-row computed tomography: the Korean Atherosclerosis Study 2. Obes. Silver Spring Md *19*, 1028–1034.

Kishimoto, T., Akira, S., Narazaki, M., and Taga, T. (1995). Interleukin-6 family of cytokines and gp130. Blood *86*, 1243–1254.

Klafke, J.Z., Porto, F.G., de Almeida, A.S., Parisi, M.M., Hirsch, G.E., Trevisan, G., and Viecili, P.R.N. (2016). Biomarkers of Subclinical Atherosclerosis and Natural Products as Complementary Alternative Medicine. Curr. Pharm. Des. *22*, 372–382.

Klatsky, A.L. (2015). Alcohol and cardiovascular diseases: where do we stand today? J. Intern. Med. *278*, 238–250.

Kleemann, R., and Kooistra, T. (2005). HMG-CoA reductase inhibitors: effects on chronic subacute inflammation and onset of atherosclerosis induced by dietary cholesterol. Curr. Drug Targets Cardiovasc. Haematol. Disord. *5*, 441–453.

Kleemann, R., Verschuren, L., van Erk, M.J., Nikolsky, Y., Cnubben, N.H.P., Verheij, E.R., Smilde, A.K., Hendriks, H.F.J., Zadelaar, S., Smith, G.J., et al. (2007). Atherosclerosis and liver inflammation induced by increased dietary cholesterol intake: a combined transcriptomics and metabolomics analysis. Genome Biol. *8*, R200.

Kleveland, O., Kunszt, G., Bratlie, M., Ueland, T., Broch, K., Holte, E., Michelsen, A.E., Bendz, B., Amundsen, B.H., Espevik, T., et al. (2016). Effect of a single dose of the interleukin-6 receptor antagonist tocilizumab on inflammation and troponin T release in patients with non-ST-elevation myocardial infarction: a double-blind, randomized, placebo-controlled phase 2 trial. Eur. Heart J.

Ko, M., Zou, K., Minagawa, H., Yu, W., Gong, J.-S., Yanagisawa, K., and Michikawa, M. (2005). Cholesterol-mediated neurite outgrowth is differently regulated between cortical and hippocampal neurons. J. Biol. Chem. *280*, 42759–42765.

Kohler, E., Prentice, D.A., Bates, T.R., Hankey, G.J., Claxton, A., van Heerden, J., and Blacker, D. (2013). Intravenous minocycline in acute stroke: a randomized, controlled pilot study and meta-analysis. Stroke J. Cereb. Circ. *44*, 2493–2499.

Kolodgie, F.D., Gold, H.K., Burke, A.P., Fowler, D.R., Kruth, H.S., Weber, D.K., Farb, A., Guerrero, L.J., Hayase, M., Kutys, R., et al. (2003). Intraplaque hemorrhage and progression of coronary atheroma. N. Engl. J. Med. *349*, 2316–2325.

Koltsova, E.K., Kim, G., Lloyd, K.M., Saris, C.J.M., von Vietinghoff, S., Kronenberg, M., and Ley, K. (2012). Interleukin-27 receptor limits atherosclerosis in Ldlr-/- mice. Circ. Res. *111*, 1274–1285.

Kondo, T., and Watanabe, Y. (1975). A heritable hyperlipemic rabbit. Jikken Dobutsu *24*, 89–94.

Kooi, M.E., Cappendijk, V.C., Cleutjens, K.B.J.M., Kessels, A.G.H., Kitslaar, P.J.E.H.M., Borgers, M., Frederik, P.M., Daemen, M.J. a. P., and van Engelshoven, J.M.A. (2003). Accumulation of ultrasmall superparamagnetic particles of iron oxide in human atherosclerotic plaques can be detected by in vivo magnetic resonance imaging. Circulation *107*, 2453–2458.

Koskinas, K.C., Feldman, C.L., Chatzizisis, Y.S., Coskun, A.U., Jonas, M., Maynard, C., Baker, A.B., Papafaklis, M.I., Edelman, E.R., and Stone, P.H. (2010). Natural history of experimental coronary atherosclerosis and vascular remodeling in relation to endothelial shear stress: a serial, in vivo intravascular ultrasound study. Circulation *121*, 2092–2101.

Kramsch, D.M., Aspen, A.J., Abramowitz, B.M., Kreimendahl, T., and Hood, W.B. (1981). Reduction of coronary atherosclerosis by moderate conditioning exercise in monkeys on an atherogenic diet. N. Engl. J. Med. *305*, 1483–1489.

Kruth, H.S. (2013). Fluid-phase pinocytosis of LDL by macrophages: a novel target to reduce macrophage cholesterol accumulation in atherosclerotic lesions. Curr. Pharm. Des. *19*, 5865–5872.

Kurose, S., Iwasaka, J., Tsutsumi, H., Yamanaka, Y., Shinno, H., Fukushima, Y., Higurashi, K., Imai, M., Masuda, I., Takeda, S., et al. (2016). Effect of exercise-based cardiac rehabilitation on non-culprit mild coronary plaques in the culprit coronary artery of patients with acute coronary syndrome. Heart Vessels *31*, 846–854.

Kurth, T., Everett, B.M., Buring, J.E., Kase, C.S., Ridker, P.M., and Gaziano, J.M. (2007). Lipid levels and the risk of ischemic stroke in women. Neurology *68*, 556–562.

Lal, B.K., Hobson, R.W., Pappas, P.J., Kubicka, R., Hameed, M., Chakhtoura, E.Y., Jamil, Z., Padberg, F.T., Haser, P.B., Durán, W.N., et al. (2002). Pixel distribution analysis of B-mode ultrasound scan images predicts histologic features of atherosclerotic carotid plaques. J. Vasc. Surg. *35*, 1210–1217.

Lamarche, B., Tchernof, A., Mauriège, P., Cantin, B., Dagenais, G.R., Lupien, P.J., and Després, J.P. (1998). Fasting insulin and apolipoprotein B levels and low-density lipoprotein particle size as risk factors for ischemic heart disease. JAMA *279*, 1955–1961.

Lambert, G., Sjouke, B., Choque, B., Kastelein, J.J.P., and Hovingh, G.K. (2012). The PCSK9 decade. J. Lipid Res. *53*, 2515–2524.

Lane, J.S., Magno, C.P., Lane, K.T., Chan, T., Hoyt, D.B., and Greenfield, S. (2008). Nutrition impacts the prevalence of peripheral arterial disease in the United States. J. Vasc. Surg. *48*, 897–904.

Lane, T., Wassef, N., Poole, S., Mistry, Y., Lachmann, H.J., Gillmore, J.D., Hawkins, P.N., and Pepys, M.B. (2014). Infusion of pharmaceutical-grade natural human C-reactive protein is not proinflammatory in healthy adult human volunteers. Circ. Res. *114*, 672–676.

van Langenberg, D.R. (2016). New choices, new challenges: Anti-TNF versus anti-integrin molecule therapy in IBD. J. Gastroenterol. Hepatol. *31 Suppl 1*, 10–11.

Lara Fernandes, J., Serrano, C.V., Toledo, F., Hunziker, M.F., Zamperini, A., Teo, F.H., Oliveira, R.T., Blotta, M.H., Rondon, M.U., and Negrão, C.E. (2011). Acute and chronic effects of exercise on inflammatory markers and B-type natriuretic peptide in patients with coronary artery disease. Clin. Res. Cardiol. Off. J. Ger. Card. Soc. *100*, 77–84.

Lee, M.-J., Wu, Y., and Fried, S.K. (2013). Adipose tissue heterogeneity: implication of depot differences in adipose tissue for obesity complications. Mol. Aspects Med. *34*, 1–11.

Lee, S., Huen, S., Nishio, H., Nishio, S., Lee, H.K., Choi, B.-S., Ruhrberg, C., and Cantley, L.G. (2011). Distinct macrophage phenotypes contribute to kidney injury and repair. J. Am. Soc. Nephrol. JASN *22*, 317–326.

Lee, T.-M., Lin, M.-S., and Chang, N.-C. (2008). Usefulness of C-reactive protein and interleukin-6 as predictors of outcomes in patients with chronic obstructive pulmonary disease receiving pravastatin. Am. J. Cardiol. *101*, 530–535.

Leening, M.J.G., Elias-Smale, S.E., Kavousi, M., Felix, J.F., Deckers, J.W., Vliegenthart, R., Oudkerk, M., Hofman, A., Steyerberg, E.W., Stricker, B.H.C., et al. (2012). Coronary calcification and the risk of heart failure in the elderly: the Rotterdam Study. JACC Cardiovasc. Imaging *5*, 874–880.

Lei, J., Vodovotz, Y., Tzeng, E., and Billiar, T.R. (2013). Nitric oxide, a protective molecule in the cardiovascular system. Nitric Oxide Biol. Chem. Off. J. Nitric Oxide Soc. *35*, 175–185.

de Lemos, J.A., Morrow, D.A., Sabatine, M.S., Murphy, S.A., Gibson, C.M., Antman, E.M., McCabe, C.H., Cannon, C.P., and Braunwald, E. (2003). Association between plasma levels of monocyte chemoattractant protein-1 and long-term clinical outcomes in patients with acute coronary syndromes. Circulation *107*, 690–695.

Ley, K., Laudanna, C., Cybulsky, M.I., and Nourshargh, S. (2007). Getting to the site of inflammation: the leukocyte adhesion cascade updated. Nat. Rev. Immunol. *7*, 678–689.

Li, J.-M., and Shah, A.M. (2002). Intracellular localization and preassembly of the NADPH oxidase complex in cultured endothelial cells. J. Biol. Chem. *277*, 19952–19960.

Li, Q., Komaba, A., and Yokoyama, S. (1993). Cholesterol is poorly available for free apolipoprotein-mediated cellular lipid efflux from smooth muscle cells. Biochemistry (Mosc.) *32*, 4597–4603.

Li, Z.-Y., Howarth, S.P.S., Tang, T., and Gillard, J.H. (2006). How critical is fibrous cap thickness to carotid plaque stability? A flow-plaque interaction model. Stroke J. Cereb. Circ. *37*, 1195–1199.

Libby, P. (2000). Changing concepts of atherogenesis. J. Intern. Med. *247*, 349–358.

Libby, P. (2013a). Mechanisms of Acute Coronary Syndromes and Their Implications for Therapy. N. Engl. J. Med. *368*, 2004–2013.

Libby, P. (2013b). Collagenases and cracks in the plaque. J. Clin. Invest. *123*, 3201–3203.

Libby, P., Ridker, P.M., and Hansson, G.K. (2011). Progress and challenges in translating the biology of atherosclerosis. Nature *473*, 317–325.

Liebig, T., Gralla, J., and Schroth, G. (2015). Endovascular Treatment of Acute Stroke: Evolution and Selection of Techniques and Instruments Based on Thrombus Imaging. Clin. Neuroradiol. *25 Suppl 2*, 299–306.

Lim, W.-S., Timmins, J.M., Seimon, T.A., Sadler, A., Kolodgie, F.D., Virmani, R., and Tabas, I. (2008). Signal transducer and activator of transcription-1 is critical for apoptosis in macrophages subjected to endoplasmic reticulum stress in vitro and in advanced atherosclerotic lesions in vivo. Circulation *117*, 940–951.

Lindmark, E., Diderholm, E., Wallentin, L., and Siegbahn, A. (2001). Relationship between interleukin 6 and mortality in patients with unstable coronary artery disease: effects of an early invasive or noninvasive strategy. JAMA *286*, 2107–2113.

Linton, M.F., Gish, R., Hubl, S.T., Bütler, E., Esquivel, C., Bry, W.I., Boyles, J.K., Wardell, M.R., and Young, S.G. (1991). Phenotypes of apolipoprotein B and apolipoprotein E after liver transplantation. J. Clin. Invest. *88*, 270–281.

LIPID Study Group (1998). Prevention of Cardiovascular Events and Death with Pravastatin in Patients with Coronary Heart Disease and a Broad Range of Initial Cholesterol Levels. N. Engl. J. Med. *339*, 1349–1357.

Liu, C.-C., Liu, C.-C., Kanekiyo, T., Xu, H., and Bu, G. (2013). Apolipoprotein E and Alzheimer disease: risk, mechanisms and therapy. Nat. Rev. Neurol. *9*, 106–118.

Liu, J., Kerwin, W.S., Caldwell, J.H., Ferguson, M.S., Hippe, D.S., Alessio, A.M., Martinez-Malo, V., Pimentel, K., Miyaoka, R.S., Kohler, T.R., et al. (2016). High resolution FDG-microPET of carotid atherosclerosis: plaque components underlying enhanced FDG uptake. Int. J. Cardiovasc. Imaging *32*, 145–152.

Liu, M.-L., Ylitalo, K., Nuotio, I., Salonen, R., Salonen, J.T., and Taskinen, M.-R. (2002). Association between carotid intima-media thickness and low-density lipoprotein size and susceptibility of low-density lipoprotein to oxidation in asymptomatic members of familial combined hyperlipidemia families. Stroke J. Cereb. Circ. *33*, 1255–1260.

Liu, Q., Fan, Z., Yang, Q., and Li, D. (2012). Peripheral arterial wall imaging using contrast-enhanced, susceptibility-weighted phase imaging. J. Comput. Assist. Tomogr. *36*, 77–82.

Lopez, D. (2008). Inhibition of PCSK9 as a novel strategy for the treatment of hypercholesterolemia. Drug News Perspect. *21*, 323–330.

Losy, J., and Zaremba, J. (2001). Monocyte chemoattractant protein-1 is increased in the cerebrospinal fluid of patients with ischemic stroke. Stroke J. Cereb. Circ. *32*, 2695–2696.

Lüscher, T.F., Dohi, Y., Tanner, F.C., and Boulanger, C. (1991). Endothelium-dependent control of vascular tone: effects of age, hypertension and lipids. Basic Res. Cardiol. *86 Suppl 2*, 143–158.

Luscinskas, F.W., and Gimbrone Jr, M.A. (1996). Endothelial-dependent mechanisms in chronic inflammatory leukocyte recruitment. Annu. Rev. Med. *47*, 413–421.

Maas, M.B., and Furie, K.L. (2009). Molecular biomarkers in stroke diagnosis and prognosis. Biomark. Med. *3*, 363–383.

Macrez, R., Ali, C., Toutirais, O., Le Mauff, B., Defer, G., Dirnagl, U., and Vivien, D. (2011). Stroke and the immune system: from pathophysiology to new therapeutic strategies. Lancet Neurol. *10*, 471–480.

Madra, M., and Sturley, S.L. (2010). Niemann-Pick type C pathogenesis and treatment: from statins to sugars. Clin. Lipidol. *5*, 387–395.

Madssen, E., Videm, V., Moholdt, T., Wisløff, U., Hegbom, K., and Wiseth, R. (2015). Predictors of Beneficial Coronary Plaque Changes after Aerobic Exercise. Med. Sci. Sports Exerc. *47*, 2251–2256.

Mahley, R.W., Weisgraber, K.H., and Huang, Y. (2006). Apolipoprotein E4: a causative factor and therapeutic target in neuropathology, including Alzheimer's disease. Proc. Natl. Acad. Sci. U. S. A. *103*, 5644–5651.

Mahmud, A., and Feely, J. (2005). Arterial stiffness is related to systemic inflammation in essential hypertension. Hypertens. Dallas Tex 1979 *46*, 1118–1122.

Malik, A.H., Akram, Y., Shetty, S., Malik, S.S., and Yanchou Njike, V. (2014). Impact of sugar-sweetened beverages on blood pressure. Am. J. Cardiol. *113*, 1574–1580.

Mallat, Z., Besnard, S., Duriez, M., Deleuze, V., Emmanuel, F., Bureau, M.F., Soubrier, F., Esposito, B., Duez, H., Fievet, C., et al. (1999). Protective role of interleukin-10 in atherosclerosis. Circ. Res. *85*, e17-24.

Malmberg, C., Ripa, R.S., Johnbeck, C.B., Knigge, U., Langer, S.W., Mortensen, J., Oturai, P., Loft, A., Hag, A.M., and Kjær, A. (2015). 64Cu-DOTATATE for Noninvasive Assessment of Atherosclerosis in Large Arteries and Its Correlation with Risk Factors: Head-to-Head Comparison with 68Ga-DOTATOC in 60 Patients. J. Nucl. Med. Off. Publ. Soc. Nucl. Med. *56*, 1895–1900.

Manolopoulos, K.N., Karpe, F., and Frayn, K.N. (2010). Gluteofemoral body fat as a determinant of metabolic health. Int. J. Obes. 2005 *34*, 949–959.

Mantovani, A., Sozzani, S., Locati, M., Allavena, P., and Sica, A. (2002). Macrophage polarization: tumor-associated macrophages as a paradigm for polarized M2 mononuclear phagocytes. Trends Immunol. *23*, 549–555.

Mantovani, A., Sica, A., Sozzani, S., Allavena, P., Vecchi, A., and Locati, M. (2004). The chemokine system in diverse forms of macrophage activation and polarization. Trends Immunol. *25*, 677–686.

Mao, J.-W., Tang, H.-Y., Zhao, T., Tan, X.-Y., Bi, J., Wang, B.-Y., and Wang, Y.-D. (2015). Intestinal mucosal barrier dysfunction participates in the progress of nonalcoholic fatty liver disease. Int. J. Clin. Exp. Pathol. *8*, 3648–3658.

Marnane, M., Merwick, A., Sheehan, O.C., Hannon, N., Foran, P., Grant, T., Dolan, E., Moroney, J., Murphy, S., O'Rourke, K., et al. (2012). Carotid plaque inflammation on 18F-fluorodeoxyglucose positron emission tomography predicts early stroke recurrence. Ann. Neurol. *71*, 709–718.

Martin, S.S., Khokhar, A.A., May, H.T., Kulkarni, K.R., Blaha, M.J., Joshi, P.H., Toth, P.P., Muhlestein, J.B., Anderson, J.L., Knight, S., et al. (2015). HDL cholesterol subclasses, myocardial infarction, and mortality in secondary prevention: the Lipoprotein Investigators Collaborative. Eur. Heart J. *36*, 22–30.

Martinon, F., Pétrilli, V., Mayor, A., Tardivel, A., and Tschopp, J. (2006). Gout-associated uric acid crystals activate the NALP3 inflammasome. Nature *440*, 237–241.

Mateo, J., Izquierdo-Garcia, D., Badimon, J.J., Fayad, Z.A., and Fuster, V. (2014). Noninvasive assessment of hypoxia in rabbit advanced atherosclerosis using ^{18}F-fluoromisonidazole positron emission tomographic imaging. Circ. Cardiovasc. Imaging *7*, 312–320.

Matsuda, A., Nagao, K., Matsuo, M., Kioka, N., and Ueda, K. (2013). 24(S)-hydroxycholesterol is actively eliminated from neuronal cells by ABCA1. J. Neurochem. *126*, 93–101.

Mattu, H.S., and Randeva, H.S. (2013). Role of adipokines in cardiovascular disease. J. Endocrinol. *216*, T17-36.

Maxwell, S.S., Jackson, C.A., Paternoster, L., Cordonnier, C., Thijs, V., Al-Shahi Salman, R., and Sudlow, C.L.M. (2011). Genetic associations with brain microbleeds: Systematic review and meta-analyses. Neurology *77*, 158–167.

Mayerl, C., Lukasser, M., Sedivy, R., Niederegger, H., Seiler, R., and Wick, G. (2006). Atherosclerosis research from past to present—on the track of two pathologists with opposing views, Carl von Rokitansky and Rudolf Virchow. Virchows Arch. *449*, 96–103.

Mazzotta, G., Sarchielli, P., Caso, V., Paciaroni, M., Floridi, A., Floridi, A., and Gallai, V. (2004). Different cytokine levels in thrombolysis patients as predictors for clinical outcome. Eur. J. Neurol. *11*, 377–381.

McAteer, M.A., Sibson, N.R., von Zur Muhlen, C., Schneider, J.E., Lowe, A.S., Warrick, N., Channon, K.M., Anthony, D.C., and Choudhury, R.P. (2007). In vivo magnetic resonance imaging of acute brain inflammation using microparticles of iron oxide. Nat. Med. *13*, 1253–1258.

McColl, B.W., Allan, S.M., and Rothwell, N.J. (2009). Systemic infection, inflammation and acute ischemic stroke. Neuroscience *158*, 1049–1061.

McEnery, M.W., Snowman, A.M., Trifiletti, R.R., and Snyder, S.H. (1992). Isolation of the mitochondrial benzodiazepine receptor: association with the voltage-dependent anion channel and the adenine nucleotide carrier. Proc. Natl. Acad. Sci. U. S. A. *89*, 3170–3174.

McGillicuddy, F.C., de la Llera Moya, M., Hinkle, C.C., Joshi, M.R., Chiquoine, E.H., Billheimer, J.T., Rothblat, G.H., and Reilly, M.P. (2009). Inflammation impairs reverse cholesterol transport in vivo. Circulation *119*, 1135–1145.

Medlow, P., McEneny, J., Murphy, M.H., Trinick, T., Duly, E., and Davison, G.W. (2015). Exercise training protects the LDL I subfraction from oxidation susceptibility in an aged human population. Atherosclerosis *239*, 516–522.

Meershoek, A., van Dijk, R.A., Verhage, S., Hamming, J.F., van den Bogaerdt, A.J., Bogers, A.J.J.C., Schaapherder, A.F., and Lindeman, J.H. (2016). Histological evaluation disqualifies IMT and calcification scores as surrogates for grading coronary and aortic atherosclerosis. Int. J. Cardiol. *224*, 328–334.

Merino, J.G., Latour, L.L., Tso, A., Lee, K.Y., Kang, D.W., Davis, L.A., Lazar, R.M., Horvath, K.A., Corso, P.J., and Warach, S. (2013). Blood-brain barrier disruption after cardiac surgery. AJNR Am. J. Neuroradiol. *34*, 518–523.

Micha, R., Imamura, F., Wyler von Ballmoos, M., Solomon, D.H., Hernán, M.A., Ridker, P.M., and Mozaffarian, D. (2011). Systematic review and meta-analysis of methotrexate use and risk of cardiovascular disease. Am. J. Cardiol. *108*, 1362–1370.

Milionis, H., Barkas, F., Ntaios, G., Papavasileiou, V., Vemmos, K., Michel, P., and Elisaf, M. (2016). Proprotein convertase subtilisin kexin 9 (PCSK9) inhibitors to treat hypercholesterolemia: Effect on stroke risk. Eur. J. Intern. Med.

Millar, P.J., McGowan, C.L., Cornelissen, V.A., Araujo, C.G., and Swaine, I.L. (2014). Evidence for the role of isometric exercise training in reducing blood pressure: potential mechanisms and future directions. Sports Med. Auckl. NZ *44*, 345–356.

Millon, A., Canet-Soulas, E., Boussel, L., Fayad, Z., and Douek, P. (2014). Animal models of atherosclerosis and magnetic resonance imaging for monitoring plaque progression. Vascular *22*, 221–237.

Millon, A., Sigovan, M., Boussel, L., Mathevet, J.-L., Louzier, V., Paquet, C., Geloen, A., Provost, N., Majd, Z., Patsouris, D., et al. (2015). Low WSS Induces Intimal Thickening, while Large WSS Variation and Inflammation Induce Medial Thinning, in an Animal Model of Atherosclerosis. PloS One *10*, e0141880.

Mills, C.D., Kincaid, K., Alt, J.M., Heilman, M.J., and Hill, A.M. (2000). M-1/M-2 macrophages and the Th1/Th2 paradigm. J. Immunol. Baltim. Md 1950 *164*, 6166–6173.

Mojtahedi, A., Alavi, A., Thamake, S., Amerinia, R., Ranganathan, D., Tworowska, I., and Delpassand, E.S. (2015). Assessment of vulnerable atherosclerotic and fibrotic plaques in coronary arteries using (68)Ga-DOTATATE PET/CT. Am. J. Nucl. Med. Mol. Imaging *5*, 65–71.

Mok, V., and Kim, J.S. (2015). Prevention and Management of Cerebral Small Vessel Disease. J. Stroke *17*, 111–122.

Monje, M.L., Toda, H., and Palmer, T.D. (2003). Inflammatory blockade restores adult hippocampal neurogenesis. Science *302*, 1760–1765.

Mono, M.-L., Karameshev, A., Slotboom, J., Remonda, L., Galimanis, A., Jung, S., Findling, O., De Marchis, G.M., Luedi, R., Kiefer, C., et al. (2012). Plaque characteristics of asymptomatic carotid stenosis and risk of stroke. Cerebrovasc. Dis. Basel Switz. *34*, 343–350.

Montagne, A., Gauberti, M., Macrez, R., Jullienne, A., Briens, A., Raynaud, J.-S., Louin, G., Buisson, A., Haelewyn, B., Docagne, F., et al. (2012). Ultra-sensitive molecular MRI of cerebrovascular cell activation enables early detection of chronic central nervous system disorders. NeuroImage *63*, 760–770.

Moody, A.R., Murphy, R.E., Morgan, P.S., Martel, A.L., Delay, G.S., Allder, S., MacSweeney, S.T., Tennant, W.G., Gladman, J., Lowe, J., et al. (2003). Characterization of complicated carotid plaque with magnetic resonance direct thrombus imaging in patients with cerebral ischemia. Circulation *107*, 3047–3052.

Moore, K.J., and Freeman, M.W. (2006). Scavenger receptors in atherosclerosis: beyond lipid uptake. Arterioscler. Thromb. Vasc. Biol. *26*, 1702–1711.

Moore, K.J., and Tabas, I. (2011). Macrophages in the pathogenesis of atherosclerosis. Cell *145*, 341–355.

Moore, K.J., Sheedy, F.J., and Fisher, E.A. (2013). Macrophages in atherosclerosis: a dynamic balance. Nat. Rev. Immunol. *13*, 709–721.

Morell, P., and Jurevics, H. (1996). Origin of cholesterol in myelin. Neurochem. Res. *21*, 463–470.

Mori, Y., Chen, T., Fujisawa, T., Kobashi, S., Ohno, K., Yoshida, S., Tago, Y., Komai, Y., Hata, Y., and Yoshioka, Y. (2014). From cartoon to real time MRI: in vivo monitoring of phagocyte migration in mouse brain. Sci. Rep. *4*, 6997.

Morohaku, K., Pelton, S.H., Daugherty, D.J., Butler, W.R., Deng, W., and Selvaraj, V. (2014). Translocator protein/peripheral benzodiazepine receptor is not required for steroid hormone biosynthesis. Endocrinology *155*, 89–97.

Mosser, D.M., and Edwards, J.P. (2008). Exploring the full spectrum of macrophage activation. Nat. Rev. Immunol. *8*, 958–969.

Moustafa, R.R., Izquierdo-Garcia, D., Fryer, T.D., Graves, M.J., Rudd, J.H.F., Gillard, J.H., Weissberg, P.L., Baron, J.-C., and Warburton, E.A. (2010). Carotid plaque inflammation is associated with cerebral microembolism in patients with recent transient ischemic attack or stroke: a pilot study. Circ. Cardiovasc. Imaging *3*, 536–541.

Myers, R., Manjil, L.G., Cullen, B.M., Price, G.W., Frackowiak, R.S., and Cremer, J.E. (1991). Macrophage and astrocyte populations in relation to [3H]PK 11195 binding in rat cerebral cortex following a local ischaemic lesion. J. Cereb. Blood Flow Metab. Off. J. Int. Soc. Cereb. Blood Flow Metab. *11*, 314–322.

Nael, K., and Kubal, W. (2016). Magnetic Resonance Imaging of Acute Stroke. Magn. Reson. Imaging Clin. N. Am. *24*, 293–304.

Nagareddy, P.R., Murphy, A.J., Stirzaker, R.A., Hu, Y., Yu, S., Miller, R.G., Ramkhelawon, B., Distel, E., Westerterp, M., Huang, L.-S., et al. (2013). Hyperglycemia promotes myelopoiesis and impairs the resolution of atherosclerosis. Cell Metab. *17*, 695–708.

Naghavi, M. (2003). From Vulnerable Plaque to Vulnerable Patient: A Call for New Definitions and Risk Assessment Strategies: Part I. Circulation *108*, 1664–1672.

Nahrendorf, M., Swirski, F.K., Aikawa, E., Stangenberg, L., Wurdinger, T., Figueiredo, J.-L., Libby, P., Weissleder, R., and Pittet, M.J. (2007). The healing myocardium sequentially mobilizes two monocyte subsets with divergent and complementary functions. J. Exp. Med. *204*, 3037–3047.

Nahrendorf, M., Sosnovik, D., Chen, J.W., Panizzi, P., Figueiredo, J.-L., Aikawa, E., Libby, P., Swirski, F.K., and Weissleder, R. (2008). Activatable magnetic resonance imaging agent reports myeloperoxidase activity in healing infarcts and noninvasively detects the antiinflammatory effects of atorvastatin on ischemia-reperfusion injury. Circulation *117*, 1153–1160.

Nahrendorf, M., Keliher, E., Panizzi, P., Zhang, H., Hembrador, S., Figueiredo, J.-L., Aikawa, E., Kelly, K., Libby, P., and Weissleder, R. (2009). 18F-4V for PET-CT imaging of VCAM-1 expression in atherosclerosis. JACC Cardiovasc. Imaging *2*, 1213–1222.

Nakashima, Y., Plump, A.S., Raines, E.W., Breslow, J.L., and Ross, R. (1994). ApoE-deficient mice develop lesions of all phases of atherosclerosis throughout the arterial tree. Arterioscler. Thromb. J. Vasc. Biol. Am. Heart Assoc. *14*, 133–140.

Namiki, M., Kawashima, S., Yamashita, T., Ozaki, M., Hirase, T., Ishida, T., Inoue, N., Hirata, K., Matsukawa, A., Morishita, R., et al. (2002). Local overexpression of monocyte chemoattractant protein-1 at vessel wall induces infiltration of macrophages and formation of atherosclerotic lesion: synergism with hypercholesterolemia. Arterioscler. Thromb. Vasc. Biol. *22*, 115–120.

Naqvi, T.Z., and Lee, M.-S. (2014). Carotid intima-media thickness and plaque in cardiovascular risk assessment. JACC Cardiovasc. Imaging *7*, 1025–1038.

Nathan, C.F., Murray, H.W., Wiebe, M.E., and Rubin, B.Y. (1983). Identification of interferon-gamma as the lymphokine that activates human macrophage oxidative metabolism and antimicrobial activity. J. Exp. Med. *158*, 670–689.

Navab, M., Berliner, J.A., Watson, A.D., Hama, S.Y., Territo, M.C., Lusis, A.J., Shih, D.M., Van Lenten, B.J., Frank, J.S., Demer, L.L., et al. (1996). The Yin and Yang of oxidation in the development of the fatty streak. A review based on the 1994 George Lyman Duff Memorial Lecture. Arterioscler. Thromb. Vasc. Biol. *16*, 831–842.

Navarese, E.P., Kolodziejczak, M., Schulze, V., Gurbel, P.A., Tantry, U., Lin, Y., Brockmeyer, M., Kandzari, D.E., Kubica, J.M., D'Agostino, R.B., et al. (2015). Effects of Proprotein Convertase Subtilisin/Kexin Type 9 Antibodies in Adults With Hypercholesterolemia: A Systematic Review and Meta-analysis. Ann. Intern. Med. *163*, 40–51.

Nerem, R.M., Levesque, M.J., and Cornhill, J.F. (1981). Vascular endothelial morphology as an indicator of the pattern of blood flow. J. Biomech. Eng. *103*, 172–176.

Nickel, T., Hanssen, H., Emslander, I., Drexel, V., Hertel, G., Schmidt-Trucksäss, A., Summo, C., Sisic, Z., Lambert, M., Hoster, E., et al. (2011). Immunomodulatory effects of aerobic training in obesity. Mediators Inflamm. *2011*, 308965.

Nidorf, S.M., Eikelboom, J.W., Budgeon, C.A., and Thompson, P.L. (2013). Low-dose colchicine for secondary prevention of cardiovascular disease. J. Am. Coll. Cardiol. *61*, 404–410.

Nighoghossian, N., Wiart, M., Cakmak, S., Berthezène, Y., Derex, L., Cho, T.-H., Nemoz, C., Chapuis, F., Tisserand, G.-L., Pialat, J.-B., et al. (2007). Inflammatory response after ischemic stroke: a USPIO-enhanced MRI study in patients. Stroke J. Cereb. Circ. *38*, 303–307.

Nighoghossian, N., Berthezène, Y., Mechtouff, L., Derex, L., Cho, T.H., Ritzenthaler, T., Rheims, S., Chauveau, F., Béjot, Y., Jacquin, A., et al. (2015). Cyclosporine in acute ischemic stroke. Neurology *84*, 2216–2223.

Nissen, S.E., Tuzcu, E.M., Schoenhagen, P., Crowe, T., Sasiela, W.J., Tsai, J., Orazem, J., Magorien, R.D., O'Shaughnessy, C., Ganz, P., et al. (2005). Statin therapy, LDL cholesterol, C-reactive protein, and coronary artery disease. N. Engl. J. Med. *352*, 29–38.

Node, K., Fujita, M., Kitakaze, M., Hori, M., and Liao, J.K. (2003). Short-term statin therapy improves cardiac function and symptoms in patients with idiopathic dilated cardiomyopathy. Circulation *108*, 839–843.

Noh, T.S., Moon, S.-H., Cho, Y.S., Hong, S.P., Lee, E.J., Choi, J.Y., Kim, B.-T., and Lee, K.-H. (2013). Relation of carotid artery 18F-FDG uptake to C-reactive protein and Framingham risk score in a large cohort of asymptomatic adults. J. Nucl. Med. Off. Publ. Soc. Nucl. Med. *54*, 2070–2076.

Nordestgaard, B.G., and Lewis, B. (1991). Intermediate density lipoprotein levels are strong predictors of the extent of aortic atherosclerosis in the St. Thomas's Hospital rabbit strain. Atherosclerosis *87*, 39–46.

Nordestgaard, B.G., Wootton, R., and Lewis, B. (1995). Selective retention of VLDL, IDL, and LDL in the arterial intima of genetically hyperlipidemic rabbits in vivo. Molecular size as a determinant of fractional loss from the intima-inner media. Arterioscler. Thromb. Vasc. Biol. *15*, 534–542.

Nordestgaard, B.G., Grønholdt, M.-L.M., and Sillesen, H. (2003). Echolucent rupture-prone plaques. Curr. Opin. Lipidol. *14*, 505–512.

Noveck, R., Stroes, E.S.G., Flaim, J.D., Baker, B.F., Hughes, S., Graham, M.J., Crooke, R.M., and Ridker, P.M. (2014). Effects of an antisense oligonucleotide inhibitor of C-reactive protein synthesis on the endotoxin challenge response in healthy human male volunteers. J. Am. Heart Assoc. *3*.

Obarzanek, E., Sacks, F.M., Vollmer, W.M., Bray, G.A., Miller, E.R., Lin, P.H., Karanja, N.M., Most-Windhauser, M.M., Moore, T.J., Swain, J.F., et al. (2001). Effects on blood lipids of a blood pressure-lowering diet: the Dietary Approaches to Stop Hypertension (DASH) Trial. Am. J. Clin. Nutr. *74*, 80–89.

O'Connor, C.M., Whellan, D.J., Lee, K.L., Keteyian, S.J., Cooper, L.S., Ellis, S.J., Leifer, E.S., Kraus, W.E., Kitzman, D.W., Blumenthal, J.A., et al. (2009). Efficacy and safety of exercise training in patients with chronic heart failure: HF-ACTION randomized controlled trial. JAMA *301*, 1439–1450.

Okello, A., Edison, P., Archer, H.A., Turkheimer, F.E., Kennedy, J., Bullock, R., Walker, Z., Kennedy, A., Fox, N., Rossor, M., et al. (2009). Microglial activation and amyloid deposition in mild cognitive impairment: a PET study. Neurology *72*, 56–62.

Olufadi, R., and Byrne, C.D. (2006). Effects of VLDL and remnant particles on platelets. Pathophysiol. Haemost. Thromb. *35*, 281–291.

Ono, H., Minatoguchi, S., Watanabe, K., Yamada, Y., Mizukusa, T., Kawasaki, H., Takahashi, H., Uno, T., Tsukamoto, T., Hiei, K., et al. (2008). Candesartan decreases carotid intima-media thickness by

enhancing nitric oxide and decreasing oxidative stress in patients with hypertension. Hypertens. Res. Off. J. Jpn. Soc. Hypertens. *31*, 271–279.

Osborn, E.A., and Jaffer, F.A. (2013). The advancing clinical impact of molecular imaging in CVD. JACC Cardiovasc. Imaging *6*, 1327–1341.

Ouchi, N., Kihara, S., Funahashi, T., Nakamura, T., Nishida, M., Kumada, M., Okamoto, Y., Ohashi, K., Nagaretani, H., Kishida, K., et al. (2003). Reciprocal association of C-reactive protein with adiponectin in blood stream and adipose tissue. Circulation *107*, 671–674.

Ouchi, N., Higuchi, A., Ohashi, K., Oshima, Y., Gokce, N., Shibata, R., Akasaki, Y., Shimono, A., and Walsh, K. (2010). Sfrp5 is an anti-inflammatory adipokine that modulates metabolic dysfunction in obesity. Science *329*, 454–457.

Owen, D.R.J., and Matthews, P.M. (2011). Imaging brain microglial activation using positron emission tomography and translocator protein-specific radioligands. Int. Rev. Neurobiol. *101*, 19–39.

Pace, J.L., Russell, S.W., Schreiber, R.D., Altman, A., and Katz, D.H. (1983). Macrophage activation: priming activity from a T-cell hybridoma is attributable to interferon-gamma. Proc. Natl. Acad. Sci. U. S. A. *80*, 3782–3786.

Packard, R.R.S., and Libby, P. (2008). Inflammation in atherosclerosis: from vascular biology to biomarker discovery and risk prediction. Clin. Chem. *54*, 24–38.

Packard, C.J., Demant, T., Stewart, J.P., Bedford, D., Caslake, M.J., Schwertfeger, G., Bedynek, A., Shepherd, J., and Seidel, D. (2000). Apolipoprotein B metabolism and the distribution of VLDL and LDL subfractions. J. Lipid Res. *41*, 305–318.

Packard, R.R.S., Lichtman, A.H., and Libby, P. (2009). Innate and adaptive immunity in atherosclerosis. Semin. Immunopathol. *31*, 5–22.

Paeng, J.C., Lee, Y.-S., Lee, J.S., Jeong, J.M., Kim, K.-B., Chung, J.-K., and Lee, D.S. (2013). Feasibility and kinetic characteristics of (68)Ga-NOTA-RGD PET for in vivo atherosclerosis imaging. Ann. Nucl. Med. *27*, 847–854.

Park, S., and Lakatta, E.G. (2012). Role of inflammation in the pathogenesis of arterial stiffness. Yonsei Med. J. *53*, 258–261.

Partovi, S., Loebe, M., Aschwanden, M., Baldi, T., Jäger, K.A., Feinstein, S.B., and Staub, D. (2012). Contrast-enhanced ultrasound for assessing carotid atherosclerotic plaque lesions. AJR Am. J. Roentgenol. *198*, W13-19.

Passlick, B., Flieger, D., and Ziegler-Heitbrock, H.W. (1989). Identification and characterization of a novel monocyte subpopulation in human peripheral blood. Blood *74*, 2527–2534.

Patel, R.S., Al Mheid, I., Morris, A.A., Ahmed, Y., Kavtaradze, N., Ali, S., Dabhadkar, K., Brigham, K., Hooper, W.C., Alexander, R.W., et al. (2011). Oxidative stress is associated with impaired arterial elasticity. Atherosclerosis *218*, 90–95.

Patel, S., Puranik, R., Nakhla, S., Lundman, P., Stocker, R., Wang, X.S., Lambert, G., Rye, K.-A., Barter, P.J., Nicholls, S.J., et al. (2009). Acute hypertriglyceridaemia in humans increases the triglyceride content and decreases the anti-inflammatory capacity of high density lipoproteins. Atherosclerosis *204*, 424–428.

Paulson, K.E., Zhu, S.-N., Chen, M., Nurmohamed, S., Jongstra-Bilen, J., and Cybulsky, M.I. (2010). Resident intimal dendritic cells accumulate lipid and contribute to the initiation of atherosclerosis. Circ. Res. *106*, 383–390.

Pedersen, B.K., and Saltin, B. (2015). Exercise as medicine - evidence for prescribing exercise as therapy in 26 different chronic diseases. Scand. J. Med. Sci. Sports *25 Suppl 3*, 1–72.

Pedersen, S.F., Sandholt, B.V., Keller, S.H., Hansen, A.E., Clemmensen, A.E., Sillesen, H., Højgaard, L., Ripa, R.S., and Kjær, A. (2015). 64Cu-DOTATATE PET/MRI for Detection of Activated Macrophages in Carotid Atherosclerotic Plaques: Studies in Patients Undergoing Endarterectomy. Arterioscler. Thromb. Vasc. Biol. *35*, 1696–1703.

Pedro, L.M., Sanches, J.M., Seabra, J., Suri, J.S., and Fernandes E Fernandes, J. (2014). Asymptomatic carotid disease--a new tool for assessing neurological risk. Echocardiogr. Mt. Kisco N *31*, 353–361.

Peluso, I., Morabito, G., Urban, L., Ioannone, F., and Serafini, M. (2012). Oxidative stress in atherosclerosis development: the central role of LDL and oxidative burst. Endocr. Metab. Immune Disord. Drug Targets *12*, 351–360.

Piepoli, M.F., Hoes, A.W., Agewall, S., Albus, C., Brotons, C., Catapano, A.L., Cooney, M.-T., Corrà, U., Cosyns, B., Deaton, C., et al. (2016). 2016 European Guidelines on cardiovascular disease prevention in clinical practice: The Sixth Joint Task Force of the European Society of Cardiology and Other Societies on Cardiovascular Disease Prevention in Clinical Practice (constituted by representatives of 10 societies and by invited experts)Developed with the special contribution of the European Association for Cardiovascular Prevention & Rehabilitation (EACPR). Eur. Heart J. *37*, 2315–2381.

Podrez, E.A., Schmitt, D., Hoff, H.F., and Hazen, S.L. (1999). Myeloperoxidase-generated reactive nitrogen species convert LDL into an atherogenic form in vitro. J. Clin. Invest. *103*, 1547–1560.

Polak, J.F., Pencina, M.J., Pencina, K.M., O'Donnell, C.J., Wolf, P.A., and D'Agostino, R.B. (2011). Carotid-wall intima-media thickness and cardiovascular events. N. Engl. J. Med. *365*, 213–221.

Pooler, A.M., Xi, S.C., and Wurtman, R.J. (2006). The 3-hydroxy-3-methylglutaryl co-enzyme A reductase inhibitor pravastatin enhances neurite outgrowth in hippocampal neurons. J. Neurochem. *97*, 716–723.

Porcheray, F., Viaud, S., Rimaniol, A.-C., Léone, C., Samah, B., Dereuddre-Bosquet, N., Dormont, D., and Gras, G. (2005). Macrophage activation switching: an asset for the resolution of inflammation. Clin. Exp. Immunol. *142*, 481–489.

Preis, S.R., Massaro, J.M., Robins, S.J., Hoffmann, U., Vasan, R.S., Irlbeck, T., Meigs, J.B., Sutherland, P., D'Agostino, R.B., O'Donnell, C.J., et al. (2010). Abdominal subcutaneous and visceral adipose tissue and insulin resistance in the Framingham heart study. Obes. Silver Spring Md *18*, 2191–2198.

Pugliese, F., Gaemperli, O., Kinderlerer, A.R., Lamare, F., Shalhoub, J., Davies, A.H., Rimoldi, O.E., Mason, J.C., and Camici, P.G. (2010). Imaging of vascular inflammation with [11C]-PK11195 and positron emission tomography/computed tomography angiography. J. Am. Coll. Cardiol. *56*, 653–661.

Putti, R., Migliaccio, V., Sica, R., and Lionetti, L. (2015). Skeletal Muscle Mitochondrial Bioenergetics and Morphology in High Fat Diet Induced Obesity and Insulin Resistance: Focus on Dietary Fat Source. Front. Physiol. *6*, 426.

Quirce, R., Martínez-Rodríguez, I., De Arcocha Torres, M., Jiménez-Bonilla, J.F., Banzo, I., Rebollo, M., Revilla, M.A., Palacio, E., Rubio-Vassallo, A., Ortega-Nava, F., et al. (2013). Contribution of 18F-

sodium fluoride PET/CT to the study of the carotid atheroma calcification. Rev. Esp. Med. Nucl. E Imagen Mol. *32*, 22–25.

Rabinovitch, M. (1995). Elastase and cell matrix interactions in the pathobiology of vascular disease. Acta Paediatr. Jpn. Overseas Ed. *37*, 657–666.

Raghavendra Rao, V.L., Dogan, A., Bowen, K.K., and Dempsey, R.J. (2000). Traumatic brain injury leads to increased expression of peripheral-type benzodiazepine receptors, neuronal death, and activation of astrocytes and microglia in rat thalamus. Exp. Neurol. *161*, 102–114.

Raines, E.W. (2004). PDGF and cardiovascular disease. Cytokine Growth Factor Rev. *15*, 237–254.

Ramlackhansingh, A.F., Brooks, D.J., Greenwood, R.J., Bose, S.K., Turkheimer, F.E., Kinnunen, K.M., Gentleman, S., Heckemann, R.A., Gunanayagam, K., Gelosa, G., et al. (2011). Inflammation after trauma: microglial activation and traumatic brain injury. Ann. Neurol. *70*, 374–383.

Ramsay, S.C., Weiller, C., Myers, R., Cremer, J.E., Luthra, S.K., Lammertsma, A.A., and Frackowiak, R.S. (1992). Monitoring by PET of macrophage accumulation in brain after ischaemic stroke. Lancet Lond. Engl. *339*, 1054–1055.

Randolph, G.J. (2014). Mechanisms that regulate macrophage burden in atherosclerosis. Circ. Res. *114*, 1757–1771.

Rastogi, S., Rizwani, W., Joshi, B., Kunigal, S., and Chellappan, S.P. (2012). TNF-α response of vascular endothelial and vascular smooth muscle cells involve differential utilization of ASK1 kinase and p73. Cell Death Differ. *19*, 274–283.

Razani, B., Feng, C., Coleman, T., Emanuel, R., Wen, H., Hwang, S., Ting, J.P., Virgin, H.W., Kastan, M.B., and Semenkovich, C.F. (2012). Autophagy links inflammasomes to atherosclerotic progression. Cell Metab. *15*, 534–544.

Rebeck, G.W., Reiter, J.S., Strickland, D.K., and Hyman, B.T. (1993). Apolipoprotein E in sporadic Alzheimer's disease: allelic variation and receptor interactions. Neuron *11*, 575–580.

Ren, X., Akiyoshi, K., Dziennis, S., Vandenbark, A.A., Herson, P.S., Hurn, P.D., and Offner, H. (2011). Regulatory B cells limit CNS inflammation and neurologic deficits in murine experimental stroke. J. Neurosci. Off. J. Soc. Neurosci. *31*, 8556–8563.

Ridker, P.M. (2016a). A Test in Context. J. Am. Coll. Cardiol. *67*, 712–723.

Ridker, P.M. (2016b). From C-Reactive Protein to Interleukin-6 to Interleukin-1: Moving Upstream To Identify Novel Targets for Atheroprotection. Circ. Res. *118*, 145–156.

Ridker, P.M., and Lüscher, T.F. (2014). Anti-inflammatory therapies for cardiovascular disease. Eur. Heart J. *35*, 1782–1791.

Ridker, P.M., Cushman, M., Stampfer, M.J., Tracy, R.P., and Hennekens, C.H. (1997). Inflammation, aspirin, and the risk of cardiovascular disease in apparently healthy men. N. Engl. J. Med. *336*, 973–979.

Ridker, P.M., Hennekens, C.H., Buring, J.E., and Rifai, N. (2000a). C-reactive protein and other markers of inflammation in the prediction of cardiovascular disease in women. N. Engl. J. Med. *342*, 836–843.

Ridker, P.M., Rifai, N., Stampfer, M.J., and Hennekens, C.H. (2000b). Plasma concentration of interleukin-6 and the risk of future myocardial infarction among apparently healthy men. Circulation *101*, 1767–1772.

Ridker, P.M., Rifai, N., Rose, L., Buring, J.E., and Cook, N.R. (2002). Comparison of C-reactive protein and low-density lipoprotein cholesterol levels in the prediction of first cardiovascular events. N. Engl. J. Med. *347*, 1557–1565.

Ridker, P.M., MacFadyen, J., Libby, P., and Glynn, R.J. (2010). Relation of baseline high-sensitivity C-reactive protein level to cardiovascular outcomes with rosuvastatin in the Justification for Use of statins in Prevention: an Intervention Trial Evaluating Rosuvastatin (JUPITER). Am. J. Cardiol. *106*, 204–209.

Ridker, P.M., Thuren, T., Zalewski, A., and Libby, P. (2011). Interleukin-1β inhibition and the prevention of recurrent cardiovascular events: rationale and design of the Canakinumab Anti-inflammatory Thrombosis Outcomes Study (CANTOS). Am. Heart J. *162*, 597–605.

Rinta-Kiikka, I., Tuohinen, S., Ryymin, P., Kosonen, P., Huhtala, H., Gorgels, A., Bayés de Luna, A., and Nikus, K. (2014). Correlation of electrocardiogram and regional cardiac magnetic resonance imaging findings in ST-elevation myocardial infarction: a literature review. Ann. Noninvasive Electrocardiol. Off. J. Int. Soc. Holter Noninvasive Electrocardiol. Inc *19*, 509–523.

Ritzenthaler, T., Lhommeau, I., Douillard, S., Cho, T.H., Brun, J., Patrice, T., Nighoghossian, N., and Claustrat, B. (2013). Dynamics of oxidative stress and urinary excretion of melatonin and its metabolites during acute ischemic stroke. Neurosci. Lett. *544*, 1–4.

Riwanto, M., Rohrer, L., Roschitzki, B., Besler, C., Mocharla, P., Mueller, M., Perisa, D., Heinrich, K., Altwegg, L., von Eckardstein, A., et al. (2013). Altered activation of endothelial anti- and proapoptotic pathways by high-density lipoprotein from patients with coronary artery disease: role of high-density lipoprotein-proteome remodeling. Circulation *127*, 891–904.

Robbins, C.S., Hilgendorf, I., Weber, G.F., Theurl, I., Iwamoto, Y., Figueiredo, J.-L., Gorbatov, R., Sukhova, G.K., Gerhardt, L.M.S., Smyth, D., et al. (2013). Local proliferation dominates lesional macrophage accumulation in atherosclerosis. Nat. Med. *19*, 1166–1172.

Robinson, J.G., Smith, B., Maheshwari, N., and Schrott, H. (2005). Pleiotropic effects of statins: benefit beyond cholesterol reduction? A meta-regression analysis. J. Am. Coll. Cardiol. *46*, 1855–1862.

Rocha, V.Z., and Libby, P. (2009). Obesity, inflammation, and atherosclerosis. Nat. Rev. Cardiol. *6*, 399–409.

Rodríguez, J.J., Noristani, H.N., Hilditch, T., Olabarria, M., Yeh, C.Y., Witton, J., and Verkhratsky, A. (2013). Increased densities of resting and activated microglia in the dentate gyrus follow senile plaque formation in the CA1 subfield of the hippocampus in the triple transgenic model of Alzheimer's disease. Neurosci. Lett. *552*, 129–134.

Rominger, A., Saam, T., Vogl, E., Ubleis, C., la Fougère, C., Förster, S., Haug, A., Cumming, P., Reiser, M.F., Nikolaou, K., et al. (2010). In vivo imaging of macrophage activity in the coronary arteries using 68Ga-DOTATATE PET/CT: correlation with coronary calcium burden and risk factors. J. Nucl. Med. Off. Publ. Soc. Nucl. Med. *51*, 193–197.

Rosenfeld, M.E. (2014). Macrophage proliferation in atherosclerosis: an historical perspective. Arterioscler. Thromb. Vasc. Biol. *34*, e21-22.

Rosenfeld, M.E., Polinsky, P., Virmani, R., Kauser, K., Rubanyi, G., and Schwartz, S.M. (2000). Advanced atherosclerotic lesions in the innominate artery of the ApoE knockout mouse. Arterioscler. Thromb. Vasc. Biol. *20*, 2587–2592.

Rosenson, R.S., Davidson, M.H., Hirsh, B.J., Kathiresan, S., and Gaudet, D. (2014). Genetics and causality of triglyceride-rich lipoproteins in atherosclerotic cardiovascular disease. J. Am. Coll. Cardiol. *64*, 2525–2540.

Rosenthal, A., Jaffer, F.A., and Ntziachristos, V. (2012). Intravascular multispectral optoacoustic tomography of atherosclerosis: prospects and challenges. Imaging Med. *4*, 299–310.

Ross, R. (1999). Atherosclerosis—an inflammatory disease. N. Engl. J. Med. *340*, 115–126.

Ross, R., de Lannoy, L., and Stotz, P.J. (2015). Separate Effects of Intensity and Amount of Exercise on Interindividual Cardiorespiratory Fitness Response. Mayo Clin. Proc. *90*, 1506–1514.

Rossebø, A.B., Pedersen, T.R., Boman, K., Brudi, P., Chambers, J.B., Egstrup, K., Gerdts, E., Gohlke-Bärwolf, C., Holme, I., Kesäniemi, Y.A., et al. (2008). Intensive lipid lowering with simvastatin and ezetimibe in aortic stenosis. N. Engl. J. Med. *359*, 1343–1356.

Rost, N.S., Wolf, P.A., Kase, C.S., Kelly-Hayes, M., Silbershatz, H., Massaro, J.M., D'Agostino, R.B., Franzblau, C., and Wilson, P.W. (2001). Plasma concentration of C-reactive protein and risk of ischemic stroke and transient ischemic attack: the Framingham study. Stroke J. Cereb. Circ. *32*, 2575–2579.

Roth, J., Harré, E.-M., Rummel, C., Gerstberger, R., and Hübschle, T. (2004). Signaling the brain in systemic inflammation: role of sensory circumventricular organs. Front. Biosci. J. Virtual Libr. *9*, 290–300.

Rousselle, A., Qadri, F., Leukel, L., Yilmaz, R., Fontaine, J.-F., Sihn, G., Bader, M., Ahluwalia, A., and Duchene, J. (2013). CXCL5 limits macrophage foam cell formation in atherosclerosis. J. Clin. Invest. *123*, 1343–1347.

Rudd, J.H.F., Warburton, E.A., Fryer, T.D., Jones, H.A., Clark, J.C., Antoun, N., Johnström, P., Davenport, A.P., Kirkpatrick, P.J., Arch, B.N., et al. (2002). Imaging atherosclerotic plaque inflammation with [18F]-fluorodeoxyglucose positron emission tomography. Circulation *105*, 2708–2711.

Rudd, J.H.F., Myers, K.S., Bansilal, S., Machac, J., Woodward, M., Fuster, V., Farkouh, M.E., and Fayad, Z.A. (2009). Relationships among regional arterial inflammation, calcification, risk factors, and biomarkers: a prospective fluorodeoxyglucose positron-emission tomography/computed tomography imaging study. Circ. Cardiovasc. Imaging *2*, 107–115.

Runge, V.M., Clanton, J.A., Price, A.C., Wehr, C.J., Herzer, W.A., Partain, C.L., and James, A.E. (1985). The use of Gd DTPA as a perfusion agent and marker of blood-brain barrier disruption. Magn. Reson. Imaging *3*, 43–55.

Rupprecht, R., Papadopoulos, V., Rammes, G., Baghai, T.C., Fan, J., Akula, N., Groyer, G., Adams, D., and Schumacher, M. (2010). Translocator protein (18 kDa) (TSPO) as a therapeutic target for neurological and psychiatric disorders. Nat. Rev. Drug Discov. *9*, 971–988.

Saavedra, J.M. (2012). Angiotensin II AT(1) receptor blockers ameliorate inflammatory stress: a beneficial effect for the treatment of brain disorders. Cell. Mol. Neurobiol. *32*, 667–681.

Sabatine, M.S., Wasserman, S.M., and Stein, E.A. (2015). PCSK9 Inhibitors and Cardiovascular Events. N. Engl. J. Med. *373*, 774–775.

Sacco, R.L., Benson, R.T., Kargman, D.E., Boden-Albala, B., Tuck, C., Lin, I.F., Cheng, J.F., Paik, M.C., Shea, S., and Berglund, L. (2001). High-density lipoprotein cholesterol and ischemic stroke in the elderly: the Northern Manhattan Stroke Study. JAMA *285*, 2729–2735.

Sacks, F.M., Pfeffer, M.A., Moye, L.A., Rouleau, J.L., Rutherford, J.D., Cole, T.G., Brown, L., Warnica, J.W., Arnold, J.M., Wun, C.C., et al. (1996). The effect of pravastatin on coronary events after myocardial infarction in patients with average cholesterol levels. Cholesterol and Recurrent Events Trial investigators. N. Engl. J. Med. *335*, 1001–1009.

Sadat, U., Jaffer, F.A., van Zandvoort, M.A.M.J., Nicholls, S.J., Ribatti, D., and Gillard, J.H. (2014). Inflammation and neovascularization intertwined in atherosclerosis: imaging of structural and molecular imaging targets. Circulation *130*, 786–794.

Saher, G., Brügger, B., Lappe-Siefke, C., Möbius, W., Tozawa, R., Wehr, M.C., Wieland, F., Ishibashi, S., and Nave, K.-A. (2005). High cholesterol level is essential for myelin membrane growth. Nat. Neurosci. *8*, 468–475.

Sakakura, K., Nakano, M., Otsuka, F., Ladich, E., Kolodgie, F.D., and Virmani, R. (2013). Pathophysiology of atherosclerosis plaque progression. Heart Lung Circ. *22*, 399–411.

Saleh, A., Schroeter, M., Jonkmanns, C., Hartung, H.-P., Mödder, U., and Jander, S. (2004). In vivo MRI of brain inflammation in human ischaemic stroke. Brain J. Neurol. *127*, 1670–1677.

Salem, M.K., Bown, M.J., Sayers, R.D., West, K., Moore, D., Nicolaides, A., Robinson, T.G., and Naylor, A.R. (2014). Identification of patients with a histologically unstable carotid plaque using ultrasonic plaque image analysis. Eur. J. Vasc. Endovasc. Surg. Off. J. Eur. Soc. Vasc. Surg. *48*, 118–125.

Salmon, D.M., and Hems, D.A. (1973). Plasma lipoproteins and the synthesis and turnover of plasma triglyceride in normal and genetically obese mice. Biochem. J. *136*, 551–563.

Santos, R.D., Nasir, K., Conceição, R.D., Sarwar, A., Carvalho, J.A.M., and Blumenthal, R.S. (2007). Hepatic steatosis is associated with a greater prevalence of coronary artery calcification in asymptomatic men. Atherosclerosis *194*, 517–519.

Scandinavian Simvastatin Survival Study Group (1994). Randomised trial of cholesterol lowering in 4444 patients with coronary heart disease: the Scandinavian Simvastatin Survival Study (4S). Lancet Lond. Engl. *344*, 1383–1389.

Schieffer, B., Selle, T., Hilfiker, A., Hilfiker-Kleiner, D., Grote, K., Tietge, U.J.F., Trautwein, C., Luchtefeld, M., Schmittkamp, C., Heeneman, S., et al. (2004). Impact of interleukin-6 on plaque development and morphology in experimental atherosclerosis. Circulation *110*, 3493–3500.

Schindhelm, R.K., van der Zwan, L.P., Teerlink, T., and Scheffer, P.G. (2009). Myeloperoxidase: a useful biomarker for cardiovascular disease risk stratification? Clin. Chem. *55*, 1462–1470.

Schlitt, A., Heine, G.H., Blankenberg, S., Espinola-Klein, C., Dopheide, J.F., Bickel, C., Lackner, K.J., Iz, M., Meyer, J., Darius, H., et al. (2004). CD14+CD16+ monocytes in coronary artery disease and their relationship to serum TNF-alpha levels. Thromb. Haemost. *92*, 419–424.

Schmidt-Ott, K.M., Kagiyama, S., and Phillips, M.I. (2000). The multiple actions of angiotensin II in atherosclerosis. Regul. Pept. *93*, 65–77.

Schumacher, A., Peersen, K., Sommervoll, L., Seljeflot, I., Arnesen, H., and Otterstad, J.E. (2006). Physical performance is associated with markers of vascular inflammation in patients with coronary heart disease. Eur. J. Cardiovasc. Prev. Rehabil. Off. J. Eur. Soc. Cardiol. Work. Groups Epidemiol. Prev. Card. Rehabil. Exerc. Physiol. *13*, 356–362.

Schwartz, E.A., and Reaven, P.D. (2012). Lipolysis of triglyceride-rich lipoproteins, vascular inflammation, and atherosclerosis. Biochim. Biophys. Acta *1821*, 858–866.

Schwartz, M., and Baruch, K. (2014). The resolution of neuroinflammation in neurodegeneration: leukocyte recruitment via the choroid plexus. EMBO J. *33*, 7–22.

Selmeci, L., Székely, M., Soós, P., Seres, L., Klinga, N., Geiger, A., and Acsády, G. (2006). Human blood plasma advanced oxidation protein products (AOPP) correlates with fibrinogen levels. Free Radic. Res. *40*, 952–958.

Selvaraj, V., and Stocco, D.M. (2015). The changing landscape in translocator protein (TSPO) function. Trends Endocrinol. Metab. *26*, 341–348.

Serres, S., Anthony, D.C., Jiang, Y., Broom, K.A., Campbell, S.J., Tyler, D.J., van Kasteren, S.I., Davis, B.G., and Sibson, N.R. (2009). Systemic inflammatory response reactivates immune-mediated lesions in rat brain. J. Neurosci. Off. J. Soc. Neurosci. *29*, 4820–4828.

Shahar, E., Chambless, L.E., Rosamond, W.D., Boland, L.L., Ballantyne, C.M., McGovern, P.G., Sharrett, A.R., and Atherosclerosis Risk in Communities Study (2003). Plasma lipid profile and incident ischemic stroke: the Atherosclerosis Risk in Communities (ARIC) study. Stroke J. Cereb. Circ. *34*, 623–631.

Sharp, F.R., Jickling, G.C., Stamova, B., Tian, Y., Zhan, X., Liu, D., Kuczynski, B., Cox, C.D., and Ander, B.P. (2011). Molecular markers and mechanisms of stroke: RNA studies of blood in animals and humans. J. Cereb. Blood Flow Metab. Off. J. Int. Soc. Cereb. Blood Flow Metab. *31*, 1513–1531.

Shih, C.-K., Chang, J.-H., Yang, S.-H., Chou, T.-W., and Cheng, H.-H. (2008). beta-Carotene and canthaxanthin alter the pro-oxidation and antioxidation balance in rats fed a high-cholesterol and high-fat diet. Br. J. Nutr. *99*, 59–66.

Shnyra, A., Brewington, R., Alipio, A., Amura, C., and Morrison, D.C. (1998). Reprogramming of lipopolysaccharide-primed macrophages is controlled by a counterbalanced production of IL-10 and IL-12. J. Immunol. Baltim. Md 1950 *160*, 3729–3736.

Shoelson, S.E., Lee, J., and Goldfine, A.B. (2006). Inflammation and insulin resistance. J. Clin. Invest. *116*, 1793–1801.

Sileikyte, J., Blachly-Dyson, E., Sewell, R., Carpi, A., Menabo, R., Di Lisa, F., Ricchelli, F., Bernardi, P., and Forte, M. (2014). Regulation of the Mitochondrial Permeability Transition Pore by the Outer Membrane Does Not Involve the Peripheral Benzodiazepine Receptor (Translocator Protein of 18 kDa (TSPO)). J. Biol. Chem. *289*, 13769–13781.

Silvera, S.S., Aidi, H.E., Rudd, J.H.F., Mani, V., Yang, L., Farkouh, M., Fuster, V., and Fayad, Z.A. (2009). Multimodality imaging of atherosclerotic plaque activity and composition using FDG-PET/CT and MRI in carotid and femoral arteries. Atherosclerosis *207*, 139–143.

Singh, N., Moody, A.R., Gladstone, D.J., Leung, G., Ravikumar, R., Zhan, J., and Maggisano, R. (2009). Moderate carotid artery stenosis: MR imaging-depicted intraplaque hemorrhage predicts risk of cerebrovascular ischemic events in asymptomatic men. Radiology *252*, 502–508.

Sjögren, P., Cederholm, T., Heimbürger, M., Stenvinkel, P., Vedin, I., Palmblad, J., and Hellenius, M.-L. (2010). Simple advice on lifestyle habits and long-term changes in biomarkers of inflammation and vascular adhesion in healthy middle-aged men. Eur. J. Clin. Nutr. *64*, 1450–1456.

Skold, B.H., Getty, R., and Ramsey, F.K. (1966). Spontaneous atherosclerosis in the arterial system of aging swine. Am. J. Vet. Res. *27*, 257–273.

Skoog, T., Dichtl, W., Boquist, S., Skoglund-Andersson, C., Karpe, F., Tang, R., Bond, M.G., de Faire, U., Nilsson, J., Eriksson, P., et al. (2002). Plasma tumour necrosis factor-alpha and early carotid atherosclerosis in healthy middle-aged men. Eur. Heart J. *23*, 376–383.

Smith, C.J., Emsley, H.C.A., Gavin, C.M., Georgiou, R.F., Vail, A., Barberan, E.M., del Zoppo, G.J., Hallenbeck, J.M., Rothwell, N.J., Hopkins, S.J., et al. (2004). Peak plasma interleukin-6 and other peripheral markers of inflammation in the first week of ischaemic stroke correlate with brain infarct volume, stroke severity and long-term outcome. BMC Neurol. *4*, 2.

Smith, D.A., Irving, S.D., Sheldon, J., Cole, D., and Kaski, J.C. (2001). Serum levels of the antiinflammatory cytokine interleukin-10 are decreased in patients with unstable angina. Circulation *104*, 746–749.

Smith, J.D., Borel, A.-L., Nazare, J.-A., Haffner, S.M., Balkau, B., Ross, R., Massien, C., Alméras, N., and Després, J.-P. (2012). Visceral adipose tissue indicates the severity of cardiometabolic risk in patients with and without type 2 diabetes: results from the INSPIRE ME IAA study. J. Clin. Endocrinol. Metab. *97*, 1517–1525.

Spann, N.J., Garmire, L.X., McDonald, J.G., Myers, D.S., Milne, S.B., Shibata, N., Reichart, D., Fox, J.N., Shaked, I., Heudobler, D., et al. (2012). Regulated accumulation of desmosterol integrates macrophage lipid metabolism and inflammatory responses. Cell *151*, 138–152.

Speliotes, E.K., Massaro, J.M., Hoffmann, U., Vasan, R.S., Meigs, J.B., Sahani, D.V., Hirschhorn, J.N., O'Donnell, C.J., and Fox, C.S. (2010). Fatty liver is associated with dyslipidemia and dysglycemia independent of visceral fat: the Framingham Heart Study. Hepatol. Baltim. Md *51*, 1979–1987.

Spence, J.D. (2006). Technology Insight: ultrasound measurement of carotid plaque--patient management, genetic research, and therapy evaluation. Nat. Clin. Pract. Neurol. *2*, 611–619.

Stamler, J. (1993). Dietary salt and blood pressure. Ann. N. Y. Acad. Sci. *676*, 122–156.

Stamler, J., Wentworth, D., and Neaton, J.D. (1986). Is relationship between serum cholesterol and risk of premature death from coronary heart disease continuous and graded? Findings in 356,222 primary screenees of the Multiple Risk Factor Intervention Trial (MRFIT). JAMA *256*, 2823–2828.

Stampfer, M.J., Krauss, R.M., Ma, J., Blanche, P.J., Holl, L.G., Sacks, F.M., and Hennekens, C.H. (1996). A prospective study of triglyceride level, low-density lipoprotein particle diameter, and risk of myocardial infarction. JAMA *276*, 882–888.

Stanhope, K.L., Medici, V., Bremer, A.A., Lee, V., Lam, H.D., Nunez, M.V., Chen, G.X., Keim, N.L., and Havel, P.J. (2015). A dose-response study of consuming high-fructose corn syrup-sweetened beverages on lipid/lipoprotein risk factors for cardiovascular disease in young adults. Am. J. Clin. Nutr. *101*, 1144–1154.

Stary, H.C., Chandler, A.B., Dinsmore, R.E., Fuster, V., Glagov, S., Insull, W., Rosenfeld, M.E., Schwartz, C.J., Wagner, W.D., and Wissler, R.W. (1995). A definition of advanced types of atherosclerotic lesions and a histological classification of atherosclerosis. A report from the Committee on Vascular Lesions of the Council on Arteriosclerosis, American Heart Association. Arterioscler. Thromb. Vasc. Biol. *15*, 1512–1531.

Stegemann, C., Drozdov, I., Shalhoub, J., Humphries, J., Ladroue, C., Didangelos, A., Baumert, M., Allen, M., Davies, A.H., Monaco, C., et al. (2011). Comparative lipidomics profiling of human atherosclerotic plaques. Circ. Cardiovasc. Genet. *4*, 232–242.

Stein, M., Keshav, S., Harris, N., and Gordon, S. (1992). Interleukin 4 potently enhances murine macrophage mannose receptor activity: a marker of alternative immunologic macrophage activation. J. Exp. Med. *176*, 287–292.

Steinberg, D., Parthasarathy, S., Carew, T.E., Khoo, J.C., and Witztum, J.L. (1989). Beyond cholesterol. Modifications of low-density lipoprotein that increase its atherogenicity. N. Engl. J. Med. *320*, 915–924.

Steinl, D.C., and Kaufmann, B.A. (2015). Ultrasound imaging for risk assessment in atherosclerosis. Int. J. Mol. Sci. *16*, 9749–9769.

Stephens, N.G., Parsons, A., Schofield, P.M., Kelly, F., Cheeseman, K., and Mitchinson, M.J. (1996). Randomised controlled trial of vitamin E in patients with coronary disease: Cambridge Heart Antioxidant Study (CHAOS). Lancet Lond. Engl. *347*, 781–786.

Stoneman, V., Braganza, D., Figg, N., Mercer, J., Lang, R., Goddard, M., and Bennett, M. (2007). Monocyte/macrophage suppression in CD11b diphtheria toxin receptor transgenic mice differentially affects atherogenesis and established plaques. Circ. Res. *100*, 884–893.

Stout, R.D., Jiang, C., Matta, B., Tietzel, I., Watkins, S.K., and Suttles, J. (2005). Macrophages sequentially change their functional phenotype in response to changes in microenvironmental influences. J. Immunol. Baltim. Md 1950 *175*, 342–349.

Strauss-Ayali, D., Conrad, S.M., and Mosser, D.M. (2007). Monocyte subpopulations and their differentiation patterns during infection. J. Leukoc. Biol. *82*, 244–252.

Sunderkötter, C., Nikolic, T., Dillon, M.J., Van Rooijen, N., Stehling, M., Drevets, D.A., and Leenen, P.J.M. (2004). Subpopulations of mouse blood monocytes differ in maturation stage and inflammatory response. J. Immunol. Baltim. Md 1950 *172*, 4410–4417.

Sung, K.-C., Wild, S.H., Kwag, H.J., and Byrne, C.D. (2012). Fatty liver, insulin resistance, and features of metabolic syndrome: relationships with coronary artery calcium in 10,153 people. Diabetes Care *35*, 2359–2364.

Survase, S., Ivey, M.E., Nigro, J., Osman, N., and Little, P.J. (2005). Actions of calcium channel blockers on vascular proteoglycan synthesis: relationship to atherosclerosis. Vasc. Health Risk Manag. *1*, 199–208.

Suzuki, S., Tanaka, K., and Suzuki, N. (2009). Ambivalent aspects of interleukin-6 in cerebral ischemia: inflammatory versus neurotrophic aspects. J. Cereb. Blood Flow Metab. Off. J. Int. Soc. Cereb. Blood Flow Metab. *29*, 464–479.

Swift, D.L., Lavie, C.J., Johannsen, N.M., Arena, R., Earnest, C.P., O'Keefe, J.H., Milani, R.V., Blair, S.N., and Church, T.S. (2013). Physical activity, cardiorespiratory fitness, and exercise training in primary and secondary coronary prevention. Circ. J. Off. J. Jpn. Circ. Soc. *77*, 281–292.

Swirski, F.K., Libby, P., Aikawa, E., Alcaide, P., Luscinskas, F.W., Weissleder, R., and Pittet, M.J. (2007). Ly-6Chi monocytes dominate hypercholesterolemia-associated monocytosis and give rise to macrophages in atheromata. J. Clin. Invest. *117*, 195–205.

Tabas, I. (2010a). The role of endoplasmic reticulum stress in the progression of atherosclerosis. Circ. Res. *107*, 839–850.

Tabas, I. (2010b). Macrophage death and defective inflammation resolution in atherosclerosis. Nat. Rev. Immunol. *10*, 36–46.

Tabas, I., and Bornfeldt, K.E. (2016). Macrophage Phenotype and Function in Different Stages of Atherosclerosis. Circ. Res. *118*, 653–667.

Takaya, N., Yuan, C., Chu, B., Saam, T., Underhill, H., Cai, J., Tran, N., Polissar, N.L., Isaac, C., Ferguson, M.S., et al. (2006). Association between carotid plaque characteristics and subsequent ischemic cerebrovascular events: a prospective assessment with MRI--initial results. Stroke J. Cereb. Circ. *37*, 818–823.

Takeda, S., Sato, N., Ogihara, T., and Morishita, R. (2008). The renin-angiotensin system, hypertension and cognitive dysfunction in Alzheimer's disease: new therapeutic potential. Front. Biosci. J. Virtual Libr. *13*, 2253–2265.

Takemoto, M., Node, K., Nakagami, H., Liao, Y., Grimm, M., Takemoto, Y., Kitakaze, M., and Liao, J.K. (2001). Statins as antioxidant therapy for preventing cardiac myocyte hypertrophy. J. Clin. Invest. *108*, 1429–1437.

Tall, A.R., and Yvan-Charvet, L. (2015). Cholesterol, inflammation and innate immunity. Nat. Rev. Immunol. *15*, 104–116.

Tancredi, V., D'Antuono, M., Cafè, C., Giovedì, S., Buè, M.C., D'Arcangelo, G., Onofri, F., and Benfenati, F. (2000). The inhibitory effects of interleukin-6 on synaptic plasticity in the rat hippocampus are associated with an inhibition of mitogen-activated protein kinase ERK. J. Neurochem. *75*, 634–643.

Tang, T.Y., Howarth, S.P.S., Miller, S.R., Graves, M.J., Patterson, A.J., U-King-Im, J.-M., Li, Z.Y., Walsh, S.R., Brown, A.P., Kirkpatrick, P.J., et al. (2009). The ATHEROMA (Atorvastatin Therapy: Effects on Reduction of Macrophage Activity) Study. Evaluation using ultrasmall superparamagnetic iron oxide-enhanced magnetic resonance imaging in carotid disease. J. Am. Coll. Cardiol. *53*, 2039–2050.

Tannahill, G.M., and O'Neill, L.A.J. (2011). The emerging role of metabolic regulation in the functioning of Toll-like receptors and the NOD-like receptor Nlrp3. FEBS Lett. *585*, 1568–1572.

Tannock, L.R., O'Brien, K.D., Knopp, R.H., Retzlaff, B., Fish, B., Wener, M.H., Kahn, S.E., and Chait, A. (2005). Cholesterol feeding increases C-reactive protein and serum amyloid A levels in lean insulin-sensitive subjects. Circulation *111*, 3058–3062.

Targher, G., Day, C.P., and Bonora, E. (2010). Risk of cardiovascular disease in patients with nonalcoholic fatty liver disease. N. Engl. J. Med. *363*, 1341–1350.

Tarkowski, E., Rosengren, L., Blomstrand, C., Wikkelsö, C., Jensen, C., Ekholm, S., and Tarkowski, A. (1995). Early intrathecal production of interleukin-6 predicts the size of brain lesion in stroke. Stroke J. Cereb. Circ. *26*, 1393–1398.

Taschner, C.A., Wetzel, S.G., Tolnay, M., Froehlich, J., Merlo, A., and Radue, E.W. (2005). Characteristics of ultrasmall superparamagnetic iron oxides in patients with brain tumors. AJR Am. J. Roentgenol. *185*, 1477–1486.

Tatano, Y., Shimizu, T., and Tomioka, H. (2014). Unique macrophages different from M1/M2 macrophages inhibit T cell mitogenesis while upregulating Th17 polarization. Sci. Rep. *4*, 4146.

Tawakol, A., Migrino, R.Q., Bashian, G.G., Bedri, S., Vermylen, D., Cury, R.C., Yates, D., LaMuraglia, G.M., Furie, K., Houser, S., et al. (2006). In vivo 18F-fluorodeoxyglucose positron emission tomography imaging provides a noninvasive measure of carotid plaque inflammation in patients. J. Am. Coll. Cardiol. *48*, 1818–1824.

Tawakol, A., Singh, P., Mojena, M., Pimentel-Santillana, M., Emami, H., MacNabb, M., Rudd, J.H.F., Narula, J., Enriquez, J.A., Través, P.G., et al. (2015). HIF-1α and PFKFB3 Mediate a Tight Relationship Between Proinflammatory Activation and Anerobic Metabolism in Atherosclerotic Macrophages. Arterioscler. Thromb. Vasc. Biol. *35*, 1463–1471.

Taylor, J.M.W., Allen, A.-M., and Graham, A. (2014). Targeting mitochondrial 18 kDa translocator protein (TSPO) regulates macrophage cholesterol efflux and lipid phenotype. Clin. Sci. Lond. Engl. 1979 *127*, 603–613.

Teupser, D., Persky, A.D., and Breslow, J.L. (2003). Induction of atherosclerosis by low-fat, semisynthetic diets in LDL receptor-deficient C57BL/6J and FVB/NJ mice: comparison of lesions of the aortic root, brachiocephalic artery, and whole aorta (en face measurement). Arterioscler. Thromb. Vasc. Biol. *23*, 1907–1913.

Thanassoulis, G., Massaro, J.M., O'Donnell, C.J., Hoffmann, U., Levy, D., Ellinor, P.T., Wang, T.J., Schnabel, R.B., Vasan, R.S., Fox, C.S., et al. (2010). Pericardial fat is associated with prevalent atrial fibrillation: the Framingham Heart Study. Circ. Arrhythm. Electrophysiol. *3*, 345–350.

Thiel, A., Radlinska, B.A., Paquette, C., Sidel, M., Soucy, J.-P., Schirrmacher, R., and Minuk, J. (2010). The temporal dynamics of poststroke neuroinflammation: a longitudinal diffusion tensor imaging-guided PET study with 11C-PK11195 in acute subcortical stroke. J. Nucl. Med. Off. Publ. Soc. Nucl. Med. *51*, 1404–1412.

Thompson, P.D., Franklin, B.A., Balady, G.J., Blair, S.N., Corrado, D., Estes, N.A.M., Fulton, J.E., Gordon, N.F., Haskell, W.L., Link, M.S., et al. (2007). Exercise and acute cardiovascular events placing the risks into perspective: a scientific statement from the American Heart Association Council on Nutrition, Physical Activity, and Metabolism and the Council on Clinical Cardiology. Circulation *115*, 2358–2368.

Thorp, E., and Tabas, I. (2009). Mechanisms and consequences of efferocytosis in advanced atherosclerosis. J. Leukoc. Biol. *86*, 1089–1095.

Thorp, E., Li, G., Seimon, T.A., Kuriakose, G., Ron, D., and Tabas, I. (2009). Reduced apoptosis and plaque necrosis in advanced atherosclerotic lesions of Apoe-/- and Ldlr-/- mice lacking CHOP. Cell Metab. *9*, 474–481.

Tillett, W.S., and Francis, T. (1930). SEROLOGICAL REACTIONS IN PNEUMONIA WITH A NON-PROTEIN SOMATIC FRACTION OF PNEUMOCOCCUS. J. Exp. Med. *52*, 561–571.

Tiozzo, E., Gardener, H., Hudson, B.I., Dong, C., Della-Morte, D., Crisby, M., Goldberg, R.B., Elkind, M.S.V., Cheung, Y.K., Wright, C.B., et al. (2014). High-density lipoprotein subfractions and carotid plaque: the Northern Manhattan Study. Atherosclerosis *237*, 163–168.

Tiret, L., Godefroy, T., Lubos, E., Nicaud, V., Tregouet, D.-A., Barbaux, S., Schnabel, R., Bickel, C., Espinola-Klein, C., Poirier, O., et al. (2005). Genetic analysis of the interleukin-18 system highlights the role of the interleukin-18 gene in cardiovascular disease. Circulation *112*, 643–650.

Tirschwell, D.L., Smith, N.L., Heckbert, S.R., Lemaitre, R.N., Longstreth, W.T., and Psaty, B.M. (2004). Association of cholesterol with stroke risk varies in stroke subtypes and patient subgroups. Neurology *63*, 1868–1875.

Toole JF, Janeway R, Choi K, and et al (1975). Transient ischemic attacks due to atherosclerosis: A prospective study of 160 patients. Arch. Neurol. *32*, 5–12.

Topper, J.N., Cai, J., Falb, D., and Gimbrone, M.A. (1996). Identification of vascular endothelial genes differentially responsive to fluid mechanical stimuli: cyclooxygenase-2, manganese superoxide dismutase, and endothelial cell nitric oxide synthase are selectively up-regulated by steady laminar shear stress. Proc. Natl. Acad. Sci. U. S. A. *93*, 10417–10422.

Torzewski, M., Suriyaphol, P., Paprotka, K., Spath, L., Ochsenhirt, V., Schmitt, A., Han, S.-R., Husmann, M., Gerl, V.B., Bhakdi, S., et al. (2004). Enzymatic modification of low-density lipoprotein

in the arterial wall: a new role for plasmin and matrix metalloproteinases in atherogenesis. Arterioscler. Thromb. Vasc. Biol. *24*, 2130–2136.

Trivedi, R.A., U-King-Im, J., Graves, M.J., Horsley, J., Goddard, M., Kirkpatrick, P.J., and Gillard, J.H. (2004). Multi-sequence in vivo MRI can quantify fibrous cap and lipid core components in human carotid atherosclerotic plaques. Eur. J. Vasc. Endovasc. Surg. Off. J. Eur. Soc. Vasc. Surg. *28*, 207–213.

Trivedi, R.A., Mallawarachi, C., U-King-Im, J.-M., Graves, M.J., Horsley, J., Goddard, M.J., Brown, A., Wang, L., Kirkpatrick, P.J., Brown, J., et al. (2006). Identifying inflamed carotid plaques using in vivo USPIO-enhanced MR imaging to label plaque macrophages. Arterioscler. Thromb. Vasc. Biol. *26*, 1601–1606.

Tsiantoulas, D., Perkmann, T., Afonyushkin, T., Mangold, A., Prohaska, T.A., Papac-Milicevic, N., Millischer, V., Bartel, C., Hörkkö, S., Boulanger, C.M., et al. (2015). Circulating microparticles carry oxidation-specific epitopes and are recognized by natural IgM antibodies. J. Lipid Res. *56*, 440–448.

Uppoor, R.B., Rajesh, A., Srinivasan, M.P., Unnikrishnan, B., and Holla, R. (2015). Oxidative Stress in Obese Postmenopausal Women: An Additive Burden for Atherosclerosis. J. Clin. Diagn. Res. JCDR *9*, OC03-05.

US Department of Health and Human Services 2015-2020 Dietary Guidelines - health.gov.

Vakkilainen, J., Mäkimattila, S., Seppälä-Lindroos, A., Vehkavaara, S., Lahdenperä, S., Groop, P.H., Taskinen, M.R., and Yki-Järvinen, H. (2000). Endothelial dysfunction in men with small LDL particles. Circulation *102*, 716–721.

Van Eck, M., Herijgers, N., Vidgeon-Hart, M., Pearce, N.J., Hoogerbrugge, P.M., Groot, P.H., and Van Berkel, T.J. (2000). Accelerated atherosclerosis in C57Bl/6 mice transplanted with ApoE-deficient bone marrow. Atherosclerosis *150*, 71–80.

Van Lint, P., and Libert, C. (2007). Chemokine and cytokine processing by matrix metalloproteinases and its effect on leukocyte migration and inflammation. J. Leukoc. Biol. *82*, 1375–1381.

VanGilder, R.L., Davidov, D.M., Stinehart, K.R., Huber, J.D., Turner, R.C., Wilson, K.S., Haney, E., Davis, S.M., Chantler, P.D., Theeke, L., et al. (2014). C-reactive protein and long-term ischemic stroke prognosis. J. Clin. Neurosci. Off. J. Neurosurg. Soc. Australas. *21*, 547–553.

Vats, D., Mukundan, L., Odegaard, J.I., Zhang, L., Smith, K.L., Morel, C.R., Wagner, R.A., Greaves, D.R., Murray, P.J., and Chawla, A. (2006). Oxidative metabolism and PGC-1beta attenuate macrophage-mediated inflammation. Cell Metab. *4*, 13–24.

Verma, S., Eikelboom, J.W., Nidorf, S.M., Al-Omran, M., Gupta, N., Teoh, H., and Friedrich, J.O. (2015). Colchicine in cardiac disease: a systematic review and meta-analysis of randomized controlled trials. BMC Cardiovasc. Disord. *15*, 96.

Vila, N., Castillo, J., Dávalos, A., and Chamorro, A. (2000). Proinflammatory cytokines and early neurological worsening in ischemic stroke. Stroke J. Cereb. Circ. *31*, 2325–2329.

Villanueva, F.S., Jankowski, R.J., Klibanov, S., Pina, M.L., Alber, S.M., Watkins, S.C., Brandenburger, G.H., and Wagner, W.R. (1998). Microbubbles targeted to intercellular adhesion molecule-1 bind to activated coronary artery endothelial cells. Circulation *98*, 1–5.

Villines, T.C., Stanek, E.J., Devine, P.J., Turco, M., Miller, M., Weissman, N.J., Griffen, L., and Taylor, A.J. (2010). The ARBITER 6-HALTS Trial (Arterial Biology for the Investigation of the Treatment Effects of Reducing Cholesterol 6-HDL and LDL Treatment Strategies in Atherosclerosis): final results

and the impact of medication adherence, dose, and treatment duration. J. Am. Coll. Cardiol. *55*, 2721–2726.

Vinegoni, C., Botnaru, I., Aikawa, E., Calfon, M.A., Iwamoto, Y., Folco, E.J., Ntziachristos, V., Weissleder, R., Libby, P., and Jaffer, F.A. (2011). Indocyanine green enables near-infrared fluorescence imaging of lipid-rich, inflamed atherosclerotic plaques. Sci. Transl. Med. *3*, 84ra45.

Virmani, R., Burke, A.P., Kolodgie, F.D., and Farb, A. (2002). Vulnerable plaque: the pathology of unstable coronary lesions. J. Intervent. Cardiol. *15*, 439–446.

Vlachopoulos, C., Xaplanteris, P., Aboyans, V., Brodmann, M., Cífková, R., Cosentino, F., De Carlo, M., Gallino, A., Landmesser, U., Laurent, S., et al. (2015). The role of vascular biomarkers for primary and secondary prevention. A position paper from the European Society of Cardiology Working Group on peripheral circulation: Endorsed by the Association for Research into Arterial Structure and Physiology (ARTERY) Society. Atherosclerosis *241*, 507–532.

Voight, B.F., Peloso, G.M., Orho-Melander, M., Frikke-Schmidt, R., Barbalic, M., Jensen, M.K., Hindy, G., Hólm, H., Ding, E.L., Johnson, T., et al. (2012). Plasma HDL cholesterol and risk of myocardial infarction: a mendelian randomisation study. Lancet Lond. Engl. *380*, 572–580.

Wang, L., Gill, R., Pedersen, T.L., Higgins, L.J., Newman, J.W., and Rutledge, J.C. (2009). Triglyceride-rich lipoprotein lipolysis releases neutral and oxidized FFAs that induce endothelial cell inflammation. J. Lipid Res. *50*, 204–213.

Wang, Q., Yan, J., Chen, X., Li, J., Yang, Y., Weng, J., Deng, C., and Yenari, M.A. (2011). Statins: multiple neuroprotective mechanisms in neurodegenerative diseases. Exp. Neurol. *230*, 27–34.

Wang, X., Dong, Y., Qi, X., Huang, C., and Hou, L. (2013a). Cholesterol levels and risk of hemorrhagic stroke: a systematic review and meta-analysis. Stroke J. Cereb. Circ. *44*, 1833–1839.

Wang, X.-F., Liu, J.-J., Xia, J., Liu, J., Mirabella, V., and Pang, Z.P. (2015). Endogenous Glucagon-like Peptide-1 Suppresses High-Fat Food Intake by Reducing Synaptic Drive onto Mesolimbic Dopamine Neurons. Cell Rep. *12*, 726–733.

Wang, Y.I., Bettaieb, A., Sun, C., DeVerse, J.S., Radecke, C.E., Mathew, S., Edwards, C.M., Haj, F.G., Passerini, A.G., and Simon, S.I. (2013b). Triglyceride-rich lipoprotein modulates endothelial vascular cell adhesion molecule (VCAM)-1 expression via differential regulation of endoplasmic reticulum stress. PloS One *8*, e78322.

Warren, R.J., Ebert, D.L., Mitchell, A., and Barter, P.J. (1991). Rabbit hepatic lipase cDNA sequence: low activity is associated with low messenger RNA levels. J. Lipid Res. *32*, 1333–1339.

Weber, L.A., Cheezum, M.K., Reese, J.M., Lane, A.B., Haley, R.D., Lutz, M.W., and Villines, T.C. (2015). Cardiovascular Imaging for the Primary Prevention of Atherosclerotic Cardiovascular Disease Events. Curr. Cardiovasc. Imaging Rep. *8*, 36.

Westlake, S.L., Colebatch, A.N., Baird, J., Kiely, P., Quinn, M., Choy, E., Ostor, A.J.K., and Edwards, C.J. (2010). The effect of methotrexate on cardiovascular disease in patients with rheumatoid arthritis: a systematic literature review. Rheumatol. Oxf. Engl. *49*, 295–307.

Whitney, N.P., Eidem, T.M., Peng, H., Huang, Y., and Zheng, J.C. (2009). Inflammation mediates varying effects in neurogenesis: relevance to the pathogenesis of brain injury and neurodegenerative disorders. J. Neurochem. *108*, 1343–1359.

Wieberdink, R.G., Poels, M.M.F., Vernooij, M.W., Koudstaal, P.J., Hofman, A., van der Lugt, A., Breteler, M.M.B., and Ikram, M.A. (2011). Serum lipid levels and the risk of intracerebral hemorrhage: the Rotterdam Study. Arterioscler. Thromb. Vasc. Biol. *31*, 2982–2989.

Willecke, F., Yuan, C., Oka, K., Chan, L., Hu, Y., Barnhart, S., Bornfeldt, K.E., Goldberg, I.J., and Fisher, E.A. (2015). Effects of High Fat Feeding and Diabetes on Regression of Atherosclerosis Induced by Low-Density Lipoprotein Receptor Gene Therapy in LDL Receptor-Deficient Mice. PloS One *10*, e0128996.

Williams, K.J., and Tabas, I. (1995). The response-to-retention hypothesis of early atherogenesis. Arterioscler. Thromb. Vasc. Biol. *15*, 551–561.

Wu, J., Leong-Poi, H., Bin, J., Yang, L., Liao, Y., Liu, Y., Cai, J., Xie, J., and Liu, Y. (2011). Efficacy of contrast-enhanced US and magnetic microbubbles targeted to vascular cell adhesion molecule-1 for molecular imaging of atherosclerosis. Radiology *260*, 463–471.

Wu, M.-C., Ho, H.-I., Lee, T.-W., Wu, H.-L., and Lo, J.-M. (2012). In vivo examination of 111In-bis-5HT-DTPA to target myeloperoxidase in atherosclerotic ApoE knockout mice. J. Drug Target. *20*, 605–614.

Xaio, H., Banks, W.A., Niehoff, M.L., and Morley, J.E. (2001). Effect of LPS on the permeability of the blood-brain barrier to insulin. Brain Res. *896*, 36–42.

Xiong, H., Callaghan, D., Jones, A., Walker, D.G., Lue, L.-F., Beach, T.G., Sue, L.I., Woulfe, J., Xu, H., Stanimirovic, D.B., et al. (2008). Cholesterol retention in Alzheimer's brain is responsible for high beta- and gamma-secretase activities and Abeta production. Neurobiol. Dis. *29*, 422–437.

Xu, P.T., Gilbert, J.R., Qiu, H.L., Ervin, J., Rothrock-Christian, T.R., Hulette, C., and Schmechel, D.E. (1999). Specific regional transcription of apolipoprotein E in human brain neurons. Am. J. Pathol. *154*, 601–611.

Yang, Q., Zhang, Z., Gregg, E.W., Flanders, W.D., Merritt, R., and Hu, F.B. (2014). Added sugar intake and cardiovascular diseases mortality among US adults. JAMA Intern. Med. *174*, 516–524.

Yang, X., Liaw, L., Prudovsky, I., Brooks, P.C., Vary, C., Oxburgh, L., and Friesel, R. (2015). Fibroblast growth factor signaling in the vasculature. Curr. Atheroscler. Rep. *17*, 509.

Yates, K.F., Sweat, V., Yau, P.L., Turchiano, M.M., and Convit, A. (2012). Impact of metabolic syndrome on cognition and brain: a selected review of the literature. Arterioscler. Thromb. Vasc. Biol. *32*, 2060–2067.

Yerramasu, A., Dey, D., Venuraju, S., Anand, D.V., Atwal, S., Corder, R., Berman, D.S., and Lahiri, A. (2012). Increased volume of epicardial fat is an independent risk factor for accelerated progression of sub-clinical coronary atherosclerosis. Atherosclerosis *220*, 223–230.

Yoo, H., Kim, J.W., Shishkov, M., Namati, E., Morse, T., Shubochkin, R., McCarthy, J.R., Ntziachristos, V., Bouma, B.E., Jaffer, F.A., et al. (2011). Intra-arterial catheter for simultaneous microstructural and molecular imaging in vivo. Nat. Med. *17*, 1680–1684.

Yousuf, O., Mohanty, B.D., Martin, S.S., Joshi, P.H., Blaha, M.J., Nasir, K., Blumenthal, R.S., and Budoff, M.J. (2013). High-sensitivity C-reactive protein and cardiovascular disease: a resolute belief or an elusive link? J. Am. Coll. Cardiol. *62*, 397–408.

Yuan, C., Kerwin, W.S., Ferguson, M.S., Polissar, N., Zhang, S., Cai, J., and Hatsukami, T.S. (2002). Contrast-enhanced high resolution MRI for atherosclerotic carotid artery tissue characterization. J. Magn. Reson. Imaging JMRI *15*, 62–67.

Yudkin, J.S., Kumari, M., Humphries, S.E., and Mohamed-Ali, V. (2000). Inflammation, obesity, stress and coronary heart disease: is interleukin-6 the link? Atherosclerosis *148*, 209–214.

Yun, M., Yeh, D., Araujo, L.I., Jang, S., Newberg, A., and Alavi, A. (2001). F-18 FDG uptake in the large arteries: a new observation. Clin. Nucl. Med. *26*, 314–319.

Yurdagul, A., Chen, J., Funk, S.D., Albert, P., Kevil, C.G., and Orr, A.W. (2013). Altered nitric oxide production mediates matrix-specific PAK2 and NF-κB activation by flow. Mol. Biol. Cell *24*, 398–408.

Zacho, J., Tybjaerg-Hansen, A., Jensen, J.S., Grande, P., Sillesen, H., and Nordestgaard, B.G. (2008). Genetically elevated C-reactive protein and ischemic vascular disease. N. Engl. J. Med. *359*, 1897–1908.

Zaremba, J., and Losy, J. (2001). Early TNF-alpha levels correlate with ischaemic stroke severity. Acta Neurol. Scand. *104*, 288–295.

Zavala, F., and Lenfant, M. (1987). Benzodiazepines and PK 11195 exert immunomodulating activities by binding on a specific receptor on macrophages. Ann. N. Y. Acad. Sci. *496*, 240–249.

Zhang, R., Brennan, M.L., Fu, X., Aviles, R.J., Pearce, G.L., Penn, M.S., Topol, E.J., Sprecher, D.L., and Hazen, S.L. (2001). Association between myeloperoxidase levels and risk of coronary artery disease. JAMA *286*, 2136–2142.

Zhang, R., Miller, R.G., Gascon, R., Champion, S., Katz, J., Lancero, M., Narvaez, A., Honrada, R., Ruvalcaba, D., and McGrath, M.S. (2009). Circulating endotoxin and systemic immune activation in sporadic amyotrophic lateral sclerosis (sALS). J. Neuroimmunol. *206*, 121–124.

Zheng, L., Nukuna, B., Brennan, M.-L., Sun, M., Goormastic, M., Settle, M., Schmitt, D., Fu, X., Thomson, L., Fox, P.L., et al. (2004). Apolipoprotein A-I is a selective target for myeloperoxidase-catalyzed oxidation and functional impairment in subjects with cardiovascular disease. J. Clin. Invest. *114*, 529–541.

Zhou, Y., Han, W., Gong, D., Man, C., and Fan, Y. (2016). Hs-CRP in stroke: A meta-analysis. Clin. Chim. Acta Int. J. Clin. Chem. *453*, 21–27.

van Zyl, C., Huisman, H.W., and Mels, C.M.C. (2016). Antioxidant enzyme activity is associated with blood pressure and carotid intima media thickness in black men and women: The SABPA study. Atherosclerosis *248*, 91–96.

APPENDICES

ADDITIONAL MATERIAL AND METHODS

Primers design and validation for Non-Human Primates tissues genomic analysis:

Primers design:

Collect sequence of cDNA of the gene of interest on NCBI gene (http://www.ncbi.nlm.nih.gov/gene) for the studied species (here, *Macaca fascicularis*). Find the NM (or XM sequence when the gene sequence is only predicted) sequence in the section "mRNA and protein" and collect the FASTA sequence for all variants. Then, using Clustal Omega software, align the FASTA sequences.

In NCBI gene, search again the gene of interest and collect the FASTA sequence in the section "Genomic regions, transcripts and products" to obtain the genome sequence. Then go to Blast (http://blast.ncbi.nlm.nih.gov/Blast.cgi): Nucleotide blast > tick the case "align two (or more) sequences" > past the cDNA sequence in the top box and the genome sequence in the bottom box > click on "Blast" > in the result file, choose "query start position" to obtain the intron position. Then, mark the intron position on the aligned sequences.

The primer had to:

- Be composed for about 20 nucleotides
- Have an amplicon size comprises between 100 and 200 nucleotides
- Have forward and reverse primers located in separate exons
- Have a 3' sequence finishing with a C or a G
- Do not count more than 3 G/C in the 5 last nucleotides
- Avoid repetition of 3 same nucleotides
- Contain minimum 9G/C and maximum 12 in their whole sequence.

Once, primer sequence was chosen, test it using Amplifix software. If primers match with the gene of interest sequence, go to Blast again for test their species and gene specificity.

Validation of primers:

Perform a qPCR at 60°C on one sample of each tissue of interest using the primers designed for each gene. Check on the melt curve of the qPCR, if only one peak is appearent, keep the qPCR samples for further validation of amplicon size. If the melt present a second peak, perform a qPCR at

62°C and see if the melt is ok. If the melt is still not neat or if it presents several peaks, new primers had to be designed.

Once primers were validated by qPCR assay, test the size of the amplicon obtained by the qPCR. There are two ways to do it: perform migration of amplicon on an agarose gel or use QIAxcel®(QIAGEN). For validate the primers, the test had to present one single peak and the amplicon size had to be similar of the expected size ± 10pb.

ARTICLE n°4

Safety and efficiency of Gadolinium-based nanoparticles for imaging in healthy and atherosclerosis non-human primates

Kotb Shady, Piraquive Joao, Lamberton Franck, Lux François, Verset Michael, Di Cataldo Vanessa, Contamin Hugues, Tillement Olivier, Canet-Soulas Emmanuelle, Sancey Lucie

Scientific Reports, October 2016, DOI: 10.1038/srep35053

ARTICLE N°4:

Main results:

No trend related to dose, sex or evaluation day was observed for both clearance, volume of distribution or $T_{1/2}$ values of Gd-nanoparticles (**Gd-NPs**) and **no evidence of an intravenous toxicity** was noted.

The **highest administered dose** – 450mg/kg – could thus be considered as the non-observed effect level (**NOEL**) **dose**.

Control animals: Gd-NPs exhibited an **excellent angiographic T1-enhancement** at first pass and bolus injected was **well tolerated**.

Atherosclerotic animals: Gd-NPs **contrast enhancement** was **similar** to what was observed in the control animals **excepted for the liver** which showed a highest enhancement. Bolus injected was **well tolerated**.

Carotid plaque imaging: both Gd-chelates and Gd-NPs allowed **good carotid wall delineation on condition that there were advanced plaques** and Gd-NPs exhibits **similar imaging properties** than Gd-chelates.

In a context of well-established atherosclerosis, **Gd-NPs enable a better identification of vulnerable plaques** than Gd-chelates.

Furthermore, **atherosclerotic** animals showed a **significant retention of Gd-NPs** compared to control animals that might be **proportional with the degree of advancement of the pathology**.

SCIENTIFIC REPORTS

OPEN

Safety Evaluation and Imaging Properties of Gadolinium-Based Nanoparticles in nonhuman primates

Received: 15 July 2016
Accepted: 13 September 2016
Published: xx xx xxxx

Kotb Shady[1,*], Piraquive Joao[2,*], Lamberton Franck[3], Lux François[1], Verset Michael[4], Di Cataldo Vanessa[2], Contamin Hugues[4], Tillement Olivier[1], Canet-Soulas Emmanuelle[2] & Sancey Lucie[1]

In this article, we report the safety evaluation of gadolinium-based nanoparticles in nonhuman primates (NHP) in the context of magnetic resonance imaging (MRI) studies in atherosclerosis bearing animals and healthy controls. In healthy NHP, the pharmacokinetics and toxicity profiles demonstrated the absence of dose, time, and sex-effects, as well as a suitable tolerance of intravenous administration of the nanoparticles. We investigated their imaging properties for arterial plaque imaging in a standard diet or a high cholesterol diet NHP, and compared their characteristics with clinically applied Gd-chelate. This preliminary investigation reports the efficient and safe imaging of atherosclerotic plaques.

Atherosclerosis is one of the main cardiovascular disorders resulting from an initial lipid accumulation in the artery wall with *in situ* lesion development as well as an unresolved chronic and complex inflammatory process[1]. This chronic and evolutive injury of the arterial wall may abruptly lead to the obstruction of the vessel itself by clot formation, or may lead to acute stroke following plaque rupture with cerebral emboli, which often leads to disastrous consequences[2]. Early imaging and monitoring of atherosclerosis and high-risk plaque is challenging as the lesion is non-obstructive and a precise non-invasive diagnosis might require the gathering of several parameters. As recent novel strategies are being developed for accurate detection, plaque burden can be measured using ultrasound exams or computed tomography (CT) for calcium scoring whereas macrophage infiltration and microcalcification can be monitored using a PET/CT or PET/MRI combination[3,4]. In parallel, high-resolution MRI allows for the depiction of angiogenesis, intraplaque hemorrhage, observation of necrotic core, or positive remodeling[5–8]. MRI can also be considered as the reference technique for vessel wall imaging and plaque characterization, especially for the carotid and peripheral arteries imaging[6]. A standard examination combines different high-resolution carotid T1-weighted and proton density-weighted, and a post-contrast agent T1-weighted acquisition[4,9]. For a better characterization of plaque microvasculature, dynamic contrast-enhanced (DCE) MRI is considered very helpful to identify leaky neovessels, a hallmark of plaque destabilization[10].

Different contrast agents containing gadolinium in the chelated form are used for T1-weighted acquisitions. Commercially available gadolinium (Gd) chelates are molecular compounds containing one single Gd atom. Nevertheless, clustering several Gd chelates will enhance the relaxivity of the probe and thus, the related contrast imaging properties[11,12]. In this context, we used Gd-based nanoparticles for MRI purposes. Nanoparticles might allow the detection of atherosclerosis plaques[13] or macrophages in inflammatory atherosclerosis[14,15]. We previously reported the efficient renal elimination (>50% of the injected dose at 74 min post injection)[16] and the safety of Gd-based nanoparticles in rodents[17,18], especially regarding the clearance mechanism[19]. Herein, we evaluated the safety and pharmacokinetics of Gd-based nanoparticles in healthy non-human primates (NHP). To further investigate the contrast potential, we reported their imaging properties in healthy and high cholesterol (HC) diet NHP and compared their characteristics to the vessel wall imaging with commercially available molecular Gd-chelate.

[1]Univ Lyon, Institut Lumière Matière, UMR5306, Université Claude Bernard Lyon 1, CNRS, Institut Lumière Matière, F-69622, Villeurbanne, France. [2]Univ Lyon, CARMEN Laboratory, INSERM INSA, INRA, Université Claude Bernard Lyon 1, Lyon, France. [3]CERMEP, Imagerie du vivant, Bron 69677, France. [4]Cynbiose SAS, Marcy-L'Etoile, France. *These authors contributed equally to this work. Correspondence and requests for materials should be addressed to S.L. (email: lucie.sancey@univ-grenoble-alpes.fr)

In life parameters	Safety Pharmacology	Clinical Pathology
Mortality/Morbidity	Electrocardiogram[a]	Haematology
Clinical signs	Blood pressure[b]	Coagulation
Local tolerance	Respiratory rate	Serum clinical chemistry
Body weight	Neurobehavioral assessment	Urinary analysis
Food consumption		Terminal parameters
Ophtalmology		Necropsy/HistoPathology

Table 1. List of the investigations performed after 2-repeated IV injection of Gd-NPs in cynomolgus monkey. [a]Includes heart rate, QRS complex duration, PR intervals, QT intervals. [b]Includes diastole and systole. No differences were reported at any dose. Details can be found in the Supplementary information Table S1.

Results

Nanoparticles characteristics. Gd-NPs were produced using reported methods, in laboratory and GMP environment[16,20]. This nanoparticle regroups gadolinium (Gd)-chelating DOTAGA (1,4,7,10-tetra-azacyclododecane-1-glutaric anhydride-4,7,10-triacetic acid) coupled to a polysiloxane network. The hydrodynamic diameter of Gd-NPs is 3.5 ± 1 nm for a mass of ≈10 kDa. Due to the presence of Gd, the nanoparticle provides positive enhancement on T1-weighted MR images and radiosensitizing properties. Its imaging properties are investigated in addition to its safety profile in NHP under normal or high cholesterol (HC) diet.

Toxicity and pharmacokinetic profile in nonhuman primates. Regulatory toxicity and pharmacokinetics were conducted in compliance with good laboratory practices (GLP), and were evaluated in nonhuman cynomolgus monkey primates at 3 different Gd-NP doses (low, 150 mg/kg body weight (b.w.); moderate, 300 mg/kg b.w.; and high, 450 mg/kg b.w.), during two-repeated injections protocol, *i.e.* once a week during two weeks. During this period, no cardiovascular or clinical signs were observed, neither in males nor females, at any dose (Table 1).

Two weeks after the last injection, all vital organs and injection sites were sampled for histological investigation. In all the tissues, no microscopic changes were evidenced after two administrations of Gd-NPs at a high dose of 450 mg/kg, compared to the control group (Fig. 1). In particular, the kidneys, which are the main organs of elimination, were similar to control kidneys, without any sign of vacuolation.

Plasma kinetics of Gd-NPs were evaluated for the treated groups after each administration, from 3 animals/sex/group, and are reported in Table 2. Blood samples were collected at 5 and 30 minutes, and 1, 2, 6, and 24 hours post-administration to determine the nanoparticles' pharmacokinetics. Following the intravenous administration of Gd-NPs, the exposure in male and female cynomolgus monkeys increased in a dose-proportional manner for both sexes on both evaluation days. The exposure on day 7 was similar to that on day 0. The accumulation ratios ranged from 0.848 to 1.04 at all dose levels. On day 0, mean clearance as well as the distribution volume were low and ranged from 0.111 and 0.187 L/h/kg and 0.176 and 0.314 L/kg, respectively. The mean blood half-life ($T_{1/2}$) ranged from 2.09 to 3.57 hours. In general, there were no trends observed related to dose, sex, or evaluation days for clearance, volume of distribution, or $T_{1/2}$ values. Under these study conditions, two intravenous administrations at one-week interval of Gd-NPs at doses of 150, 300, and 450 mg/kg to the cynomolgus monkey were not associated with any overt evidence of intravenous toxicity. Consequently, the high dose (450 mg/kg/administration) could be considered to be the NOEL (non observed effect level). This dose corresponds to a mean area under the curve determined between 0 to 24 h ($AUC_{0\text{-}24h}$) normalized to a unit dose (1 mg/kg b.w.) of 9.00/7.60 mg.h/mL (Day 0/Day 7) in males and of 6.42/6.32 mg.h/mL (Day 0/Day 7) in females.

Imaging properties of the Gd-NPs in control (Cont) healthy monkeys. The T1-MRI properties of Gd-NPs were first studied in healthy monkeys to observe the general biodistribution of the particles. After the intravenous injection of Gd-NPs, the main vascular network was clearly identified, and the main organs, *i.e.* heart, liver, and kidneys. One should note that there was a marked enhancement of blood vessels at first-pass (Fig. 2, see also Figure S1) and the bolus injection was very well tolerated without any changes in hemodynamic, cardiac, or ventilation parameters. Within the first 30 minutes, most of the nanoparticles were eliminated by the kidney route, as observed in Fig. 2A (last panel). Low T1 contrast was persistent in the muscles, liver, and kidneys. The contrast enhancement indicated a rapid renal washout of the nanoparticles: the T1 contrast enhancement strongly increased in the ureters within the first 150 seconds, before it was drastically reduced during the next minute (Fig. 2B). Moreover, at 35 min post-administration, the T1 contrast of the ureters was once more very intense, indicating a continuous washout of Gd-NPs. The main MRI findings were in accordance with the pharmacokinetics' profiles, which indicated a Gd-NPs blood half-life of ≈2 hours at the administrated dose (*i.e.* 200 mg/kg for MRI investigations).

Imaging properties of Gd-NPs in old animals under a high cholesterol (HC) diet for 24 months. Similarly to the previous investigation, MRI was performed on old monkeys under a 24-months HC diet (referred as HC^{++} animal, Fig. 3A). The contrast enhancements were similar to healthy animals except for the liver, which indicated a highest enhancement (Fig. 3B). Similar to healthy animals, the Gd-NPs were well tolerated without any changes in hemodynamic, cardiac or ventilation parameters.

Contrast properties for vulnerable carotid plaque. The contrast properties of Gd-NPs were evaluated for vulnerable carotid plaques and compared to the ones of Gd-DOTA. In this pathology, unspecific accumulation

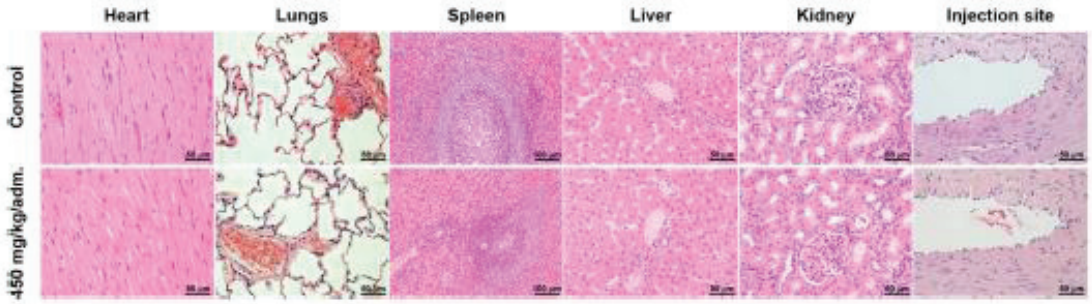

Figure 1. Examples of histological sections of vital organs and injection site of the control and the high-dose group. Hematoxylin and eosin staining revealed similar microscopic profiles when comparing control and high-dose group samples, in both males and females.

Day, Gender		Dose (mg/kg/day)	$AUC_{0\text{-}24h}$ (h*mg/mL)	DN $AUC_{0\text{-}24h}$	C_{max} (mg/mL)	DN C_{max}	$T_{1/2}$ (h)	Cl (L/h/kg)	V_{ss} (L/kg)	Acc. Ratio
Day 0	M	150	812	5.41	1,429	9.53	2.13	0.187	0.195	
	M	300	1,866	6.22	3,305	11.02	2.17	0.162	0.176	
	M	450	4,051	9.00	4,792	10.65	3.57	0.111	0.314	
	F	150	884	5.89	1,422	9.48	2.21	0.171	0.225	
	F	300	1,695	5.65	3,216	10.72	2.09	0.178	0.184	
	F	450	2,890	6.42	4,541	10.09	2.34	0.150	0.185	
Day 7	M	150	828	5.52	1,437	9.58	2.29	NA	NA	1.02
	M	300	1,934	6.45	3,198	10.66	2.22	NA	NA	1.04
	M	450	3,419	7.60	4,779	10.62	NA	NA	NA	0.848
	F	150	831	5.54	1,528	10.19	2.30	NA	NA	0.948
	F	300	1,665	5.55	2,984	9.95	2.19	NA	NA	0.983
	F	450	2,842	6.32	4,979	11.06	NA	NA	NA	0.991

Table 2. Mean pharmacokinetic parameters in male and female cynomolgus monkeys following two intravenous administrations of Gd-NPs. M: Male; F: Female; AUC: Area under the curve; DN: Dose-Normalized; C_{max}: Maximum plasma concentration; T½: blood half-life; Cl: Clearance; V_{ss}: Volume of distribution at the steady state. Units for DN $AUC_{0\text{-}24h}$ is (mg*h/mL)/(mg/kg) and units for DN C_{max} is (mg/mL)/(mg/kg). Acc. Ratio = Accumulation Ratio. The values were determined at 5 and 30 minutes, 1, 2, 6, and 24 hours post-administration.

of contrast agent may occur due to the leaky wall's endothelial layer and the inflammation, which recruits highly active macrophages[21]. In our condition, the 24-months HC diet induced moderate and more advanced atherosclerosis, as indicated by the ultrasound and biochemical parameters recorded from the treated animals (Supplementary information Table S2). As indicated by pre-contrast T1 MRI (Fig. 4), the carotid walls were not observable before the administration of any contrast agent. In absence of vulnerable plaque, both Gd-DOTA and Gd-NPs allowed very minimal carotid wall delineation. In presence of vulnerable plaque, both Gd-DOTA and Gd-NPs delineated the carotid wall with similar contrast properties. Gd-NPs appeared to have similar imaging properties as compared to Gd-DOTA. In the case of a well-established pathology (Fig. 4, HC^{++}), the vulnerable plaques were better identified by Gd-NPs, in comparison to Gd-DOTA. The T1-contrast obtained after Gd-NPs was measured with time and the elimination kinetics of Gd-NPs were determined (Fig. 5). In healthy animals, Gd-NPs were rapidly washed out, whereas a significant retention was observed in HC animals. Gd-NPs retention might be proportional with the stage of the pathology, as the highest retention was observed for the most developed pathology (right carotid of HC^{++} animal).

Discussion – Conclusion

The use of nanoparticles as a contrast imaging agent requires their specific distribution in the body after intravenous injection, a rapid clearance from the body without undesired accumulation, a safe profile, and good contrast properties. Gd-NPs present the above mentioned properties with a fine distribution within the entire body starting at the first heartbeats following the intravenous administration, as well as a fast renal clearance as demonstrated with healthy NHP. After high-dose repeated IV administration, the particles were well tolerated, without modification of the antemortem and post-mortem parameters as compared to untreated animals. In particular, H&S staining indicated a safe renal elimination of Gd-NPs. Transient and minimal vacuolations of the proximal convoluted tubules was observed in rodents as previously reported[18,19], but the NHP did not present such transient alteration for similar equivalent doses, indicating a strong tolerance and safe elimination in NHP.

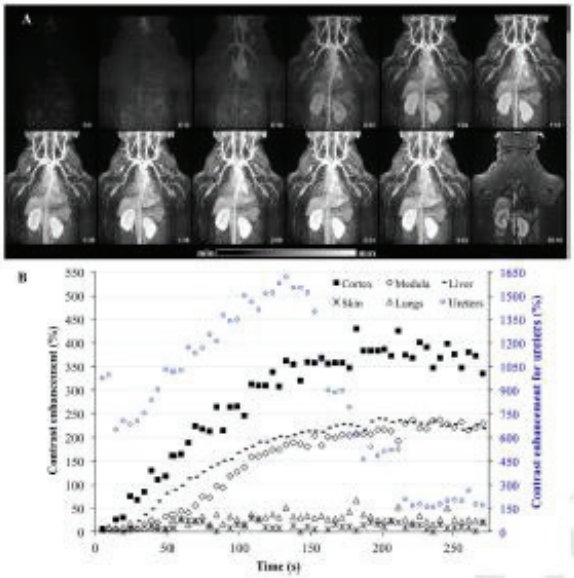

Figure 2. MRI first-pass kinetics of Gd-NPs in different tissues (liver, kidneys' cortex and medulla, skin, and lungs) in a male control subject with a slow injection. (**A**) During the first minutes of the acquisition, Gd-NPs were administrated intravenously, allowing a clear observation of the blood network and main organs, such as the heart, liver, and kidneys, *i.e.* an excellent T1 enhancement for angiographic studies and fast renal excretion. Then, at 35 minutes, the kidneys and ureters were mainly observed, demonstrating the washout of the nanoparticles. (**B**) The contrast enhancement was determined on the main organs. The highest contrast enhancements were observed for the kidneys, liver, and ureters.

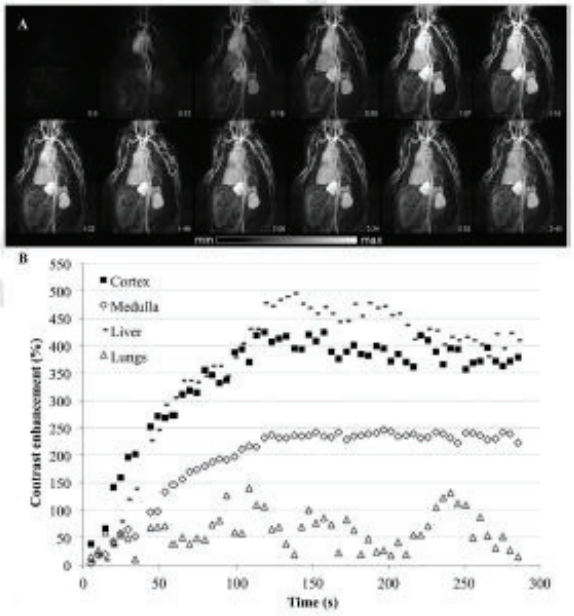

Figure 3. MRI first-pass kinetics of Gd-NPs in different tissues (liver, kidneys' cortex and medulla, lungs) in a female HC subject with a slow injection. (**A**) Similar to healthy animals, Gd-NPs were distributed in the vascular network and the main organs, and rapidly reached the kidneys. (**B**) The contrast enhancements were determined for the kidneys, livers, and lungs.

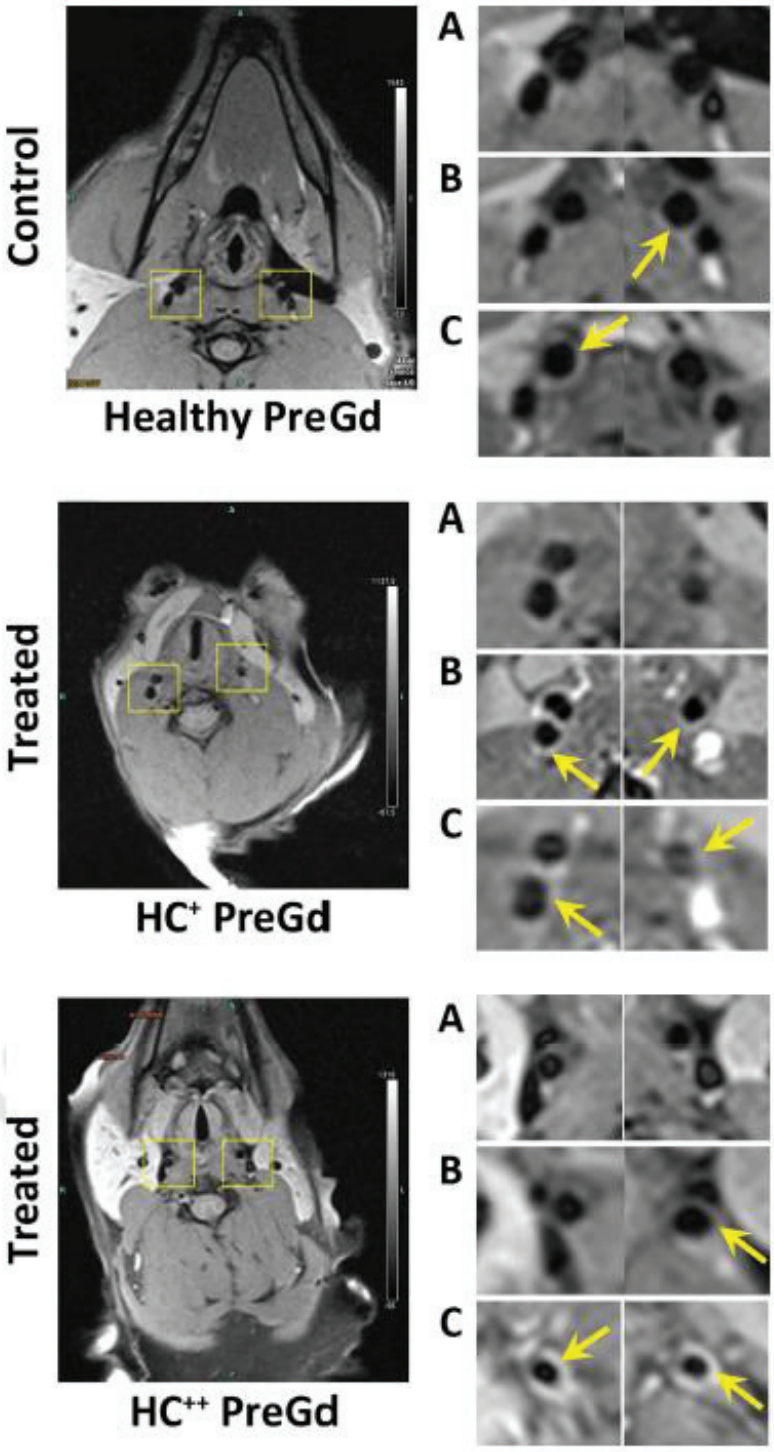

Figure 4. High-resolution vessel wall carotid MRI in control (upper panel) and HC animals (middle and lower panel). Enlarged views of the carotids (right panels) with pre-contrast T1 images (**A**), post-Gd-DOTA (**B**) and post-Gd-NPs (C) respectively. In HC animals, post-contrast enhancement of the vessel wall is characteristic of atherosclerotic lesions with inflammation and increased vessel wall permeability. Arrows: vessel wall.

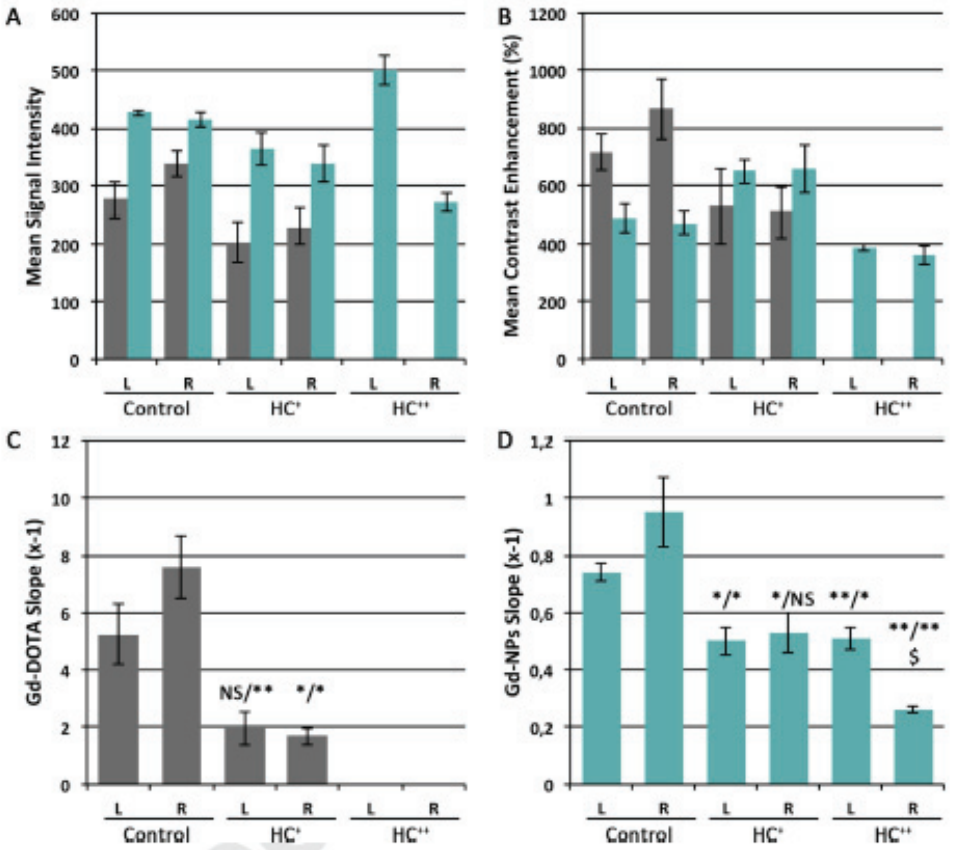

Figure 5. MRI characteristics of the left and right carotids after intravenous administrations of Gd-NPs. The uptake of Gd-NPs in the vulnerable carotid plaque was followed as function of time for signal intensity (**A**), and contrast enhancement (**B**). The calculated slopes of the washout were determined for Gd-DOTA (**C**) and Gd-NPs (**D**). They were significantly different for vulnerable carotid plaques *versus* healthy carotids. L: left. R: right. HC: High cholesterol. For HC^{++} animal, Gd-DOTA values were not determined due to movements during the acquisition. $^{*}P < 0.05$, $^{**}P < 0.01$ HC *versus* healthy NHP. $^{\$}p < 0.05$ for HC^{++} left *versus* right carotid.

Mean blood half-life measured in NHP was very similar to the one measured in rats for equivalent doses, with 2.35 hours *versus* 2.31 hours, respectively[18]. Altogether, the safety profile indicated a NOEL of 450 mg/kg/administration, which corresponds to 145 mg/kg/administration for Humans[22,23].

In contrast to intravascular ultrasound which accurately image the vessel wall at high resolution[24], MRI is noninvasive. Combined to a T1-weighted contrast agent, MRI also allows to assess the morphological plaque characteristics. In particular, the local lesion and its evolution could be monitored using a carotid MRI protocol, considering the vessel wall permeability on gadolinium-enhanced MRI[5]. Under high cholesterol diet, old NHP had at-risk plasmatic profile (high LDL/HDL ratio, high triglycerides (see Table S3) and high hsCRP levels) and developped atherosclerosis lesions similar to human plaques at the same vascular sites[25]. As shown by MRI, our animals had carotid plaques with the same advanced and vulnerable characteristics as in patients.

For similar contrast properties[16,20], Gd-DOTA is a cyclic ionic chelate, and Gd-NPs possess DOTA-derivatives. Both compounds possess very strong complexation for Gd ($\log\beta_{110} = 25.58$ for Gd-DOTA, and $\log\beta_{110} = 25.58$ for Gd-NPs), preventing the release of free Gd[20]. Safe administration was observed for old atherosclerosis NHP. Imaging of the vessel's wall in this pathologic animal was demonstrated using both chelates and chelates bound to NPs. The signal measured in the vessel wall was correlated to the plaque development for Gd-NPs investigations; the former agent possesses a longer circulation time as compared to Gd-DOTA that is rapidly cleared from the body which may have favored its retention in the plaque (13.2 min *vs.* 6.8 min in mice, respectively)[19]. Therefore, this agent has more suitable properties to quantify neovessels leakiness using DCE-MRI, another important functional parameters to define vulnerable plaques[10]. Thanks to the high safety of Gd-NPs, this could be studied longitudinally in the near future using kinetic modeling in order to assess the vessel's wall permeability over time and correlate it with the plaque's evolution and downstream clinical events.

MRI data treatment. MRI data analysis was performed using the Inveon® Research Workplace 4.1 software (Siemens, Erlangen, Germany). The regions of interest were drawn in the carotid vessel wall and in the artery's lumen to obtain the dynamic contrast information during the contrast agent first-pass, and in the different organs of interest for the contrast distribution at a steady state.

Statistical analysis. Statistical analysis was performed using unpaired T-Test (Excel software) for the vulnerable plaque contrast.

References

1. Yahagi, K. *et al.* Pathophysiology of native coronary, vein graft, and in-stent atherosclerosis. *Nat Rev Cardiol* **13,** 79–98, doi: 10.1038/nrcardio.2015.164 (2016).
2. Libby, P. Mechanisms of acute coronary syndromes and their implications for therapy. *The New England journal of medicine* **368,** 2004–2013, doi: 10.1056/NEJMra1216063 (2013).
3. Adamson, P. D., Vesey, A. T., Joshi, N. V., Newby, D. E. & Dweck, M. R. Salt in the wound: (18)F-fluoride positron emission tomography for identification of vulnerable coronary plaques. *Cardiovasc Diagn Ther* **5,** 150–155, doi: 10.3978/j.issn.2223-3652.2015.03.01 (2015).
4. Dweck, M. R., Puntman, V., Vesey, A. T., Fayad, Z. A. & Nagel, E. M. R. Imaging of Coronary Arteries and Plaques. *JACC Cardiovasc Imaging* **9,** 306–316, doi: 10.1016/j.jcmg.2015.12.003 (2016).
5. Canet-Soulas, E. & Letourneur, D. Biomarkers of atherosclerosis and the potential of MRI for the diagnosis of vulnerable plaque. *Magma* **20,** 129–142, doi: 10.1007/s10334-007-0078-y (2007).
6. Kramer, C. M. & Anderson, J. D. MRI of atherosclerosis: diagnosis and monitoring therapy. *Expert Rev Cardiovasc Ther* **5,** 69–80, doi: 10.1586/14779072.5.1.69 (2007).
7. Moody, A. R., Allder, S., Lennox, G., Gladman, J. & Fentem, P. Direct magnetic resonance imaging of carotid artery thrombus in acute stroke. *Lancet* **353,** 122–123 (1999).
8. Murphy, R. E. *et al.* Prevalence of complicated carotid atheroma as detected by magnetic resonance direct thrombus imaging in patients with suspected carotid artery stenosis and previous acute cerebral ischemia. *Circulation* **107,** 3053–3058, doi: 10.1161/01.CIR.0000074204.92443.37 (2003).
9. Dweck, M. R. *et al.* Imaging of coronary atherosclerosis - evolution towards new treatment strategies. *Nat Rev Cardiol*, doi: 10.1038/nrcardio.2016.79 (2016).
10. van Hoof, R. H., Heeneman, S., Wildberger, J. E. & Kooi, M. E. Dynamic Contrast-Enhanced MRI to Study Atherosclerotic Plaque Microvasculature. *Curr Atheroscler Rep* **18,** 33, doi: 10.1007/s11883-016-0583-4 (2016).
11. Fries, P. *et al.* Evaluation of a Gadolinium-Based Nanoparticle (AGuIX) for Contrast-Enhanced MRI of the Liver in a Rat Model of Hepatic Colorectal Cancer Metastases at 9.4 Tesla. *RoFo: Fortschritte auf dem Gebiete der Rontgenstrahlen und der Nuklearmedizin* **187,** 1108–1115, doi: 10.1055/s-0035-1553500 (2015).
12. Lux, F. *et al.* Gadolinium-based nanoparticles for theranostic MRI-radiosensitization. *Nanomedicine* **10,** 1801–1815, doi: 10.2217/nnm.15.30 (2015).
13. Lobatto, M. E. *et al.* Atherosclerotic plaque targeting mechanism of long-circulating nanoparticles established by multimodal imaging. *ACS nano* **9,** 1837–1847, doi: 10.1021/nn506750r (2015).
14. Majmudar, M. D. *et al.* Polymeric nanoparticle PET/MR imaging allows macrophage detection in atherosclerotic plaques. *Circ Res* **112,** 755–761, doi: 10.1161/CIRCRESAHA.111.300576 (2013).
15. Bagalkot, V. *et al.* Hybrid nanoparticles improve targeting to inflammatory macrophages through phagocytic signals. *J Control Release* **217,** 243–255, doi: 10.1016/j.jconrel.2015.09.027 (2015).
16. Lux, F. *et al.* Ultrasmall rigid particles as multimodal probes for medical applications. *Angew Chem Int Ed Engl* **50,** 12299–12303, doi: 10.1002/anie.201104104 (2011).
17. Detappe, A. *et al.* Advanced multimodal nanoparticles delay tumor progression with clinical radiation therapy. *J Control Release* **238,** 103–113, doi: 10.1016/j.jconrel.2016.07.021 (2016).
18. Verry, C. *et al.* MRI-guided clinical 6-MV radiosensitization of glioma using a unique gadolinium-based nanoparticles injection. *Nanomedicine*, doi: 10.2217/nnm-2016-0203 (2016).
19. Sancey, L. *et al.* Long-term *in vivo* clearance of gadolinium-based AGuIX nanoparticles and their biocompatibility after systemic injection. *ACS nano* **9,** 2477–2488, doi: 10.1021/acsnano.5b00552 (2015).
20. Mignot, A. *et al.* A top-down synthesis route to ultrasmall multifunctional Gd-based silica nanoparticles for theranostic applications. *Chemistry* **19,** 6122–6136, doi: 10.1002/chem.201203003 (2013).
21. Ronald, J. A. *et al.* Comparison of gadofluorine-M and Gd-DTPA for noninvasive staging of atherosclerotic plaque stability using MRI. *Circ Cardiovasc Imaging* **2,** 226–234, doi: 10.1161/CIRCIMAGING.108.826826 (2009).
22. Blanchard, O. L. & Smoliga, J. M. Translating dosages from animal models to human clinical trials--revisiting body surface area scaling. *FASEB J* **29,** 1629–1634, doi: 10.1096/fj.14-269043 (2015).
23. Reagan-Shaw, S., Nihal, M. & Ahmad, N. Dose translation from animal to human studies revisited. *FASEB J* **22,** 659–661, doi: 10.1096/fj.07-9574LSF (2008).
24. Celeng, C., Takx, R. A., Ferencik, M. & Maurovich-Horvat, P. Non-invasive and invasive imaging of vulnerable coronary plaque. *Trends Cardiovasc Med*, doi: 10.1016/j.tcm.2016.03.005 (2016).
25. Di Cataldo, V. *et al.* Mr and pet/ct imaging use to stratify cardiovascular risks in non-human primates under atherogenic diet. *Atherosclerosis* **241,** E161–E161 (2015).

Acknowledgements

The authors gratefully acknowledge the LABEX PRIMES (ANR-11-LABX-0063) of Lyon 1 University within the program "Investissements d'Avenir" (ANR-11-IDEX-0063) and the French National Research Agency (ANR) within the ANR Cyclops (ANR-15-CE17-0020) for financial support. The authors gratefully acknowledge Fabrice Taborik and the animal care technicians at Cynbiose, and Stéphanie Simonet for editing and proofreading.

Author Contributions

K.S., P.J. and D.C.V. performed MRI data processing and experiments. L. Franck created the MRI sequences. L. François and T.O. developed and produced the particles. V.M. and C.H. developed the HC diet for NHP. C.-S.E. developed the MRI project and performed investigations. S.L. performed investigations and article writing. The project was designed by L. Franck, L. François, T.O., C.H., C-S.E. and S.L. All the authors participated to the writing of the manuscript.

Additional Information

Supplementary information accompanies this paper at http://www.nature.com/srep

Competing financial interests: F.L. and T.O. have to disclose the patent WO2011/135101. The patent protects the nanoparticles described in this publication: AGuIX® .

How to cite this article: Shady, K. *et al.* Safety Evaluation and Imaging Properties of Gadolinium-Based Nanoparticles in nonhuman primates. *Sci. Rep.* **6**, 35053; doi: 10.1038/srep35053 (2016).

SUPPLEMENTAL DATA

Table S1 **In vivo *safety pharmacology studies in Cynomolgus Monkeys: detailed data on Blood Pressure, Heart Rate, and ECG before and after treatment of Gd-NPs***

Before treatment (Day -9)							
		Electrocardiogram			Blood pressure		Respiratory rate (breaths /min)
Group	Heart Rate (beats/min)	QRS complex duration (ms)	PR interval (ms)	QT intervals (ms)	Diastolic (mm Hg)	Systolic (mm Hg)	
M-0	246.7 ± 15.3	76.7 ± 3.5	60.3 ± 5.8	172.3 ± 4.0	89 ± 12.2	163.7 ± 20.4	49.0 ± 3.6
M-150	256.7 ± 15.3	78.7 ± 5.1	54.3 ± 2.3	174.3 ± 19.6	102 ± 8.5	179.3 ± 9	48.0 ± 2.6
M-300	253.3 ± 20.8	77.7 ± 4.0	58.0 ± 1.7	172.0 ± 1.7	93.3 ± 6.1	156.3 ± 13.3	41.3 ±2.9
M-450	266.7 ± 15.3	76.6 ± 6.5	51.3 ± 5.1	165.3 ± 6.8	88.7 ± 5.1	147 ± 22.6	48.3 ± 2.9
F-0	243.3 ± 20.8	78.0 ± 1.7	56.7 ± 3.5	175.7 ± 5.1	94.7 ± 10.2	159.3 ± 13.6	56.0 ± 5.2
F-150	223.3 ± 32.1	75.7 ± 5.1	61.0 ± 1.7	177.7 ± 13.6	99.7 ± 14	168.3 ± 27	52.0 ± 3.5
F-300	250 ± 10	74.3 ± 5.1	59.0 ±3.5	177.7 ± 6.8	100.3 ± 2.5	170.7 ± 15.6	55.3 ± 6.7
F-450	240 ± 10	81.0 ± 3.5	55.7 ± 7.5	192.3 ± 6.8	97 ± 10.1	171 ± 14.9	49.7 ± 4.7
Before treatment (Day -9)							
		Electrocardiogram			Blood pressure		Respiratory rate (breaths /min)
Group	Heart Rate (beats/min)	QRS complex duration (ms)	PR interval (ms)	QT intervals (ms)	Diastolic (mm Hg)	Systolic (mm Hg)	
M-0	226.7 ± 51.3	84.3 ± 7.5	62.0 ± 11.5	190.0 ± 28.8	100 ± 5.3	177.3 ± 6.4	46.7 ± 11.6
M-150	250 ± 10	77.7 ± 5.0	57.0 ± 0.0	175.7 ± 18.0	102.7 ± 23.4	185.7 ± 36.1	53.0 ± 7.8
M-300	230 ± 17.3	79.0 ± 1.7	64.3 ± 7.5	185.7 ± 5.1	90.3 ± 12.1	158 ± 25.6	47.0 ± 5.2
M-450	260 ± 17.3	71.3 ± 5.1	55.3 ± 4.0	180.0 ± 13.0	97 ± 15.5	180.3 ± 11	44.0 ± 1.0
F-0	263.3 ± 5.8	73.0 ± 0.0	51.0 ± 8.5	167.7 ± 10.8	96 ± 10.8	163.3 ± 20.4	47.7 ± 5.5
F-150	223.3 ± 25.2	79.0 ± 1.7	63.3 ± 5.8	181.3 ± 5.1	101 ± 12.1	172 ± 13	48.7 ± 12.5
F-300	263.3 ± 15.3	75.7 ± 2.3	54.7 ± 4.0	174.7 ± 13.7	97.7 ± 8.1	174.7 ± 13.3	46.3 ± 4.2
F-450	246.7 ± 25.2	79.0 ± 1.7	58.7 ± 9.8	189.0 ± 18.5	102.7 ± 5.7	182.7 ± 7	40.7 ± 6.4

Example of MR imaging in NHP:

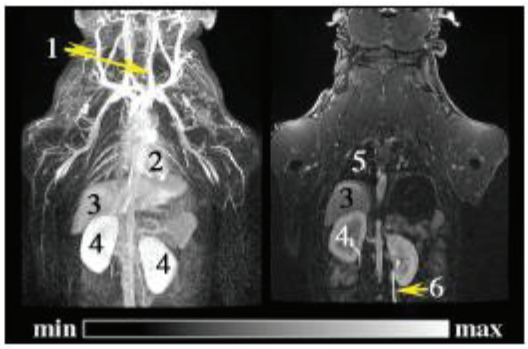

Figure S1: Example of MR Imaging of Gd-NPs in healthy NHP. 1: Main vascular network; 2: Heart; 3: Liver; 4: Kidneys; 5: Lungs; 6: Ureters.

Atherosclerosis characteristics:

The two old HC NHP included in this study (respectively 16 and 17 years old) had increased total cholesterol (respectively, 402 and 386 mg/dL compared to 100 mg/dL in normal NHP), and high LDL (220 and 258 mg/dL compared to 50 mg/dL in normal NHP). The two ultrasonography exams showed evolving atherosclerosis as at least two vascular beds (iliac arteries and carotids) showed lesion progression between 12 and 18 months. At the last time point, the inflammatory plasma profiles (high TNFalpha, respectively 125 and 157 pg/mL *versus* 38 pg/mL in normal NHP) were in agreement with increased cytokines in the heart, aortic arch, and carotids (increased IL1-beta and IL6 production, >0.2 pg/mg and >1 pg/mg of proteins respectively), further assessed by increased inflammatory macrophage gene expressions in the same tissues.

Table S2 ***Main atherosclerosis characteristics of the NHP (HC+ with moderate carotid plaque evolution between the two ultrasound exams, HC++ more advanced lesions)***

NHP	Age (y.o.)	Total cholesterol (mg/dL)	High LDL (mg/dL)	hsCRP (µg/mL of serum)	TNFalpha (pg/mL)	IL production (pg/mg of proteins)
Control	8	100	50	18	38	Low
HC^{+}	16	402	220	38	125	>0.2
HC^{++}	17	386	258	55	157	>1

Table S3 ***Serum clinical chemistry parameters. Liver and Kidney enzymes were measured at 12-months of diet.*** ALT: Alanine Amino-Transferase, AST: Aspartate Amino-Transferase, CREAT: creatinine, GGT: Gamma Glutamyl-Transferase, ALP: alkaline phosphatase, Trigs: Triglycerides, *elevated values.

NHP	ALT (U/L)	AST (U/L)	CREAT (µmol/L)	GGT (U/L)	Glucose (mmol/L)	ALP (U/L)	Trigs mg/dL
Control	68	50	71	150	2.2	460	54
HC^{+}	48	93*	105*	115	3.4	204	229*
HC^{++}	56	61*	93*	142	3.2	248	262*